Multi-Scale Investigation of Low Salinity Water Flooding for Enhanced Oil Recovery

Arije Ali Hussein Al-Khafaji

Submitted in accordance with the requirements for the degree

of Doctor of Philosophy

The University of Leeds

School of Chemical and Process Engineering

March 2019

The candidate confirms that the work submitted is her own, except where work, which has formed part of jointly authored publications has been included. The contribution of the candidate and the other authors to this work has been explicitly indicated below. The candidate confirms that appropriate credit has been given within the thesis where reference has been made to the work of others.

Publications

Chapter 4 results in a published paper. Al-Khafaji, A. and Wen, D. Quantification of Wettability Characteristics for Carbonates Using Different Salinities. Journal of Petroleum Science and Engineering, 2018, 173, 501-511. As a primary author, I was responsible for conducting the experimental work, analysing the obtained results, and writing the draft paper. The contribution of Dongsheng Wen was on the supervision and revision of the paper.

Chapter 6 results in a published paper. Al-Khafaji, A., Neville, A., Wilson, M., and Wen, D. Effect of Low Salinity on the Oil Desorption Efficiency from Calcite and Silica Surfaces. Energy & Fuels, 2017, 31(11), 11892-11901. I was responsible for conducting the experiments, interpreting and analysing the data, and writing the draft paper. The co-authors supervised the experimental work and reviewed the paper.

Chapter 8 results in a published paper. Al-Khafaji, A., Wilson, M., Neville, A., and Wen, D. Pore-Scale Displacement Efficiency during Different Salinity Water Flooding in Hydrophilic and Hydrophobic Microstructures. Energy & Fuels, 2019, 33(5), 3859-3870. As a main author, I was responsible for carrying out all the microfluidic experiments, images processing and analysis, drafting the figures and the paper. The co-authors reviewed the paper and provided some editorial suggestions.

Acknowledgements

First and foremost, I would like to express my sincere appreciation and deep gratitude to my supervisors Prof. Dongsheng Wen, Prof. Anne Neville, and Dr. Mark Wilson for their continuous guidance and encouragement throughout all stages of my PhD work. Their deductive critical reviews, productive discussions, and precious advice have undoubtedly helped me to further improve my project.

I would like to express my utmost appreciation to Shell and BP for providing financial support for the duration of my study and their technical assistance by providing me with the samples to experiment with.

Appreciation is also extended to Prof. Xianfeng Fan and his research group for their collaboration to accomplish a part of my research work at the University of Edinburgh /Institute of Materials and Processes. I would like to thank Dr. Simon Connell for giving me the opportunity to perform the lab work that related to Atomic Force Microscopy (AFM) at the School of Physics and Astronomy. His technical skills, valuable feedback, and suggestions were helpful in data interpretation.

I gratefully like to thank all my close friends in my home country and all my research colleagues at the University of Leeds for giving me a lot of inducement and support to finish my study.

Last but not least, special words of kinds and love feelings are dedicated to my parents, sisters, and brothers for their continuous encouragement, moral support, and patience during the years of my PhD journey.

Abstract

Injecting low salinity water in sandstone reservoirs is the most practical example of smart water technology. However, the feasibility of low salinity flooding for enhanced oil recovery is controversial for carbonates due to the poor understanding of the displacement mechanisms, which should be potentially responsible for low salinity effect.

This project presents a novel concept to study the complicated interactions in solid/brine/crude oil systems at multiple scales with more insight on the physicochemical mechanisms affecting the wettability trend and hence, the potential of low salinity flooding. Different microscopic and macroscopic apparatuses were used including atomic force microscopy (AFM), quartz crystal microbalance (QCM), microfluidic system, goniometer, and core flooding setup.

Studying the rock/brine/oil interactions at a macroscopic-scale shows that the salinity effect is more salient at the rock/liquid interface than the liquid/liquid interface, and the response to the brine composition is dominated by the chemical composition of crude oil with respect to its content of polar organic components, as well as the rock mineralogy. These results have been corroborated by a series of macroscopic core flooding experiments conducted at *in-situ* reservoir conditions. Molecular level QCM study also shows that increasing the content of negative polar components in crude oil leads to less desorption from calcite surface compared to the silica surface upon exposure to low saline solutions, verifying the macroscopic core flooding findings. Two times diluted seawater yielded the highest desorption efficiency as a result of a reduction in the adhesion forces, as detected by AFM study.

Investigating the potential of enhancing oil recovery by low salinity flooding at the pore-scale, however, did not show any positive effect on the microscopic sweeping efficiency for the oil-wet system compared to the water-wet system. No change in the *in-situ* wettability was observed

during a sequential low salinity injection in a hydrophobic microstructure, and the pore surfaces stay within a strongly oil-wet condition.

The work described in this thesis revealed that there is a critical brine concentration for EOR in carbonates that should be considered, after which no measurable effect is detected. Low salinity flooding is an inappropriate technique for enhanced oil recovery for the strongly oil-wet formations saturated with heavy-polar crude oils. In addition, while the expansion of the electric double layer at lower salt is likely to be responsible for reduced oil adhesion on carbonates, it is modulated by surface ions binding. Therefore, a combination of these two mechanisms, as well as the salting-out phenomenon has a dominating effect on low salinity flooding performance. The pore-flow of brine in the water-wet system is different from that of a completely oil-wet system, and thereby the potential and associated mechanisms of low salinity flooding are expected to be different.

Table of Contents

List of Tables

List of Figures

List of Abbreviations

AFM	Atomic Force Microscopy
AIM$_{SM}$	Advanced Ion Management by Exxon Mobil
AN	Acid Number
API	American Petroleum Institute
ASP	Alkali Surfactant Polymer
BJH	Barret Joyner and Halenda Pore Model
CA	Contact Angle
CBR	Crude Oil/Brine/Rock
Cos	Cosine
CSW	Control Low Salinity Water Flooding
DLVO	Derjaguin-Landau-Verwey-Overbeek
DWF	Designer Water Flood
EDL	Electrical Double Layer Expansion
E_{do}	Microscopic Displacement Efficiency
EDX	Energy Dispersive X-ray
EOR	Enhanced Oil Recovery
E_{OR}	Overall Oil Recovery Efficiency
Ea	Areal Displacement Efficiency
Ev	Vertical Displacement Efficiency
Ev_o	Macroscopic Sweep Efficiency
FW	Formation Water
HPHT	High Pressure-High Temperature
HS	High Salinity
IEP	Isoelectric Point
IFR	Infrared
IFT	Interfacial Tension
IOR	Improved Oil Recovery
LoSal	Low Salinity
LS	Low Salinity
LSF	Low Salinity Flooding
NMR	Nuclear Magnetic Resonance
N_C	Capillary Number

nN	nano-Newtons
ODE	Oil Desorption Efficiency
OOIP	Original Oil in Place
pN	pico-Newtons
PV	Pore Volume
PZC	Point of Zero Charges
QCM	Quartz Crystal Microbalance
SARA	Saturates Aromatic Resin Asphaltenes
SEM	Scanning Electron Microscopy
SP	Surfactant Polymer
SW	Seawater
SWCTT	Single Well Chemical Tracer Test
SWF	Smart Water Flooding
TAN	Total Acid Number
W_A	Work of Adhesion
XRD	X-ray Diffraction
2dSW	2 Times-Diluted Seawater
5dSW	5 Times-Diluted Seawater
10dSW	10 Times-Diluted Seawater
20dSW	20 Times-Diluted Seawater
50dSW	50 Times-Diluted Seawater

List of Symbols

C	Constant of quartz crystal
cP	Centipoise
d	Cantilever deflection
de	Equatorial diameter
F	Force applied to the cantilever
f	Fundamental frequency of the crystal
g	Gravitational acceleration
H	Drop-shape dependent parameter
K	Permeability
k_c	Cantilever spring constant
M	Mobility ratio
N	Ultimate oil recovery
n	Harmonic number
R_A	Mean roughness
S_{oi}	Initial oil saturation
S_{or}	Residual oil saturation
S_{wi}	Initial water saturation
S_{wir}	Irreducible water saturation
v	Velocity of displacing fluid
ρ_q	Specific density of quartz
υ_q	Shear wave velocity in quartz
$\Delta\rho$	Difference between densities
Γ_{QCM}	Adsorbed mass
Δf	Frequency changes
Δm	Desorbed mass
μ_o	Viscosity of oil

μ_w	Viscosity of water
σ_A	Adhesion tension
σ_{os}	Oil/Solid interfacial tension
σ_{ow}	Oil/ Water interfacial tension
σ_{ws}	Water/Solid interfacial tension
η	Viscosity of solution
θ	Contact angle
μ	Viscosity of displacing fluid
ρ	Density of solution
σ	Interfacial tension

Chapter 1

Introduction

1.1 Motivation

A considerable amount (45-90%) of light and heavy oils is retained in hydrocarbon reservoirs after using primary and secondary recovery processes, as illustrated in Figure 1.1. The growing demand for energy resources has led to the development and application of various tertiary or enhanced oil recovery (EOR) techniques to improve oil recovery from carbonate and sandstone reservoirs. EOR refers specifically to methods for extracting residual oils trapped in reservoirs once conventional primary and secondary extraction have been exhausted. The main EOR techniques that have been developed at different times are thermal recovery, miscible or immiscible gas injection, and chemical techniques. Increasing recovery factor from high-temperature carbonate reservoirs is the primary target of using most of these methods. This significantly affects global reserves, since a large quantity of about 60% of the world's oil reserves exists in carbonate reservoirs [1]. Figure 1.2 shows the most widely applied enhanced oil recovery techniques for extracting trapped oil from carbonate reservoirs.

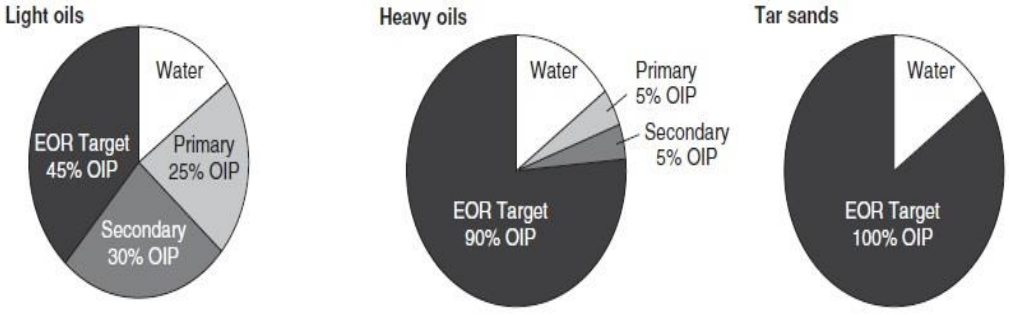

Figure 1.1: Percentage of oil recovered at the end of conventional operations and EOR target for different hydrocarbons [2].

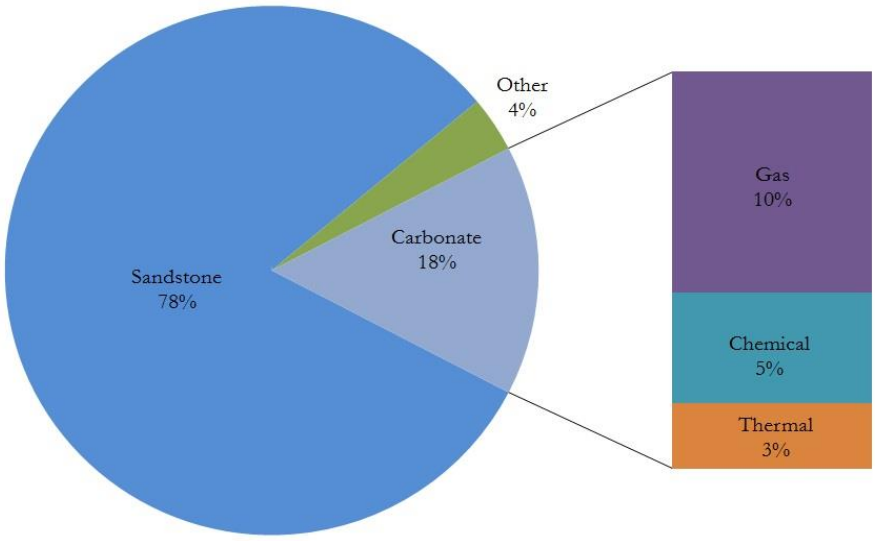

Figure 1.2: EOR technologies in carbonate formations depending on the universal database [3,4].

It is clear from Figure 1.2 that gas injection represents the most applicable EOR method in carbonates; however, gas availability and high operational costs preclude its application [2,3]. The second method used for EOR in carbonate reservoirs is chemical techniques. While most of the chemical processes are applicable at only small laboratory scale such as surfactant-polymer (SP) and alkali-surfactant-polymer (ASP), polymer flooding is technically successful for EOR at the field scale [3]. However, polymer flooding is not suitable for implementation in formations with low permeability (<5 md), which thereby makes its application much more suitable to sandstone reservoirs than carbonate formations. Furthermore, the practical feasibility of thermal techniques for EOR in carbonate reservoirs is not high; making their implementation in carbonates unpopular.

Despite the fact that the above EOR methods have been used to extract oil from some of the carbonate reservoirs around the world, the ultimate oil recovery from these reservoirs is generally less than that of sandstone reservoirs [5]. Comparing the screening criteria for each type of the EOR

processes indicates that the application of these processes is still strongly affected by the restrictions of reservoir characteristics, as many of the carbonate reservoirs are naturally fractured and preferentially oil-wet with low matrix permeability [6]. Also applying conventional EOR techniques are relatively expensive compared with secondary recovery methods. Consequently, the fluctuation in the oil prices would aggravate the risks, making most of these techniques economically unfavourable [7]. Therefore, using a new enhanced oil recovery technique will be essential to reaching the maximum and economic production rate from carbonate reservoirs.

Improving enhanced oil recovery (EOR) techniques would bring a large positive economic impact. Recently, many considerable efforts have been devoted to finding an innovative method that can alter the initial wetting properties of the surfaces from oil-wet to intermediate or water-wet. Smart water has been suggested as an emerging EOR technique for this purpose.

Smart water technology commonly refers to a method of injecting water with an optimized ionic and salinity composition that can change the initial equilibrium of the crude oil/brine/rock (CBR) system in a good way to improve oil recovery. The most general practical example of applying smart water technology is low salinity water flooding in sandstones and high salinity water flooding in carbonates. Different names have been given in the literature to identify smart water injection, such as Designer Water Flood (DWF) by Shell [8], LoSal^{TM} by BP [9], Smart Water Flooding (SWF) by Saudi Aramco [10], and Advanced Ion Management (AIM$_{SM}$) by Exxon Mobil [11]. Availability of water at a low price, an easy injection process during the early life cycle of the reservoirs, and attaining higher ultimate oil recovery with minimal investment, have all been cited as variables contributing to making smart water technology as an encouraging process compared to other conventional EOR methods [1].

A broad range of studies has been recently conducted to study the effect of low salinity water flooding in sandstone reservoirs and identify the

potential recovery mechanisms. Laboratory observations showed that injecting brines with salinities below a certain level (4000-5000 ppm) can improve oil recovery from sandstone reservoirs. These laboratory core flooding tests have been confirmed to a limited extent at the field scale as well [12-15]. However, the feasibility of low salinity flooding in carbonates is still questionable. It has been reported that low salinity water flooding cannot be used in carbonate reservoirs and its effect has only been detected for sandstones with high clay minerals [16,17].

In a major advance in 2011, a new understanding of low salinity water flooding has been demonstrated after several laboratory experiments conducted by a Saudi Aramco research group, who verified that there is an increment in oil recovery of approximately 17-20% of the OOIP by reducing the salinity and ionic composition of the injected seawater [10]. Later, a single well chemical tracer test (SWCTT) was performed by the same group to confirm the potential of low salinity water flooding at a large pilot scale. The results showed a reduction of about 7 units in the residual oil saturation compared to the injection of normal seawater.

Though few studies have been achieved as an attempt to evaluate the potential recovery into carbonate reservoirs by using chemically modified water, up to date, there has been no conclusive evidence on the potential of low salinity water flooding for EOR in carbonates. Therefore, its application in the field scale is still doubtful. The main reason behind that is the composite chemical interactions between rock/brine and crude oil, which lead to a poor understanding of the chemical mechanisms responsible for oil recovery improvement [17-19].

After extensive experimental work by some researchers, it is supposed that wettability alteration from oil-wet to intermediate-wet is the most probable mechanism that affects significantly the EOR during low salinity water flooding in carbonates [20-22]. However, consistent mechanistic clarification behind this alteration is not fully understood due to the lack of *in-situ* wettability assessment at the pore-scale, calling for more efficient

methods for evaluating wettability changes and low salinity potential at the level of pore surface heterogeneities.

1.2 Challenges and Objectives

It is found that most of the previously published studies to date have tended to focus on macroscopic measurements to assess the low salinity effects. However, one major drawback of these measurements is that they cannot provide precise elucidations and micro-level details of the physicochemical interactions taken place between rock/brine/oil interfaces during low salinity injection. This raises many questions about the interactions between polar oil components and mineral surfaces at the pore scale, which lead to a difficulty in predicting or interpreting the effect of low salinity flooding on reservoir performance. To meet these challenges, a multi-scale understanding of low salinity effects based on Quartz Crystal Microbalance (QCM), Atomic Force Microscopy (AFM), microfluidic measurements, macroscopic core flooding, and contact angle measurements have been explored and examined in this project. The main objectives of this study are briefly summarised as:

1. To understand the solid/brine/oil interactions at multiple scales to elucidate the probable mechanisms of wettability modification during low salinity flooding in carbonates.
2. To demonstrate any symbiotic impact of rock mineralogy and oil composition on the potential of low salinity flooding.
3. To evaluate the influence of low salinity injection on the macroscopic oil displacement efficiency under reservoir-like conditions (HPHT).
4. To investigate whether low salinity flooding can affect the trapped oil at the pore-scale level, i.e., pore sweeping efficiency.

1.3 Thesis Outline

This dissertation is organised as follows:

Chapter 1 includes a brief overview and motivation for the project, the overall challenges and objectives, as well as the structure of the thesis. A graphical overview of the work presented in this thesis is given in Figure 1.3.

Chapter 2 presents an extensive overview of the related literature on the feasibility of saline solutions in carbonate and sandstone reservoirs and suggested mechanisms of wettability modification. The literature on using different quantitative and qualitative approaches such as QCM, microfluidics, and AFM is also demonstrated.

Chapter 3 provides a detail description of the instruments, materials, procedures and experimental methods used in this dissertation.

Chapter 4 discusses the results of quantifying wettability characteristics and its associated mechanisms at the macroscopic scale based on the brines, oils, and carbonate rocks used. Throughout this Chapter, the impact of ionic strength and brine salinity on the electrostatic surface charges and the interfacial properties are thoroughly assessed. The probable adsorption of potential determining ions into the surfaces is also investigated. The key parameters that govern the complex interactions of rock/brine/crude oil at the macroscopic scale are discussed.

Chapter 5 presents the results from the Atomic Force Microscopy (AFM) study. In this Chapter, the molecular interaction of polar components in crude oil with the carbonate minerals at different salinities is extensively investigated by measuring the adhesion forces at the micro-scale level.

Chapter 6 describes and discusses the effect of polar components on the oil adsorption based on the Quartz Crystal Microbalance (QCM) findings. The impact of saline solutions on the desorption of crude oils from calcite and silica surfaces is also discussed.

Chapter 7 provides a description of the macroscopic core flooding results. Throughout this Chapter, the symbiotic effect of crude oil composition and rock mineralogy on the potential of low salinity flooding for EOR under *in-situ* (HPHT) reservoir conditions is extensively investigated.

Chapter 8 discusses the obtained findings from the drainage and imbibition displacements by using a microfluidic system. In this Chapter, the pore-scale sweeping efficiency and flow behaviour of different saline solutions in hydrophilic and hydrophobic microstructures are systematically studied.

Chapter 9 exhibits the overall conclusions of this research, subsequent discussions, and future work recommendations.

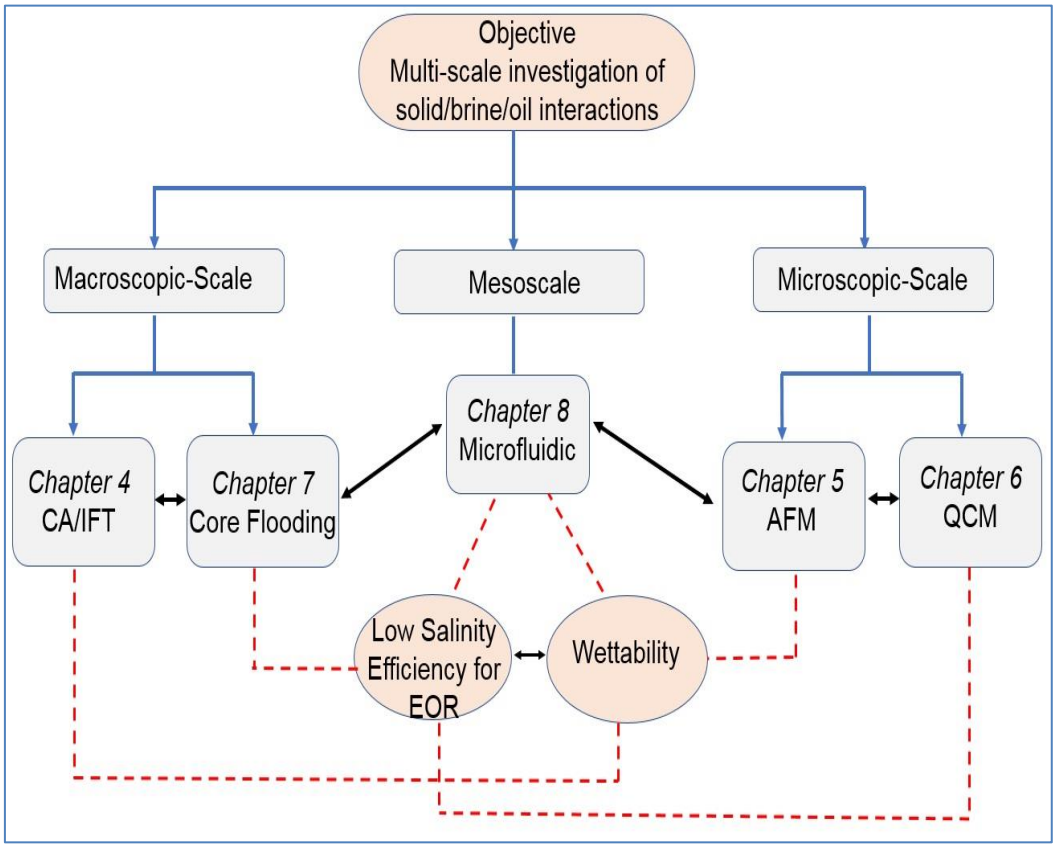

Figure 1.3: Schematic diagram of thesis layout.

Chapter 2

Literature Review

2.1 Overview

More than 60% of the world's oil reserves exist in carbonate reservoirs. However, enhanced oil recovery from these reservoirs has been demonstrated as a great challenge because many of the carbonate formations are naturally fractured and preferentially oil-wet with very low permeability. Previously, many technologies have been performed for enhanced oil recovery from carbonates by improving reservoir characterization through adding polymers, surfactants, and alkaline to the injected water. While some of these methods are applicable and successful, simple economics precludes their application, leading to thinking of finding another economic method. Over the last decade, the pioneering study by the research group at the University of Stavanger [23] has pointed out that adjusting the ionic composition of the injected seawater can positively influence the ultimate oil recovery for carbonate reservoirs as will be extensively clarified in this chapter.

This chapter provides an extensive overview of the theoretical background and related literature on the feasibility of saline solutions in sandstone and carbonate reservoirs which is organized as follows: section 2.2 and 2.3 give a brief clarification of the overall oil recovery efficiency and the wetting state of carbonate reservoirs. This will be followed by a review of the previous studies focusing on using high salinity (seawater) flooding in carbonate reservoirs, section 2.4. The potential of low salinity water flooding in carbonate reservoirs will be discussed in section 2.5. Then, the effect of low salinity and ionic composition on the interfacial properties represented by the contact angle and interfacial tension will be illustrated in section 2.6. This will be followed by clarifying the proposed mechanisms of wettability modification during low salinity flooding, section 2.7. In sections 2.8 and 2.9, a review of the previous literature about using

atomic force microscopy (AFM) and quartz crystal microbalance (QCM) apparatus respectively will be demonstrated. Section 2.10 will include a discussion of the research conducted on fluid displacement at the pore-scale level using a visualized microfluidic technique. Finally, we finish with a summary in section 2.11.

2.2 Theoretical Background

As mentioned in Chapter 1, enhanced oil recovery refers to the techniques used to extract residual oils trapped in reservoirs once conventional primary and secondary extraction have been exhausted. Increasing the overall oil recovery efficiency (E_{OR}) is the main target of implementing most of the EOR methods. The E_{OR} generally refers to the ratio of the ultimate oil (N) recovered by one of the recovery methods to the original amount of oil present in the pore space (OOIP), as given below [24]:

$$E_{OR} = \frac{N}{OOIP} \tag{2.1}$$

It is important here to clarify that the overall oil recovery efficiency (E_{OR}) includes both macroscopic (volumetric) displacement efficiency (E_{vo}) and microscopic sweeping efficiency (E_{do}), as illustrated in Figure 2.1. The macroscopic displacement efficiency is defined as the efficiency of the invading fluid to displace the bearing zone of oil either areally or vertically into the production wells, while the microscopic displacement efficiency refers to the measurable efficiency of the displacing fluid to release the oil trapped by capillary forces at the micro-scale level [24,25].

$$E_{OR} = E_{do}\, E_{vo} = E_{do}\, E_a\, E_v \tag{2.2}$$

where E_a is the areal displacement efficiency, and E_v is the vertical displacement efficiency.

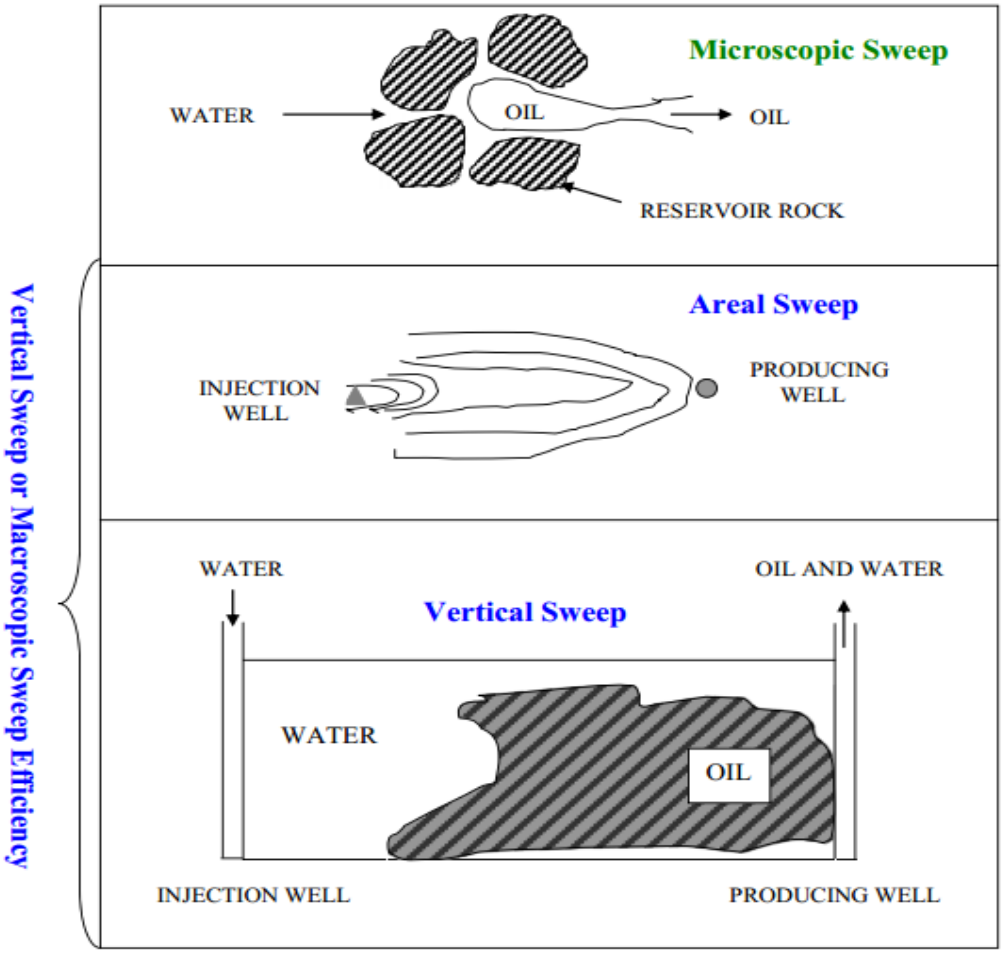

Figure 2.1: Schematic diagram of macroscopic and microscopic displacement efficiencies [24,26].

Many factors affect the macroscopic displacement efficiency. These include heterogeneity and thickness of the reservoir, mobility ratio, flow rate, density and viscosity contrast between the invading and displaced fluid, and fracture in the invaded zones [24]. On the other hand, it is found that the microscopic sweeping efficiency is mainly governed by the interfacial tension and fluid viscosity, as well as the reservoir characterization such as wettability, pore geometry, and relative permeability [24]. For utmost recovery efficiency, either an improvement in the mobility ratio (i.e., increasing the viscosity of the invading fluid) or an increase in the capillary number (N_C) (i.e., decreasing the IFT and/or

contact angle) should be achieved, which represent the main goal of known recovery techniques.

The capillary number can be defined as the ratio of viscous to capillary forces, as given in equation 2.3 [27].

$$N_C = \frac{v\mu}{\sigma cos\theta} \quad (2.3)$$

where v and μ represent the velocity (m/s) and viscosity (Pa.s) of the displacing fluid, respectively, θ is the contact angle between the fluid/fluid interface and the solid surface. σ is the interfacial tension between aqueous phases (N/m). An equilibrium between the capillary forces and viscous forces occurs as the capillary number falls within the range of 10^{-4} to10^{-5} [28].

It is known that the stability of the displacement front strongly depends on the capillary forces and viscous forces. Accordingly, the flow pattern takes one of these regimes: capillary fingering, viscous fingering, and stable displacement, as shown in Figure 2.2 [29,30]. An unstable displacement front will be observed when the contrast between the viscosity of the injecting and displaced fluid is very high, i.e., when the mobility ratio M >1. Consequently, viscous fingering will be developed, which leads to a decrease in the ultimate oil recovery [31].

It is also found that when the flow falls within the capillary regime, the fluid can move randomly and transport reversely towards the new pores, leading to trapping of the wetting fluid inside these pores [31]. For this, a reduction in the interfacial tension of the oil/water system to ultra-low values (< 0.001 N/m) and/or contact angle are needed to reduce the capillary effect and extract the trapped oil in the pore space, and hence achieve higher microscopic sweeping efficiency.

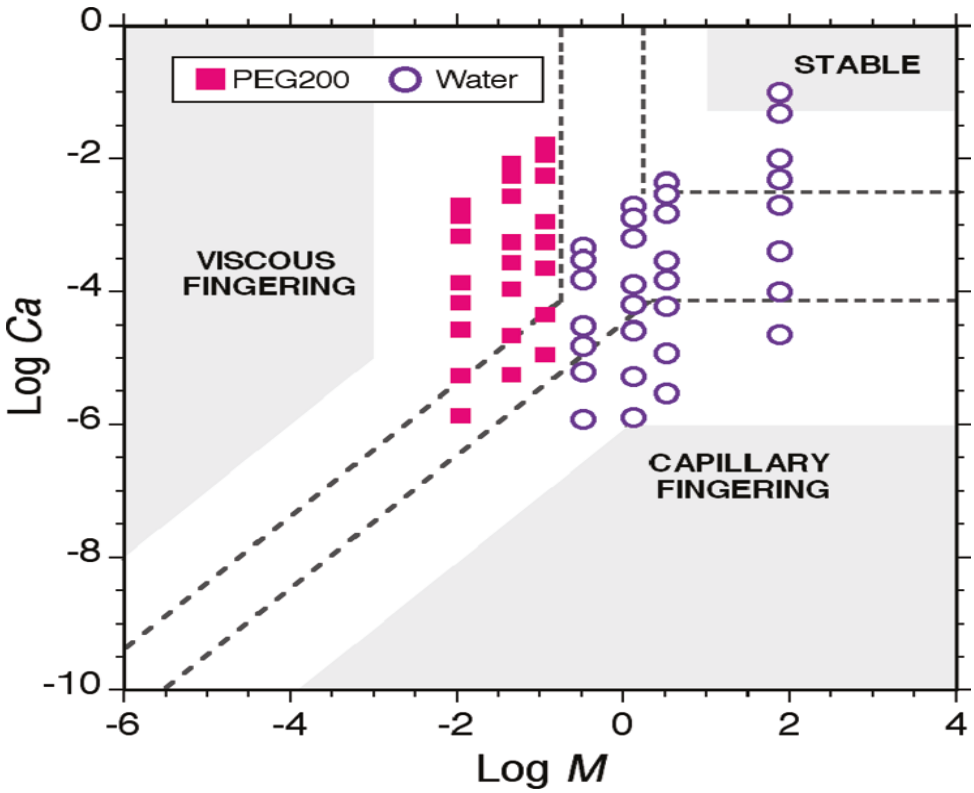

Figure 2.2: Flow regimes based on the displacements of polyethylene glycol 200 (PEG200) and water [30].

2.3 Wettability of Carbonate Reservoirs

As mentioned in the previous section, wettability can play a crucial role in the efficiency of the oil displacement process. This is related to the fact that it has a great effect on the distribution and movement of water and oil through the porous media, and therefore it is used to assess the performance of recovery processes such as water flooding. Anderson and William [6] have specified the best definition for wettability as "the tendency of one fluid to spread on a solid surface in the presence of other immiscible fluids." As a result, depending on the intermolecular interactions between fluid, rock and crude oil at reservoir conditions, the rock surfaces can be classified as (1) water-wet, $\theta = 0^{o}$-75^{o}, (2) intermediate-wet, $\theta = 75^{o}$-115^{o}, or (3) oil-wet, $\theta = 115^{o}$-180^{o} [6]. The contact angle with interfacial tension at the oil/fluid interfaces can be used to describe the adhesion properties, represented by dispersive adhesion tension (σ_A). The relation is given by the Young-Dupre equation (2.4) [6].

$$\sigma_A = \sigma_{os} - \sigma_{ws} = \sigma_{ow} \cos \theta \quad (2.4)$$

where:

σ_{os}: The interfacial tension between oil and solid surface, dynes/cm.

σ_{ws}: The interfacial tension between water and solid surface, dynes/cm.

σ_{ow}: The interfacial tension between oil and water, dynes/cm.

θ : Contact angle between the fluid/fluid interface and the solid surface.

Generally, higher adhesion tension per unit area corresponds to a high degree of wetting. In contrast, the system is poor wetting at weak adhesion tension [32].

A majority (80%) of the carbonate reservoirs are oil-wet or mixed-wet with a positively charged surface, while most of the sandstone rocks are preferential water-wet [22,33]. It is noteworthy that most of the carbonate surfaces are initially strongly water-wet, due to the assumption that the reservoir was originally occupied by water before the migration of the hydrocarbon, then rock surfaces turn into more oil-wet after aging with crude oil present in the reservoir [34]. Naturally, after the migration of oil to carbonate reservoirs, an unstable water film between rock and oil will be formed due to the positively charged rock/water interface and negatively charged oil/water interface. Consequently, the presence of polar organic compounds in crude oil will help to diffuse the thin water film; then oil is attracted to the rock surfaces rendering it to oil-wet [35,36]. As a result, the displacement process of the oleic phase from the pore throats will be more difficult due to the strong capillary forces. Therefore, improving the wetting state of carbonate reservoirs to more water-wet conditions for maximum oil recovery has been the major focus of many researchers [10, 20, 37-39].

The recent work by Al-Attar et al. [40], however, revealed that the most efficient oil displacement by water flooding was observed by changing the wettability of carbonates to intermediate-wetness. It has also been reported that adsorption or desorption of polar organic compounds in

crude oil, brine salinity, rock mineralogy, and temperature are strongly contributed to affecting the initial wetting conditions of carbonate rocks over geological time [36]. Thus, determining the wetting state of the carbonate surfaces will be helpful to evaluate the effectiveness of oil recovery processes and understanding the associated production mechanisms as will be seen later in this thesis.

2.4 Smart Water in Carbonate Reservoirs

Injection smart water or specifically modified seawater is comparatively new. Austad and co-workers [23] have first reported that injection seawater in the Ekofish chalk reservoir showed an improvement in oil recovery. Later extensive laboratory studies at various conditions have been conducted to evaluate the feasibility and understand the mechanisms of smart water flooding in carbonate reservoirs [41-44]. In this section, we consider a comprehensive review of the most relevant publications about the effect of active and non-active ions on spontaneous and forced displacements. The impact of temperature on EOR in carbonate reservoirs and suggested recovery mechanisms of high salinity seawater will also be demonstrated.

2.4.1 The Influence of Active and Non-Active Ions in Seawater

Seawater is enriched with divalent ions such as SO_4^{2-}, Ca^{2+}, and Mg^{2+}. Previous studies indicated that among these ions, SO_4^{2-} has an extreme affinity toward the carbonate surfaces and plays a vital role in shifting the surface charges of the carbonates to negative [37,45,46]. For instance, research by Strand et al. [45] gives insights into the impact of brine salinity and ionic components on oil recovery revealed that adding sulphate to the imbibed fluid could improve spontaneous displacement from chalk reservoirs, and an increase in the sulphate concentration caused more

increase in the oil recovery (Figure 2.3). They also stated that the effect of sulphate concentration on the dolomite rock was less pronounced in comparison with chalk. Another investigation by Webb et al. [46] pinpointed that a significant increase in oil recovery was obtained by imbibing seawater containing SO_4^{2-} into carbonate cores as compared to the formation water (SO_4^{2-} free brine).

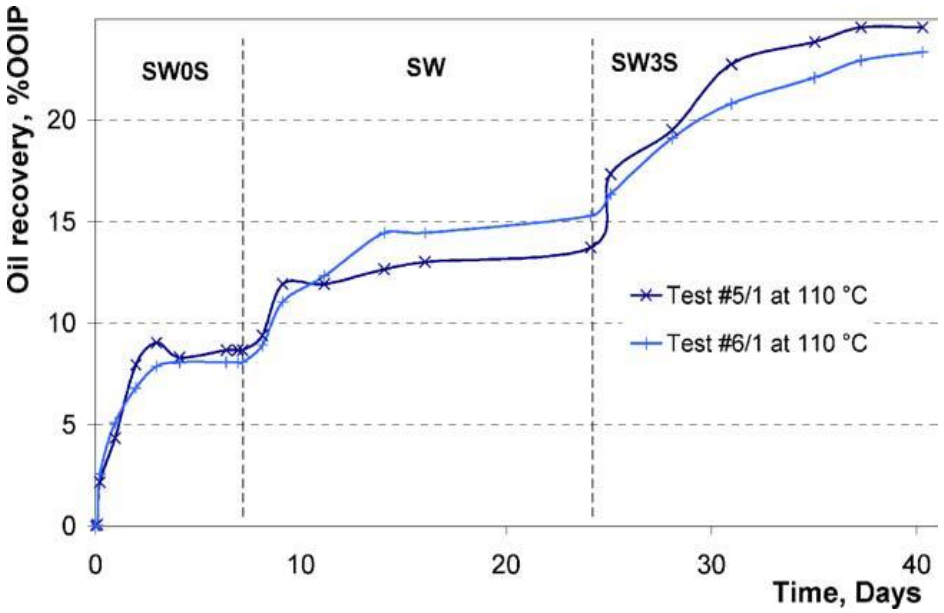

Figure 2.3: Spontaneous imbibition of a sequence of SW without sulfate (SW0S), SW, and SW with three times sulfate (SW3S) into preferential oil-wet chalk cores at 110 ◦C [45].

Another important aspect to be considered to improve oil recovery is that SO_4^{2-} has to interact simultaneously with either Ca^{2+} and/ or Mg^{2+} ions, so using Ca^{2+} or Mg^{2+} alone did show a strong impact on improving oil recovery [42]. The first work on the synergetic ionic effect was by Strand et al. [37]. They studied the symbiotic effect between SO_4^{2-} and Ca^{2+} ions at different ranges of temperature. Their results demonstrated that as the concentration of Ca^{2+} and temperature increased the adsorption of the SO_4^{2-} onto chalk surface increased. The impact of sulphate ions alone and with the presence of cationic surfactant on the wetting properties of the oil-wet calcite surface was also discussed by Karimi et al. [47]. They claimed that the improvement in wettability of calcite surface could be

attributed to the interactions between sulphate ions and calcium ions attached to the carboxylate groups on the surface.

The combined effect of Mg^{2+} and SO_4^{2-} ions on oil recovery in carbonate reservoirs has also been experimentally investigated. The concentration of Mg^{2+} in seawater is higher than the concentrations of SO_4^{2-} and Ca^{2+} by factors of two and four, respectively. Zhang et al. [41] argued that under spontaneous imbibition, Mg^{2+} without SO_4^{2-} showed insignificant improvement in oil recovery, however, a combination of Mg^{2+} and SO_4^{2-} caused a considerable increase in oil production, as shown in Figure 2.4. Similarly, Karoussi et al. [48] found that saturated and imbibed chalk samples by fluids containing just Mg^{2+} yielded the lowest recovery factor at high temperature.

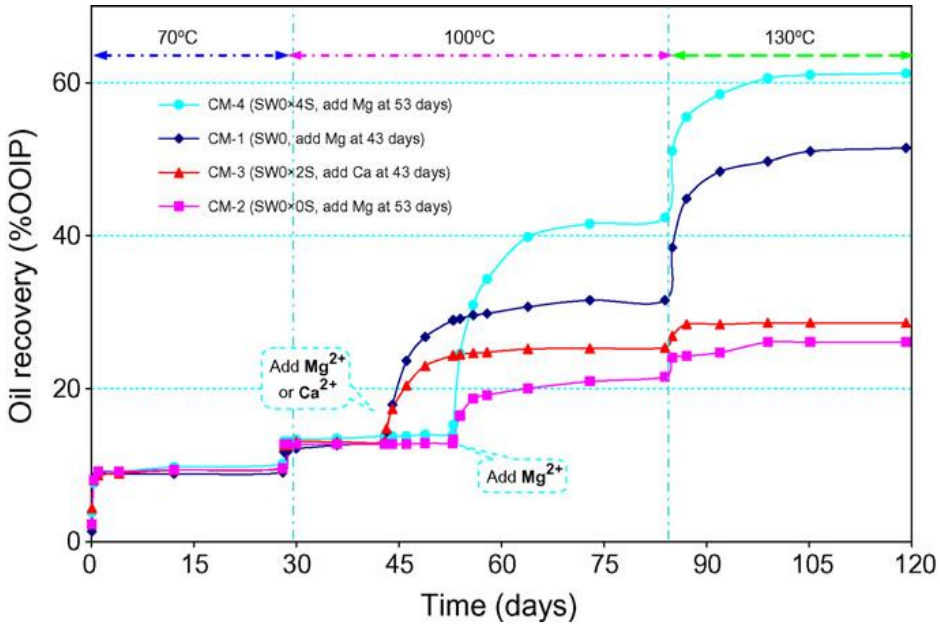

Figure 2.4: Spontaneous imbibition tests at 70, 100 and 130 °C of modified seawater [41].

On the other hand, it has been emphasized that the amount of non-active ions in seawater represented by NaCl can also contribute to EOR, i.e., not only the concentrations of the potential determining ions (SO_4^{2-}, Ca^{2+}, and Mg^{2+}). Fathi et al. [39] performed spontaneous and forced

displacement experiments on the Stvens Klint chalk cores at different temperatures to investigate the link between the ionic composition and the concentration of non-active salt. An increase in the oil recovery of about 10% of OOIP was observed with the modified seawater (depleted in NaCl) in comparison with ordinary seawater at high temperatures. They also claimed that four times increment in the concentration of NaCl in seawater caused a reduction in the ultimate oil recovery of about 5% of OOIP. The spontaneous imbibition results are illustrated in Figure 2.5.

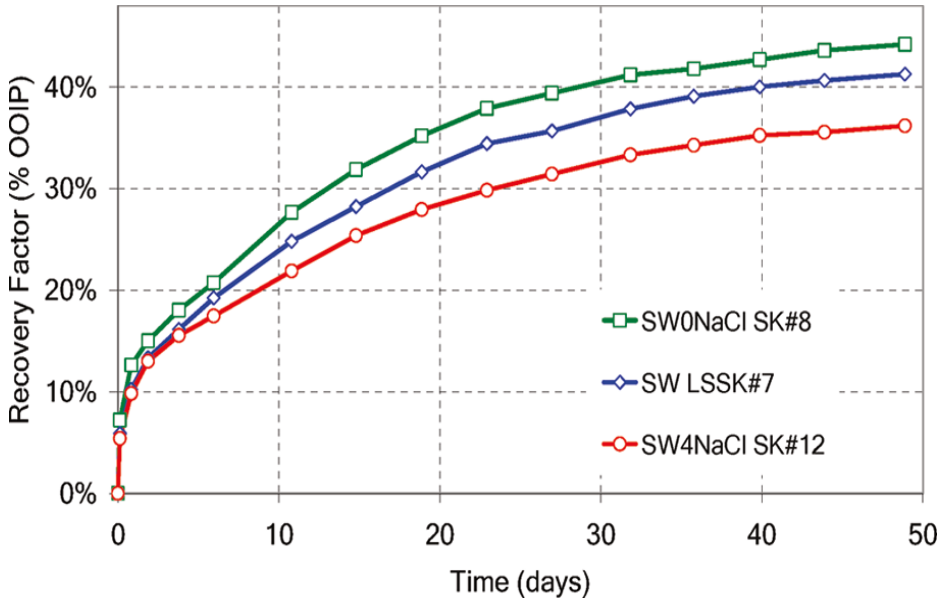

Figure 2.5: Spontaneous imbibition into oil-saturated chalk cores using SW, SW0NaCl, and SW4NaCl at 100 °C [39].

In another article, Fathi et al. [18] examined the effect of SO_4^{2-} and Ca^{2+} in modified seawater (depleted in NaCl). They concluded that both non-active salt (NaCl) and active ions (SO_4^{2-}) in seawater have an enormous impact on oil recovery. Increasing the concentration of SO_4^{2-} ions four times in the seawater that depleted in NaCl at high temperature (70-120 ºC) led to an increase in oil recovery by about 5-18%. No significant improvement in oil recovery was observed by increasing the amount of Ca^{2+} ions in the modified seawater at 100 ºC, as shown in Figure 2.6.

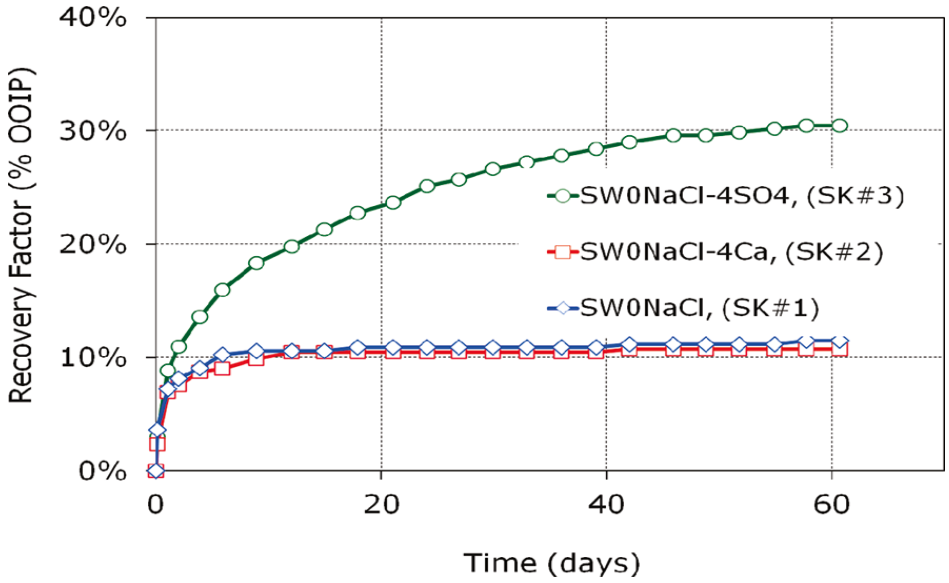

Figure 2.6: An example of spontaneous imbibition into chalk samples at 100 ^{o}C using different imbibing fluids with different salinities and ionic compositions [18].

2.4.2 The Influence of Temperature

Temperature is another critical parameter that affects EOR during smart water injection. It has been verified by the previous publications that an increase in the temperature to more than 90 °C was required to obtain a significant improvement in oil recovery by spontaneous imbibition of seawater [43,49]. Hence, the symbiotic interactions and the affinity of active ions (SO_4^{2-}, Ca^{2+}, and Mg^{2+}) toward the carbonate surface increased as the temperature increased, leading to shifting in wettability to a more water wetness. The first systematic study on the influence of temperature on the reaction of the active ions was reported by Hognesen et al. [33]. They conducted spontaneous imbibition tests using outcrop chalk and reservoir limestone cores over a range of temperatures (70-130 °C). They observed an increase in oil recovery from 22-45% as the temperature increased from 90-130 °C by imbibing modified seawater (seawater with 3 times the initial SO_4^{2-} concentration). Hognesen et al. suggested that the increment in oil recovery was due to the high affinity of sulphate to the rock surfaces as the temperature increased.

Strands' et al. [43] comparative study also showed that a significant impact of high salinity seawater on oil recovery was noticed at 110 and 120°C. In another study, Puntervold et al. [44] reported that seawater seems to be much more effective at high temperature (> 100°C) and no remarkable increase in oil recovery was observed at 50 and 70 °C for seawater and produced water.

Based on the previously discussed results, there seems to be some evidence to indicate that the potential determining ions (SO_4^{2-}, Ca^{2+}, and Mg^{2+}) and high temperature are the key parameters for EOR into oil-wet carbonate rock by using seawater. The main observation is that seawater could work as a wettability modifier toward a more water-wet surface during spontaneous imbibitions and forced displacement as will be discussed later in this chapter [33,37,38,41,50].

2.4.3 Proposed Chemical Recovery Mechanism of Seawater

As we alluded to before, seawater has been supposed to act as a wettability modifier by many researchers, and therefore several studies have been carried out to characterize the mechanism behind wettability alteration. In this section, the suggested chemical recovery mechanism by seawater is summarized.

The chemical mechanism for wettability alteration during seawater injection involves mutual interactions between SO_4^{2-} and Ca^{2+} at the rock surface, Figure 2.7 [17,41]. It has been hypothesized that injecting seawater into a positively charged carbonate rock would promote the adsorption of sulphate ions to the rock surface, resulting in an improvement in the electrostatic repulsion forces between negatively charged polar oil components and carbonate surface.

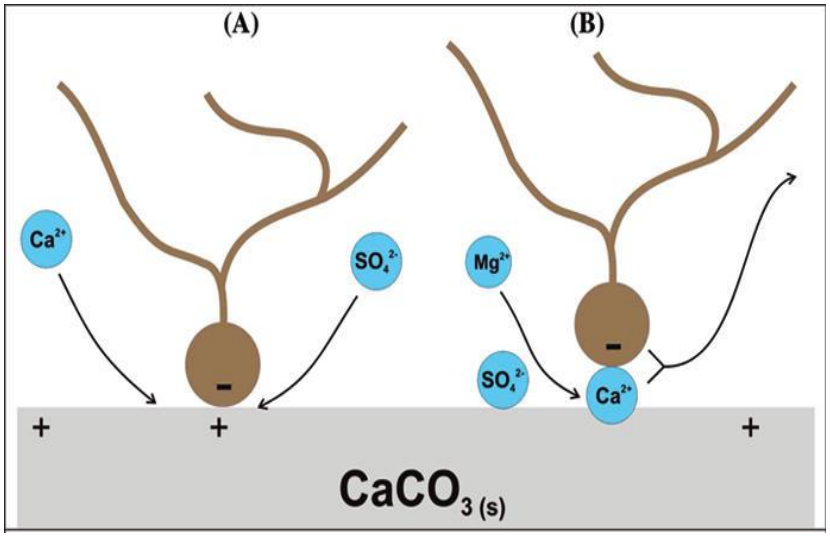

Figure 2.7: Chemical mechanism for wettability alteration caused by seawater. A: Wettability alteration when SO_4^{2-} and Ca^{2+} are active ions in seawater. B: Wettability alteration when SO_4^{2-} and Mg^{2+} are active ions in seawater [41].

This leads to extracting some of the adsorbed oil components from the surface, rendering it to more water-wetness. Simultaneously, calcium ions could also attach to the rock, bonding with the calcium carboxylate group and removing them from the rock surface [37,41]. The chemical reactions are illustrated by the following equation:

$$RCOO^-\text{--}Ca\text{--}CaCO_3\,(s) + Ca^{2+} + SO_4^{2-} = RCOO\text{--}Ca^+ + Ca\text{--}CaCO_3\,(s) + SO_4^{2-} \quad (2.5)$$

It is also suggested that the reactivity of Mg^{2+} ions increased in water at high temperature (90-100) °C, and they can even subrogate Ca^{2+} ions on the surface, which are linked to carboxylic polar components, causing displacement of the calcium-carboxylate bonds and thus more oil desorption [41].

$$Ca\text{--}CaCO_3(s) + Mg^{2+} = Mg\text{--}CaCO_3(s) + Ca^{2+} \quad (2.6)$$

2.5 The Performance of Low Salinity Flooding for EOR in Carbonate Reservoirs

Over the last two decades, low salinity water flooding has been confirmed as an innovative method for improved oil recovery in sandstone reservoirs. The efficiency of low salinity in sandstone has been approved by various lab core flooding tests, as well as by limited fields scale tests. A large number of published studies showed that lowering the salinity of water below 5000 ppm revealed positive results for sandstone reservoirs [13-16, 51-54]. An improvement in the ultimate oil recovery of about 15-20 % was stated. However, some of these studies have shown that low salinity water flooding is not sufficient for carbonate reservoirs and its effect has only been detected for sandstones with high clay minerals. For instance, Lager et al. [16] claimed it is difficult to detach oil polar organic components that bond strongly to the positively charged carbonate surfaces by low salinity water flooding. In their conclusions, the only way to remove the organic components is by increasing the salinity of the injected water, which could promote the reactivity of the carbonate surfaces and modify the wettability to water-wetness.

Fathi et al. [39] added their experimental observations which are consistent with what was previously suggested by Lager et al. [16]. Fathi et al. found that injecting diluted seawater in tertiary mode after flooding with traditional seawater did not improve oil recovery. They stated that the reduction in the concentration of the multivalent ions as the seawater was diluted seems to be the main reason behind the failure of low salinity injection for EOR. Three years later, Fathi et al. [18] achieved another work to evaluate the efficiency of using low salinity in carbonate reservoirs. Corresponding with their previous work, they found that diluting seawater to the range of 1000-2000 ppm revealed a reduction in oil recovery due to the decline of active ions.

Recently, a new understanding of low salinity water flooding has been demonstrated. A strategic research program by Saudi Aramco, Advanced Research Centre, has been initiated to explore the impact of low salinity flooding on IOR in carbonates. In 2011, Yousef et al. [10] carried out the first representative core flooding experiments using composite rock samples from the carbonate reservoir at reservoir conditions. Contrary to the previous studies, this survey indicated that extra ultimate oil recovery of approximately 17-20% was reported by reducing the salinity and ionic composition of the injected fluid. No extra oil recovery was noticed with 100 times dilution of seawater. Subsequent research performed by Austad et al. [55] who also pointed out that additional oil recovery of 2-5% of OOIP was obtained by tertiary flooding into limestone cores by using 10 times diluted Gulf seawater and 100 times diluted formation water at 110°C. Austad et al. [55] suggested the cause of a small increment in oil recovery could be traced back to the presence of anhydrite $CaSO_4$ in the rock formation, as conducting similar tests using outcrop chalk samples free from anhydrite did not show any positive effect on oil recovery when exposed to diluted seawater and formation water.

Based on the encouraging recovery results by Yousef et al. [10], low salinity flooding has become an object of research interest recently, and several attempts have been made to address the effect of low salinity water flooding for EOR. Al-Harrasi et al. [56] performed spontaneous imbibition and core flooding tests at the ambient temperature of 25 ºC. They used carbonate rock samples and various proportions of diluted synthetic brine. Their results revealed that in both core flooding and spontaneous imbibition tests, an increase in oil recovery of 3-5% and 6-21% of OOIP was observed when the salinity of water was reduced. Aladasani et al. [57] used a simulation model to examine the potential of low salinity flooding in carbonate reservoirs by using the published data of Yousef et al. [10]. Based on the matched modelling data, they found that wettability alteration from oil-wet to intermediate-wet led to increasing the oil relative permeability, resulting in higher ultimate oil recovery. Also, the

presence of potential determining ions in brine could enhance the modification of wettability.

Al-Attar et al. [40] conducted numerous core flooding experiments on carbonate samples from the Bu Hasa field in Abu Dhabi. All the tests were performed at the ambient temperature of 25 ºC. In their study, Al-Attar et al. found that diluting Um-Eradhuma formation water to 5000 ppm caused extra oil recovery of 21% of the OOIP, while low oil recovery of 2% of the OOIP was observed by diluting seawater to the same level of salinity. In addition, it was found that there is a critical sulphate concentration of 46.8 ppm in the dilution formation water (5000 ppm), and a negative impact on oil recovery was obtained beyond this concentration.

Similarly, Hamouda and Maevskiy [58] examined the efficiency of the brines with different ionic strengths on oil recovery. They conducted secondary and tertiary water flooding experiments using outcrop chalk from Denmark with synthetic oil and various diluted versions of regular seawater. All core flooding experiments were performed at 70 ºC. The results showed that highest oil recovery was reported when using 10 times diluted seawater in secondary mode at flooding rate 4 PV/day, and this increment coincides with the highest calcium concentration and pH at the effluent. However, no additional oil recovery was noticed in tertiary mode by using seawater and 10 times diluted at the same flow condition, which is in line with the Fathi et al. [39] observations. Hamouda and Maevskiy also argued that the higher calcium concentration at the effluent might be contributed to the dissolution and calcium/magnesium ions exchange process, which might lead to altering the wettability of the chalk surface.

Finally, Austad and his colleagues [59] carried out core flooding tests on the limestone cores from the formation similar to that used by Yousef et al. [10]. The major focus of this research was to get a better understanding of the mechanism for low salinity effect to improve oil recovery. They conducted force displacement tests at 100 ºC using 100 times diluted sulphate-free formation water (d_{100}FW0S), 10 times diluted

Gulf seawater (d_{10}GSW) and 30 times diluted Gulf seawater (d_{30} GSW). In their work, an increase in oil recovery of 22% of the OOIP was noticed by injected diluted formation water in tertiary mode after first pumping ordinary formation water. Similarly, injection of 30 times diluted seawater in a tertiary flood after secondary flooding with formation water showed an improvement in oil recovery by about 18% of the OOIP. Also, a stepwise increase in oil recovery (25, 30, 33 %) of the OOIP was observed after flooding the sample sequentially with FW, GSW, and d_{10}GSW, as illustrated in Figure 2.8.

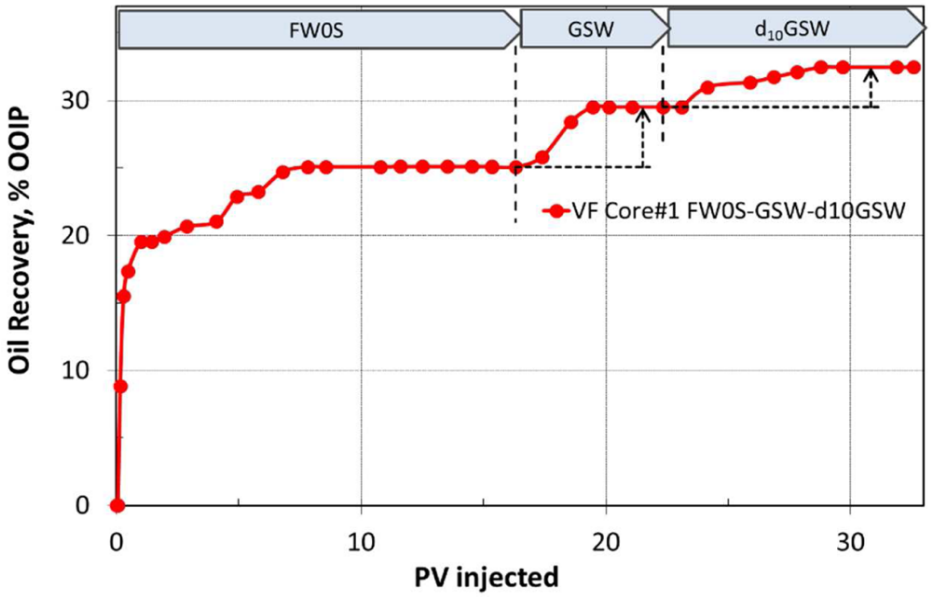

Figure 2.8: Oil recovery test at 100 °C [59].

In summary, it can be seen from the literature the observations of core flooding experiments concerning low salinity effect on EOR in carbonates are rather controversial, and the existing studies failed to identify whether the variation in the chemical composition of crude oil could affect the potential of low salinity. Therefore, systematic core flooding experiments under various kinds of crude oil and carbonate rocks need to be conducted to realize the multiple perceptions of low salinity effect.

2.6 Effect of Low Salinity and Ionic Composition on the Interfacial Properties in Carbonate Reservoirs

As it was stated in section 2.3, a majority of the carbonate reservoirs are preferentially oil-wet, and this could provide an explanation why the ultimate oil recovery for these reservoirs is less than that of sandstone formations. A number of researchers have stated that for a successful EOR process, an increase in the capillary work (N_C) is required by decreasing the IFT and/or contact angle as will be reviewed in the next sections.

2.6.1 Effect of Low Salinity Flooding (LSF) on Wetting State

Many researchers have sought to find a well-established EOR method that can alter the initial wetting state of carbonate rock from oil-wet to intermediate or water-wet conditions. Wettability alteration to favourable wet conditions due to modifying the ionic composition and salinity of the injected water has been confirmed by numerous recent studies [10,33,37,38,41,43]. Most of these studies have used a macro-scale contact angle measurement as the conventional means to characterize wettability alteration of carbonate reservoirs. However, measurement of this kind has some restrictions to provide *in-situ* molecular-level details of the physicochemical interactions that take place between interfaces as will be discussed in section 2.8 of this chapter.

In 2008, Gupta and Mohanty [60] studied the impact of active ions (SO_4^{2-}, Ca^{2+}, and Mg^{2+}) and temperature on wettability change through measuring the contact angle for the calcite/brine system using a model oil. They found that using divalent ions at high temperature (≥ 90 ºC) could alter the wettability of oil-wet carbonates to water-wetness. Their results also revealed that sulphate and calcium ions had a significant effect on the wettability alteration compared to magnesium ions. Sulphate ions along with the two other active ions (Ca^{2+} and Mg^{2+}) showed, however, a more significant effect on the wettability alteration. Calcium ions alone

were able to modify the wettability when its concentration increased five times from the base value, while magnesium ions alone did not yield any wettability modification.

Further extensive research was performed by Alotaibi et al. [61] to evaluate the wettability of carbonate rocks with more focus on the salinity of brines. In their study, the wettability of the dolomite and limestone rocks was qualitatively and quantitively assessed by using contact angle and Amott imbibition methods at high pressure and temperature. They used three different synthetic brines: formation brine (230,000ppm), seawater brine (54,000ppm), and aquifer brine (4000 ppm). Alotaibi et al. experimentally detected that the pressure had an insignificant effect on the wettability alteration while increasing the temperature to 90 ºC shifted the contact angle toward water-wet conditions. In their analysis of the contact angle measurements, Alotaibi et al. also found that seawater and formation water altered the wettability of dolomite surface to intermediate-wet at 90 ºC, whereas the rock's wettability changed to water-wet when aquifer water was used at the same test conditions. For limestone rocks, similar results were observed by using aquifer water, as the wetting state improved to water-wetness.

The first proof of oil recovery improvement due to wettability alteration during low salinity water flooding in carbonate reservoirs was stated by Yousef et al. [10]. They used contact angle measurement to evaluate the effect of low salinity water on the wettability alteration of carbonates. As indicated in Figure 2.9, seawater did not show any positive impact on the wetting state, while a definite change in the contact angle values was observed with twice and ten times diluted seawater. As with these two different slugs of seawater, the wettability of the rock altered toward a water-wet condition.

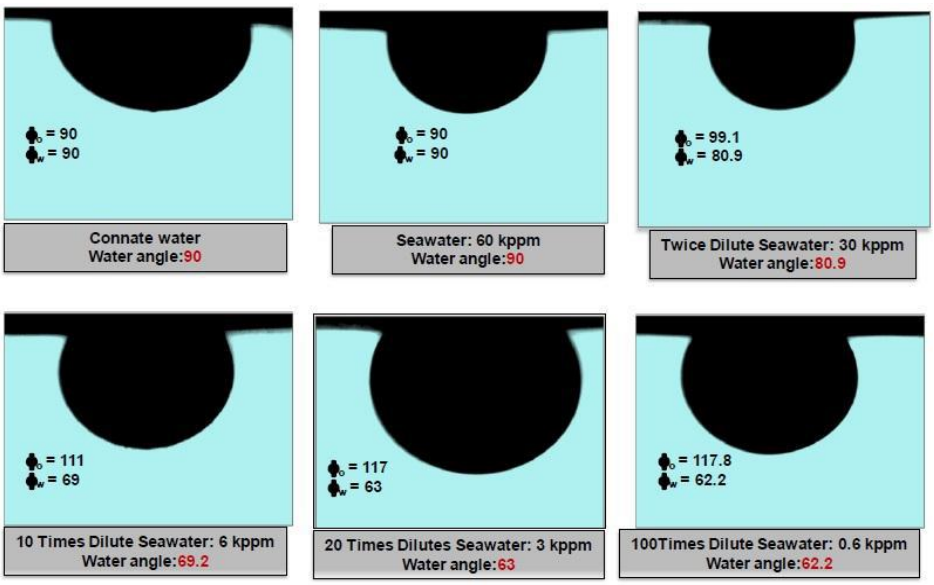

Figure 2.9: Images of contact angles measurements of carbonate rock samples with reservoir live oil and connate water, seawater, and dilution of seawater [10].

In 2013, Al-Attar et al. [40] published a paper in which they performed contact angle measurements using a sessile drop method to identify the reason behind oil recovery improvement when diluted formation water and diluted seawater used. The contact angle measurements indicate that reducing the salinity of the formation water with an optimum sulphate concentration altered the wettability of the system to an intermediate-wet, resulted in increased oil recovery. Conversely, no distinction in the contact angle values between the original seawater and diluted seawater (5000 ppm) were observed, which might be the major cause of reporting low recovery (2% of OOIP).

Lashkarbolooki and his colleagues [62] also considered the impact of the type and concentration of salts on the wetting state of carbonate rocks. They used carbonate rock samples with acidic and asphaltenic crude oils from Iranian reservoir, and different single component brines involving NaCl, KCl, Na_2SO_4, $MgSO_4$, $CaSO_4$, $CaCl_2$, and $MgCl_2$ with a wide range of concentrations. Their results showed that changing in brine salinity from deionized water (0 ppm) to high salinity water (30000-45000 ppm) resulted in a higher contact angle. In their detailed study, Lashkarbolooki

et al. [62] also found that the highest effect on the wetting state was detected by divalent ions, especially $MgCl_2$ which changed the wettability to a less water-wet condition, while monovalent ions such as NaCl and KCl did not show a substantial effect on the wettability alteration, as the contact angle remains within a strong water wetness.

From the aforementioned literature, it can be seen that many authors have sought to study the effect of salinity and type of ions on the wetting state of carbonates; however, far less attention has been paid to the impact of active polar components of crude oil on the wettability of carbonates. Thus, there is a practical need to determine the specific effect of low salinity water on the wetting state of carbonates under various kinds of crude oil with particular emphasis on its acidity value.

2.6.2 Effect of Low Salinity Flooding (LSF) on Interfacial Tension

From equation 2.3, the interfacial tension (IFT) of the oil/brine system is another critical parameter that affects the capillary forces, and hence the trapped oil mobilization and sweeping efficiency. Many studies have been conducted to evalaute the IFT between the oil/brine interfaces but with conflicting results, as will be reviewed below.

To begin with, Vijapurapu and Rao [63] studied the effect of brine dilution and surfactant addition on the IFT of Yates dead crude oil. Various proportions of diluted Yates formation brine were used to measure the IFT of the oil/water system. Their study confirmed that there was a critical brine concentration reporting a minimum IFT value, after which the oil/brine IFT increased with further dilution brine. Xu [64] also performed detailed IFT experiments using Yates live crude oil from west of Texas and different aqueous solutions including Yates formation water, 50 times diluted formation water, NaCl, and $CaCl_2$ solutions. Their results showed that a higher IFT was obtained with the dilution formation brine compared to the original Yates brine. Xu's comparative study also revealed that

using a pure $CaCl_2$ solution yielded the highest IFT among other examined solutions.

In 2011, Yousef et al. [10] presented a convenient procedure to measure the IFT between the oil/brine interface. Their study indicated that an insignificant impact on the IFT values was observed by using reservoir live oil and different diluted versions of seawater. A later survey of Al-Attar et al. [40] also suggested that no clear correlation was found between the interfacial tension and the performance of low salinity water flooding for EOR at the ambient conditions.

Further research carried up by Lashkarbolooki et al. [62] who found that using divalent cations along with chloride ions especially $MgCl_2$ reported lowest IFT values compared to monovalent ions (NaCl and KCl), showing unpredicted behaviour for IFT values as the salt concentration was raised to 1000 ppm. Moeini et al. [65] also investigated the impact of monovalent and divalent ions on IFT. In their study, heavy crude oil and two simple component brines including $CaCl_2$ and NaCl with a wide range of concentrations were used. They observed that there was a critical brine concentration (20000-40000 ppm), after which an adverse effect on IFT was reported, as shown in Figure 2.10. In addition, the general trend of IFT was higher for $CaCl_2$ solution compared to NaCl; however, this variation was insignificant at low salt concentrations.

On the other hand, the amount and type of polar organic components and hetero-atoms such as oxygen, nitrogen, and sulphur found in the heavy fractions of crude oil could contribute to the IFT reduction [66-69]. The polar groups are mainly carboxylic acid, but also phenolic acids, alcohols, thiols, ketones and esters [70]. The quantity of petroleum acids is characterized by the total acid number (TAN), equivalent to the milligrams of potassium hydroxide (KOH) required to neutralize the acidity of 1g of oil, a value that can range from negligible up to around 3 mg KOH/g.

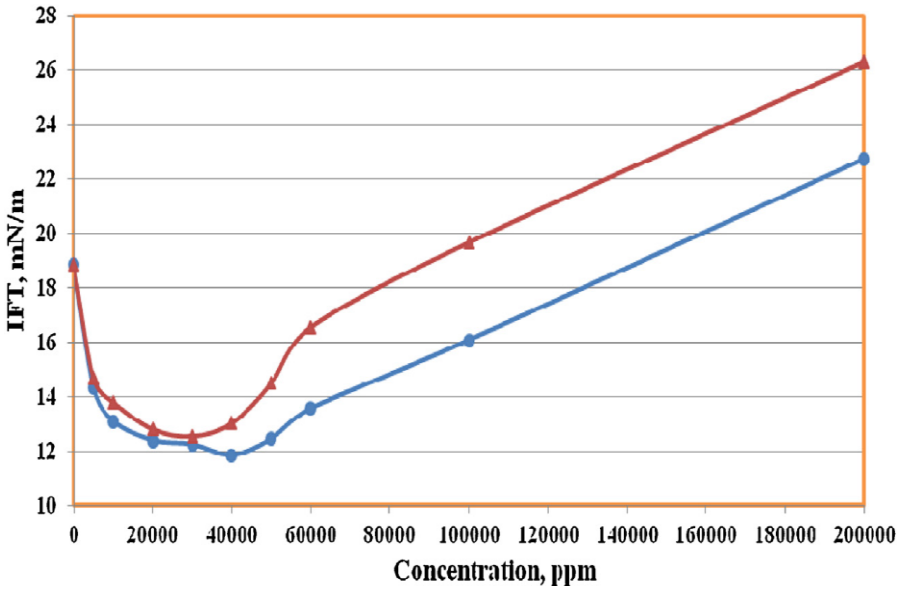

Figure 2.10: IFT of crude oil and NaCl/$CaCl_2$ brine at various salt concentrations [65].

However, even quantities in the lower range could have an influence as a strong surface-active polar molecule so that they will have a disproportionate effect on interfacial tension [67,68,71].

Preliminary study on the impact of polar components and salinity on the IFT was undertaken by Abdel-Wali [72]. In their work, different amounts of oleic acid and octadecylamine were used to change the concentration of acidic and basic polar compounds of crude oil. Their results demonstrated that increasing the concentration of oleic acid to 0.028 mol/l with 40000 ppm NaCl led to a more considerable decrease in IFT values as a result of increasing the solubility of oleic acid in the aqueous phase, acting as an anionic surfactant. When the basic polar compound (octadecylamine) was used an optimum salt concentration ranging from 4000-10000 ppm was required to get a minimum IFT value.

In 2005, Brandal et al. [73] examined the impact of naphthenic acid and divalent cations on the dynamic interfacial tension. They reported that a substantial decrease in the interfacial tension values was observed when saturated naphthenic acid combined with divalent cations, creating positively charged monoacid complexes occupying the oil/water interface, causing higher interfacial activity. A recent study by Lashkarbolooki et al.

[74] which set out to investigate the symbiotic effects of salt, resin, and asphaltene on the IFT activity, revealed that high IFT values were reported for the resin/brine system at low concentrations of $MgCl_2$, $CaCl_2$, and NaCl due to the low interfacial activity. However, their results showed that at high $MgCl_2$ concentration, a complex ion of MgCl-resin occupying the interface would be formed, leading to lower IFT values. For the case of asphaltene, Lashkarbolooki et al. [74] stated that asphaltene molecules could easily transfer from bulk to interface in comparison with resin molecules, resulting in positive interfacial activity. This effect was more pronounced when Ca^{2+} ions were used due to the higher attraction forces between Ca^{2+} and asphaltene molecules.

In 2018, more evidence of the opposite effect of asphaltene and resin fractions on the IFT behaviour was presented by Lashkarbolooki and Ayatollahi [75]. They found that resin fraction exhibited less contribution to decrease the IFT compared to asphaltene fraction in the presence of ionic solution, and this effect is dominated by the concentration and aromaticity of asphaltene and resin.

It can be seen from the literature that a number of studies have been conducted to study the effect of brine salinity on IFT. Despite this interest, however, the experimental data are rather controversial. In addition, quite little attention has been paid to the diversity of the crude oil composition and its corresponding effect on the IFT of the oil/brine system.

2.7 Suggested Mechanisms of Wettability Alteration during Low Salinity Flooding

As pointed out in the previous section, wettability alteration from oil-wet to intermediate-wet or water-wet has been demonstrated as a plausible mechanism, which affects the IOR significantly during low salinity water flooding [10,20-22]. Many theories concerning the alteration of wettability have been suggested, but none are commonly accepted. The main individual mechanisms proposed by the researchers will be illustrated below.

2.7.1 Electrical Double Layer Expansion

The theory of electrical double layer expansion has been suggested as one of the mechanisms involved in the process of wettability alteration during low salinity injection [76]. According to the Derjaguin-Landau-Verwey-Overbeek (DLVO) theory, the competitive interactions between the repulsion forces and attractive van der Waals forces when the charged rock surfaces exposed to the saline solution will lead to creating an electrical double layer along the interface, which is different from the bulk solution [77]. This layer is divided into two regions. These are the Stern layer and diffusive layer. In the Stern layer, the ions are strongly bonded to the rock surface, and they cannot move. However, the ions within the diffusive layer are loosely associated with the surface and thereby can pass through easily. The two parts of the electrical double layer are illustrated in Figure 2.11. The concentration and type of ions existing in the electrolyte solution play a crucial role in the magnitude of the conductivity and thickness of the electrical double layer [78]. Increasing the concentration of the electrolyte causes a shrinkage in the thickness of the electrical double layer and vice versa.

As a result of the intermolecular interaction, a potential at the shear (slipping) plane, located between the Stern layer (stagnated ions) and the diffusive layer (moving ions) will be developed. The difference in the potential between the slipping plane and bulk solution has been commonly referred to as the zeta potential, which is affected by the nature of the surrounding medium and the surface charges [77]. The surface charges are strongly related to pH. The pH value at which the rock surface charges change from positive to negative is identified as the point of zero charges (PZC). It was supposed that the carbonate surfaces are positively charged at pH ≤ 7 [6].

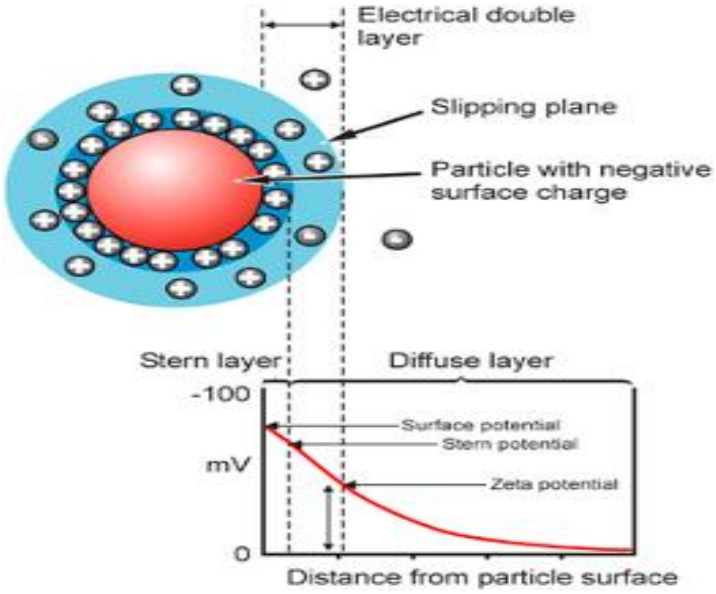

Figure 2.11: Electrical Double Layer [76].

At a low electrolyte concentration and a relatively high surface charge density, the repulsive energy due to the electrical double layer expansion (EDL) will dominate the interaction at the rock/brine interface, leading to negative charges at the carbonate surfaces. As the oil/brine phase become negatively charged at high pH (pH >3.5) [79], thereby creating more negative charges on the rock sites will promote the detachment of oil components from the surface and change the wettability of carbonates to a desirable state [80]. It should, however, be noted that van der Waals attractive forces can facilitate the adsorption of cations and anions on the surfaces, but it has not been disturbed by the alterations of the ionic strength of electrolytes and pH.

For the effect of electrical double layer expansion on the wettability alteration of carbonates, a number of studies have been published recently. In 2010, the experimental work was conducted by Alotaibi et al. [80] to study the surface charges of the outcrop limestone and dolomite rocks by measuring the zeta potential. Alotaibi et al. used seawater, aquifer water, and modified aquifer water involving a different concentration of divalent and monovalent ions. Their study suggested that the expansion of the electrical double layer (EDL) caused by pH and

salinity change led to the more negatively charged surface, helping to improve the wettability of carbonate rock surface to water wet, as shown in Figure 2.12.

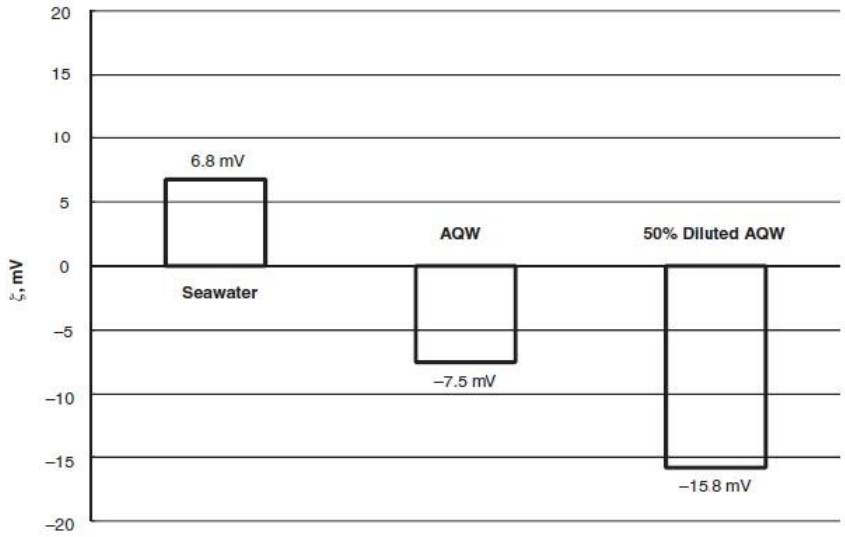

Figure 2.12: Effect of seawater and aquifer water on zeta potential at 25 °C and pH 7 [80].

In the same vein, Mahani et al. [81] examined the zeta potential to quantify the surface charges at the rock/brine interface. To perform their experiments, high salinity formation water, seawater, and 25 times diluted seawater with and without crushed carbonate rocks (limestone and dolomite) were used. In their comparative study, Mahani et al. found that more negative surface charges at the limestone/brine interface were obtained at lower salinities, consisting with the observed change in the contact angle value to a less oil-wet condition. In contrast, dolomite reported less decrease in the positive surface charges upon exposure to the low saline solution, supported by a smaller reduction in the contact angle value. According to Mahani et al., the change in the surface charges seems to be the primary mechanism that responsible for the positive low salinity effect in carbonates while rocks dissolution did not show any relevant effect.

Another study by Kasha et al. [82] investigated the impact of potential determining ions (Ca^{2+}, Mg^{2+}, and SO_4^{2-}) on the surface charge of aged

calcite and dolomite particles. They used stearic acid as a model oil to age the carbonate particles and synthetic brines with various ions concentration. In their detailed analysis of electrokinetics of the two types of carbonate rocks, Kasha et al. found that increasing the concentration of Ca^{2+} and Mg^{2+} ions made the dolomite rock more positively charged, but it changed the original negative charges of aged calcite rock to positive values. They also stated that increasing the concentration of SO_4^{2-} ions could alter the positive zeta potential of dolomite particles to negative.

2.7.2 Rock Dissolution

Injected low salinity brines with low calcium concentration into carbonate reservoirs could properly cause calcite dissolution to return the equilibrium in low salinity brines. Consequently, the adsorbed polar components of oil would detach from the rock surfaces when the calcite dissolution occurred, and this can improve water wetness. The connectivity between the pores might also be enhanced due to the change in the porous structure during the calcite dissolution, which could lead to an increase in the permeability and sweep efficiency.

The calcite dissolution hypothesis was first suggested by Hiorth et al. [83,84] who developed a geochemical model for the system consisting of seawater-CO_2-$CaCO_3$. They considered the previous experimental data of Austad et al. [23] in their model to assess whether the calcite dissolution or the change in the surface charges dominate the wettability alteration of carbonates. From their analysis of matched data, Hiorth et al. suggested that the surface charges change could not explain the observed difference in the wettability, while the calcite dissolution seems to be the major cause behind wettability alteration and higher potential oil recovery at a certain temperature. Hiorth et al. also pointed out that the effect of calcite dissolution could be enhanced with a high acid number crude oil (high organic components). Later, Austad et al. [85] published a paper in which they refuted the calcite dissolution theory proposed by Hiorth et al. [83,84]. They gave strong arguments that Hiorth et al. used seawater with

high ionic strength to mimic the chemistry of water in their chemical model. One question that has been raised, however, is whether their observations will be valid when the low salinity brine used. Another criticism of Hiorths' et al. work is that their analyses are mainly based on the numerical study but without further empirical evidence. Therefore, it seems that the results are questionable.

Another technique, nuclear magnetic resonance (NMR), was used by Yousef et al. [10] to evaluate the wettability alteration during low salinity flooding in carbonate reservoirs. NMR data gave an indirect indication of calcite dissolution upon exposure to low saline solutions since a damped signal was reported, referring to an improvement in the pores connectivity. However, Yousef et al. argued that NMR data could not prove the calcite dissolution during low salinity injection, it is just an indicator. Further investigation was experimentally achieved by Mahani et al. [86] to assess whether the calcite dissolution is responsible for the wettability alteration and low salinity effect. They examined the mineral dissolution by using 25 times diluted seawater saturated with calcite minerals, to ensure that the mineral dissolution would not occur during the experiment. From their analysis of the contact angle measurements, Mahani et al. found that wettability alteration to more water-wetness was observed even without mineral dissolution.

2.8 Evaluating the Wettability Change by Atomic Force Microscopy (AFM)

The literature mentioned above so far demonstrates that contact angle between crude oil and rock surfaces, mediated by the aqueous phase has been mainly used to evaluate the wettability of rock surfaces. However, the macroscopic contact angle measurement has a limitation to provide molecular-level detail of the physicochemical interactions that take place between interfaces, which can help to understand the complexities of the various interfacial phenomena governing surface wetting of crude oil on

carbonates in a brine environment. This leads to a lack of reliable predictions of reservoirs' performance under low salinity flooding, calling for a more efficient method for assessing wettability at the microscopic-scale. Atomic force microscopy (AFM) has been recently used to investigate the effect of some solutions on surface wettability by measuring the adhesion forces between a probe and the mineral surface at pico-Newtons (pN) or nano-Newtons (nN) [87,88]. As decreasing adhesion force would contribute to the release of polar organic components from the surface, rendering it with a favourable wetting state [89,90].

For instance, Kumar et al. [91] studied the mechanism behind the changes in surface wettability caused by surfactants. Kumar et al. measured the force of adhesion for aged silicon and mica substrates before and after exposure to anionic and cationic surfactants. Their results confirmed that a significant change in the adhesion force values was observed when the ionic surfactants used as a result of removing adsorbed oil molecules from the surfaces, helping to change the wettability to preferential water condition. In the same vein, to assess the pore-scale wettability modification, Seiedi et al. [92] examined the properties of the aged mica surfaces before and after exposing to the two kinds of surfactants (Triton X-100 and C_{16}TAB) by using AFM topographies and phase images. From their analysis of the topographical images, Seiedi et al. suggested that using cationic surfactant C_{16}TAB was less efficient than non-ionic surfactant Triton X-100 to modify the wettability of aged mica plate, confirming by contact angle measurements, showing oil-wetness when C_{16}TAB used.

The first serious work and analysis of low salinity effect on micro-scale wettability alteration were undertaken by Hassankam et al. [89]. They examined wettability alteration of the natural sandstone samples using -COOH functionalized AFM tip to mimic the polar oil components-rock interactions under a range of salt concentration. From the force maps, Hassankam and co-workers found that an average decrease in adhesion

forces of about 30% was reported as the salinity of solution decreased from 36000 ppm to 1400 ppm, and the same behaviour was observed for the outcrop and reservoir sandstones. They claimed that a reduction in the adhesion could be explained by the electrical double layer expansion combined with the presence of clay particles, responding obviously to the low salinity effect.

Hssankams' et al. work [89] is supported by Hilner et al. [93] who also studied wettability alteration of natural sandstone samples containing quartz and clay minerals. They measured the adhesion forces between a non-polar oil droplet using -CH3 functionalized AFM tips and the sandstone minerals as a function of salinity. Like Hssankam et al., Hilners' et al. analyses revealed that no change in adhesion was observed at high salinity solution (28000 ppm), while a clear reduction in adhesion was reported when the salinity decreased below a threshold of 5000 ppm, rendering the surface with a favourable wetting state. Hilner et al. also proposed that the strong repulsive force of the electrical layer at low salinity conditions was contributed in the observed change of adhesion values and this effect was higher on clay minerals than on quartz.

In 2014, Mathiesene and his colleagues [94] conducted a comparative study in which they examined the adhesion forces of kerosene-treated-sandstone and solvent-cleaned-sandstone samples to explore the effect of adsorbed organic material on the performance of low saline solutions. Like previous studies, Mathiesene et al. concluded that a reduction in the adhesion force values was reported for both types of samples used when the solution changed from high salinity (35600 ppm) to low salinity (1500 ppm). However, the change in adhesion was more pronounced on kerosene-preserved grains than on clean-solvent grains, confirming the association between the adsorbed polar organic material and low salinity effect to EOR in sandstones.

From the researches mentioned above, there is a general agreement of the positive low salinity effect at the micro-scale level in sandstones. However, a discussion about the molecular interactions of carbonates is

rare. Preliminary work by Pedersen et al. [95] studied the effect of the presence of organic material on surface wettability upon exposure to different saline solutions by using two kinds of natural limestone grains and non-polar –CH3 functionalized AFM probes, with inconclusive results. The surface response was heterogeneous, with no overall correlation found between probe adhesion and salinity, although some small patches of the surface did respond. Unexpectedly, some areas of low adhesion became more adhesive upon exposure to lower salinity solution. More recently, Generosi et al. [96] performed a study in which they examined the adhesion between the non-polar -CH_3 tip and calcite surface in the presence of different saline solutions (NaCl, $MgCl_2$, $MgSO_4$, and Na_2SO_4) at high temperature. Their results exhibited that a considerable decrease in the adhesion force was observed upon exposure to $MgSO_4$ solution and this response was reversible when a solution of pure NaCl used. Generosi et al. findings confirm the association between SO_4^{2-} and Mg^{2+} to enhance the wettability change of carbonates.

In summary, the majority of previous studies have focused on measuring the change in adhesion forces between the molecules on the functionalized tips and the natural grains as an attempt to evaluate the wettability at the micro-scale and to assess the response to the changes in salinity, with very limited work on carbonate minerals. In addition, while the study of the minerals in their natural form is preferable in many ways, the granular structure has a very high roughness which can interfere with the AFM adhesion measurements due to changes in the surface contact area. With that said, the data presented seemed to be influenced by the topography. Therefore, further studies need to be done.

2.9 Assessment of Adsorption/Desorption of Crude Oil onto/from Surfaces by Quartz Crystal Microbalance (QCM)

Throughout years, Quartz Crystal Microbalance (QCM) technique has been generally used in various research areas. A number of studies have been conducted to evaluate the adsorption of polymers on the surfaces using a QCM approach. An example of this is the work performed by Guo et al. [97] and Li et al. [98] in which they investigated the adsorption behaviour of different kinds of polymers on gold and silica surfaces. The adsorption/desorption of asphaltene onto/from surfaces has also been extensively considered by many researchers [99,100]. For instance, Ekholm et al. [101] compared the adsorption of asphaltene and resin on the gold surfaces with crude oil diluted in heptane/toluene mixtures. Their findings suggested that the adsorption of crude oil on the gold surface was comparable to the adsorption of the asphaltene solution but significantly different from that of asphaltene/resin mixtures. A recent study by Tapio et al. [102] evaluated the desorption efficiency of asphaltene from stainless steel surfaces by using different organic solvents such as Pyridine, Carbon disulphide, Aniline, Quinoline, and Ethanol. Tapio et al. [102] found that the polarity of solvent affects significantly on the desorption of asphaltene from the surfaces, as the least desorption efficiency of 18% was reported with a non-polar carbon disulphide solution compared to 70% for Pyridine.

Based on the fact that the polar organic components of crude oil may also have a role to play in the wettability alteration of reservoir rock during brine injection, there have been some efforts recently to investigate the adsorption/desorption of crude oil components onto/from various surfaces [103,104]. A preliminary study was conducted by Farooq et al. [105] who assessed the desorption of asphaltene from coated silica surfaces at low electrolytes concentration. According to Farooq et al. [105], the type and ionic strength of saline solutions play a vital role in the amount of desorption. In another work, Farooq and co-worker [106] studied the

desorption of acidic and basic crude oils from coated silica surfaces after exposing to seawater, NaCl, and $CaCl_2$ solutions with the concentration varied between 35000 to 1500 ppm. Their results revealed that the acidic crude oil had less affinity to the silica surface compared to the basic crude oil and the presence of acidic components seems to have an adverse impact on the oil desorption efficiency upon exposure to low salinity solution. In contrast, using basic crude oil showed substantial desorption after exposing to a low salinity solution. Farooq et al. concluded that the pH and the composition of the aqueous solutions affect the desorption of oil from silica surfaces.

In the same vein, Nourani et al. [107] compared the desorption efficiency of different kinds of crude oils from silica and alumin silica upon exposure to low salinity and a hybrid of low salinity and surfactant solutions. They found that as the amounts of polar components (asphaltenes and resins) in the crude oil and aluminium content at the surface increased, the desorption of crude oil components decreased. In terms of low salinity effect, Nourani et al. concluded that injecting low salinity solution revealed some desorption from the surfaces, however, the desorption efficiency was significantly enhanced by injecting a hybrid of low salinity and sodium dodecylbenzene sulfonate (SDBS) surfactant.

From above, it is found that all the previously mentioned works have focused on evaluating the adsorption and/or desorption efficiency of asphaltene or crude oil onto/from silica surfaces. So far, however, there are very few studies that surveyed the crude oil adsorption/ desorption efficiency onto/from carbonate minerals. The first experimental realisation of assessing the desorption of crude oil from the carbonate surface has been undertaken by Liu et al. [108]. They used single component brines including NaCl and $CaCl_2$ with a series of decreasing salt concentrations (33000 ppm, 1600 ppm, and 300 ppm). Liu et al. confirmed that the oil detached from the carbonate surface upon exposure to both high and low salinity solutions of NaCl, but no desorption was seen by injection high salinity solution of $CaCl_2$.

2.10 Fluid Displacements at the Pore-Scale Using a Visualized Microfluidic Technique

As we alluded to in the introduction, forced and imbibed core flooding are the most common methods used to examine the feasibility of different solutions to displace oil from carbonate and sandstone reservoirs. However, it is important to emphasize here that performing conventional imbibition or core flooding experiments exhibit some restrictions to provide *in-situ* visualization of multi-phase flow and oil recovery at the pore-scale level. For this, many considerable attempts have been made to finding an innovative method that can visualize the movement of fluids at a mesoscale, helping to characterize the flow inside sedimentary rock structures and evaluate the effectiveness of different flood processes for enhanced oil recovery. Microfluidics is the ideal technique for this purpose.

Previously, the microfluidic system has been extensively used as a diagnostic platform in biological and chemical processes [109,110]. In recent years, microfluidic technology has gained a wider acceptance for use in the oil and gas sector, specifically for the studies targeting the mechanisms of immiscible displacements with particular attention to pore geometry and fluid properties. This is exemplified in work conducted by Xu et al. [111] who considered the effect of variation in the pore geometry on pore-scale displacement efficiency by water flooding. They used hydrophobic polydimethylsiloxane (PDMS) microfluidic porous media with random geometry and various periodic pore networks, including triangles, squares, diamonds, and hexagons. Xu and his co-workers noticed that there was an improvement in oil displacement efficiency when the flow was within the pores of the same size, while vugs and pore width distribution affected negatively on the microscopic displacement efficiency.

Another example is given by Joseph et al. [112] who studied the petrophysical properties on-chip porous media with different pore structures in an attempt to characterize the association between porosity

and permeability at the pore-scale level. Their results revealed that the range of porosity in the on-chip pore networks was between 0.39 and 0.67, determined by the image analysis technique. Whereas, the permeability values were within the range of 2.66-15.93 Darcy, estimated by measuring the pressure difference across the chip. Joseph et al. concluded that increasing the number of pores-throats in a micromodel resulted in an increase in the porosity and permeability.

Later, researchers have examined the effect of liquid properties on the oil displacement efficiency at the pore level. In 2013, Nilsson et al. [113] developed a microfluidic microstructure to test the activity of non-Newtonian fluids, having various rheological properties on the oil recovery factor. Their results revealed that using a surfactant as a displacing fluid showed an improvement in oil recovery by about 15% compared to that of water flooding under the same flow conditions. They also stated that shear-thinning and viscoelastic fluids yielded a much better effect on oil displacement efficiency in comparison with the water and surfactant solutions.

Conn et al. [114] studied foam flooding and its impact on oil displacement efficiency by using an oil-wet micromodel with the heterogeneous pore networks. They found that foam flooding improved the recovery efficiency by increasing the resistance of flow in the regions with the high permeability (fracture), causing an increase in the local pressure gradients and diverting the flow toward low permeability regions, mobilizing trapped oil. Another comparative research carried out by He et al. [115] to evaluate the performance of non-emulsifying surfactant (NES) and weakly emulsifying surfactant (WES) on oil productivity in unconventional reservoirs. They used a micromodel with pore geometry analogous to that in the shale formation. He et al. stated that a better oil displacement efficiency was observed when weakly emulsifying surfactant was used due to its tendency to form emulsion, without blocking the formation.

In 2016, Xu and Zhu [116] published a paper in which they examined the symbiotic effect of nanoparticles and surfactants in macro-emulsion on

sweeping efficiency by using a dual-permeability micromodel. Xu and Zhu found that stable emulsion improved the flux by blocking the high-permeability pathway and diverting the invading fluid toward low-permeability layers, helping to enhance sweep efficiency.

It is clear that the performance of different displacing fluids to improve the sweeping efficiency at the pore-level has been studied by many researchers; however, little attention has been paid to the low salinity effect except in recent few studies. These studies simulated the low salinity flooding in the clean and clay-functionalized water-wet micromodels to advance the understanding of the micro-mechanisms responsible for oil recovery enhancement in natural sandstone reservoirs. This is exemplified by the work of Barnaji et al. [117] who concluded that low salinity water flooding did not show any positive effect on the oil recovery in the non-coated pore network, i.e., with no clay minerals.

Unlike Barnaji et al. [117], Amirian et al. [118], however, argued that no correlation was found between the presence of clay minerals and the potential of low salinity water flooding for EOR. According to Amirian et al., the most acceptable mechanism behind the low salinity effect was related to the formation of a viscoelastic oil-water interface. Another experimental work by Emadi and Soharbi [119] showed that when high salinity water was replaced by low salinity solution, micro-dispersions (water-in-oil emulsion) at oil/water interfaces were formed and considered as an underlying mechanism affecting the fluid redistribution and sweep efficiency in a homogenous water-wet system. A very recent study by Fredriksen et al. [120] in which they examined the mobilization of oil using silicon-wafer micromodels, demonstrated that osmosis and diffusion of water molecules driven by salinity contrasts represented the main pore-scale mechanisms responsible for oil mobilization during low salinity flooding.

It can be seen from the literature that there is no consensus on the underlying pore-scale mechanisms affecting oil recovery during low salinity flooding in sandstones and much uncertainty still exists. On the

other hand, most of the previous pore-scale studies up to now have been conducted on the water-wet microstructures, therefore not considering the sweeping efficiency of low salinity flooding in a completely oil-wet system to resemble carbonates, which prevail in most of the world's oil reserves (> 60%). Thus, further pore-scale studies need to be conducted.

2.11 Summary

In this Chapter, the related literature of the quantitative and qualitative techniques used to evaluate the salinity effect on EOR in carbonates and sandstones has been thoroughly reviewed. The aim was to understand the general concepts and commence critical analysis as a logical preliminary step for advanced research and new contributions. The following conclusions can be drawn:

- It is clear that complex interactions occur between rock/brine/oil, leading to wettability alteration. However, there is no universal agreement on the physicochemical mechanisms behind this alteration. Characterization of the carbonate surface and how it interacts with the polar oil components under various electrolyte solutions will be necessary for a careful evaluation of low salinity performance, and it can help to find a unified interpretation of wettability alteration mechanisms. On the other hand, as reviewed in section 2.6.2, it seems to be that there is no conclusive statement regarding the impact of salinity on the fluid/fluid interaction. Thus, the oil/brine interaction needs to be studied well with particular emphasis on oil polar content to unveil whether it can affect oil recovery during low salinity flooding. To address the above limitations, the key parameters that govern the complex interactions of rock/brine and oil/brine interfaces are systematically investigated in this thesis as will be discussed in Chapter 4.

- As reviewed in section 2.9, although evaluating the adsorption and desorption efficiencies of crude oil under different aqueous phases has generated research interest lately, limited work on carbonate surfaces can be found. To address this limitation, more studies need to be performed on carbonates to explore whether the desorption of crude oil is influenced by its chemical composition and/or the ionic strength and salinity of the injected fluids. Such a study would be of great help to estimate the potential of enhancing oil recovery from carbonate reservoirs before committing to the conventional core flooding test. The empirical findings that exhibit some crucial insights into this concept will be given in Chapter 6 of this thesis.

- Most of the previously published studies to date have tended to focus on macroscopic contact angle measurements to assess the change in wettability. However, even though such type of measurement can give an indication of wettability alteration, it cannot provide molecular-level details of the interactions that take place between interfaces. This leads to a difficulty in predicting the microscopic efficiency of low salinity flood. To address this problem, a more systematic approach should be considered to simulate solid/brine/oil interactions at the meso to micro scale level. In this research, the high spatial resolution techniques such as Atomic Force Microscopy (AFM) and visualized microfluidic have been used. Using these techniques can make a big contribution to the existing studies by extending our knowledge of the pore-scale mechanisms affecting oil sweep efficiency and providing insights into the feasibility of low salinity flooding for enhanced oil recovery at the pore-level. The experimental findings of micro-scale and mesoscale investigations will be given in Chapters 5 and 8 in this thesis.

- Based on this review of the state-of-the-art studies, it is worthwhile to mention that due to the late interest about the impact of low salinity flooding on improving oil recovery in carbonate reservoirs and the limited number of successful core flooding experiments, no solid proof

has yet been gained and hence, its application at a large field scale is still doubtful. In addition, a comprehensive review of many technical publications covering low salinity effects, section 2.5, demonstrated that researchers have tended to focus primarily on investigating the impact of salinity and ionic strength reduction on oil recovery, but without taking into consideration the combined effect of oil composition and rock mineralogy on the real low salinity potential. Therefore, systematic macroscopic core flooding experiments with various kinds of crude oil and carbonate rocks need to be conducted at *in-situ* reservoir conditions to realize the various perceptions of low salinity effect, which will represent the basis of Chapter 7 in this research.

- Finally, the experimental studies on the feasibility of low salinity for EOR have mostly been designed to focus on an individual specific aspect by either measuring macroscopic contact angle or macroscopic displacement efficiency. However, to date, no integrated study has been carried out to carefully examine the low salinity potential and its possible mechanisms at multiple scales, which represents one of the main objectives of this research.

Chapter 3

Instrumentation and Methodology

This Chapter describes detailed information about a set of qualitative and quantitative approaches used in this thesis to identify the potential of low salinity flooding for EOR in hydrocarbon reservoirs and to understand the underlying mechanisms related to its effect. The Chapter includes seven main sections, each of which explains materials, equipment, and methodology related to one of the certain measurements.

3.1 Zeta Potential Measurement

3.1.1 Materials

3.1.1.1 Rock Samples

Homogenous Estaillades limestone outcrop rock and subsurface dolomite rock were used in the zeta potential measurements. The core samples were supplied by Shell. The average grain density is 2.74 g/cc, measured by Micromeritics Acupyc-1330.X-ray. The average porosity and permeability of the Estaillades core are 25 % and 100 md, respectively. Reservoir rock has a range of permeability between 30-380 md and 25-30% of porosity.

X-ray Diffraction (XRD) analysis was carried out by an XRD Bruker D8 Diffractometer to quantify the mineral composition of the outcrop and subsurface rock. The intensity of the reflected X-rays was recorded over a range of diffraction angles (2θ) from 20° to 70°, and the diffraction peaks were then detected. Figure 3.1 shows the XRD response of Estaillades outcrop and subsurface rocks. The data were analysed and matched with a reference pattern by using XRD data collector software. According to the matched data, the minerals reference codes in Figure 3.1A reveal that the powder of outcrop rock was composed of mainly (94%) calcite with a

small amount (6%) of Dolomite, while the intensity peaks of reservoir rock, Figure 3.1B, matched dolomite and anhydrite structure. No clay minerals were detected for both rock samples.

The specific surface area of carbonate samples was measured using Tristar 3000. The carbonate powder was first put in the vacuum oven for 18 hours at 400 °C to evacuate the pore surface. Nitrogen was then used as an adsorptive material on a degassed sample. The adsorption of nitrogen per mass was determined at 77K, and the physisorption isotherm was obtained. Figure 3.2 provides information about the pores structure and the physisorption isotherm. It is found that subsurface dolomite rock has a relatively large surface area (1.25 m^2/g) compared to limestone rock, which revealed only 0.56 m^2/g.

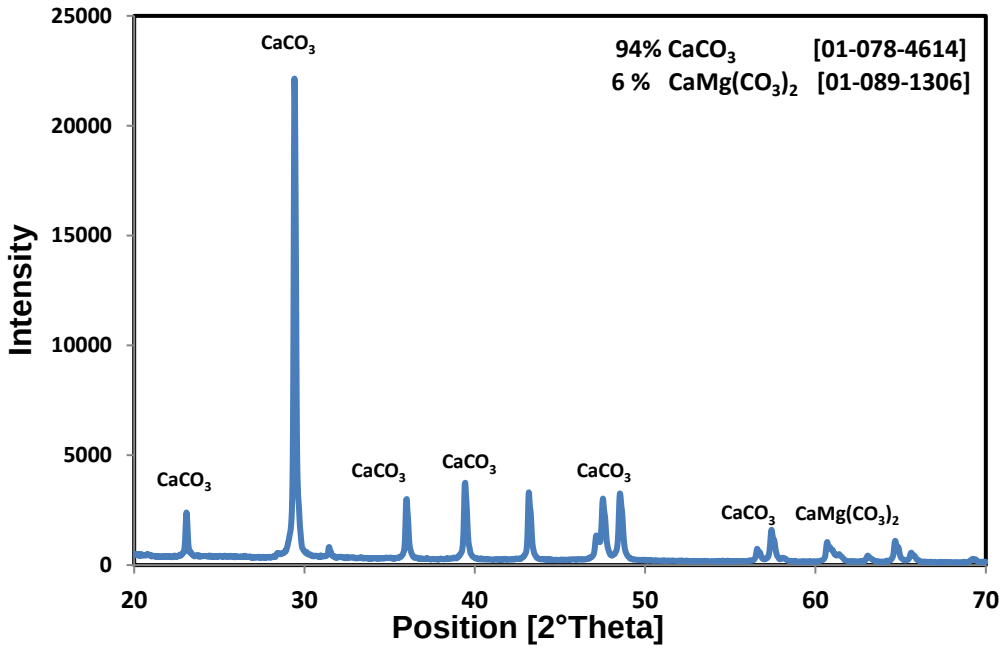

(A)

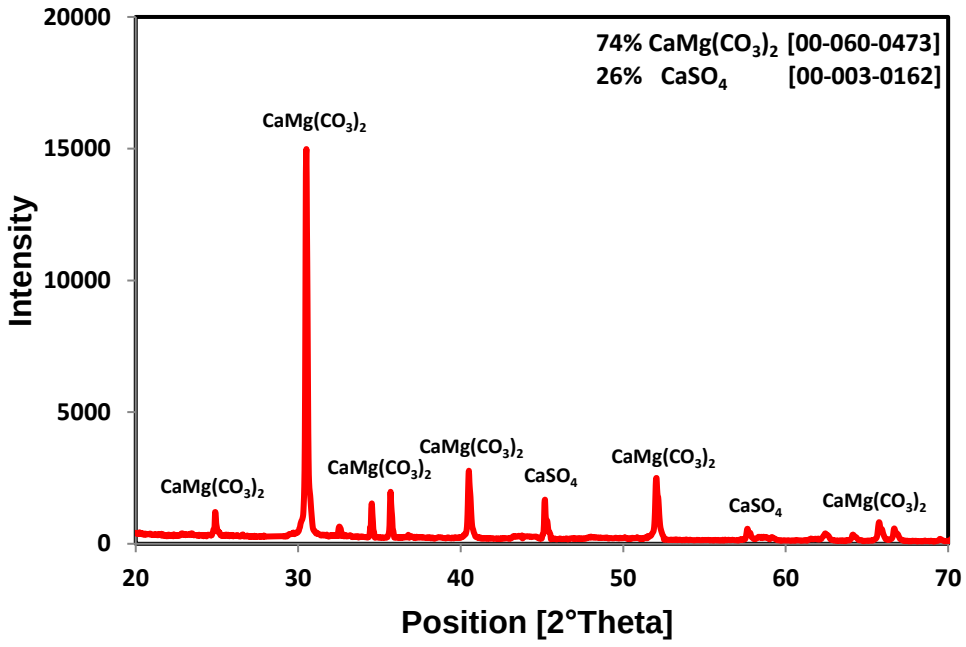

(B)

Figure 3.1: XRD response of (A) Estaillades outcrop and (B) subsurface reservoir rocks.

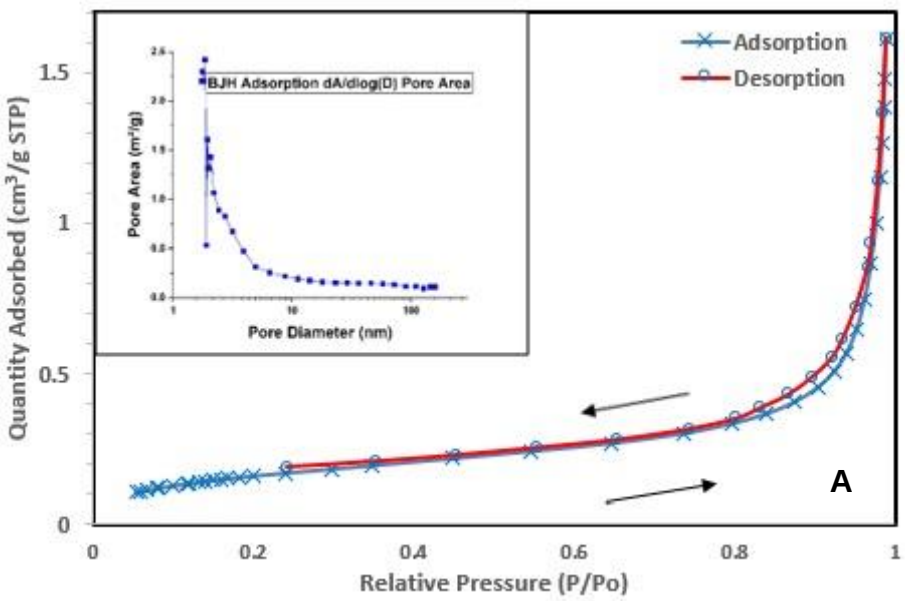

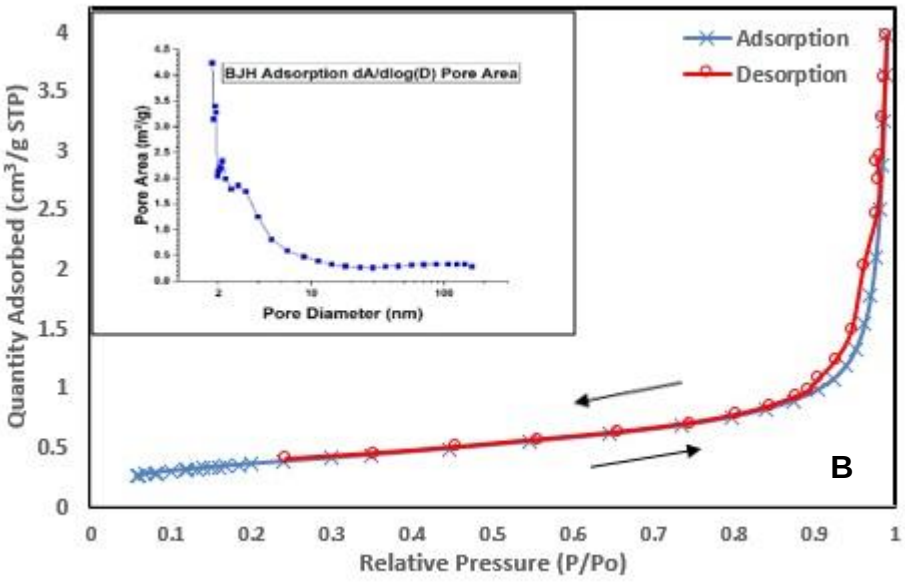

Figure 3.2: N_2 Physisorption isotherms and BJH pore area distribution at 77 K for (A) Limestone particles. (B) Dolomite particles.

3.1.1.2 Brine Preparation and Physical Properties

In this study, synthetic seawater and artificial formation water were used as the base brines. All brines were prepared in the lab by mixing deionized water (Milli-Q, resistivity >18.2 MΩ.cm) with reagent grade salts, which supplied by Merck and Sigma with a purity grade > 99%. The salinity of seawater and formation water solutions were 43650 ppm and 200000 ppm, respectively; representing the high salinity (HS) solutions. The artificial low salinity (LS) solutions were then made by diluting the prepared seawater with different proportions of Milli-Q water. This includes twice-diluted seawater (2dSW), 5 times-diluted seawater (5dSW), 10 times-diluted seawater (10dSW), 20 times-diluted seawater (20dSW), and 50 times-diluted seawater (50dSW). The composition of all brine solutions is given in Table 3.1.

Table 3.1: The composition of high salinity and low salinity brines

Salts	FW (mg/L)	SW (mg/L)	2dSW (mg/L)	5dSW (mg/L)	10dSW (mg/L)	20dSW (mg/L)	50dSW (mg/L)
Na^+	59498	13847	6924	2769	1384	692	277
Cl^-	117626	24141	12071	4828	2414	1207	483
Ca^{2+}	19040	513	256	103	51	25	10
Mg^{2+}	3248	1618	809	324	162	81	32
SO_4^{2-}	234	3355	1677	671	335	167.7	67
HCO_3^-	354	176	88	35	17.6	8.8	3.5
Salt Concentration (ppm)	200000	43650	21825	8730	4365	2182	873

The physical properties of all prepared brines were characterized as below:

- **Density Measurement**

Helium pycnometry Micromeritics Acupyc-1330 was used to measure the densities of all prepared brines. First, the mass of the sample was determined using an accurate balance. Then, the sample was loaded into the pycnometry, and its volume was precisely measured by the gas displacement technique. The volume data together with the sample mass was collected to calculate the density.

- **Viscosity Measurement**

A Malvern Bohlin Gemini Rheometer was used to measure the dynamic viscosity of all brines. Prior to the measurement, a standard liquid was used to calibrate the rheometer. The sample was then put in 2 mL small cell, and viscosity values were determined at a shear rate region of 10-1000 1/s.

- **Conductivity Measurement**

Brine conductivity was determined by using the S70 Seven Multi conductivity meter. A standard solution of 0.01 M KCl was used for calibration before the conductivity of different brines measured.

- **pH Measurement**

The pH of different brines solutions was detected by a pH meter (MP-225). Firstly, the meter was calibrated using high, neutral, and low pH buffer solutions, subsequently. Then the pH of different samples was measured.

All the measurements were carried out at ambient temperature. Table 3.2 summarizes the details of physical properties for different brines used in this study.

Table 3.2: Physical properties of high salinity and low salinity brines

Brines Types	Salt (ppm)	Density (kg/m^3)	Viscosity (cP)	Conductivity (S/m)	pH
FW	200000	1188.65	1.995	14.92	6.7
SW	43650	1043.94	1.142	4.27	7.96
2dSW	21825	1041.38	1.125	1.617	7.58
5dSW	8730	1038.75	1.012	0.88	7.34
10dSW	4365	1035.79	1.002	0.497	7.24
20dSW	2182	1028.48	0.989	0.277	7.15
50dSW	873	1009	0.936	0.111	7.01

3.1.1.3 Crude Oil

Three kinds of dead crude oil were supplied by Lundin and Shell from oil fields in Alta and the North Sea, respectively. A Malvern Bohlin

Rheometer and Micromeritics Acupyc-1330 were used to measure viscosity and density. SARA fractionation was used to analyze the bulk composition of oils to saturates, aromatics, resin, and asphaltenes. The mass ratios of N, S, and O were determined by an Elemental Analyzer (Thermo EA2000). The physicochemical properties of the crude oils are given in Table 3.3.

Table 3.3: Physicochemical properties of crude oils

Specification	Crude Oil A	Crude Oil B	Crude Oil C
Specific gravity at 25 °C, kg/m^3	827	835	933
°API	39.5	38	20
Dynamic viscosity at 20 °C, cP	5.5	7.4	50
Dynamic viscosity at 50 °C, cP	2.94	4.5	28
Total acid number (TAN), mg KOH/g	0.25	0.46	2.54
Composition (wt. %)			
Saturates	73.7	64.53	32.25
Aromatics	22.75	28.81	44.91
Resin	3.34	6.19	11.71
Asphaltenes	0.21	0.47	11.13
Elemental analysis (wt. %)			
Nitrogen	1.14	0.88	1.06
Sulphur	0	0.19	0.32
Oxygen	2.2	5.12	10.33

3.1.2 Experimental Procedure

A Colloidal Dynamics Zeta-Probe was used to determine the zeta potential of different calcite-brine suspensions, which is an accurate instrument based on electro-acoustic measurements without the need for sample dilution, Figure 3.3**.** Hence, optical techniques such as the light-scattering technique need the sample to be entirely transparent by diluting it down to a minimum concentration. This dilution can lead to significant

errors in the values of zeta potential. The Colloidal Dynamics Zeta-Probe measures the dynamic mobility of charged colloidal suspensions at different frequencies in the MHz range.

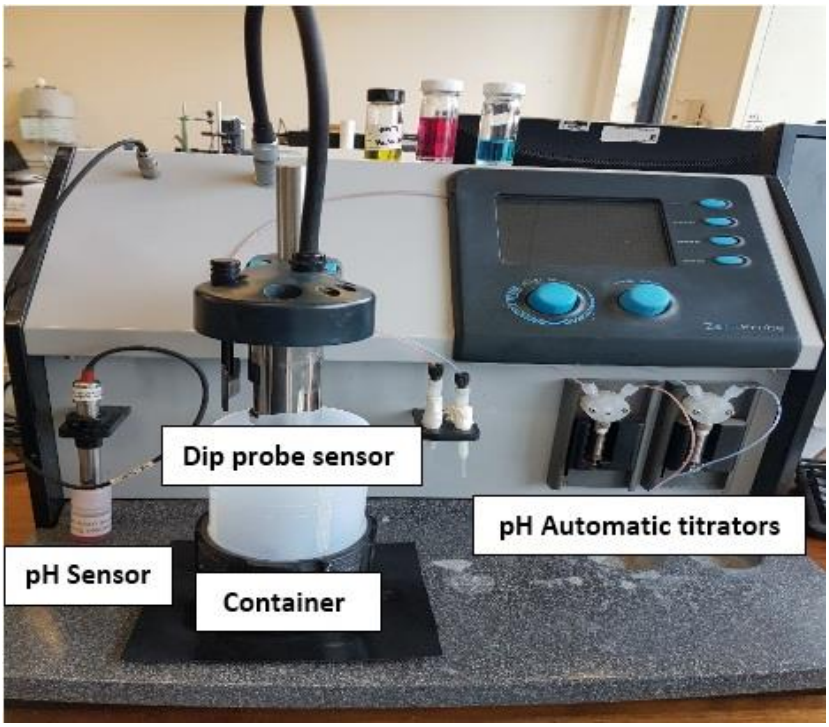

Figure 3.3: Colloidal dynamics zeta-probe.

First, the outcrop and reservoir rock samples were crushed using a mill disc to get a very fine powder of carbonate particles. To prepare suspensions, 2% weight of limestone and dolomite powder were added to various brine solutions under magnetic stirring to maintain homogeneity and left one day to reach equilibrium. Then, we analysed the particles size distribution using Malvern Mastersizer-2000E. Figure 3.4 shows a typical example of the grains size distribution in seawater. It is evident that the limestone particles have a median size of 2.5 μm, while the average size of dolomite particles is about 3.2 μm. It should, however, be noted that the largest particles size for the two types of particles examined did not exceed 20 μm, which can provide a way of proper dispersing in the aqueous phase and satisfy the range of zeta potential measurement.

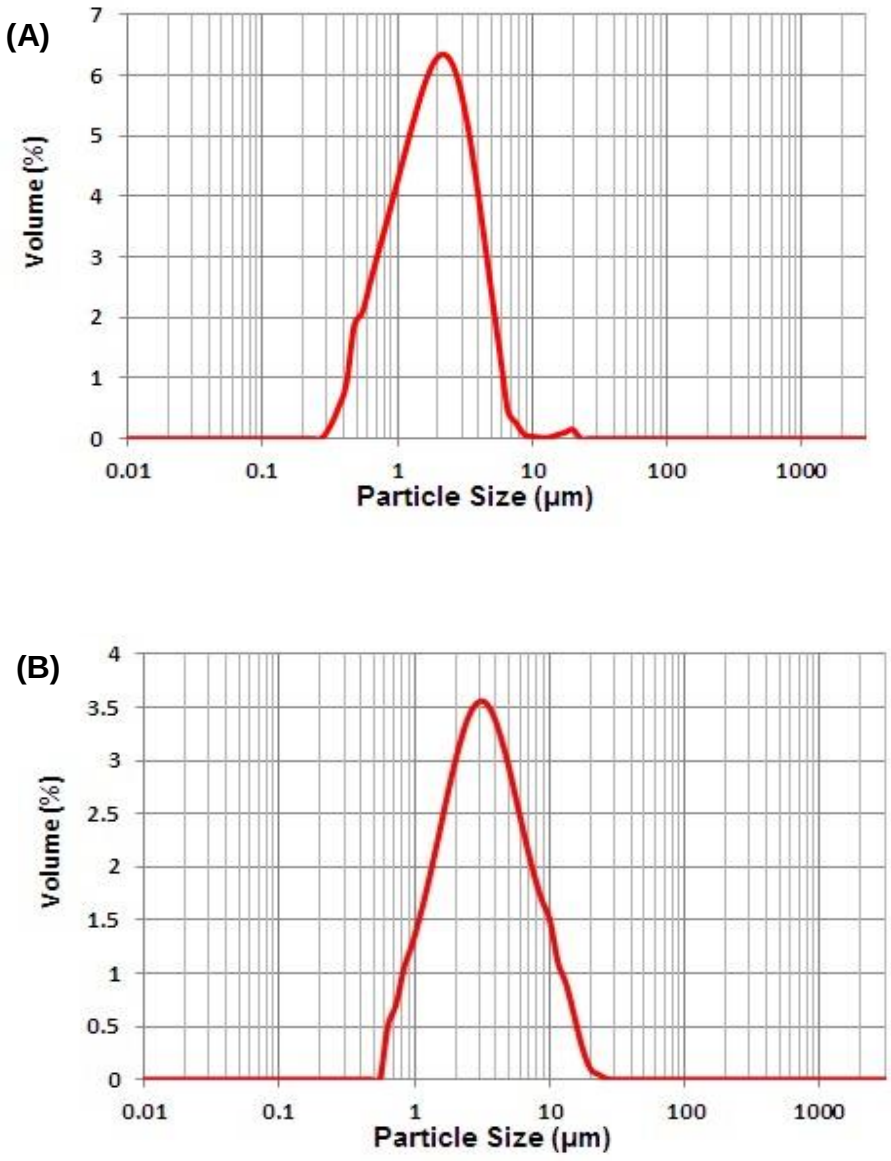

Figure 3.4: Particles size distribution in low saline solution of (A) limestone outcrop rock and (B) subsurface dolomite rock.

The zeta potential measurements of the various carbonate-brine suspensions were conducted at a constant pH value of 8, typical of carbonate reservoir conditions. 0.1 mole/L for HCl and NaOH solutions was used to adjust the pH of suspensions. All zeta potential measurements were conducted at 25 °C. Three runs were carried out for each sample with five cycles' measurement for each run, and an average value of zeta potential was evaluated within this range. The standard deviation of repeated zeta potential measurements is about 0.5 mV.

3.2 Scanning Electron Microscopy and Infrared Spectroscopy Measurements

Different apparatuses, including infra-red spectroscopy (Thermo Scientific Nicolet iS10 FTIR Spectrometer) and scanning electron microscopy (SEM, Carl Zeiss EVO MA15) coupled with integrated energy-dispersive X-ray spectroscopy (EDX, Oxford X-mass 80 SDD) were used to examine the morphology of the carbonate grains and to check whether there were potential bonding effects and mutual ions interactions formed between carbonate minerals and surrounding brines.

The same carbonate-brine suspensions that were prepared for zeta potential measurements have been used for the SEM-EDX test. The Megafuge 16R was then used to separate the solid particles from suspensions. The samples were rotated at 5600 rpm for 20 minutes. Afterwards, the powder was dried in the oven for 24 hours at 70 °C.

The fresh carbonate particles (i.e., prior to being contacted with saline solutions) and treated particles (separated from saline solutions) were put on the aluminium stub that was covered with a carbon adhesive disk. To avoid samples charging during the test, the samples were placed in high-resolution iridium (Ir) coater for 10 minutes. The samples were then loaded into the SEM chamber, and the morphology of surfaces was examined. After imaging the surface by SEM, EDX elemental test was performed on different locations for the same sample to detect the mineral composition and check whether there were compositional changes occurred after exposure to saline solutions, which may reveal indicative information for a better understanding of the rock-brine interaction.

For the infrared measurement, the powder of carbonate rocks was put on the Dimond crystal of infrared spectroscopy, and the light beam of infrared was passed through the sample. As the vibrational frequency of bonds within the atoms coincides with the infrared radiation, the atoms absorb frequencies. The infrared spectrum of absorbed energy (transmitted light) at a specific wavelength was determined, and the mid-infrared region

(4000-500 cm^{-1}) was then compared with the reference patterns to determine the chemical bonds.

3.3 Interfacial Tension and Contact Angle Measurements

3.3.1 Interfacial Tension (IFT)

The interfacial tension measurements of the oil-brine system were performed to evaluate the impact of ionic strength and brine salinity on the fluid-fluid interaction. CAM 2008-KSV equipment was used to determine the interfacial tension of dead crude oils with different saline solutions. It is accurate equipment that depends on the drop-shape analysis technique by using the LED light source. Figure 3.5 illustrates the main parts of the KSV instrument.

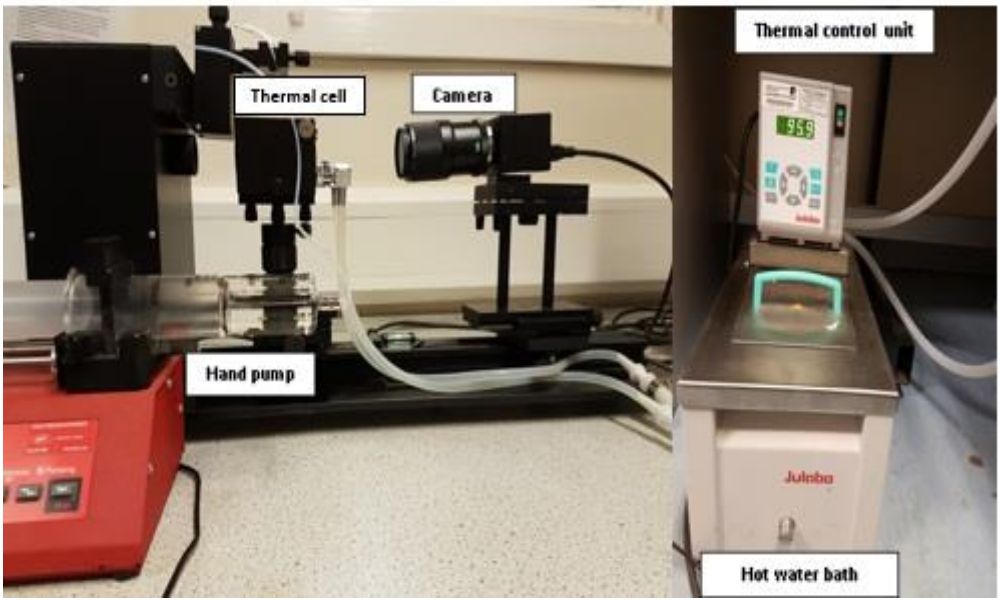

Figure 3.5: KSV pendant drop equipment.

To perform IFT measurements, a calibration test was run firstly by using a stainless-steel ball, which placed inside a glass vessel, filled with water. Then the position and the magnification of the camera were adjusted. This is considered an important step before starting the measurements, as insufficient pixels with poor accuracy could be obtained if the camera has

not been fixed well. To validate the equipment calibration, the interfacial tension of deionized water with air was measured with the value of 71.66 dynes/cm. For IFT measurements of oil/brine system, a hooked (U-shape) needle with an outer diameter of 0.7 mm was fitted with a micro syringe that filled with low density fluid (i.e., crude oil) and immersed in an optically clear thermal cell filled with the aqueous phase. The crude oil droplet was then manually injected upwards, and a stable pendant oil droplet was recorded by a camera, Figure 3.6. The same drop size of 12 µl was used for all experiments, which is the most crucial factor when the analysis depends on the Young-Laplace equation. Previous studies showed that an identical IFT value was obtained if the drop volume falls within the range of 7 µl to 30 µl [69]. A pendant drop shape was then processed by the software to fit the Young-Laplace equation, and the IFT values were determined using the following equation [121]:

$$\sigma_{ow} = \frac{\Delta\rho g d e^2}{H} \tag{3.1}$$

where σ_{ow} is the liquid/oil interfacial tension (mN/m), $\Delta\rho$ is the difference between crude oil droplet and the surrounding aqueous phase densities (kg/m^3), g is the gravitational acceleration (m/s^2), H is the drop-shape dependent parameter, and de is the equatorial diameter from the bottom line of the droplet (m).

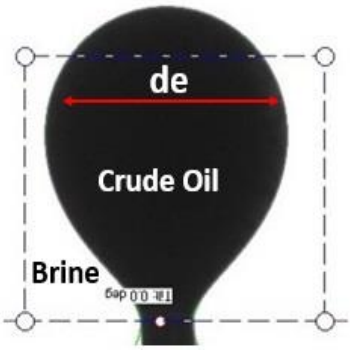

Figure 3.6: Schematic diagram of crude oil droplet at the tip of inverted needle.

A high IFT value was observed at the beginning of the test, and then it decreased gradually with passing times to reach a constant value which is commonly known as the equilibrium interfacial tension. The equilibrium IFT value was observed after about 30 minutes. The measurements were repeated several times for each oil/brine system, and a similar trend was yielded with the standard deviation of about ±2 unit. All the interfacial measurements were conducted at a high temperature (80°C) and atmospheric pressure.

3.3.2 Contact Angle

A goniometer (CAM 2008, KSV instrument Ltd. Finland) was used to determine the static contact angle of oil on carbonate rocks upon exposure to different saline solutions. Carbonate rocks and three types of dead oil with the properties given in sections 3.1.1.1 and 3.1.1.3 were used in the contact angle measurements.

For a reasonable estimation of contact angle, 10 core slices with the thickness of 0.5 cm were extracted from selected low permeability core plugs (outcrop and subsurface) to avoid the imbibition of the liquid when the drop attached to the rock surface. The rock slices were then ground using silicon carbide grinding discs-600 grit and a finer 1200 grit to reduce the roughness of the surface that can lead to the contact angle hysteresis. Next, the rock plates were saturated with synthetic formation water (200000 ppm) and left for 4 days. The rock slices were then dried in the oven for 48 hours at 70 °C. Finally, the rock plates were aged in the oil for 8 weeks to restore the wettability of the substrates (3 rock plates for crude oil A, 3 rock plates for crude oil B, and 3 rock plates for crude oil C). After aging, the slices were washed with Isopropyl alcohol (Sigma-Aldrich, purity grade > 99%) to detach the oil from the surface and left to dry in the air.

To measure contact angle, the sessile drop method has been used instead of the pendant drop method, since introducing the oil pendant

droplet to the surface submerged in the aqueous phase did not show a permanent attachment. The slices were first placed inside the cell, a sessile oil droplet of 10 µl was attached carefully to the surface using a pipette and left for 24 hours to attain the adsorption equilibrium with the surface. A drop size of 10 µl has been chosen to minimize the gravity effects on the drop shape [122]. Then, formation water was injected into the cell by using a hand pump until the rock slice is completely covered. Afterwards, the temperature of the water bath was set up at 80 °C, and the liquid cell was left for 1 hour to bring the sample to the desired test conditions. To ensure accuracy, the temperature inside the liquid cell was measured by a digital thermometer.

The sessile drop was monitored until the variation of the contact angle was insignificant, and a sequence of images was captured for the oil contact angle. The average value of the right and left contact angles was then calculated for each picture. The above procedure was repeated for the brines with different salinities, injecting in a sequential manner. The contact angle measurements were repeated for each rock slice/oil/brine system, and the values reported in this study represent the average of 5 separate droplets of crude oil at different locations on the same substrate with the standard deviation of about ±4°. Figure 3.7 illustrates a schematic diagram of the contact angle measurement [123].

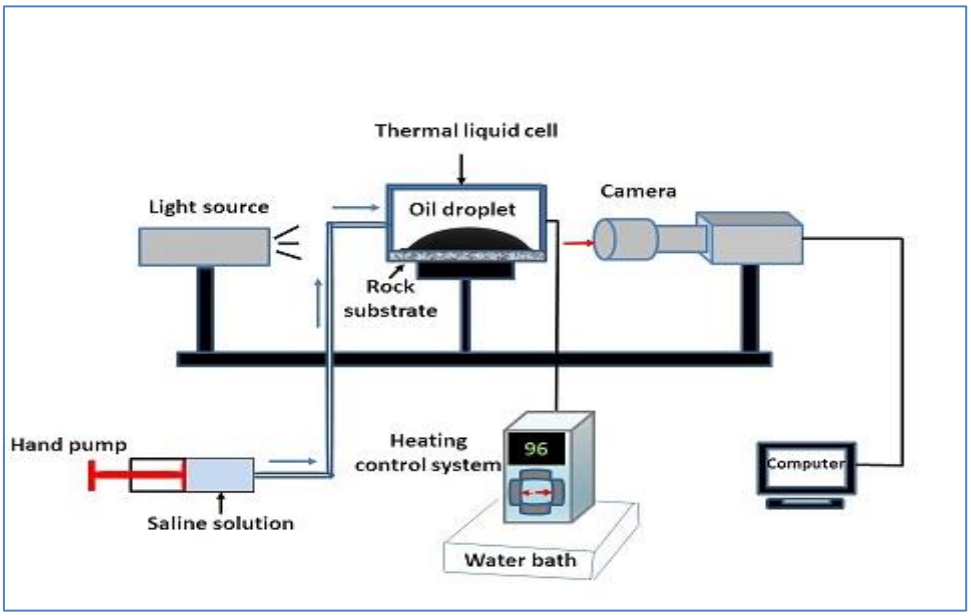

Figure 3.7: Schematic diagram of experimental setup for contact angle measurement.

3.4 Quartz Crystal Microbalance (QCM) Measurement

3.4.1 Principles and Calculations

In this study, a Q-Sense D300 was used to detect the adsorption/ desorption of crude oil onto/from the calcite and silica coated crystals. Figure 3.8 shows a schematic diagram of the Q-Sense. Q-Sense is a nanogram sensitive technique that used to detect the amount of substance adsorbed or desorbed onto/from a coated crystal [124]. The coated crystal consists of a single quartz crystal with two metal electrodes on each side. The crystal vibrates with a characteristic frequency when the electric voltage is applied, and Q-Sense measures the change in resonant frequency and dissipation energy of the coated crystals used. The change in frequency when the oscillating crystal exposed to an aqueous phase can be attributed to the mass loading, liquid loading, and liquid trapping.

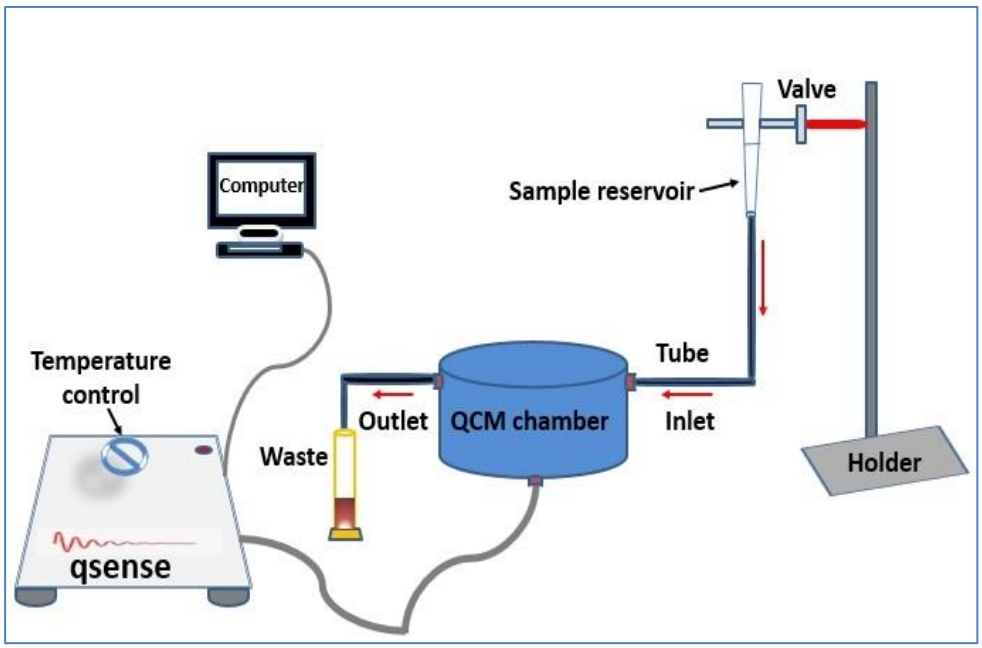

Figure 3.8: Schematic diagram of Q-Sense D-300.

The adsorbed mass of a thin and rigid adhering layer is determined by the Sauerbrey equation (Eq.3.2) [125]. When Newtonian fluids come into contact with the oscillating crystal, an additional shift in frequency is observed due to the change in density and/or viscosity of the medium (Eq.3.3) [126]. The liquid trapping effect can be neglected because of the atomic smoothness of the crystal surfaces. The principle calculations of mass and liquid loading are described by the following equations:

$$\Delta f_{ads.} = -\frac{n\Gamma_{QCM}}{C} \tag{3.2}$$

$$\Delta f_{liq.load} = -\sqrt{\frac{nf^3}{\pi\rho_q \upsilon_q}}\left(\sqrt{\rho_1\ \eta_1} - \sqrt{\rho_2\ \eta_2}\right) \tag{3.3}$$

where Γ_{QCM} is the adsorbed mass (mg/m^2), n is the harmonic number, C is the constant of quartz crystal (0.177 mg/m^2 Hz), f is the fundamental frequency of the crystal (5 MHz), ρ_q is the specific density of quartz (2650 kg/m^3), υ_q is the shear wave velocity in quartz (3340 m/s), ρ is the density

of solution, kg/m^3, and η is the viscosity of solution, kg/m.s. Subscription 1 and 2 refer to the solutions of different densities and viscosities.

3.4.2 Materials

To perform the experiments, the same crude oils and saline solutions that have been described in the previous section were used to assess the adsorption /desorption of oil by QCM-D. Calcite and silica crystals were used to mimic carbonates and sandstones. $CaCO_3$ (QSX 999) and SiO_2 (QSX 303) standard coated sensors were purchased from Q-Sense Biolin Scientific. The sensors consist of a quartz crystal disk with metal electrodes on each side. One of the electrodes was covered with thin surface layers to simulate either carbonate or sandstone minerals. The fundamental resonant frequency for the crystals is 5 MHz.

3.4.3 Experimental Procedure

Prior to each experiment, the sensor was immersed in 2 wt. % Hellmanex cleaning solutions for 30 minutes, and then washed several times with Milli-Q water to get the cleanest possible surface. Afterwards, the sensor was blow-dried with air duster removal and put in a UV-ozone chamber for 10 minutes. The chemical resistant tubes and QCM chamber were also cleaned with Milli-Q water and Iso-Propanol many times to remove any organic contamination. All adsorption /desorption QCM experiments were conducted at 22 °C.

In order to get a stable baseline, toluene was first injected. This was achieved by flushing toluene into the chamber for 20 minutes until the oscillation in frequency was about ± 2 Hz. After that, 2mL of dead crude oil was injected by gravitative flow into the chamber. After oil saturated the crystal surface and equilibrium was reached (30-50 minutes), toluene was injected again to detach loosely held oil components. Next, a high salinity solution represented by seawater was injected. Finally, different diluted versions of seawater were flooded sequentially through the QCM

chamber. When the frequency was stabilized for each particular solution (20-25 min), the changes in frequency were detected. The amount of desorbed oil after exposure to different aqueous salt solutions was calculated by the difference between the measured frequency shift and liquid loading shift due to the small difference in densities and viscosities, i.e., $\Delta f_{des} = \Delta f_{measured} - \Delta f_{liquid\ load}$. The desorption efficiency was calculated by (desorbed mass/adsorbed mass) x100. The measurements were repeated three times for each type of crude oil to ensure the accuracy and reliability of the results. The relative standard deviation of repeated measurements was less than 5%.

3.5 Atomic Force Microscopy (AFM) Force Imaging

3.5.1 Materials

The intermolecular interactions of polar components in crude oil with carbonate minerals at different levels of salinity were examined by using a Multi-Mode 8 SPM (Nanoscope V controller, Bruker). For AFM measurements, calcite crystals (Island Spar, Ward's Science, USA) were used as a model surface that could represent the most common mineral in carbonate. The calcite crystals were mechanically cut to small (10 mm) square plates with a thickness of 3 mm. The substrates were polished using AutoMet polisher and then re-polished by hand lapping process with 50 nm Aluminum oxide slurry to obtain smooth surfaces appropriate for AFM imaging. Figure 3.9A illustrates an example of the calcite substrate before and after the polishing process. Following the polish, the calcite surfaces were washed thoroughly in Milli-Q water and dried with a strong jet of nitrogen gas. EDX elemental analysis was carried out using integrated energy-dispersive X-ray spectroscopy (EDX, Oxford X-mass 80 SDD) to confirm the mineral composition of the substrate, Figure 3.9B.

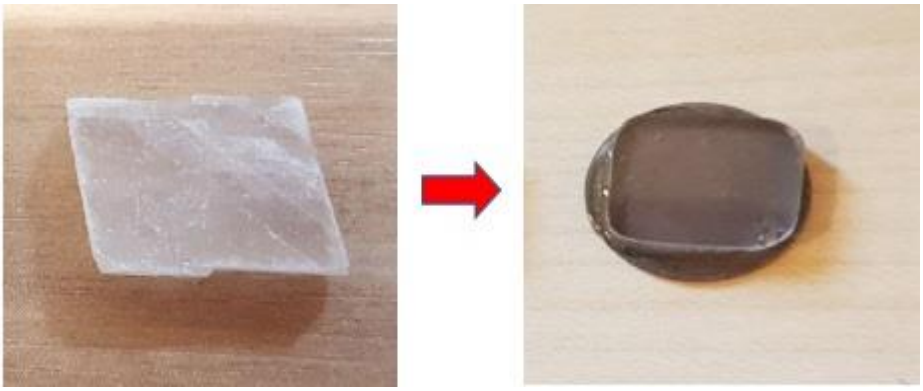

(A)

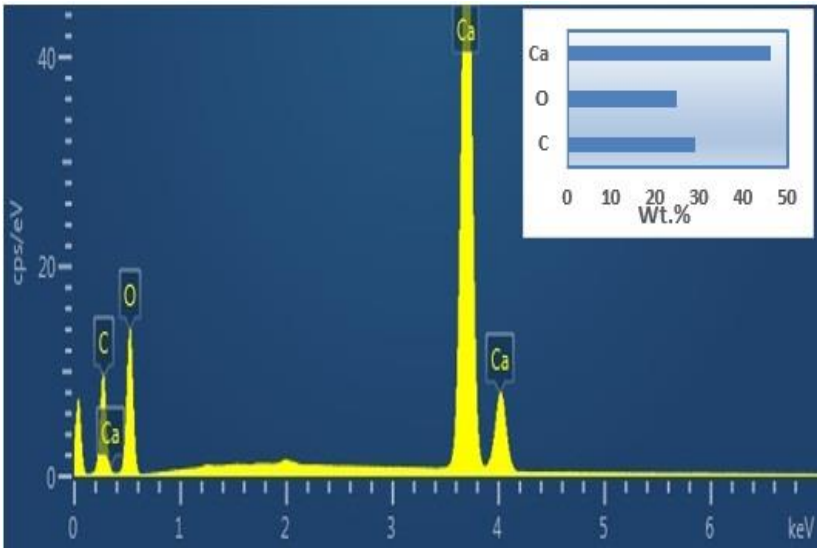

(B)

Figure 3.9: (A) Calcite substrate before and after the polishing process. (B) EDX spectrum with the elemental weight percentages.

The calcite surface was imaged in tapping mode using silicon probes (TESPA-V2) from Bruker, with a resonant frequency of 320 kHz and a spring constant (k) of 40 N/m. For force mapping, the probes were chemically modified with a –COOH termination (ST-PNP-COOH, Windsor Scientific), which represent the surface-active properties of crude oil. The tips were supplied with two different cantilevers with force constants of 0.08 N/m and 0.32 N/m. Each probe was rinsed in a small quantity of ethanol before use. The same synthetic brines with the properties given in Table 3.2 were used in the AFM work.

3.5.2 Principles and Calculations

Before starting the experiments, the deflection sensitivity was calibrated against the calcite surface, and the spring constant was evaluated using the thermal tune method [127]. An area of 10 µm x 10 µm was then mapped as an array of 32 x 32 force curves at a z-resolution of 1024 pixel with the scan rate of 1.5 Hz. Figure 3.10 illustrates an example of a force spectroscopy plot. The horizontal axis represents the vertical motion of the probe tip movements corresponding to the surface. As the tip descends toward the sample and the tip-sample distance decreases, the attractive electrostatic force near the surface transcended the cantilever spring constant, the tip clings to the surface, leading to deflection of the cantilever. The tip remains in touch with the surface until the maximum force of 685 pN was attained. It was then withdrawn from the surface and rebounded sharply upward to a certain distance (in this example, 160 nm). The minimum repulsion force, in this example, -940 pN, that needed to pull the tip away from the sample is known as the force of adhesion or pull off force. The adhesion force for each x, y point over the scanned area was determined by Hook's law (Eq.3.4) [128], and then plotted to construct the force maps as will be shown in Chapter 5.

$$\mathrm{F} = -k_c \times d \tag{3.4}$$

where F is the force applied to the cantilever (nN), k_c is the cantilever spring constant (nN/nm), and d is the cantilever deflection (nm).

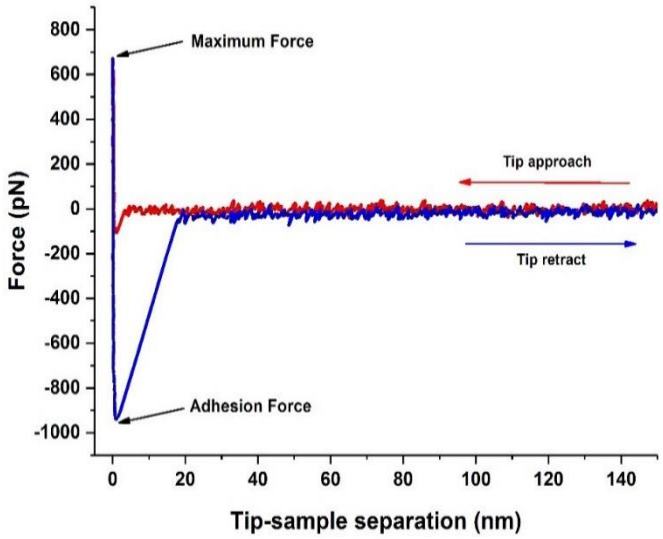

Figure 3.10: A typical force plot as obtained by AFM. The horizontal axis represents the vertical motion of the probe tip movements corresponding to the surface. The tip approach (Red), tip presses into the surface with a maximum force of 685 pN. The tip retracts (blue), tip breaks free of surface attraction. Adhesion force, is the minimum force required to move the tip away from the surface, - 940 pN in this test.

3.5.3 Experimental Procedure

To begin the AFM imaging experiments, polished calcite substrate, attached to steel AFM stubs was placed on the AFM scanner, and the height of the sample was adjusted to prevent the risk of a crash when the probe holder installed. The chemically modified probe was then loaded into the AFM fluid cell and given one final rinse of ethanol. Figure 3.11 shows the experimental setup and a schematic diagram for the AFM measurement. Next, 1 mL of super saline solution represented by formation water was slowly injected through the fluid cell using a micro syringe and flushed through. The probe and calcite plate were entirely immersed in the solution for 20 minutes to reach thermal stability before measurement. Three force maps were acquired on each sample in

succession (with each map taking 10-15 minutes) at fixed time points of 10, 30, and 50 minutes, to establish that the adhesion measurements were repeatable, and the sample was at equilibrium, and there was no further variation with exposure time. From the set of force maps collected, no variation in the adhesion values was observed over time. The solution was then replaced by seawater without moving the sample, allowing the acquisition of force maps on the same imaging area on the same calcite plate, with the same chemical probe whilst only varying the saline solutions.

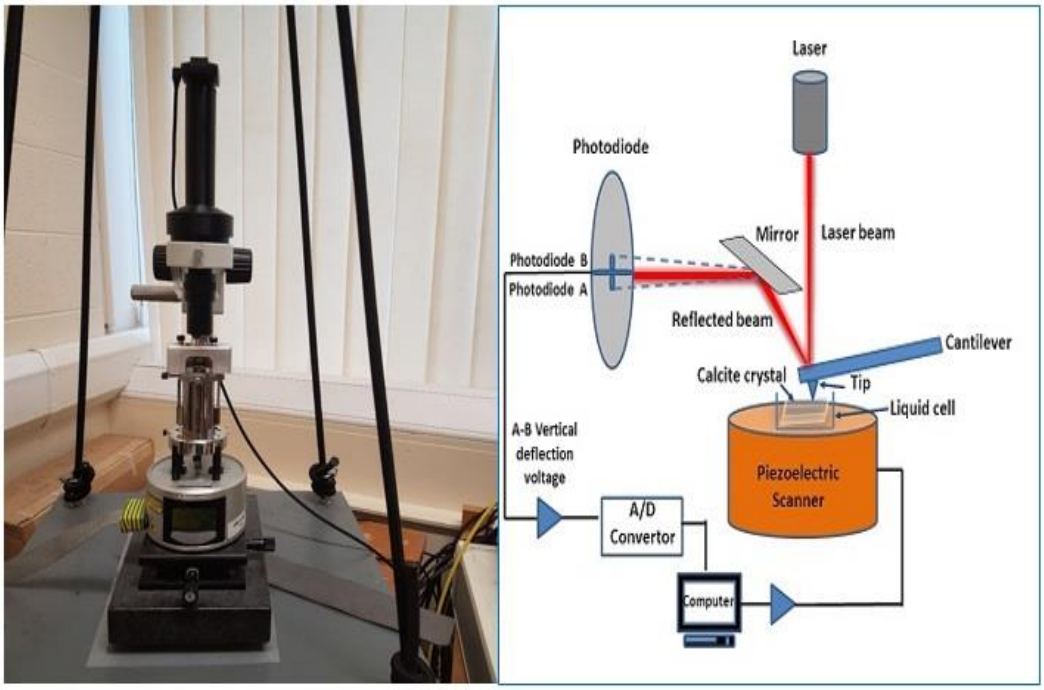

Figure 3.11: (A) Multi-Mode Nanoscope with a J-scanner. (B) A schematic diagram of the AFM measurement.

To change the solution, 1 mL of the saline solution was slowly flushed through the fluid cell volume, ensuring complete removal of the previous solution in the 100 µl sample area, and in the dead volumes in the tubing and inlet/outlet ports. This procedure was repeated several times, to be sure that the solution was properly replaced, and the conditions of the

new injected solution were attained. The above procedure was repeated for the brines with different salinities, and the solutions were sequentially exchanged, finishing with the lowest saline solution.

Topographical images of the calcite surface before and after exposure to saline solutions were collected in tapping imaging mode in the air at 22°C, but all force maps were acquired in the force-volume mode in the fluid at 26°C.

3.6 High Pressure-High Temperature (HPHT) Core Flooding Experiments

3.6.1 Materials

For macroscopic core flooding experiments, the same brines, crude oils, and rocks that have been used in the previous contact angle measurements were also used in this test. Further core analyses were carried out, including brine permeability, porosity, pore volume, and initial water saturation. The physical properties of the carbonate samples are summarized in Table 3.4.

Table 3.4: Petrophysical properties of outcrop and reservoir core samples used in core flooding experiments

Core ID	Rock type	K (md)	Bulk volume (cm^3)	Pore volume (cm^3)	Porosity (%)	S_{wi} (%)
EST-24	Outcrop	101	47.50	12.5	26.3	25
EST-25	Outcrop	115	47.97	13	27.1	24
EST-26	Outcrop	108	47.66	11.4	24	28
EST-30	Outcrop	90	47.65	12	25.2	23
EST-31	Outcrop	112	47.12	13.4	28.5	26
EST-33	Outcrop	120	47.50	14	29.4	30
EST-36	Outcrop	129	47.64	13.2	27.8	22
M-01	Reservoir	75	47.30	10.8	23	27
M-02	Reservoir	90	47.23	11	23.3	33
M-03	Reservoir	290	47.71	14.3	30.5	29

3.6.2 Experimental Setup

The core flooding experimental work was carried out by the author at the University of Edinburgh/Institute of Materials and Processes. A high pressure-high temperature core flooding setup was used for the oil/brine displacement in carbonate rock samples, as shown in Figure 3.12. The main parts of the system include a high-pressure core holder with an internal diameter of 1.5 inches, equipped with the rubber sleeve, two ISCO-100DM syringe pumps for oil and brine injection with the range of flowrate varied between 0.0001 to 25 ml/min, and a Milton Roy-CM4000 overburden pressure pump. For temperature control, a water path connected to the electrical heater was used, while a back-pressure regulator was connected to the outlet of the core holder to maintain the pore pressure to the desired test conditions. The differential pressure across the core sample was measured by pressure transducers (UNIK, 0-100 bar), and the data were recorded by the LabVIEW data acquisition. The produced liquids were collected using a graduated cylinder.

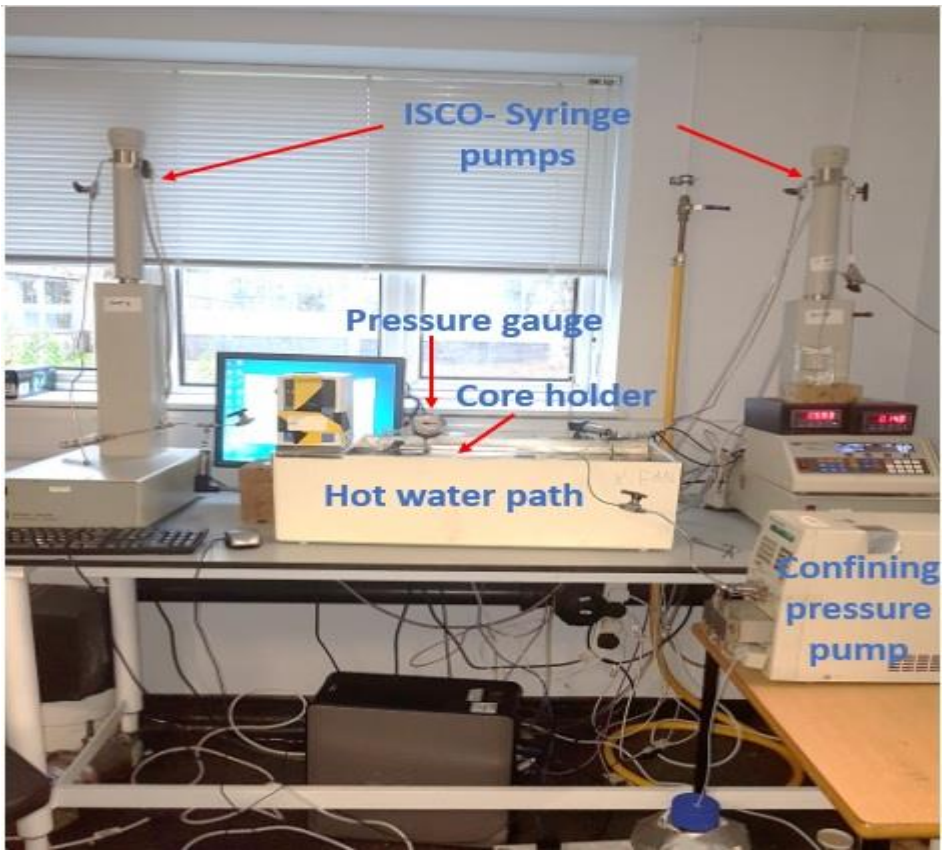

(A)

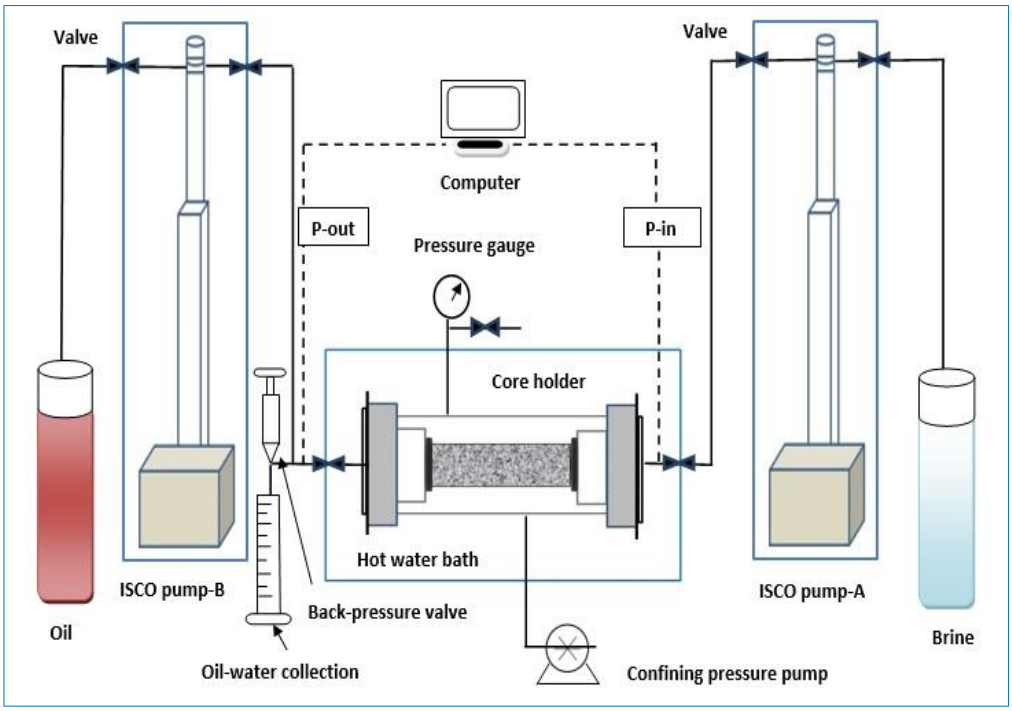

(B)

Figure 3.12: (A) Core flooding experimental set-up. (B) Schematic diagram for the core flooding system.

3.6.3 Experimental Procedure

Horizontal oil-brine macroscopic displacements were carried out to study the impact of low salinity water flooding on oil recovery under reservoir-like conditions (HPHT). Outcrop and reservoir carbonate core plugs with a diameter of 1 inch and a length of 3.5 inches were used. A standard core flooding experimental procedure has been followed for all the tested samples.

To begin with, 2 to 3 pore volumes (PV) of toluene were injected in the carbonate rock samples for cleaning, followed by washing thoroughly with methanol and deionized water. After that, the core plugs were dried in the oven for 48 hours at 100 °C. Clean samples were then saturated with formation water under vacuum for three days. To ensure that no air trapped in the pores and the porous media is completely saturated with formation water, the core plug was set into the core holder, and 4 PVs of

connate water were injected under a confining pressure of 115 bar and a constant injection pressure of 40 bar. The absolute brine permeability was then determined using Darcy's law. The pore volume of each sample was also estimated by determining the weight difference of the dried-saturated plug and the density of the formation water. Next, 3 PVs of dead crude oil were flooded at a constant pore pressure of 50-60 bar to displace the connate water and establish the irreducible water saturation (S_{wi}), see Table 3.4. To restore the wettability to an oil-wet condition, the core samples were put in a sealed container and aged in crude oil for 10 days at 80 °C. Figure 3.13 shows one of the core samples before and after the aging process.

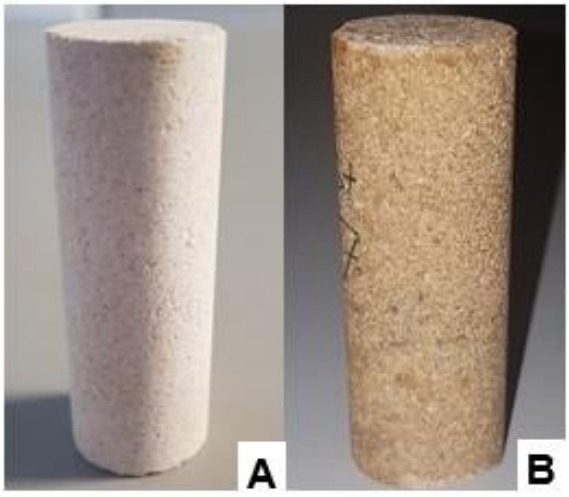

Figure 3.13: Carbonate rock sample (A) before aging in crude oil and (B) after aging in crude oil.

After the aging process, the core sample is enclosed in an elastic rubber sleeve and put into the core holder which was then loaded into the water bath. The temperature of the water bath was set up at 80 °C and the core holder left for two to three hours to bring the core sample to the desired test temperature. The injected pore pressure was maintained at about 82 bar using a regulator back pressure valve, whereas the confining pressure of 120 bar was applied to avoid the bypass of injection fluid. A high salinity

solution represented by seawater or formation water was then injected in a secondary mode recovery. Tertiary mode recovery was performed by sequentially injecting different diluted versions of seawater, finishing with the lowest saline solution. For each saline solution, 3 to 4 pore volumes were injected until the oil production is stopped. During the flooding process, the injection rate was kept low at 0.1 ml/min. To ensure that the residual oil saturation was reached, and all the movable oil was recovered, the injection rate was increased to 0.5 ml/min then to 1 ml/min, but no more oil was produced. The produced oil and differential pressure were determined. To verify whether these experimental observations were changeable, two cycles of core flooding experiments were performed for each type of core plug examined.

3.7 Microfluidic Measurements

3.7.1 Materials

To achieve this work, two-dimensional silicon glass and polymer-coated chips (45 × 15 mm^2; length × width) from Micronit were used to mimic natural hydrophilic and hydrophobic surfaces. The chip has a physical pore network to resemble a real physical rock pattern with the total internal volume of 5.7 µl, 50 µm channel width, and 20 µm channel height. The average porosity and permeability of the physical pore network are 0.57 and 2.5 Darcy, respectively. Figure 3.14 gives a schematic diagram of the physical pore network considered in this test. Saline solutions and crude oils that have been used before were also used in the displacements at the pore-scale.

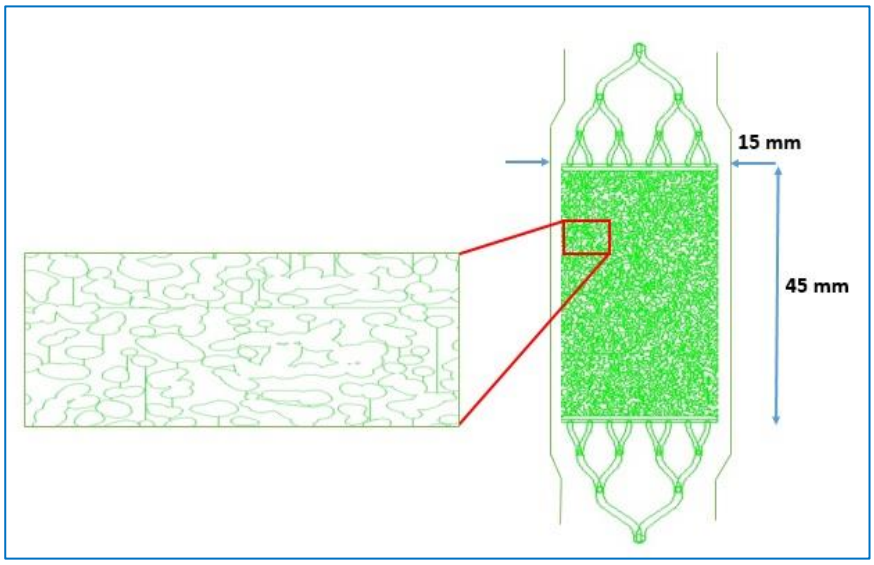

Figure 3.14: Schematic diagram of the physical structure micromodel with a small section magnification of the pores pattern. Pores are displayed in green and grains in white.

3.7.2 Experimental Procedure

In this work, the microfluidic apparatus was used to visualize oil displacement in porous media during secondary and tertiary flooding, as shown in Figure 3.15. The system consisted of a microfluidic solid casing to hold the chip with inlet and outlet ports, high pressure syringe pump (Nexus 6000) with a minimum flow rate of 0.0001 µl/min, PEEK tubing (OD= 1/16″, IDEX) to join the inlet of the chip to the pump, a controlling valve to control the direction of flow, and pressure transducers. A high magnification microscope (Olympus SZX16-ILLT) was used to visualize the chip with the view area up to 50 mm, which was outfitted with a digital camera (5 M pixel, Colour USP3 Vision, Sony Pregius IMX250, Canada) to capture digital images when the fluids flow along the pore channels. The images were recorded every 20 seconds by Point Grey Fly Cap 2 software.

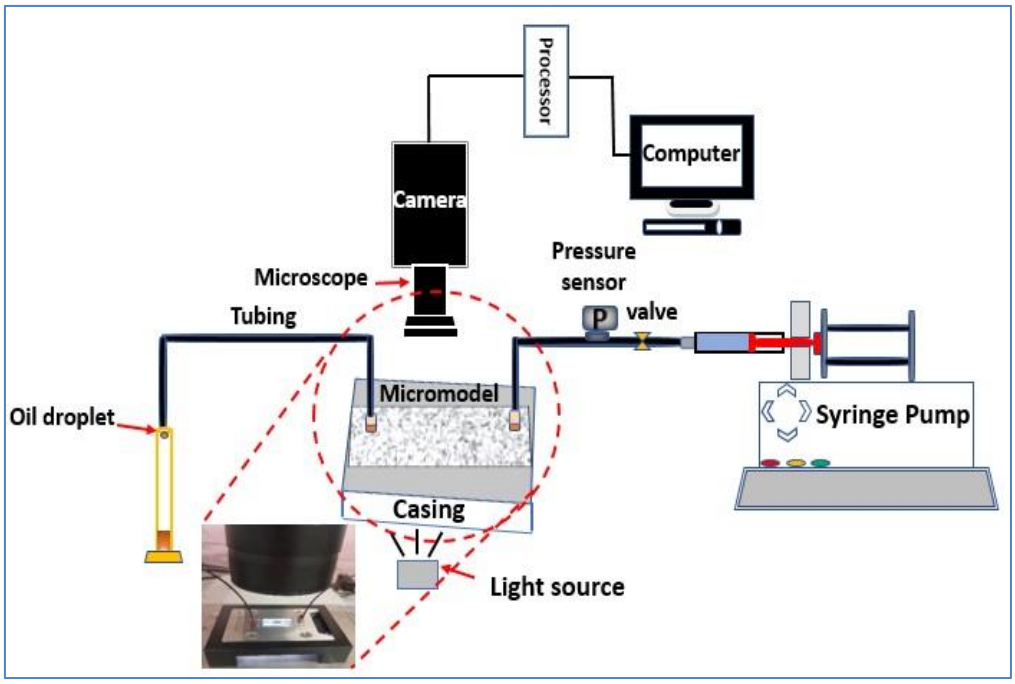

Figure 3.15: Schematic diagram of microfluidic system used in the experiments.

To perform the experiments, the microfluidic physical chip was put into the casing, and an isopropyl alcohol, IPA (Sigma-Aldrich, purity grade of > 99%) was first flushed through the chip to remove trapped air bubbles, followed by rinsing with a sufficient amount of Milli-Q water. Afterward, the clean pore network was saturated with a super saline solution (200000 ppm), representing formation water in the real reservoirs. Next, 10 pore volumes of dead crude oil were injected at a steady flow rate of 50 µl/hr to displace formation water and establish initial water saturation (S_{wi}). The saturated microchip was then left for about 24 hours to attain the adsorption equilibrium conditions.

To increase the distinction between high and low salinity solutions during the pore-scale displacement, a red tracer dye (Rhodamine B base, Sigma-Aldrich) was mixed with the injected low saline solutions. Seawater was then pumped in a secondary mode recovery, whereas tertiary mode recovery was performed by sequentially injecting different diluted versions of seawater through the microphysical chip. The low injection rate of 5

μl/hr was used in all cycles of the injection, representing the typical pore velocity (1 m/day) in real reservoir water flooding. After oil production is stopped, the flow rate was increased to 10 and 15 μl/hr for each cycle of brine injection to ensure that the remaining oil saturation was reached, and no more oil was visibly removed with the higher flow rate. For each stage of the displacement, the saline solution was continuously flooded for 6-12 hours. Optical images for fluid distribution were recorded at different stages of secondary and tertiary flooding. The pore-scale displacements were conducted at ambient temperature (23°C) and atmospheric pressure. For data reliability, the flooding tests were repeated two times for both microstructures examined.

3.7.3 Image Analysis

A set of digital images acquired during the displacement process were quantitatively analysed using image processing software FIJI to evaluate the quantity of oil recovered after each stage of brine injection. The digital images were first segmented to distinguish between solid and liquid phases. The oil-filled pore spaces were then identified by thresholding of its pixels' intensity, Figure 3.16B, and the oil area was represented totally by red, while non-oil zone appeared as black. After that, the images were binarized, and the pixels of oil were counted (see Figure 3.16C). The sweeping efficiency during brine flooding was determined by the following equation [129]:

$$E_m = \frac{1-S_{or}-S_{wir}}{1-S_{wir}} \quad (3.5)$$

where E_m is sweeping efficiency at the pore-scale level, S_{or} is residual oil saturation upon exposure to the saline solution, and S_{wir} is irreducible water saturation, i.e., the percentage determined when the chip was saturated with oil and before starting the displacement process. The *in-situ* contact angle was also assessed by a random selection of different

locations at the micromodels. The contact angle plugin in FIJI was used for this purpose, and the uncertainty in measurements was about ± 2°.

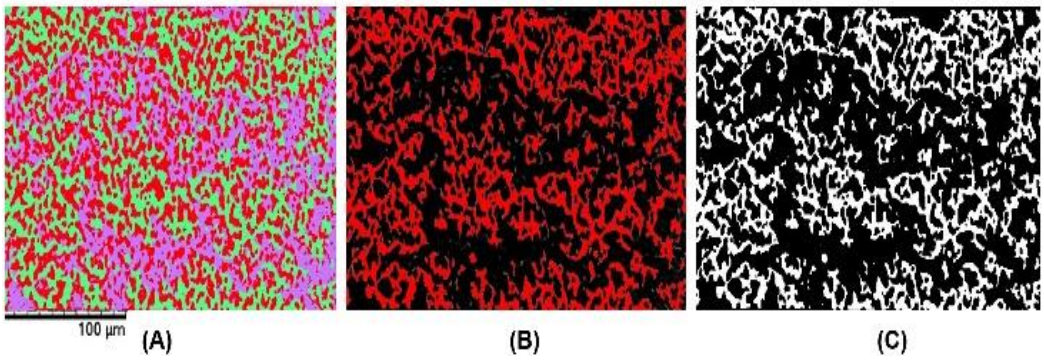

Figure 3.16: Typical example of the image analysis procedure by FIJI for determining the residual oil saturation after brine flooding. (A) Segmented image with red for grains, light green for oil, and pink for brine. (B) Image after thresholding to distinguish between oil phase in red and background in black. (C) Binary image with oil phase in white.

Chapter 4

Quantification of Wettability Characteristics for Carbonates Using Different Salinities

4.1 Introduction

As we alluded to in the literature review, injecting low salinity water could improve oil recovery in carbonate reservoirs through wettability alteration, whose mechanism, however, remains unclear. In this Chapter, the key parameters that govern the complex interactions of rock/brine/crude oil at the macroscopic scale are systemically investigated with the aim of finding a unified interpretation of possible wettability alteration mechanisms. The effect of crude oil composition on surface characterization upon exposure to different saline solutions is studied by using three types of dead oil with various acid numbers and two types of carbonate rocks (outcrop-limestone and subsurface-dolomite). The surface charges of carbonate rocks are first characterized by zeta potential measurement. Ions-substitution-adsorption is then evaluated using the infrared spectrometer (IFR) and energy-dispersive X-ray spectroscopy (EDX). Oil/brine interaction by means of the interfacial tension (IFT) is then measured. Contact angle as a function of oil composition, rock type, and salinity is also experimentally investigated under high temperature.

The obtained results are classified into six main sections. In the first section, we discuss the impact of ionic strength and brine salinity on the electrostatic charges of carbonate rocks. In the next part, the probable adsorption of potential determining ions into the carbonate surfaces will be demonstrated. The effect of salt concentration, oil composition, and types of cations on interfacial tension (IFT) activity will be then clarified in sections three and four, respectively. In the following section, the detailed effects of active polar components and salinity on the wetting state of

carbonates will be extensively explained. In the final section, the wettability alteration mechanisms will be discussed.

4.2 Effect of High and Low Salinity on Rock Surface Charges

It was found that the change in surface charge of the minerals is one of the proposed mechanisms for wettability alteration in carbonates during low salinity flooding. Carbonates display complex behaviour in the aqueous media mainly because of its solubility, which is dominated by surface electrical charge and chemical equilibrium [80]. As mentioned in Chapter 2, the surface electrical charge is characterized by zeta potential, which is strongly affected by the pH and ionic strength. The current investigation involved measuring the surface potential of limestone and dolomite particles in different saline solutions at ambient temperature, aiming to evaluate the effect of ionic strength and brine salinity on surface electrical change. For the pH effect, the results of the previous work have been considered to understand the electrostatic behaviour of carbonate minerals in deionized water at different pH.

The effect of pH on the surface electrical charge of carbonate minerals has been studied by some researchers [22,80,82,130]. For instance, Kasha et al. [82] measured the zeta potential of pure calcite particles in deionized water over a wide range of pH (3.5-11.5). Their results showed that the isoelectric point (IEP) for calcite surface was observed at pH 5.4. The sensitivity of zeta potential of dolomite particles to pH was also evaluated by other researchers [131,132]. It is found that the isoelectric point (IEP) of pure dolomite is within the range of pH 6.3-8. It has also been reported that at high pH value the concentration of Mg^{2+} $(OH)^{+}$ will be less than that of HCO_3^-, and thus the electrokinetics of dolomite particles become more negative [133].

The zeta potential values of limestone and dolomite particles in formation water, seawater, and different dilution versions of seawater were measured at pH 8. The measured values as a function of elapsed time for different saline suspensions are given in Appendix A. While the averaged zeta potential values of these measurements are shown in Figure 4.1. It can be seen that the zeta potential of limestone and dolomite particles was positive (+10.37 mV and +6.96 mV) in formation water, which represents the highest brine concentration (200000 ppm) used in this study. This result is consistent with the findings from Mahani et al. [81] that the zeta potential for the different types of carbonate particles in high salinity water is positive due to the high concentration of Ca^{2+} and Mg^{2+} ions, leading to a shrinkage of the EDL and shift of the zeta potential to a positive value. In comparison, the zeta potential of limestone particles in seawater was less positive than formation water (+3.6 mV) at the same pH value, while the value overturned to negative (-3.73 mV) for dolomite particles. This could be attributed to the reduction in the total dissolved solids (43650 ppm) and an increase of the concentration of the SO_4^{2-} ions in seawater, which is supported by the previous studies [5,47,82].

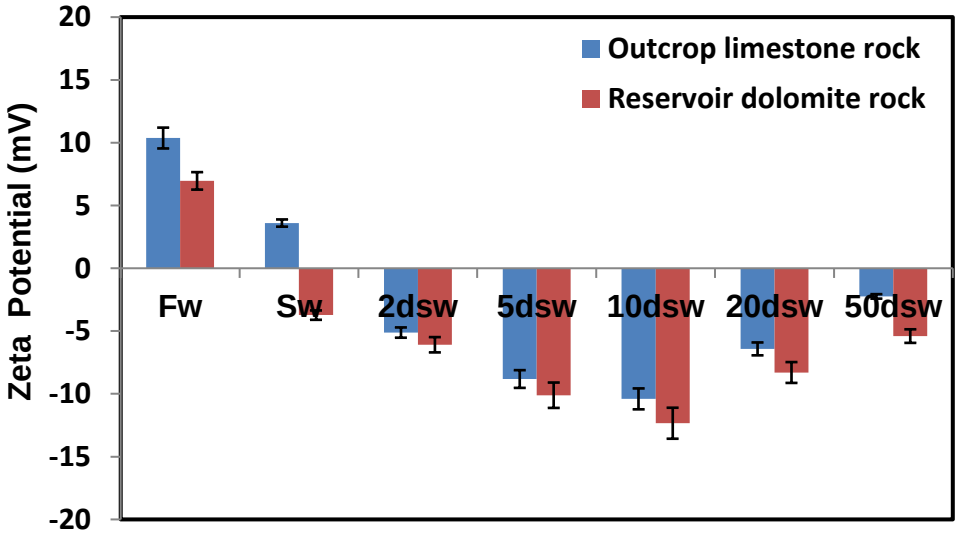

Figure 4.1: Averaged zeta potential of calcite and dolomite particles in high and low salinity solutions at pH 8.

The results also reveal that the magnitude of the negative charges generally increases as the salinity and ionic strength of suspensions decreases up to 10 times dilution. For instance, the zeta potential of limestone and dolomite particles for twice-diluted seawater was -5.12 mV and -6.09 mV, respectively, and it reached to -10.62 and -12.3 mV at 10 times dilution. It is logical that as the salinity of suspension decreases, the adsorption of Mg^{2+} and Ca^{2+} ions surrounding the particles decreases with continuous adsorb of SO_4^{2-}. This leads to the expansion of the EDL and an increase in the magnitude of the negative surface charges [81]. However, further brine dilution causes more reduction in the concentration of SO_4^{2-} and therefore less negative charges were observed, i.e., a zeta potential of -2.24 mV and -5.4 mV were obtained for limestone and dolomite suspensions, respectively at 50 times dilution. Alotaibi et al. [80] also confirmed that less negative charges were observed by using aquifer water without sulphate at a certain pH.

It is also evident from the results that, the subsurface dolomite particles are more negatively charged than outcrop limestone particles. This could be linked to the presence of dissolvable anhydrite ($CaSO_4$) as a part of the rock material, as was mentioned in section 3.1. This could provide an *in-situ* source of sulphate ions, affecting the net surface charges, and therefore more negative charges on dolomite sites would be expected as the salinity was decreased. Another possible explanation could be that the dolomite particles used in this study have a large specific area (1.25 m^2/g) compared to that of limestone (0.56 m^2/g). Therefore, it is expected that the reaction surface of dolomite molecules would be larger and consequently, high negative surface charges have been reported. A study performed by Vdovic [134] showed that a significant difference in the zeta potential values was observed for the two synthetic calcite samples, having a different surface area. He concludes that the specific surface area and grain size could affect the magnitude of electric charges or energy stored on the calcite surface.

4.3 Scanning Electron Microscopy and Infrared Spectroscopy Results

As reviewed in Chapter 2, many previous studies proposed that wettability alteration of carbonates during seawater flooding is mostly because of the potential determining ions adsorption into the positively charged rock surface, i.e., mutual interactions between Ca^{2+}, SO_4^{2-}, and Mg^{2+} occurred at the rock surface, leading to improving the electrostatic repulsion forces [12,41,135]. To validate whether such a hypothesis is relevant to the low salinity flooding or not, IFR absorbance of fresh limestone and dolomite particles prior to coming in contact with saline solutions was first measured, as the basis for differentiation with those treated with seawater and different diluted versions of seawater. From Figure 4.2, it can be clearly seen that the same general pattern of the IFR spectrum is observed for the particles before and after treatment. However, there is a variation in the intensity of absorbance between the fresh and aged particles.

It is also obvious that there is a substantial decrease in the intensity of C-O stretching vibration at 1391-1392 cm^{-1} as well as in that of the bands located at the 871 cm^{-1} and 712 cm^{-1}. This might be due to the chemical substitution of the CO^{3-} and Ca^{2+} ions by the anions and cations that adsorbed from brines on the mineral surface. It has been previously reported that any change in the strength of the corresponding peaks of the specific absorption bands could be referred to the gain or loss of the particular compounds [136]. The additional small peak between 620-680 cm^{-1} of the wavenumber, represented by red stippled lines, Figure 4.2, can give an indication that the sulphate adsorption had happened on the mineral surface after treated with seawater and different diluted versions of seawater [47,137]. On the other hand, Fig. 4.2C specifies that no sign of SO_4^{2-} bending band in the range of 620-680 cm^{-1} when the limestone minerals exposed to 20dSW and 50dSW. It seems likely that no sulphate molecules adsorbed on the mineral surface as the sulphate concentration decreased with the further dilutions. Previous studies stated that the

catalytic agent sulphate is created in the matrix because of the dissolution of anhydrite. These findings confirm the above zeta potential measurements for limestone rock that less negative charges were observed when 20dSW and 50dSW were used.

For dolomite particles, Figures 4.2D, E, and F show that SO_4^{2-} bending band at 620-680 cm^{-1} is relatively more intense for treated dolomite surface compared with that of treated limestone surface. A possible explanation for this observation could be that the treatment of dolomite surface with various saline solutions can lead to the adsorption of sulphate ions on the surface, as dolomite mineral contained anhydrite in their crystalline lattice, which could cause a further increase in the intensity of the SO_4^{2-} bending band of dolomite compared to the limestone. In addition, inspection of Figures 4.2D, E, and F indicate that there is a symmetric vibration band at the wave number of 842 cm^{-1} for all treated dolomite particles, which is referred to the $MgCl_2$ compound [137]. This gives sufficient evidence that magnesium adsorption was taken place on the dolomite surface after exposure to various saline solutions, which might substitute calcium ions on the surface, leading to a decrease in the strength of the carbonate absorption bands.

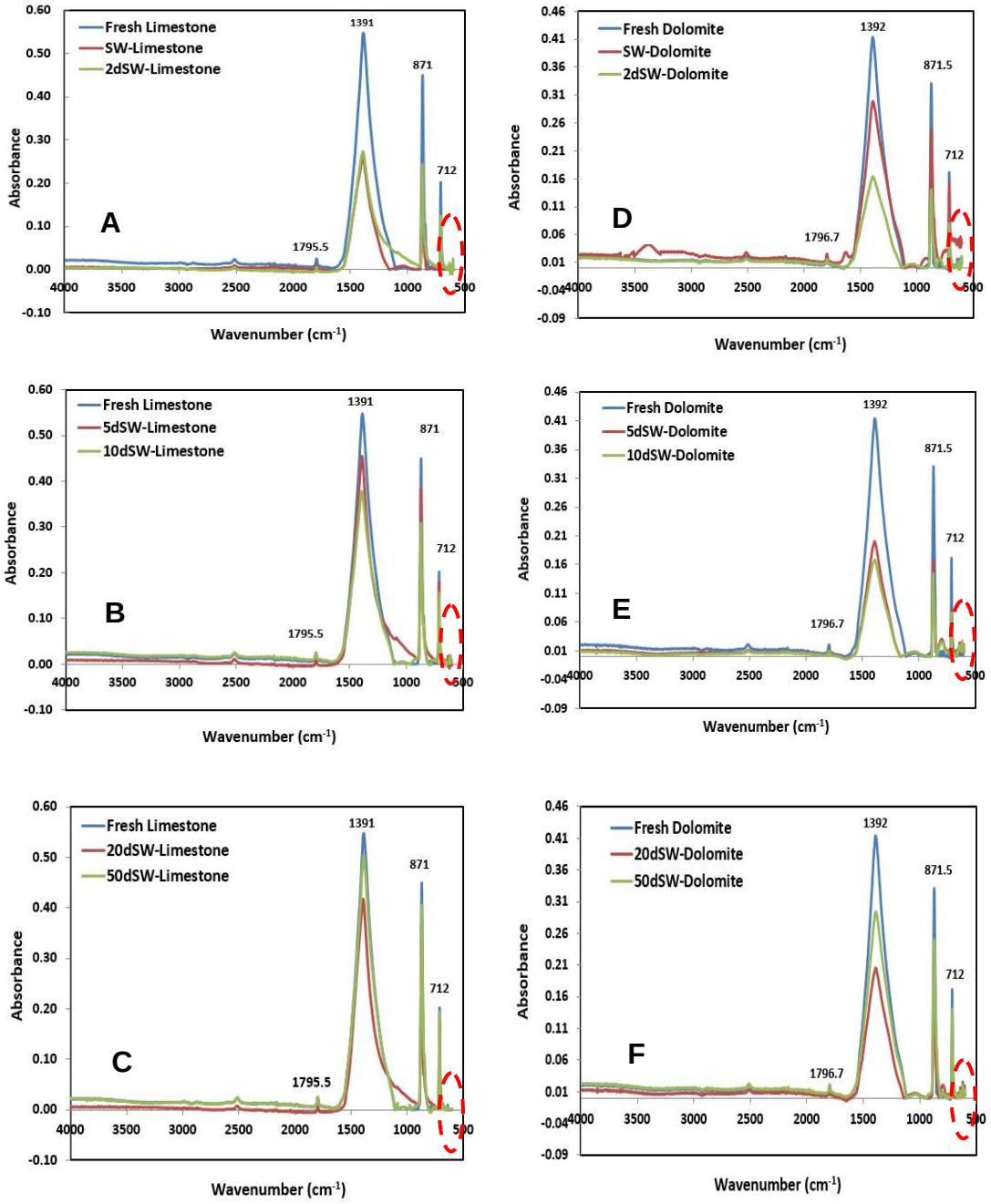

Figure 4.2: Infrared spectra of fresh and treated limestone and dolomite particles.

To further investigate the possible adsorption of potential determining ions into the carbonate surface, a second set of experiments have been conducted using EDX elemental analysis apparatus. The elemental analysis of the fresh carbonate minerals prior to coming in contact with the saline solutions were taken as the basis sample with which all other

samples that exposed to brines were compared, Fig 4.3A. Figures 4.3B-D show a typical example for the EDX spectra and the elemental analysis for the outcrop limestone grains after exposure to seawater, 2dSW and 5dSW.

Apparently, the same general pattern of the EDX spectrum was observed for the limestone grains before and after treatment. However, there are additional small peaks were detected, referring to the elements of sulphate, sodium, chloride, and magnesium with the various weight proportions. It is highly probable that these compounds came from the saline solutions that were come in contact with the carbonate surfaces [41]. Similarly, the EDX analysis was performed for fresh dolomite particles (Fig 4.4A) and those aged in different saline solutions, Figures 4.4B-D. From the weight composition proportions, it is obvious that the concentration of sulphate ions is relatively higher than that of limestone particles aged in 2dSW. As mentioned earlier, this could be linked to the presence of dissolvable anhydrite ($CaSO_4$), as a part of the dolomite particles material, leading to an increase in the weight proportions of this compound.

Another possible explanation could be that the dolomite particles have a large specific area (1.25 m^2/g) compared to that of limestone (see section 3.1). Therefore, it is expected that the reaction surface of dolomite molecules will be larger and consequently, more ions could be adsorbed on the surface [134]. The SEM images also displayed clear morphological changes over the limestone and dolomite grains upon exposure to saline solutions, which could be related to the adsorbed salt on the surface of the grains. Thus, the SEM and EDX elemental analysis provides compelling evidence that chemical interactions between carbonate minerals and surrounding brine had likely happened, which could affect the net surface charges of carbonates.

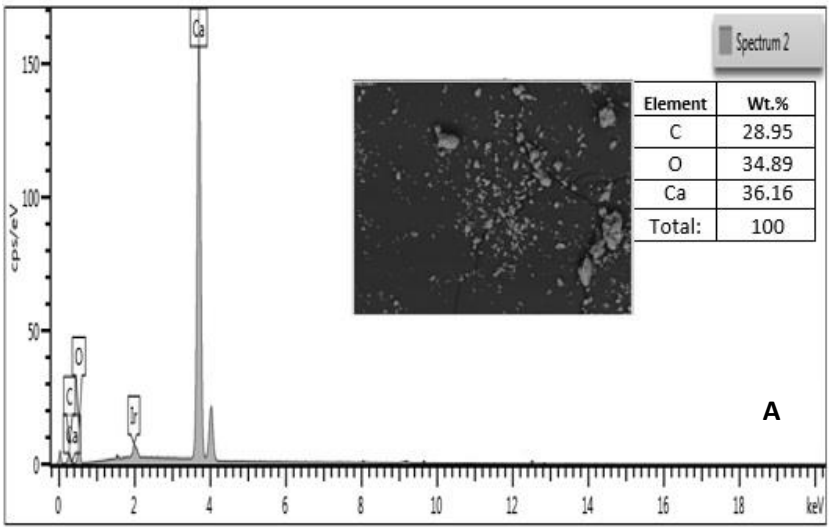
Spectrum 2
Element Wt.%
C 28.95
O 34.89
Ca 36.16
Total: 100
A
cps/eV
keV

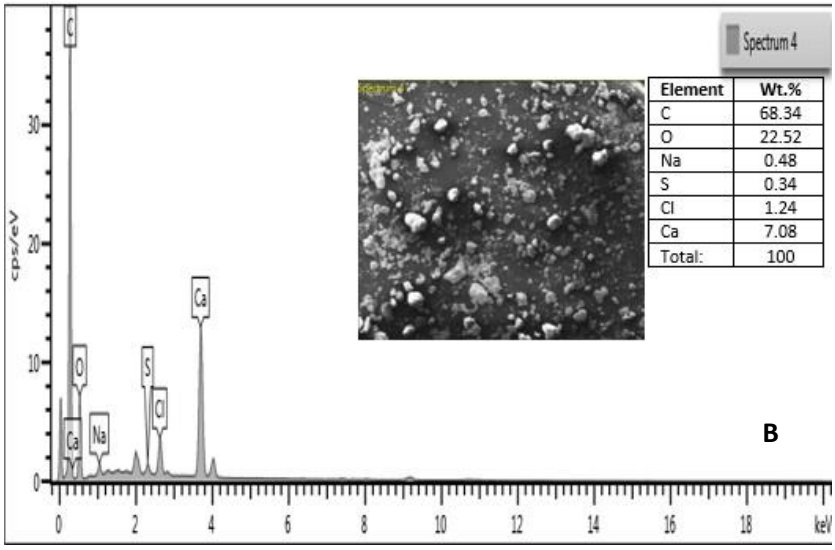
Spectrum 4
Element Wt.%
C 68.34
O 22.52
Na 0.48
S 0.34
Cl 1.24
Ca 7.08
Total: 100
B
cps/eV
keV

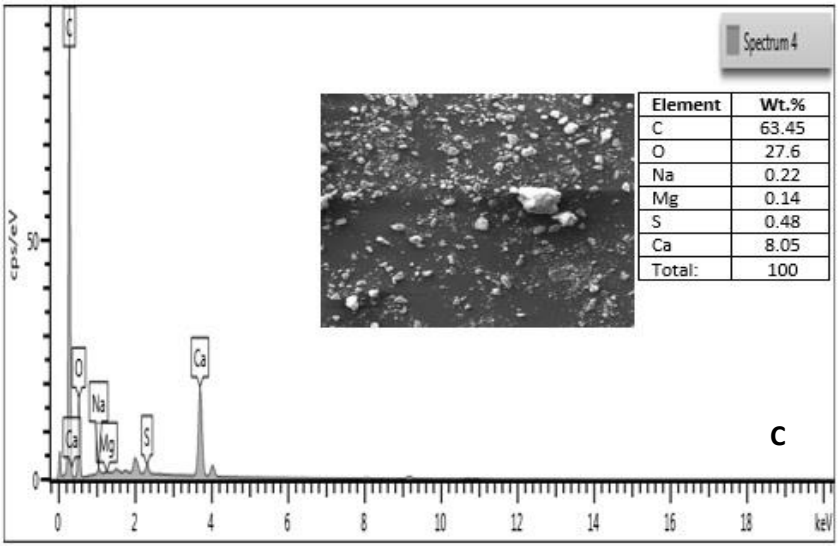
Spectrum 4
Element Wt.%
C 63.45
O 27.6
Na 0.22
Mg 0.14
S 0.48
Ca 8.05
Total: 100
C
cps/eV
keV

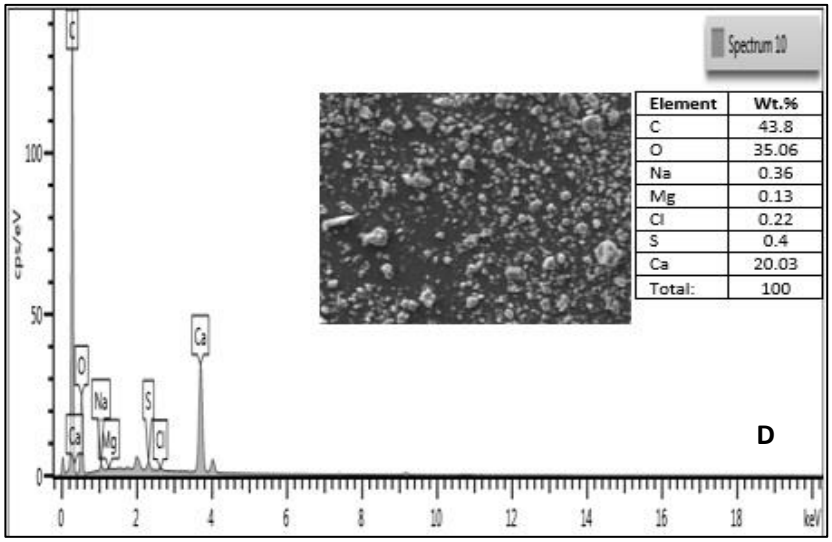

Figure 4.3: SEM and EDX elemental analysis for (A) Fresh limestone, (B) particles aged in SW, (C) particles aged in 2dSW, and (D) particles aged in 5dSW.

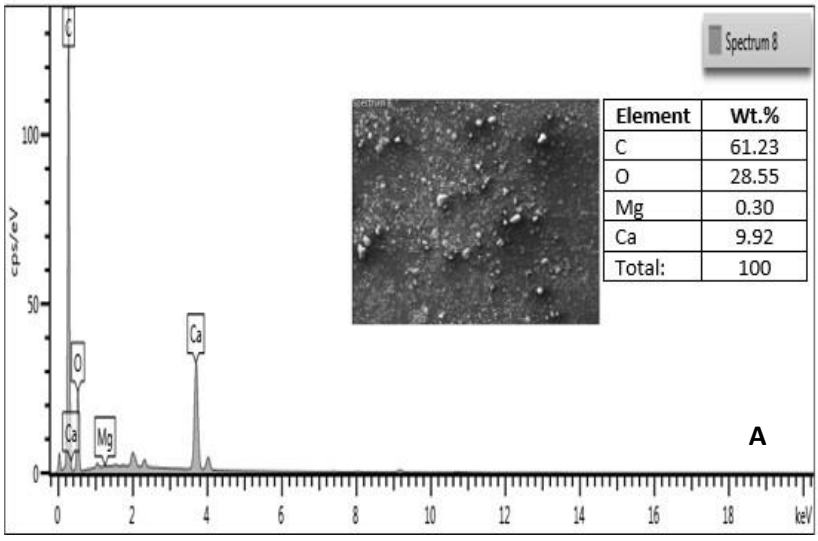

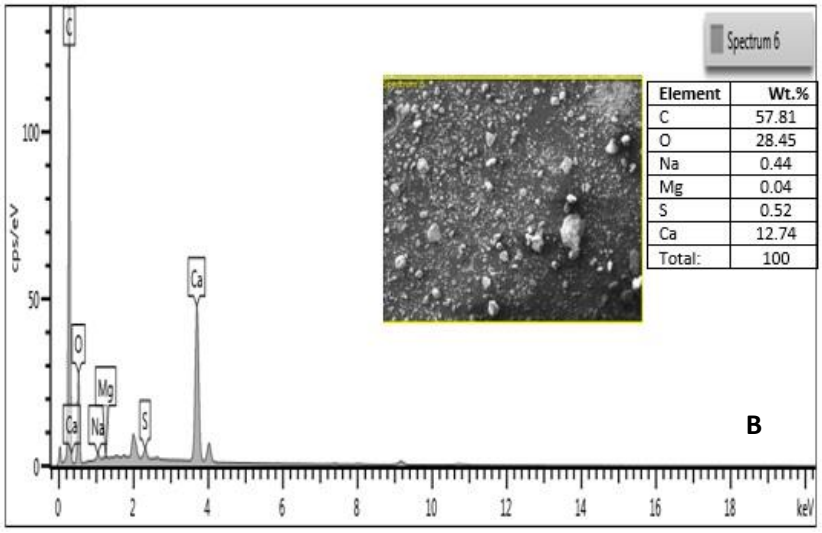

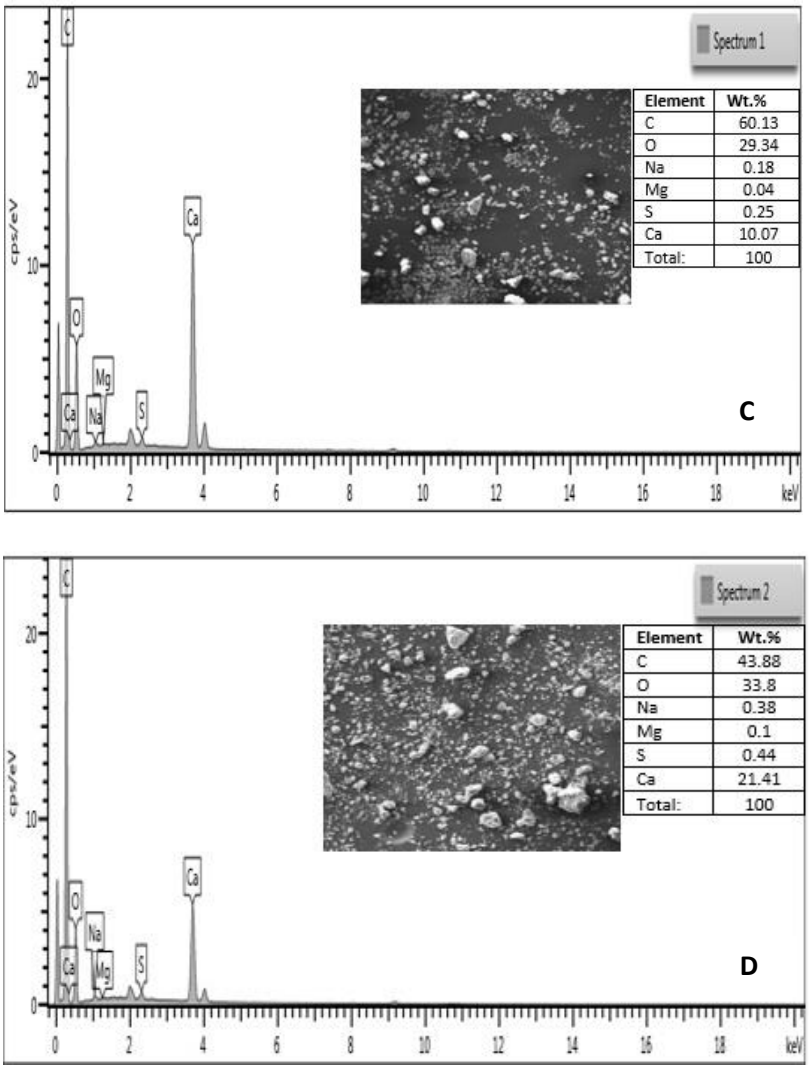

Figure 4.4: SEM and EDX elemental analysis for (A) Fresh dolomite, (B) particles aged in SW, (C) particles aged in 2dSW, and (D) particles aged in 5dSW.

4.4 Interfacial Tension (IFT) as a Function of Brine and Oil Composition.

IFT measurements were carried out between different dead crude oils and compound aqueous phases to examine the impact of salinity and the presence of polar organic components in crude oil on the IFT variation. The obtained IFT results are illustrated in Figure 4.5, and the averaged values of equilibrium IFT are summarized in Table 4.1.

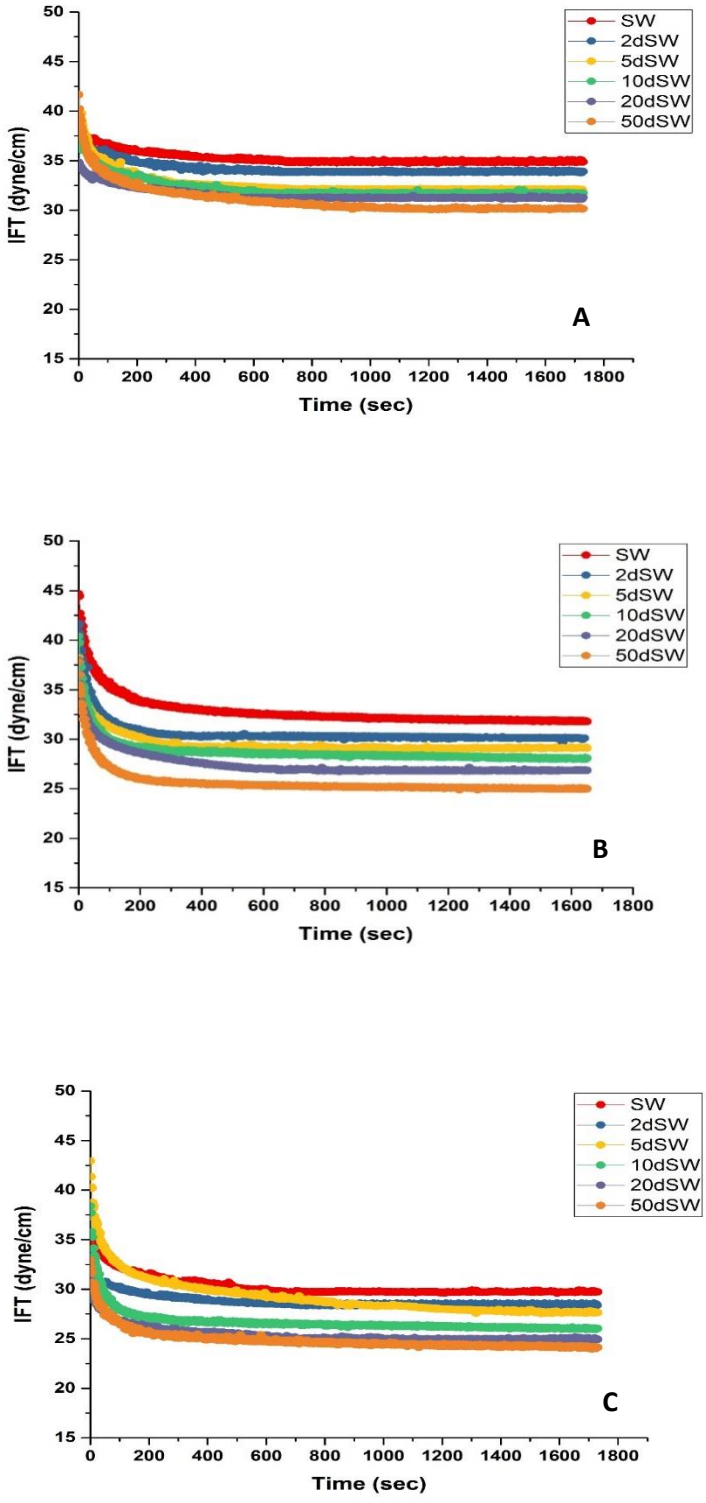

Figure 4.5: IFT measurements as a function of brine salinity for (A) Crude oil A. (B) Crude oil B. (C) Crude oil C.

Table 4.1: Equilibrium IFT values of different brines and crude oils examined.

Brines	IFT (dynes/cm) Crude Oil A	IFT (dynes/cm) Crude Oil B	IFT (dynes/cm) Crude Oil C
Formation Water	37.5	35	34
Seawater	34.6	31.8	29.7
2 diluted seawater	33.7	30.5	28
5 diluted seawater	32.8	29.5	27
10 diluted seawater	31.7	28.8	26
20 diluted seawater	31	27	25
50 diluted seawater	30.6	25.7	24

It is evident that the IFT values decreased steadily as the salinity of water declined. Hence replacing formation water with seawater promotes IFT drop by about 2.9, 3.2, and 4.3 units for crude oils A, B, and C, respectively. Further reduction of 4-6 units was observed when seawater was changed to 50dSW for the three kinds of crude oils used. This can be attributed to the salting-out effect, so at a very high salt concentration, the solubility of polar organic components of oil in aqueous phase decreases causing an increase in the IFT value [67,93]. On the other hand, minor IFT decrease (0.4-1 dynes/cm) was obtained under different dilution proportions of seawater. This trend is in line with previously discussed work by Yousef et al. [10].

From Table 4.1, it is clear that the IFT values for crude oil C are relatively less than those of crude oil A and B. According to the elemental analysis (Table 3.3), crude oil C has a higher mass ratio of hetero-atoms than crude oil A and B. This means that an alteration in the fluid/fluid interactions occurred when the oil solvent character changed. It has previously been reported that the hetero-atoms play a vital role in interfacial activity since they can transfer from bulk solution and accumulate at the oil-water interface acting as a weak to moderate ionic

surfactant [74,138,139]. It should, however, be noted that the activation of the acidic species causes more reduction in IFT values compared with activation of basic species [79]. This means that more acidic components present in the interface region the positive IFT contribution will be obtained.

The results acquired in this study are consistent with Skauge et al. [140] findings that a significant reduction in IFT values was reported for oil with the highest acid number. In addition, the light crude oils A and B have a higher resin to asphaltene ratio (15.90 and 13.17) compared to the heavy crude oil C (resin/asphaltene ratio =1), see Table 3.3. Therefore, the interface of light oil/brine was more affected by the resin fraction than the asphaltene fraction. The previous study by Lashkarbolooki and Ayatollahi [75] showed that the IFT of crude oil as a function of salinity mainly affected by the wt. % of asphaltene and resin fractions and resin had less surface excess activity as the salt concentration increased, thereby less contribution to decreasing the IFT of light oil/brine system. We can thus expect higher IFT values when crude oil A and B were used compared to crude oil C with almost the same resin/asphaltene ratio, showing the determining impact on the IFT, and therefore more IFT contribution.

Given the minor decrease in the IFT values for all crude oils tested, it is found that the changes in the IFT of the crude oil/brine system would not contribute to any considerable alterations in the capillary forces when brine composition is changed [123].

4.5 Interfacial Tension (IFT) as a Function of Monovalent and Divalent Cations

In this section, the effect of monovalent and divalent ions on IFT was studied with the aim of examining the probable synergism between the type of salts and the polar surface components of crude oil. The IFT between crude oil C, which contains the highest amount of active polar components and monovalent ($NaCl/Na_2SO_4$) or divalent ($MgCl_2/CaCl_2$)

ions was measured. Figure 4.6 shows the measured IFT as a function of various concentrations of monovalent and divalent ions. The summary of IFT results for the four types of salts examined is illustrated in Figure 4.7. It is evident from the results that no clear trend for IFT values was noticed for NaCl and Na_2SO_4. It appears that monovalent ions did not have a considerable contribution to the IFT activity. The obtained results extend those of previous studies, confirming that monovalent salts have less affinity to interact with polar organic components (asphaltene and resin) present in the oleic phase, resulting in no noticeable IFT variation [74,141].

In the case of divalent ions, similar behaviour was observed for $MgCl_2$ and $CaCl_2$ saline solutions, since the IFT gradually decreased as the divalent concentrations increased. These observations are likely linked to the tendency of Mg^{2+} and Ca^{2+} cations to interact with the natural polar compounds creating positive complex ions, which are preferably soluble in the aqueous phase and thus further decrease in the IFT values obtained [142,143]. It should, however, be noted that $MgCl_2$ solution showed more reduction in IFT compared with the $CaCl_2$ solution. This observed trend could be explained by Mg^{2+} cations have high affinity to interact with the oxygen-atom in the asphaltene than that of Ca^{2+} cations [42]. Brandal et al. [142] also found that the difference in the degree of hydration between Mg^{2+} and Ca^{2+} cations could affect the IFT activity. Since magnesium attaches six water molecules compared to the two molecules for Ca^{2+}, consequently the magnesium-complex ions would be preferable to dissolve in the water phase, leading to more decrease in IFT values.

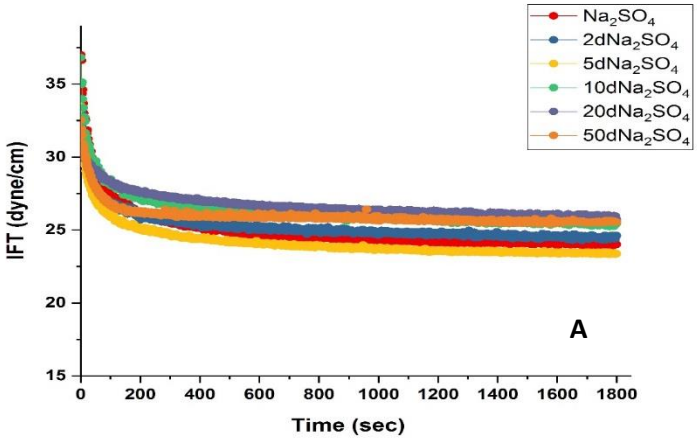
Na_2SO_4
$2dNa_2SO_4$
$5dNa_2SO_4$
$10dNa_2SO_4$
$20dNa_2SO_4$
$50dNa_2SO_4$
IFT (dyne/cm)
Time (sec)
A

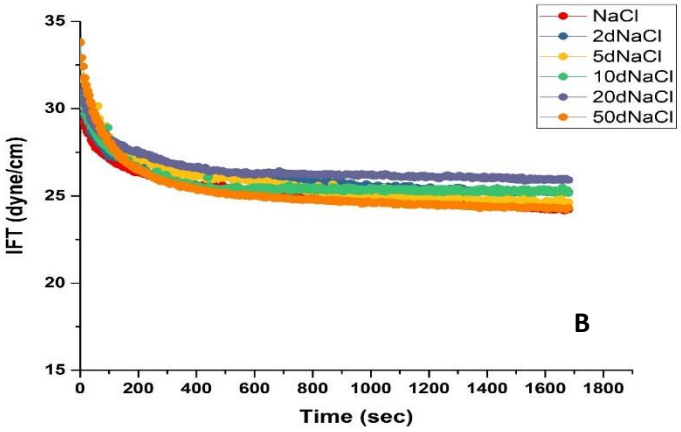
NaCl
2dNaCl
5dNaCl
10dNaCl
20dNaCl
50dNaCl
IFT (dyne/cm)
Time (sec)
B

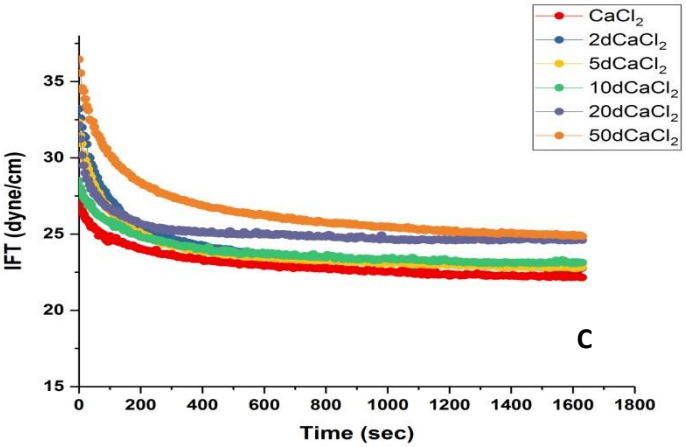
$CaCl_2$
$2dCaCl_2$
$5dCaCl_2$
$10dCaCl_2$
$20dCaCl_2$
$50dCaCl_2$
IFT (dyne/cm)
Time (sec)
C

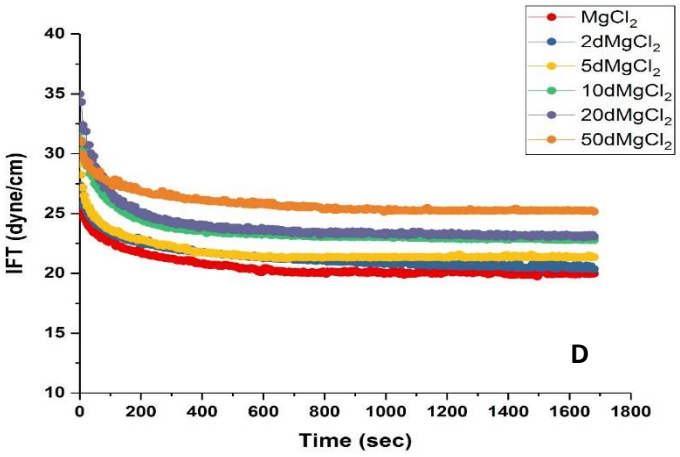

Figure 4.6: IFT measurements as a function of monovalent and divalent cations for crude oil C.

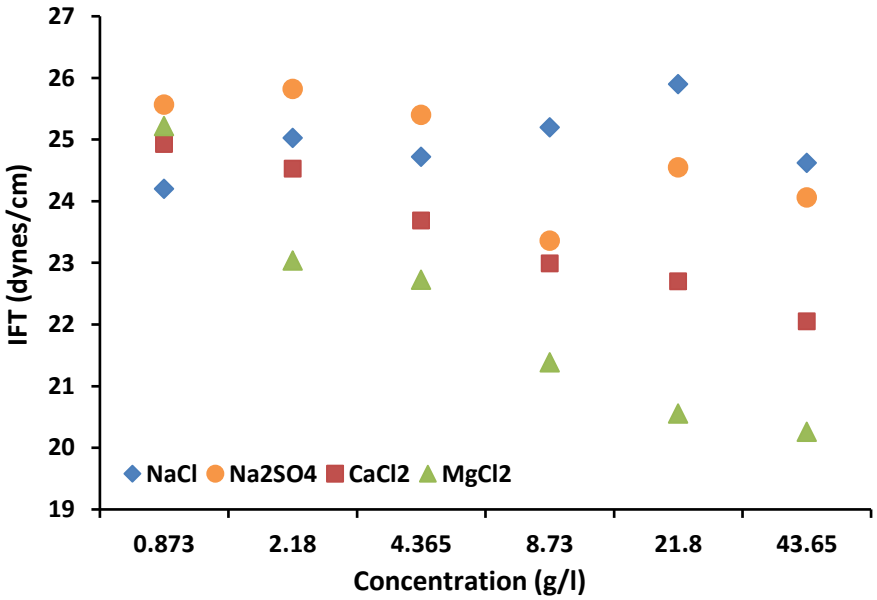

Figure 4.7: Averaged IFT values as a function of monovalent and divalent salts concentration.

4.6 Contact Angle Alteration as a Function of Rock Mineralogy, Brine Salinity, and Oil Composition

The impact of brine concentration on the wettability alteration of the limestone and dolomite plates aged with different types of dead crude oil is investigated in this section. Figures 4.8 and 4.9 show a summary for measured contact angle values of aged dolomite and limestone substrates upon exposure to various brines for the crude oil A, B, and C, respectively. The results revealed that an overall decrease of about 5 to 9 degrees in the water contact angle was detected as the salinity of the solution decreases up to 21828 ppm for crude oil A, but with insignificant changes for crude oil B and C.

For crude oil A, it is clear from Figure 4.8A that a weakly oil-wet with the contact angle of 120° was recorded when the aged dolomite substrate was subjected to formation water. Subsequently, a reduction in the water contact angle to 112° was reported after exposure to seawater. A similar trend was observed by Mahani et al. [81] who noted that a change of 5-17° in the contact angle was observed when switching from formation water to seawater. An obvious decrease in the contact angle value to 107° was for the dolomite plate when switching to twice-diluted seawater (21828 ppm), which reveals that the rock substrate is changed to intermediate-wet. As mentioned in Chapter 2, when the contact angle is between 0 to 75° and 115°-180°, the system is defined as water wet and oil-wet state, respectively, and when the contact angle falls within the range of 75º-115º, the system is neutrally wet [6]. An insignificant effect on the contact angle was recorded with a further reduction in the salt concentration, as the contact angle showed almost a fluctuation within the value of 106 ± 2°.

In the second and third set of contact angle tests, we measured the contact angles of dolomite substrates with other kinds of crude oils under various salinities. The aim was to verify if changing the type of crude oil affects the wetting state or not. Unlike crude oil A, the more hydrophobic surface was observed for crude oil B when using formation water with the

contact angle value of 135°. As identified by Al-Hashim et al. [22], positive surface charges on the dolomite surfaces were reported when the saline solutions with a high concentration of Ca^{2+} and Mg^{2+} ions were used. Therefore, we expect that the dolomite surface is likely to be acting as an attractive site for the negative ends of polar organic components in crude oil upon exposure to formation water, i.e., a strong interaction between ionized acidic and basic sites could happen, resulting in an oil-wet surface [79,80]. The dolomite surface was then changed to less oil-wet when the concentration of brines was decreased to 43650 and 21828 ppm. In the case of oil C, the oil contact angle displayed a gradual small decrease as the concentration of brines was decreased, but the substrate remains within a strongly oil-wet condition, Figure 4.8C.

For the limestone/brine/oil system, as can be seen in Figure 4.9A, there was a change in the contact angle to less oil-wet when the super saline solution (200000 ppm) replaced by seawater and twice-diluted seawater. These results are consistent with the previous findings in the literature [74]. It should, however, be noticed that the limestone/crude oil B regime showed relatively a fixed trend with the various salt concentration used (Figure 4.9B), indicating more hydrophobic surface than limestone/crude oil A. These results may have been linked to the difference in the solvent character of crude oil A and B with respect to their polar components, as detailed in Table 3.3, and to the effect of surface properties.

It is also apparent that the contact angle of limestone and crude oil C showed a strong oil-wet surface upon exposure to different brines with the water contact angle varies between 151° and 140°.

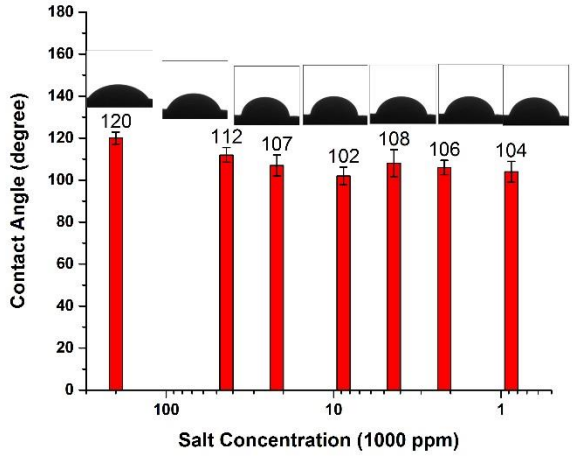

A

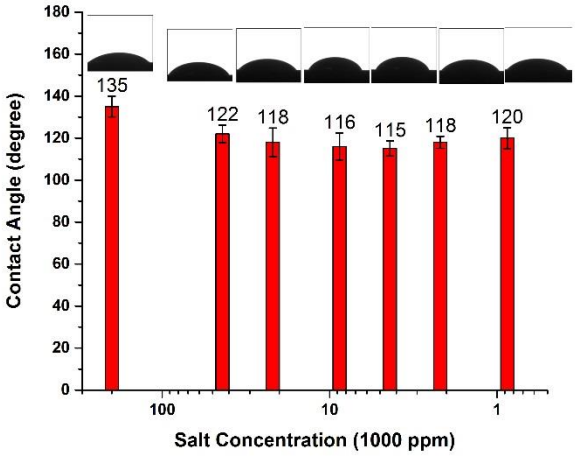

B

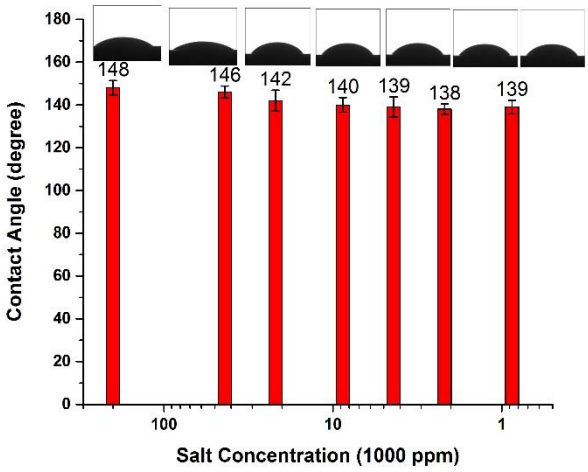

C

Figure 4.8: Contact angle values of dolomite rock as a function of salt concentration for (A) Crude oil A. (B) crude oil B. (C) crude oil C.

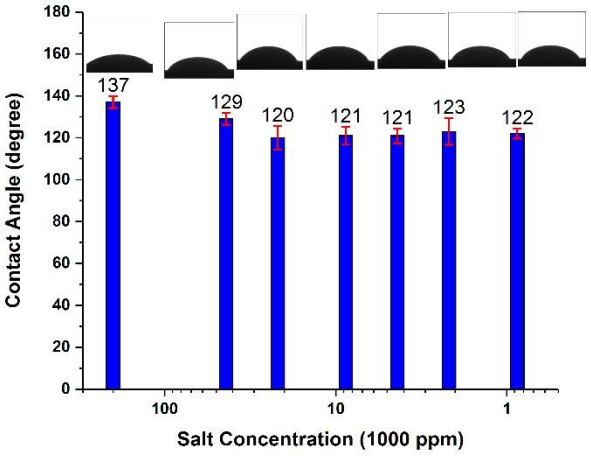

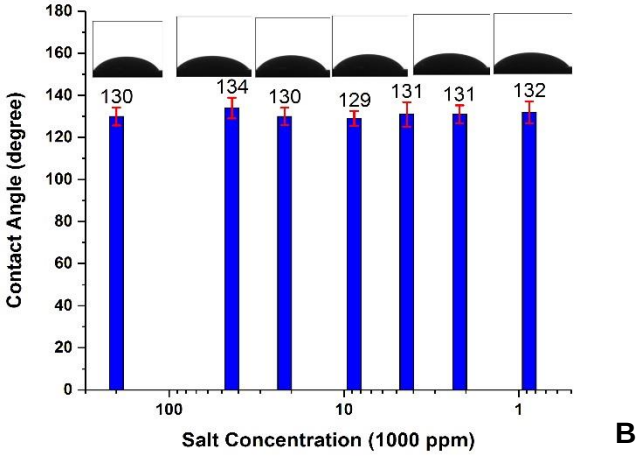

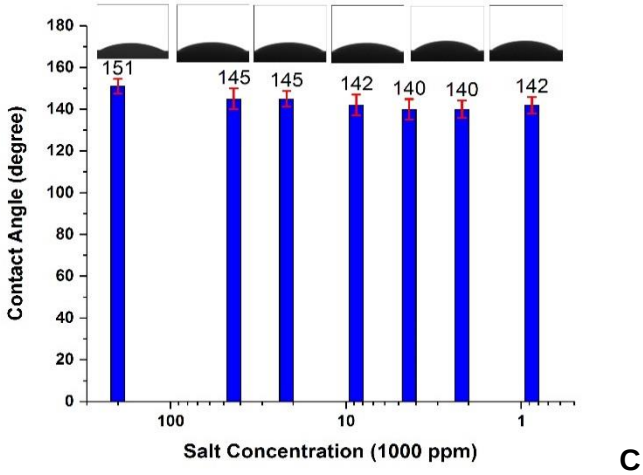

Figure 4.9: Contact angle values of limestone rock as a function of saline concentration for (A) Crude oil A. (B) crude oil B. (C) crude oil C.

4.7 Wettability Alteration Mechanisms

Based on the above results, we found that the wetting state is likely to be affected by three factors including minerals composition of the rock, brine concentration, and chemical composition of the crude oil. To better understand the role of each factor and to explain the main cause of wettability alteration and oil release, we evaluate the work of adhesion (W_A) "The work that required to separate a liquid/solid phase from one another to a certain distance" using Young-Dupre equation [144]:

$$W_A = \sigma_{ow} (1+\cos \theta) \quad (4.1)$$

where σ_{ow} is the measured oil/brine interfacial tension (dynes/cm), as given in Table 4.1, θ is the measured contact angle between oil/brine interface and the solid surface. The calculated values for both surfaces examined are plotted as a function of salt concentration, as shown in Figure 4.10.

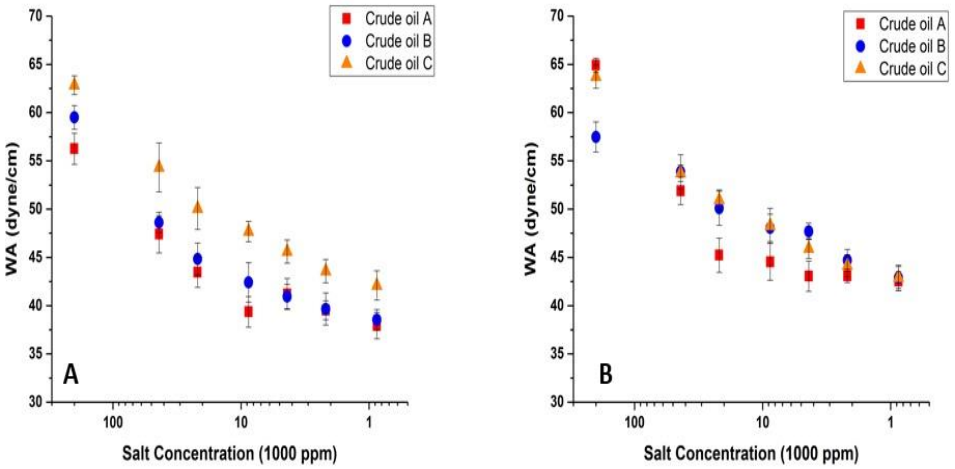

Figure 4.10: Work of Adhesion of (A) Dolomite surfaces. (B) Limestone surfaces as a function of brine salinity and crude oil composition.

From Figure 4.10A, it is apparent that a relatively sharp decrease in the work of adhesion values was observed when switching from super saline solution (200000 ppm) to seawater and then to twice-diluted seawater, and the effect was more pronounced for crude oil A. This means that a decrease in the electrostatic adhesive force had likely happened as will be explored in the next chapter, thereby less work was needed to separate the aqueous phase from the solid. In comparison, the variation in the adhesive forces for limestone surfaces for the three oils used showed the same pattern to that displayed in Fig. 4.10A, although the response to the change in the chemical composition of the oil is even less marked. These findings are in line with the recent observations by Lashkarbolooki and Ayatollahi [145], who found that the type of crude oils did not reveal a substantial impact on the work of adhesion and spreading coefficient and therefore, on the wettability alteration of the calcite surface. The small variation in adhesion values may have been linked to the difference in the rock characteristics of limestone and dolomite minerals with respect to the content of anhydrite and to the concentration of sulphate ions that adsorbed on minerals surface as discussed in section 4.3.

It has been previously reported that pure dolomite surfaces react differently to the change of brine salinity and composition in comparison to the other carbonate minerals. Dolomite also tends to show more positive surface changes compared to the pure limestone as the seawater was diluted up to 25 times [81,86]. In this study, as mentioned earlier, dolomite particles contained dissolvable anhydrite ($CaSO_4$), as a part of the rock material, providing an *in-situ* source of sulphate ions as the salinity was decreased, affecting the net surface charges, and therefore more negative charges on dolomite sites would be expected. This theory is qualitatively confirmed by the previously measured zeta potential and infrared absorbance data. On the other hand, at low electrolyte concentration and a relatively high surface charge density, an expansion in the thickness of the electrical double layer (EDL) to a few Angstroms would occur, leading to an increase in the EDL repulsion forces [39,146]. Thereby, preventing a close approach of negatively charged oil components to the surface,

resulting in a decrease in the adherence tendency of the oil to the dolomite surface and less hydrophobic surface in comparison with limestone.

From above, by consideration of the relation between work of adhesion per unit area W_A of the solid/brine/oil system and wetting properties of surfaces by using Young-Dupre Equation ($1+\cos\theta = W_A/\sigma_{OW}$) [5], and with a small change in the IFT values (σ_{ow}) between the high and low salinity solutions (Table 4.1), it is speculated that any small change in the adhesion energy will cause an abrupt change in the wettability. This assumption is qualitatively in good agreement with the above macroscopic contact angle observations.

It is also clear that the adhesive forces of dolomite and limestone rocks for crude oil C is relatively higher than of crude oil A with the low acid number, resulting in a high degree of oil-wetting. As mentioned earlier, crude oil C contained the highest concentration of polar organic components, which are strongly surface active so that they will have a disproportionate effect on the wetting properties of the system. It is supposed that the ionized polar components at the oil/water interface could adsorb at the carbonate surfaces and the strongest interactions between these polar atoms and polar surface site may occur, i.e., adhesive force will compensate the repulsive force, leading to preferentially oil-wet surface and low wettability alteration for the rock/brine/crude oil C regime [68]. The contact angle results support that the observed wettability alteration is mostly affected by the variation in the oil composition. Our current findings expand prior work [5, 20, 79, 80,147-149].

To sum up, it is found that three possible explanations are leading to a general trend of adhesion drop when the salinity was decreased up to two-times dilution. Firstly, *in-situ* chemical interactions between divalent ions and carbonate molecules and ion binding at the solid/water interface could happen, preventing oil from contacting the surface. Such mechanism is supported by the evidence of the infrared absorbance and

EDX elemental analysis, section 4.3, that sulphate ions are adsorbed on the limestone and dolomite surfaces, turning the net surface charges of carbonate particles to negative values. As a result, the repulsion force is likely to be increased, and consequently, the affinity of polar oil components into the rock surface would decrease, presenting less adhesion work. Such results are consistent with the previous studies by the researcher's group in BP [9,16] that the cause of an increment in oil recovery by specific brine composition containing a high concentration of SO_4^{2-} and Mg^{2+} could be traced back to the multi-ionic exchange, which results in a detachment of organic polar components from the surface by divalent cations.

The second mechanism is the electrical double layer and DLVO theory, which illustrates the competitive interactions between repulsive electrostatic forces and van der Waals attractive forces [75]. At a low electrolyte concentration and a relatively high surface charge density, the repulsive energy of the EDL plays a vital role in the interactions between rock/brine/oil interfaces. A thin water film on the rock surface becomes stable and thicker (i.e., positive disjoining pressure), thereby receding the three-phase contact line and preventing oil from contacting the surface [150]. As mentioned in section 4.2 of this chapter, the surface charges of carbonate rocks become more negative when the salinity of suspensions decreased up to 10 times dilution, which can indicate the occurrence of EDL expansion [19]. The expansion of EDL could, therefore, improve the electrostatic repulsion between oil components and carbonate surfaces, thereby resulting in a considerable change in the rock wettability, evidenced by the reduction in adherence tendency of oil components to the surface as the salinity is diluted twice from its original concentration, Figure 4.10.

Finally, the salting-out effect could also be considered as another possible mechanism for the wettability alteration during low salinity injection. Increasing the salinity can lead to a decrease in the solubility of polar organic components in the aqueous phase, resulting in the thin oil film being close to the rock surface. Consequently, the adherence tendency of

polar components to the rock surface will be increased, leading to a more hydrophobic surface. In contrast, decreasing the ionic strength and salinity of solutions can cause an increase in the solubility of polar organic components in the aqueous phase, resulting in a less hydrophobic surface. This could explain why the formation water had the highest adhesion values (strongly oil-wet) for three kinds of crude oil examined.

The proposed low salinity mechanisms in this study are consistent to some extent with what was previously suggested by Lashkarbolook et al. [151]. It should, however, be noted that the dissolution of carbonates ($CaCO_3$) seems not to be justified by the experimental findings of this study. Instead, the results of this work confirmed the mutual intermolecular interactions between the divalent ions and carbonate surfaces, which seem likely to act as a wettability modifier during low salinity flooding.

4.8 Summary

This Chapter provides insights on the oil/brine and carbonates/brine interactions under various kinds of crude oil with particular emphasis on its polar content. The objective was to understand precisely the possible wettability alteration mechanisms during low salinity flooding under various conditions. In the first section, the impact of ionic strength and brine salinity on the zeta potential of carbonates is described. The overall results demonstrate that as the salinity and ionic strength of suspensions decreases up to 10 times dilution, the magnitude of the negative charges increases. The dolomite surface, containing some amount of anhydrite, is more negatively charged than the limestone surface.

The results of IFR and SEM-EDX tests show that sulphate and magnesium ions are adsorbed on limestone and dolomite surfaces when using highly concentrated solutions, giving an indication that multiple ions interaction has happened, which affects the net surface charges and influences the wetting properties of carbonates.

It is found that there is a general trend of IFT reduction as the salinity of water is decreased, however, the reduction is very small, which suggests that low salinity water flooding has an insignificant effect on the fluid/fluid interaction compared to the fluid/rock interaction. The results also exhibit that monovalent ions did not show a considerable contribution to the IFT activity in comparison with the divalent ions, showing a gradual decrease in the IFT as the salts concentration of divalent ions increased.

For contact angle measurements, different effects on the contact angle are obtained for the same rock/brine system but with different kinds of crude oil. The results reveal that a change in the contact angle to intermediate-wet is seen for dolomite/oil A system by decreasing the salinity twice from the seawater water, but with an insignificant effect on the contact angle thereafter. No dramatic wettability alteration is observed for crude oil B and C, and the contact angle of dolomite substrates remains within the oil-wet conditions. This suggests that wettability alteration of carbonate rock under high temperature is highly influenced by the chemical composition of crude oil existing in the porous media. The limestone surfaces also show strong hydrophobic conditions at different salinities for different crude oils examined.

In general, the work described in this study demonstrated that a combination of three mechanisms, including multiple ions exchange, EDL expansion (electrokinetics repulsive), and salting-out are responsible for the wettability alteration during low salinity injection.

The next Chapter moves on to study the solid/brine/oil interactions at a micro-scale level using AFM technique, which would provide further explanation for the main findings emerged from this Chapter.

Chapter 5

Estimation of Carbonates/ brine/Crude Oil Interactions Using Microscopic Apparatus

5.1 Introduction

Although the visible macroscopic contact angle measurements outlined in Chapter 4 provide a fundamental understanding of the carbonates/brine interaction, the micro level details of the physicochemical interactions taken place between interfaces, however, are not entirely understood. Thus, the complexities of various interfacial phenomena governing surface wetting of crude oil on carbonates in a brine environment require further elucidation.

Crude oil can contain quantities of polar molecules. The polar molecules are strongly surface active so that they will have a disproportionate effect on the wetting properties of the system. Therefore, decreasing adhesion force would lead to the release of polar organic components from the surface, rendering it with a favourable wetting state [89,90]. Despite this practical importance, however, no experimental works are found in the literature on simulating the micro-interaction of carbonate surfaces and active polar components, which forms the basis of this study.

In this work, a molecular-level systematic study using Atomic Force Microscopy (AFM) apparatus was conducted with the aim of characterizing the interaction of polar components in crude oil with carbonate minerals at different levels of salinity. As mentioned in Chapter 3-section 3.5, the laboratory experiments were designed to measure the change in adhesion forces between the molecules on the carboxylic acid (-COOH) functionalized tips, representing the surface-active properties of crude oil and the flat calcite crystal, the most stable form of calcium carbonate under a range of saline solutions. The findings drawn would be

of a crucial significance for assessing the wettability of the surface as well as its associated mechanisms at the micro-scale.

Throughout this Chapter, the obtained data set were divided into two main sections. Section one will outline the detailed effects of formation water, seawater, different diluted versions of seawater, and a simple model of $NaCl/Na_2SO_4$ on adhesion force values. This will be followed by giving a discussion of the impact of sulphate (SO_4^{2-}) and magnesium (Mg^{2+}) ions on the overall adhesion attractive forces, section 2.

5.2 Effect of Seawater and Dilution of Seawater on Adhesion Force

Before measuring the adhesion forces, the topography of the calcite substrate was examined using tapping mode in air to confirm a smooth flat surface. Figure 5.1 illustrates a 10 µm x 10 µm scan area of calcite substrate before and after exposure to different saline solutions. The mean roughness of the fresh calcite surface (i.e., before exposing to saline solutions) was determined, R_A = 1.9 nm. Due to the fact that imaging the surface was performed in dry mode, i.e., the solution had to be removed, the imaged area was not the same. However, this would not significantly affect the obtained results because the examined surface was uniform, with no heterogeneity.

In comparison to the first image, Figure 5.1B shows a noticeable change in the topographical features occurring after exposure to saline solutions with the mean roughness of 8-10 nm, suggestive of a very slight dissolution of the polished calcite surface, accentuating some of the peaks of salt crystal deposited. Surface adsorbates arising from the solution are also present. To ensure repeatability, another position on the treated calcite substrate was chosen to scan, and the same topographical feature was observed, Figure 5.1C.

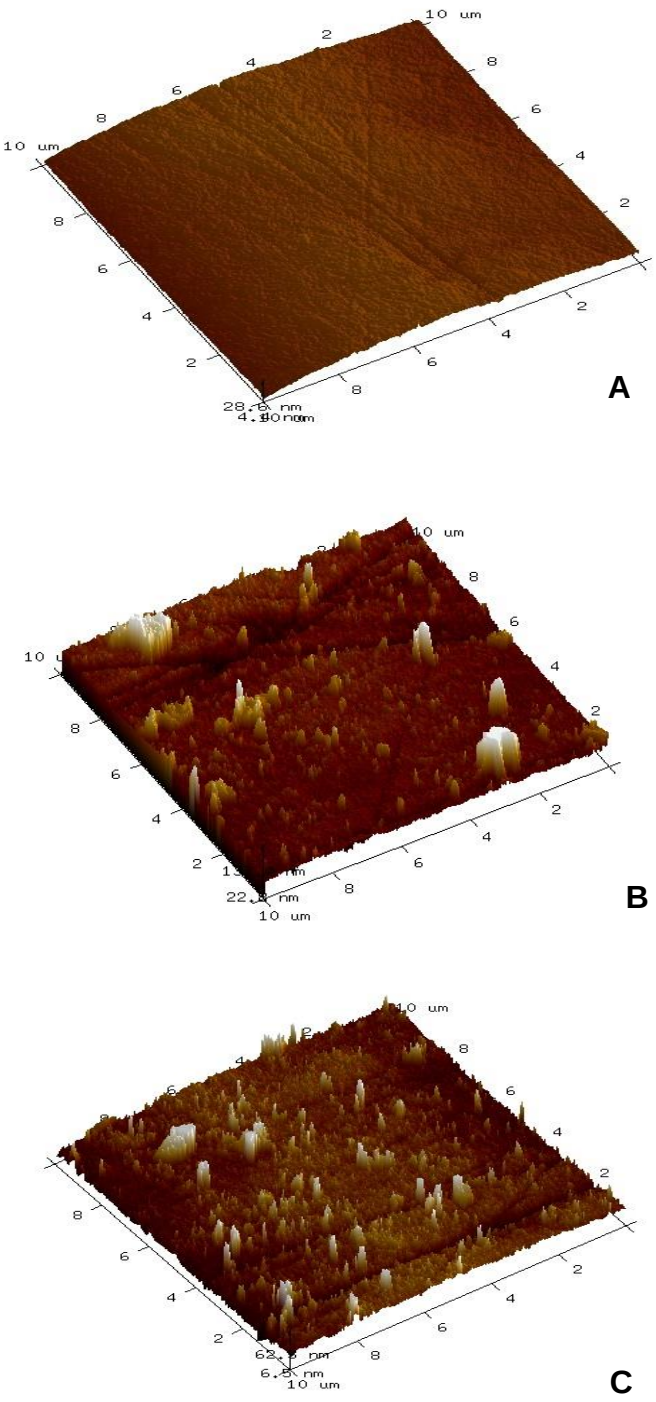

Figure 5.1: Topographical images of calcite surface (A) before exposure to saline solutions. (B) and (C) after exposure to saline solutions.

For adhesion force measurements, Figure 5.2 shows the adhesion force maps for the same scanned area with the same probe upon exposure to formation water, seawater, and different dilutions of seawater, which were injected in a sequential manner. The corresponding adhesion force histograms extracted from these maps are shown in Figure 5.3.

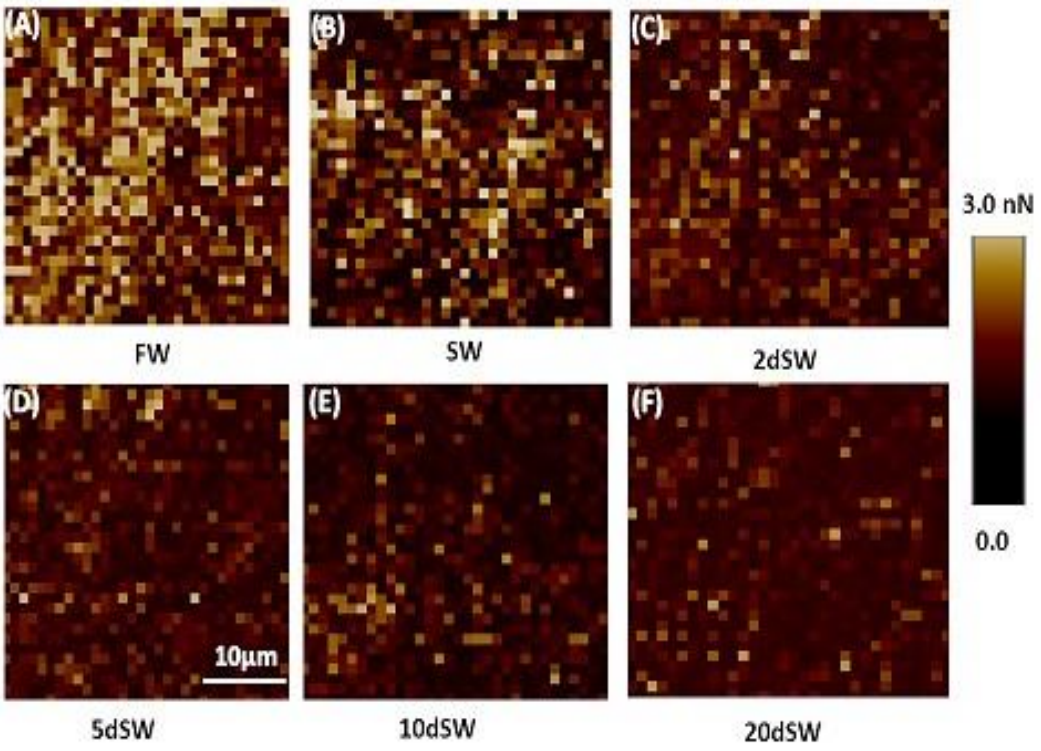

Figure 5.2: Adhesion force maps acquired in formation water, seawater, and different dilutions of seawater, varying in salinity and ionic strength from high to low. For each map, the ranges of adhesion vary from very low adhesion, dark brown, through medium adhesion, light brown, pale brown, and finally the highest adhesion, yellow.

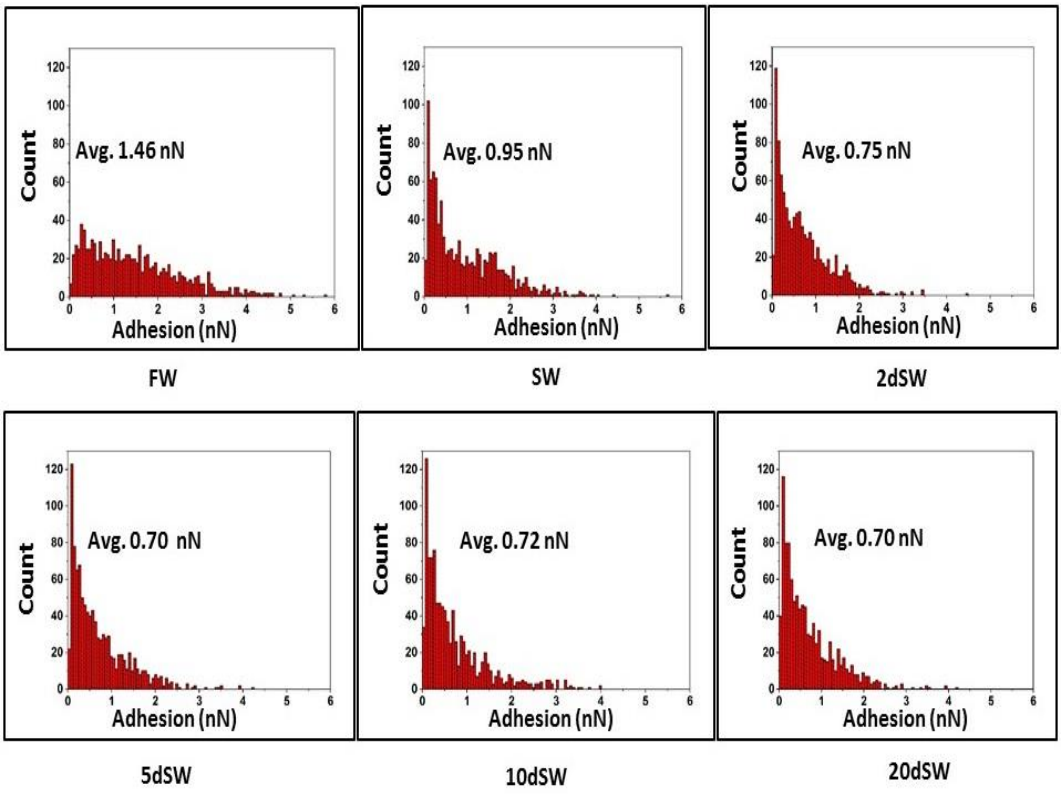

Figure 5.3: Adhesion force histograms extracted from force maps for different saline solutions.

It can be clearly seen that there is a wide statistical spread in the adhesion measurements which tend to have a maximum at low force. This type of Poisson distribution is typical of a probabilistic interaction which is related to the probability of an adhesive bond forming. This will also be a function of the nanoscale roughness at that particular point of the surface in the force map. However, it is also apparent that the high adhesive forces are encountered far more frequently at high salt. This is quantified most straightforwardly by taking the average adhesion for the whole area scanned. As shown in Figure 5.4, an overall decrease in the average adhesion force of about 48.6% was observed when switching from super saline solution (i.e., formation water, 200000 ppm) to twice-diluted seawater (21828 ppm). This indicates that the wetting of the calcite by the polar oil components will be substantially reduced when twice-diluted was injected, but any further decrease in salinity had little effect. These results contrast markedly from the observations by Pedersen et al. [95] who

found little impact of saline solutions on natural grains using a non-polar – CH_3 terminated probe. This contradiction is mainly attributed to the fact that Pedersen et al. [95] used natural heterogeneous grains, therefore the tip-surface interaction area would not be the same for each point, which highly affected the adhesion results.

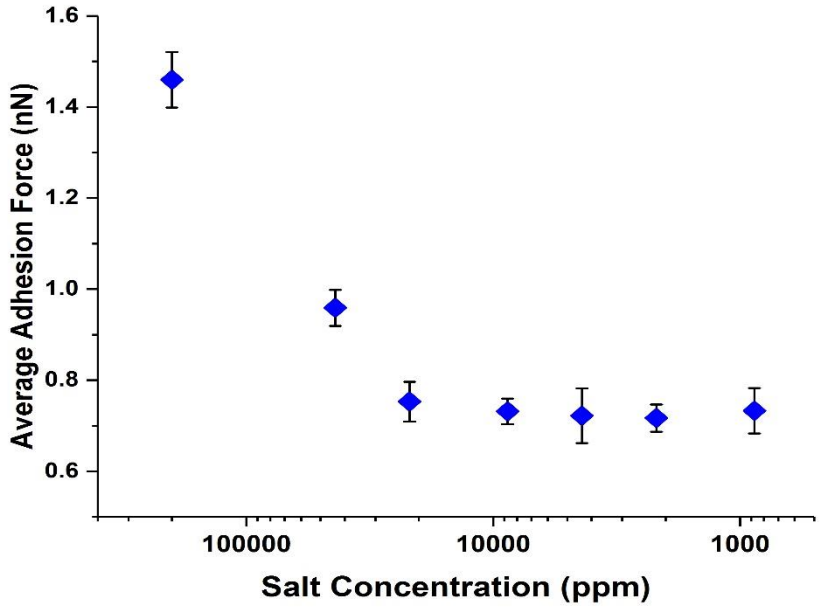

Figure 5.4: Average adhesion force as a function of salt concentration.

Based on the relation between work of adhesion per unit area (W_A) and wetting properties of calcite surface by using equation 5.1 [144,146], and with a minor change in the IFT values (σ_{ow}) for different saline solutions (Table 4.1), it is expected that any small alteration in the adhesion force will produce an abrupt change in the wettability. From Figure 5.4, it is evident that a significant decrease in the adhesion force value from 1.46 nN to 0.75 nN occurred upon exposure to twice-diluted seawater, which is in agreement with the macroscopic contact angle observation for the dolomite/oil A system, Chapter 4. It is thus concluded that the reduction in the adhesive force results in a substantial decrease in the W_A/σ_{ow} ratio, and therefore wettability alteration to a less hydrophobic condition. For

other diluted versions of seawater, the variation in adhesion force was insignificant, and hence the W_A/σ_{ow} ratio remains relatively unchanged, leading to a minor effect on the wetting state.

$$(1+ \cos \theta) = \frac{W_A}{\sigma_{ow}} \quad (5.1)$$

A change in adhesion when the salinity of the solutions is reduced could be explained by the DLVO theory. This theory explains the forces between charged surfaces interacting through a liquid medium. “It combines the competitive interactions of the double layer repulsive forces and van der Waals attractive forces” [152]. Hence, the Debye length (k^{-1}), the thickness of the diffuse EDL, controls the interaction between two charged surfaces to be either attractive or repulsive. In our system, the interaction was between the calcite sample and the apex of the carboxyl-functionalized tip. At very high salinity and ionic strength, i.e., super saline solution, a shrinkage in the thickness of the EDL to a few Angstroms would occur due to the high concentration of NaCl in the double layer. The Debye length (k^{-1}) for FW is approximately 0.2 nm, for SW 0.4 nm, and for 2dSW 0.6 nm. This leads to a decrease in the EDL repulsion forces, and hence the tip could approach to a closer distance and experience higher Van der Waals adhesive forces [39,71,146]. In contrast, decreasing the salinity of solution would cause an expansion in the electrical double layer, thereby preventing the close approach of the polar tip to a point where the very close-range van der Waals forces would dominate, resulting in a decrease in the adhesion between the polar components and the calcite surface [146,153].

To verify the impact of salinity on adhesion forces, a simple model system of NaCl and Na_2SO_4 was used with the salinity equal to that of original seawater (i.e., 43650 ppm). The concentration was then diluted with the same proportions of that when the composite saline solution used, starting from 2 times dilution (21828 ppm) to 20 times dilution (2183 ppm). Figures 5.5 and 5.6 show the acquired force maps and corresponding force

histograms for the same scanned area with the same probe upon exposure to different concentrations of NaCl/Na_2SO_4 salt solution. The average values for the above measurements are illustrated in Figure 5.7. It was interesting to observe that the variation in the adhesion forces showed the same pattern to that displayed in Figure 5.4, although the response is even more marked. Hence, the average adhesion decreased by about 70% as the saline solution was diluted twice from its original concentration. This stronger response is a consequence of the adhesion continuing to reduce rapidly below 2 times dilution to a final adhesion of approximately 100 pN, in contrast to the minimum adhesion of around 700 pN in seawater, plateauing after two times dilution. This could be due to the presence of complicating additional ionic components in the seawater.

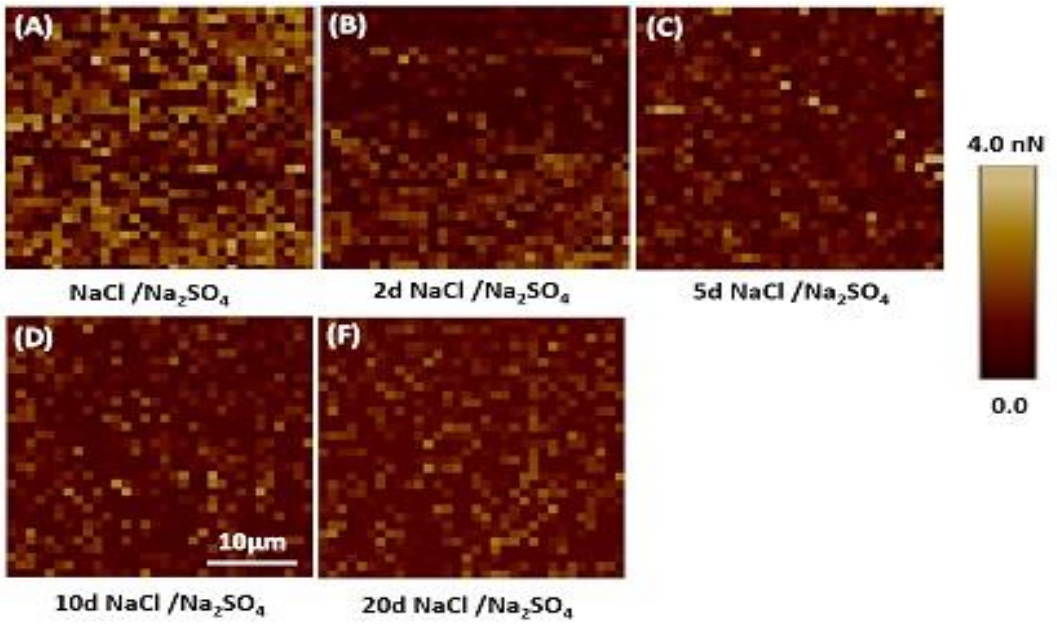

Figure 5.5: Adhesion force maps acquired in various solutions of NaCl/Na_2SO_4, varying in salinity and ionic strength from high to low. For each map, the ranges of adhesion vary from very low adhesion, light brown, through medium adhesion, pale brown, and finally the highest adhesion, yellow.

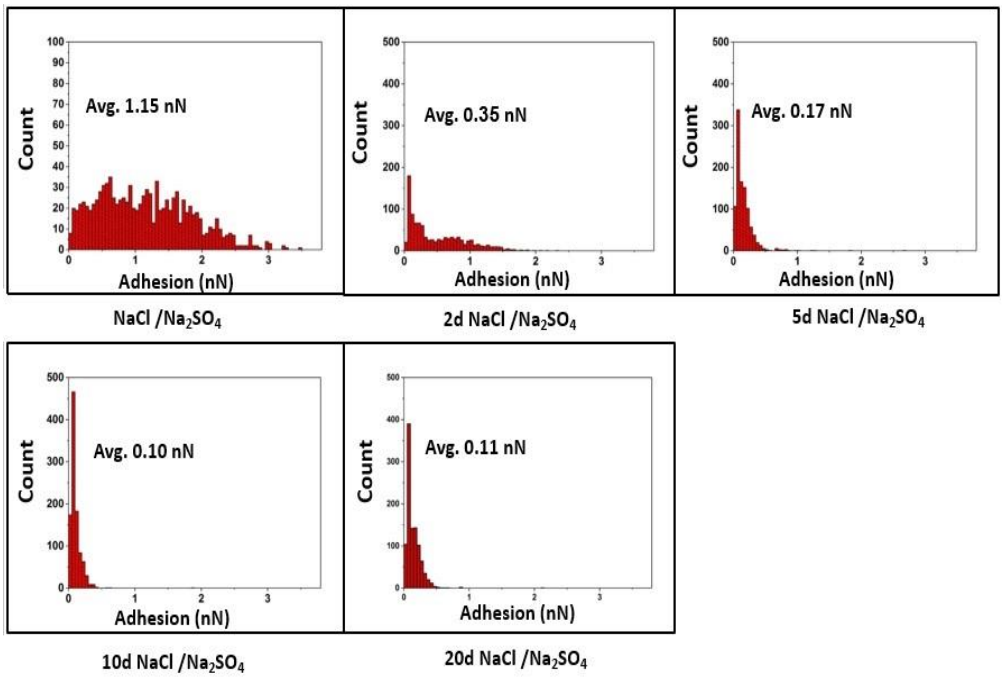

Figure 5.6: Adhesion force histograms extracted from force maps for different concentrations of $NaCl/Na_2SO_4$ saline solution.

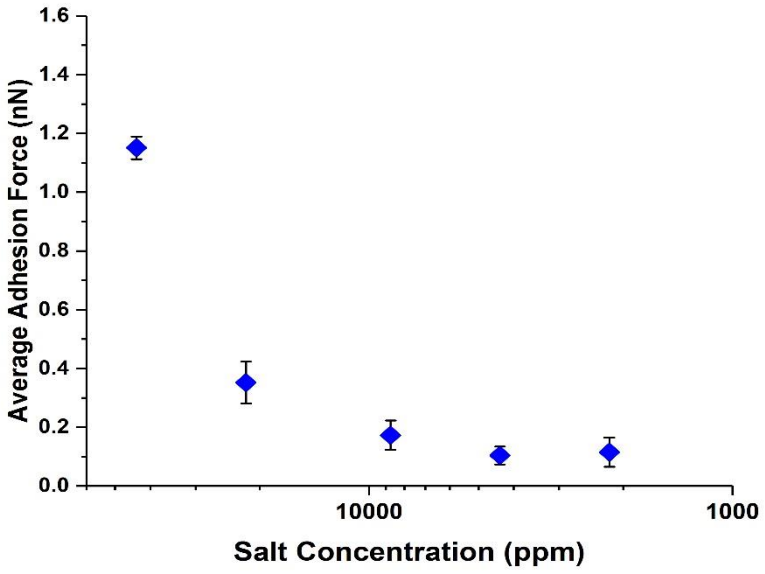

Figure 5.7: Average adhesion force of $NaCl/Na_2SO_4$ saline solution as a function of salt concentration.

It is proposed that while the expansion of the electric double layer (EDL) at lower salt is responsible for changing oil adhesion on carbonates, it can be modulated by binding of divalent ions such as SO_4^{2-} at the solid/water

interface. The potential chemical interactions between the calcite surface and AFM probe with polar components under saline solution is illustrated in Figure 5.8, and detailed discussion on this will be given in Chapter 9.

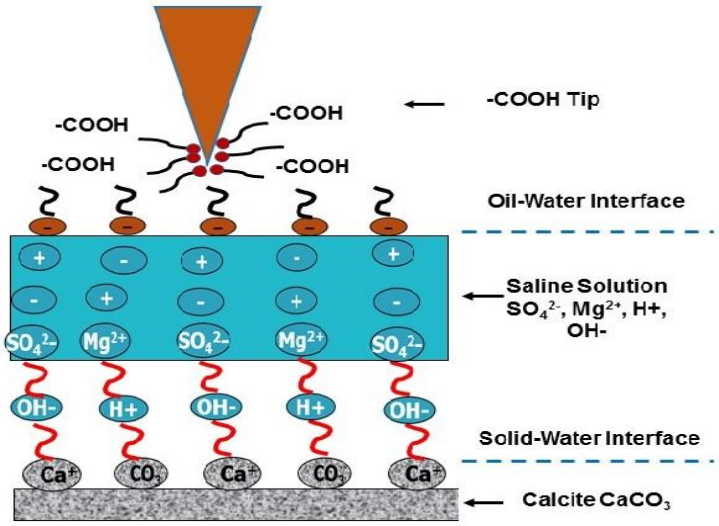

Figure 5.8: Potential chemical interactions between calcite/ functionalized AFM tip and saline solution.

5.3 Effect of SO_4^{2-} and Mg^{2+} Ions on Adhesion Force

As mentioned in the previous Chapter, the adsorption of SO_4^{2-} into carbonate surfaces has been supposed to work as a wettability modifier by changing the surface charge during water injection, affecting the wetting state. Such a hypothesis has also been confirmed by current molecular-level observations that seawater and twice-diluted seawater, containing a high concentration of SO_4^{2-} revealed less adhesion, as illustrated in section 5.2. Mg^{2+} is another active ion that could contribute to the chemical interaction process, helping to promote the wettability of carbonates. In this section, the experimental findings of the molecular study on the influence of potential determining ions on oil adhesion are presented. The adhesion force between the polar-functionalized tip (-COOH) and the calcite surface in the presence of saline solution, containing different concentrations of SO_4^{2-} and Mg^{2+} ions was measured.

NaCl solution was used as the base brine with a salinity equal to that of twice-diluted seawater (2 wt. %), as the highest change in the adhesion value was observed upon exposure to this solution. The modified brines of $NaCl/Na_2SO_4$ and $NaCl/MgCl_2$ were prepared by increasing the concentration of sulphate and magnesium ions gradually with the proportion of 0x, 1x, 2x, 3x, 4x, the concentration of twice-diluted seawater, while the concentration of NaCl was kept constant. It should, however, be noted that the concentration of sulphate ions in seawater is about half that of Mg^{2+} ions [37]. For this, we initially adjusted the concentration of Mg^{2+} to be more than that of SO_4^{2-}. A set of adhesion force maps and corresponding histograms are extracted under these conditions, as shown in Figures 5.9 through 5.12 while the average adhesion values for each type of saline solution examined are summarized in Figure 5.13.

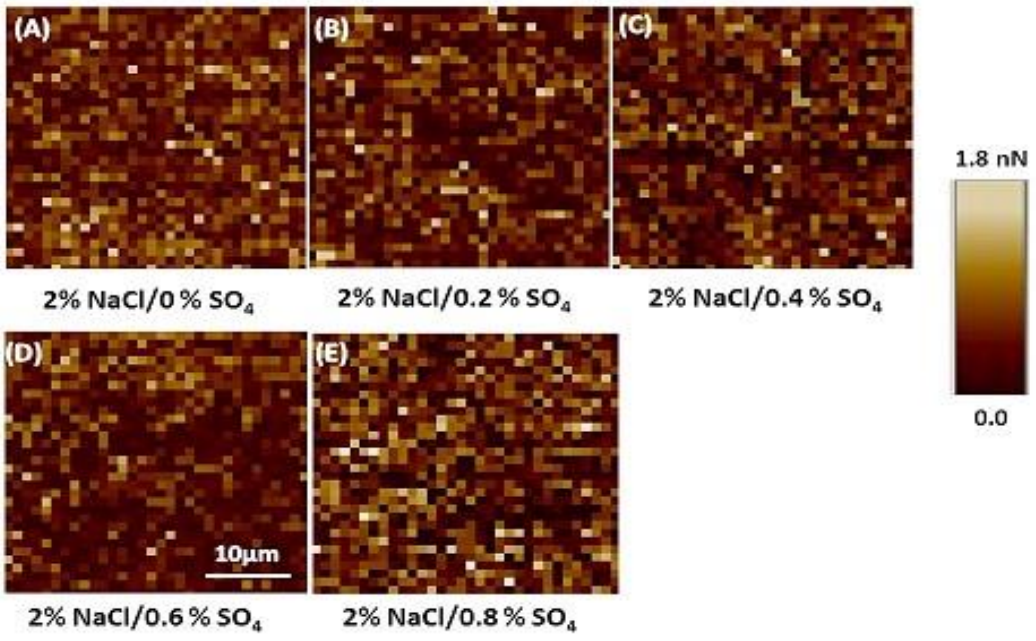

Figure 5.9: Adhesion force maps acquired in solution of $NaCl/Na_2SO_4$, varying in SO_4^{2-} concentration at a constant salinity 2 wt. % NaCl. For each map, the ranges of adhesion vary from very low adhesion, light brown, through medium adhesion, pale brown, and finally the highest adhesion, pale yellow.

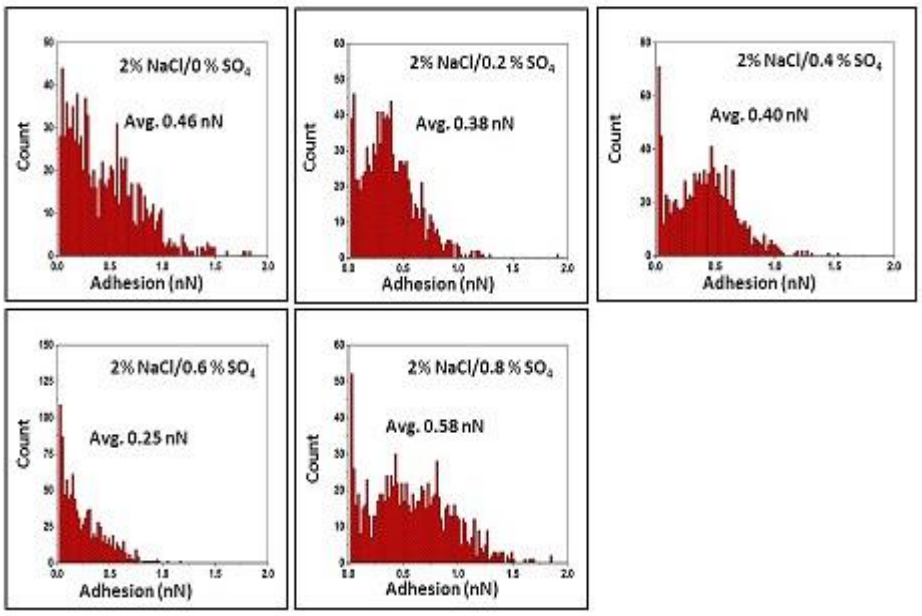

Figure 5.10: Adhesion force histograms for fluids, varying in ionic concentration of SO_4^{2-} at a constant salinity 2 wt. % NaCl.

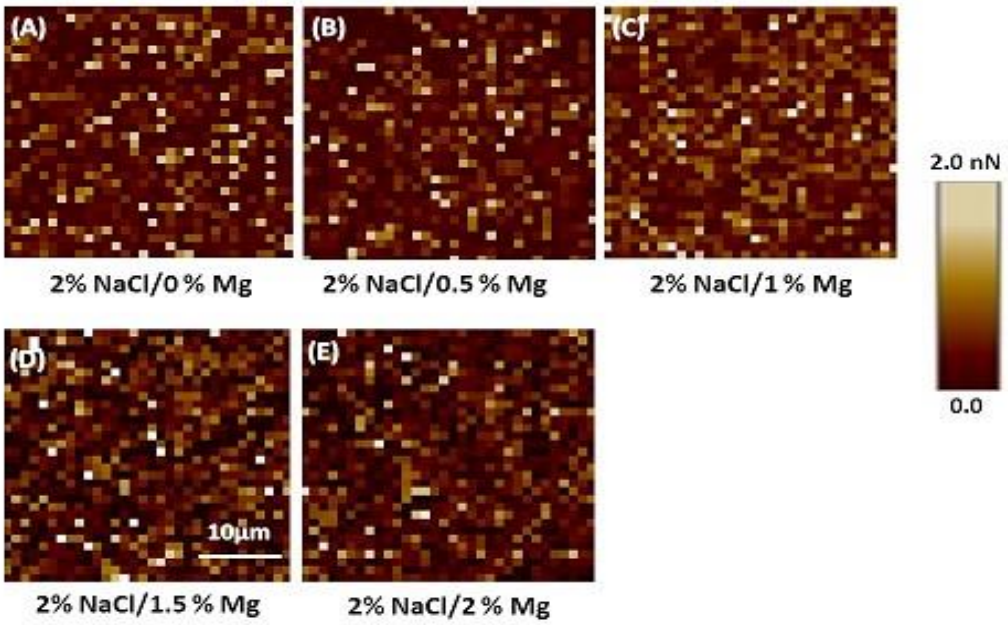

Figure 5.11: Adhesion force maps acquired in solution of $NaCl/MgCl_2$, varying in SO_4^{2-} concentration at a constant salinity 2 wt. % NaCl. For each map, the ranges of adhesion vary from very low adhesion, light brown, through medium adhesion, pale brown, and finally the highest adhesion, pale yellow.

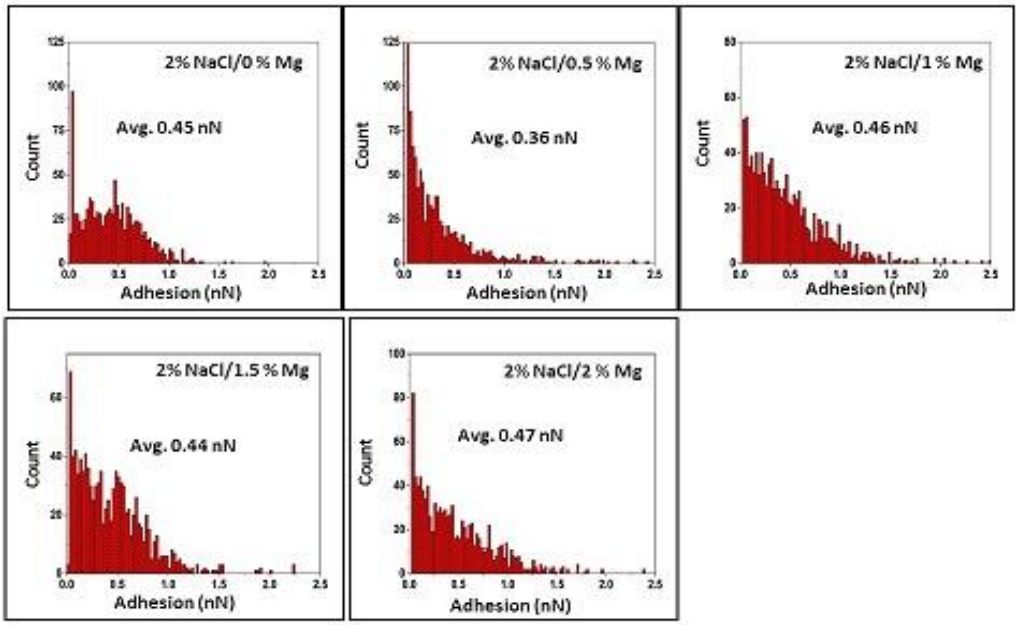

Figure 5.12: Adhesion force histograms for fluids, varying in ionic concentration of Mg^{2+} at a constant salinity 2 wt. % NaCl.

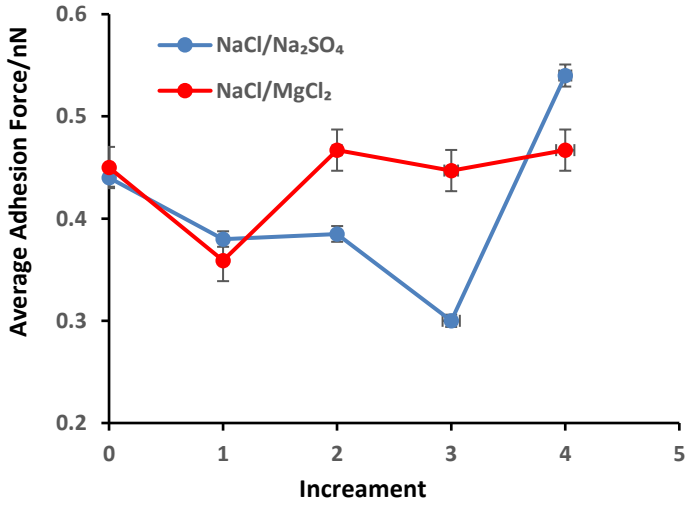

Figure 5.13: Average adhesion force as a function of SO_4^{2-} and Mg^{2+} concentration increment.

Generally, it is obvious from Figure 5.13 that the effect of SO_4^{2-} and Mg^{2+} additional ions on the surface adhesion is not large in comparison to the salinity; however, it is still apparent and measurable. The change in the adhesion force values with the concentration is more pronounced for the SO_4^{2-} ions than that of Mg^{2+} ions. Hence, the adhesion was relatively reduced when the concentration of sulphate was increased 3 times (0.6

wt. %) the concentration of twice-diluted seawater. This result is in line with those of Strand et al. [37] who noted that the imbibition oil recovery increased as the concentration of sulphate increased to 3 times. The results also demonstrate that the adhesion force reaches its peak value with the further increase in the sulphate concentration (0.8 wt.%). This might be commonly linked to the precipitation of $CaSO_4$ (which possibly represent the small accretions found on the calcite surface after the experiments). It appears from the evidence that the effect of sulphate ions will be reversible when the concentration increases beyond a certain level.

It is also interesting to note that sulphate and magnesium ions show approximately similar adhesion values when both ions have a concentration equal to that in twice diluted seawater, as illustrated in Figure 5.13. Nevertheless, increasing the concentration of magnesium ions beyond that of 2dSW displayed a negligible change in the adhesion values. The same results were noticed by Generosi et al. [96] who found that the surface did not become more hydrophilic and the change in the average adhesion was small when a solution of $MgCl_2$ used. It has previously reported that the affinity of magnesium toward carbonate surface increases as the temperature increases [43]. Since magnesium becomes more reactive and partial dehydrated when the temperature rises to 130 °C, it is, therefore, speculated that no strong interaction between magnesium and calcite surface had been occurred under ambient conditions, leading to an insignificant effect on the average adhesion values when Mg^{2+} ions used.

5.4 Summary

This study is conducted to provide insightful information on the carbonates/brine/oil interactions at the micro-scale level by using the AFM apparatus. The aim was to gain a better understanding of the possible microscopic mechanisms related to the wettability alteration, hence the potential oil recovery enhancement during low salinity flooding.

Compared to the previous AFM researches, this work is the first to provide a detailed analysis of microscopic AFM measurement by using a very smooth calcite crystal, and therefore less prone to topographic effects. The magnitude of adhesion between the polar end (-COOH) functionalized tips and calcite substrate is determined upon exposure to various saline solutions.

A decrease in the average adhesion value from 1.46 nN to 0.75 nN is observed when switching from formation water (200000 ppm) to twice-diluted seawater (21828 ppm). However, an insignificant effect on the average adhesion values is reported with further dilutions, revealing no measurable difference in the W_A/σ_{ow} ratio when the concentration of ions decreased, i.e., minor effect on the carbonates' wettability. The results are supported to some extent by previously measured macroscopic contact angle, demonstrating a change from oil-wet to intermediate-wet condition for dolomite/oil A system when the salinity reduced to 21828 ppm, showing a decrease in the oil/surface interaction. A model system of NaCl /Na_2SO_4 also shows similar results as the salinity reduced, suggesting that there is an optimal brine concentration, beyond which the salt concentration has a small impact on the oil/carbonate rock interaction. The results also reveal that magnesium ions did not show a strong effect on the adhesion values, while there was a critical sulphate concentration existing for a given amount of NaCl that should be considered to make adsorption onto the carbonate surface rather than precipitation.

It is also found that the adhesion changes occur through a combination of ions binding and EDL expansion (electrokinetics repulsive) mechanisms, with the latter having by far the larger effect. Further follow-up work is required to shed more light on how the variation in the adhesion forces and improving the electrostatic repulsion of the surfaces could affect oil desorption efficiency, which will represent the basis of the next Chapter.

CHAPTER 6

Effect of Low Salinity on the Oil Desorption Efficiency from Calcite and Silica Surfaces

6.1 Introduction

The conclusions drawn from the previous chapters proposed that decreasing the salinity beyond certain concentration has contributed to reducing the adhesion forces, which can assist in detaching the active polar components of oil from the surfaces. Therefore, assessing the desorption efficiency of crude oil upon exposure to different saline solutions will help to understand and corroborate the earlier findings, helping to reveal the potential of enhancing oil recovery from carbonates and sandstones.

As outlined in Chapter 2, Quartz Crystal Microbalance (QCM) has been extensively used to detect the adsorption and interaction of polymers, surfactants, and asphaltene at solid surfaces [97,98]. Recently, QCM has been used to assess the adsorption/desorption of crude oil onto/from different surfaces, however, previous work on carbonate surfaces is very scarce [17,19,99,100]. In this study, we used QCM as a simple and quick method to assess the adsorption/desorption of crude oils onto/from calcite and silica crystal surfaces. The work aims to understand the influence of the ionic strength and brine salinity on the desorption of crude oils with various chemical composition and polar content from crystal surfaces. Such a study will help to evaluate the potential of low salinity water flooding before conducting conventional macroscopic core flooding experiments. The same synthetic brines that used in our previous work were used in the QCM study, including seawater and different proportions of diluted seawater. Crude oils with the physicochemical properties given in Table 3.3 were also used in this work.

This Chapter is organized as follows: the first section will outline and discuss the experimental findings of oil adsorption onto the calcite and silica surfaces, while the second section moves on to discuss the obtained results of oil desorption from the same crystal surfaces upon exposure to different saline solutions.

6.2 Adsorption of Crude Oil on Calcite and Silica Surfaces

In this section, the adsorption of three kinds of crude oil into the calcite and silica surfaces, having different electrostatic properties is compared. Q-Sense measures the change in resonant frequency and dissipation energy of the coated crystals. An indicative example of the frequency and dissipation changes when calcite and silica surfaces were exposed to dead crude oil, followed by flushing with toluene and subsequent exposure to seawater and different slugs of diluted seawater, is illustrated in Figure 6.1 [19]. It is obvious that a frequency shift on the silica surface is higher than that on the calcite surface, suggesting that the mass adsorbed rapidly on the surface [106]. These results are in line with those of Guo et al. [97], who noted that a higher shift in the frequency was on the silica surface than that on the gold surface. They stated that silica (SiO_2) has higher electrostatic contact sites compared to the other surfaces, leading to more molecules adsorbed on the SiO_2 surface through the electrostatic attraction. It can also be seen from Figure 6.1 that the corresponding dissipation shift increases during the adsorption of crude oil onto the investigated surfaces, but it decreases upon exposure to toluene, meaning that loosely bound oil molecules were detached from the surface and the residual components represent a rigid oil layer [107]. It can also be noted that injecting 2dSW and 10dSW show an increase in the frequency shifts, coinciding with a decrease in the corresponding dissipation shifts, indicating that desorption happened as will be discussed in the next section. Moreover, the overall dissipation shifts for the calcite and silica surfaces are relatively small (less than 10). Similar behaviours have been observed previously [98,102,106,107].

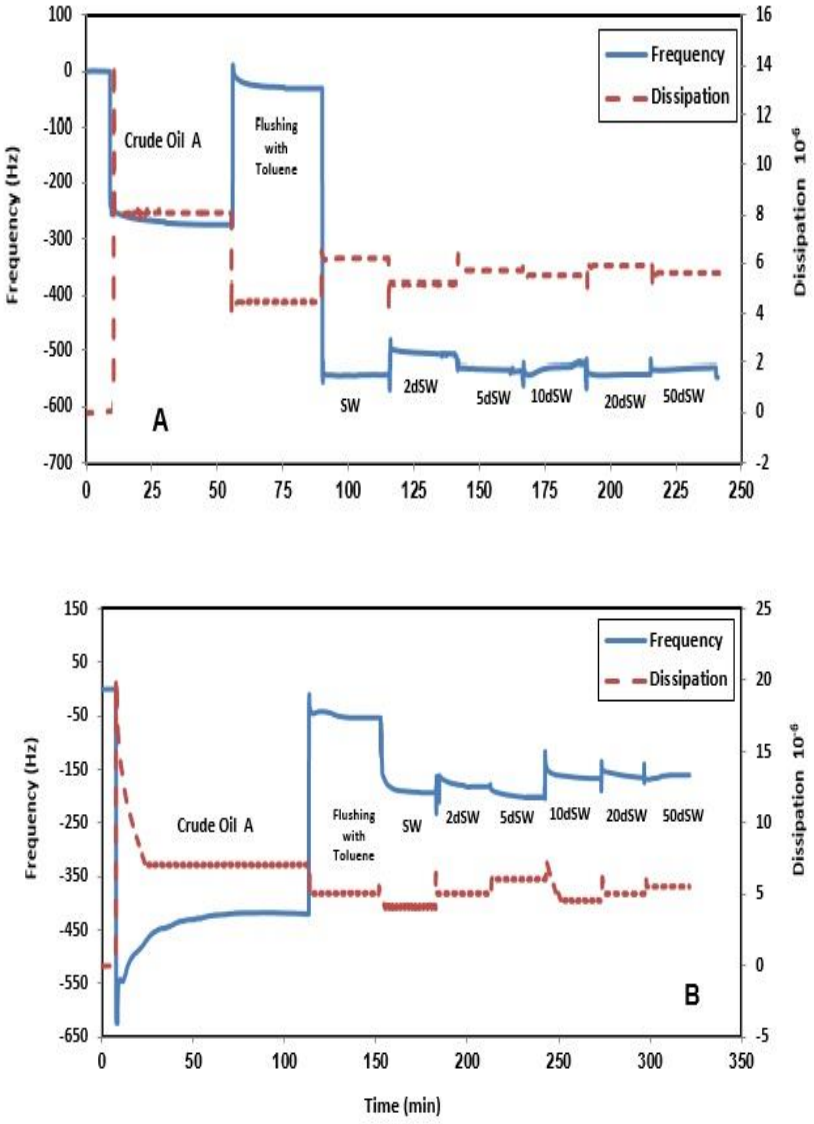

Figure 6.1: Frequency and dissipation shifts (third overtone) versus time for typical adsorption/desorption sequences onto (A) calcite and (B) silica surfaces.

The adsorbed mass was determined by the Sauerbrey equation (Eq.3.2) as mentioned before in Chapter 3, and the results are shown in Figure 6.2. For calcite surfaces, the highest adsorption was observed for crude oil C, which contained a high acid number (2.54 mg KOH/g) and the highest mass ratio of the oxygen atom, as illustrated in Table 3.3. On the other hand, the lowest adsorption was for crude oil A with no significant

acidity and less oxygen content. For silica surfaces, an opposite trend was observed since the adsorption is decreased as the acidity of crude oil and oxygen heteroatom increased. This observation is consistent with the study by Liu et al. [108], who confirmed that the oil components adsorbed to silica surfaces were different from those on calcite surfaces.

Based on the fact that silica surface is dominated by silanol (Si-OH) groups, the surface will be negatively charged, which can promote the adsorption of positively charged nitrogen-based components present in oil [6, 68,107]. Thus, it might be speculated that more layers are adsorbed to silica surfaces compared to calcite surfaces when crude oils with insignificant acidity have been used (Crude Oil A and B). Overall, the variation in the amount of mass adsorbed can be attributed to the difference in the chemistry of the adsorbed oil.

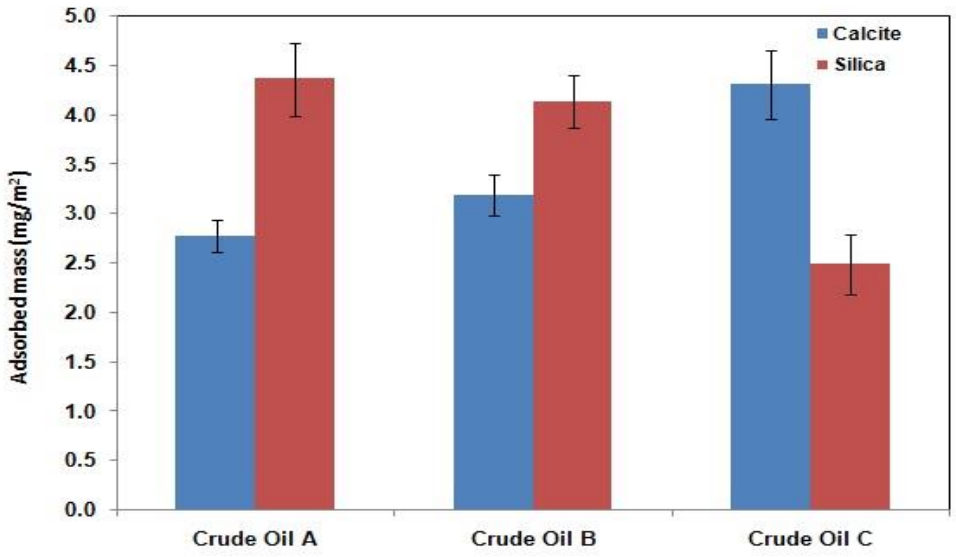

Figure 6.2: Amount of adsorbed crude oils on the calcite and silica surfaces.

To support the observations mentioned above, Infra-Red Spectroscopy (FTir-Thermo iS10) was used to determine the organic functional groups present in the crude oils. The IR spectra obtained for three crude oil samples are illustrated in Figure 6.3. Considering the functional groups of crude oils, it can be seen that the absorption bands of aliphatic hydrocarbon (CH_2 and CH_3) represent the major functional groups in crude oils A, B, and C, including C-H stretching of the saturate (2800-2921 cm^{-1}), C-H deformation of saturate (1455.25 cm^{-1}) and C-H symmetric deformation of saturate (1376.56 cm^{-1}) [154]. The region between 1640-1737 cm^{-1} was consistent with the stretching carboxylic groups C-O, such as carboxylic acid. This region depicted two small peaks for crude oil C, which showed the highest adsorption on the calcite surface, referring to the presence of the C-O functional group in this kind of oil. The peak at 1141.6 cm^{-1} in crude oil A and B was assigned to the presence of amine C-N stretch.

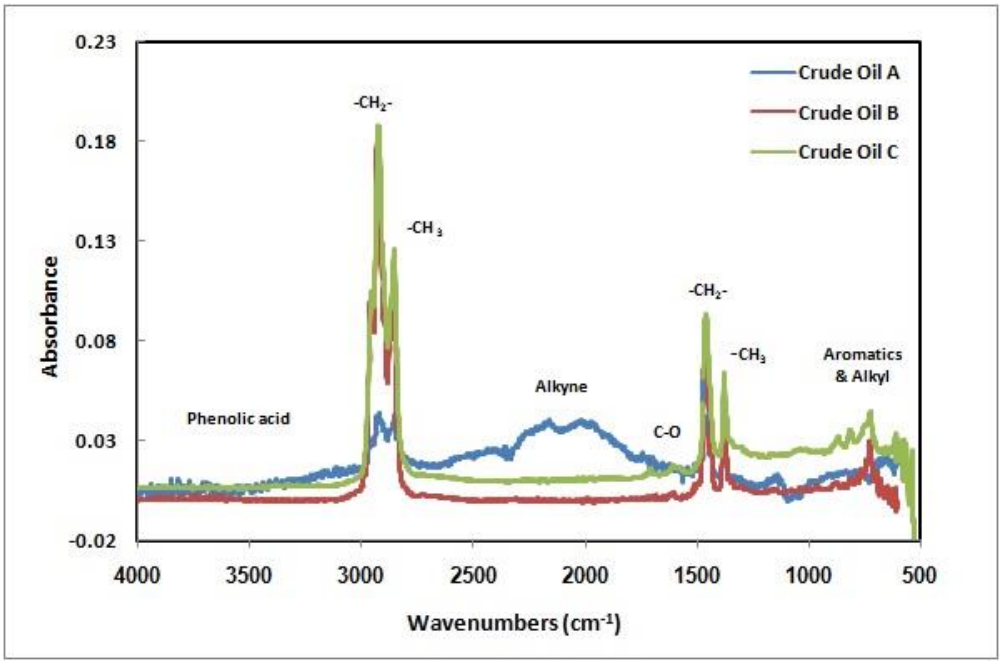

Figure 6.3: Infra-Red spectra of the three crude oils used in this study.

The results also revealed that the three crude oil samples contain an amount of phenolic functional groups in the range of 3107-3938 cm^{-1}. Finally, the wave number in the range between 1505.6-1538 cm^{-1} corresponded to aromatics ring stretch C-C, while the band between 800-600 cm^{-1} was assigned to the aromatics C-H deformations and alkyl groups [107]. Notably, the aromatic bands were more intense for crude oil C, which gives an indication of high aromaticity for this sample compared to crude oils A and B. SARA analysis also confirmed that crude oil C has a high aromatic weight ratio 44.91%, as illustrated in Table 3.3.

In general, IR spectra indicate that the saturated hydrocarbon bands seem to be the predominant function groups for all types of crude oils. However, there is variation in the abundance of polar groups such as carboxylic acid, amine, and phenolic acid. IR spectroscopy observations have also been supported by SARA and elemental analyses, which showed equivalent contents of saturate and polar hetero atoms groups (NO). These results are consistent with the amount of adsorbed oil layers on the calcite and silica surfaces. It has previously been reported that the surface energy seems likely to be dominated by the basic, acidic, and crude oil solvent character with respect to its polar content which showed a considerable impact on deposition or precipitation at the solid surface [79,108].

6.3 Desorption of Crude Oil from Calcite and Silica Surfaces

The desorption efficiency of oils from calcite surfaces upon exposure to various saline solutions was calculated, more details on this are given in Table 6.1.

Table 6.1: Desorption of dead crude oils from calcite surface upon exposure to different saline solutions

Dead Oil A-Calcite Surface						
Aqueous Solution	**SW**	**2dSW**	**5dSW**	**10dSW**	**20dSW**	**50dSW**
Desorbed Frequency Change Δf (Hz)	-5.60	-14.89	-3.30	8.30	-2.19	-0.80
Desorbed Mass Δm (mg/m^2)	0.33	0.87	0.19	0.49	0.13	0.04
Desorption Efficiency (%)	14.35	37.82	8.26	21.30	5.62	2.05

Dead Oil B-Calcite Surface						
Aqueous Solution	**SW**	**2dSW**	**5dSW**	**10dSW**	**20dSW**	**50dSW**
Desorbed Frequency Change Δf (Hz)	-5.50	-13.93	-2.60	-6.50	-2.00	-1.00
Desorbed Mass Δm (mg/m^2)	0.32	0.82	0.15	0.38	0.11	0.059
Desorption Efficiency (%)	10.20	25.62	4.68	11.87	3.43	1.84

Dead Oil C-Calcite Surface						
Aqueous Solution	**SW**	**2dSW**	**5dSW**	**10dSW**	**20dSW**	**50dSW**
Desorbed Frequency Change Δf (Hz)	-5.00	-10.00	-2.10	-5.00	-1.50	-1.00
Desorbed Mass Δm (mg/m^2)	0.29	0.59	0.12	0.29	0.09	0.059
Desorption Efficiency (%)	6.74	13.72	2.76	6.74	2.09	1.37

The calculated values are summarized in Figure 6.4. It is obvious that the desorption efficiency is generally decreased as the acidity of crude oil is increased. The lowest desorption efficiency was for crude oil C, which contained the highest acidic components (O= 10.33%). Whereas the highest desorption efficiency was for crude oil A, having the lowest amount of acidic components (O= 2.2%). These observations could be attributed to the high bonding strength of negatively charged acidic components onto the positively charged calcite surface, i.e., the attractive adhesion forces are higher than the electrostatic repulsion forces. Such results are strongly supported by our previous work [123], exhibiting a minimal change in the wetting condition of carbonates when crude oil C with a high polar content was used. Fathi et al. [39] also found that the oil depleted in water-soluble acids can be displaced easily from the chalk cores compared to the original oil with a high acid number (1.8 mg KOH/mg).

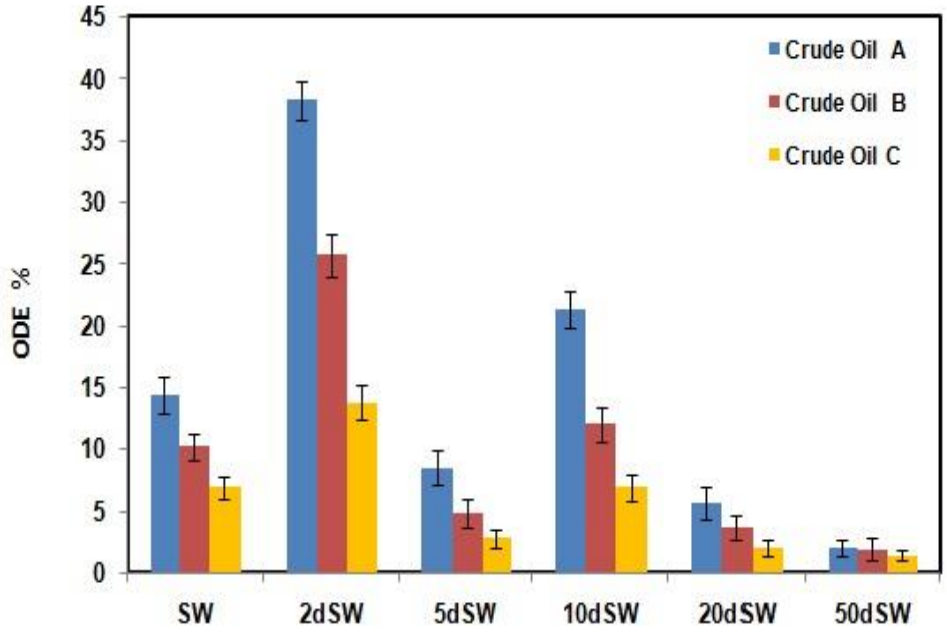

Figure 6.4: Oil desorption efficiency (ODE) from the calcite surface upon exposure to seawater and different diluted versions of seawater.

Injecting seawater showed some desorption of the adsorbed layer from the calcite surface, and not much difference in desorption efficiency was observed for various types of oils used. As mentioned in the previous chapters, this result may originate from the mutual interactions between sulphate ions (SO_4^{2-}) and calcium ions (Ca^{2+}), i.e., multiple ions exchange on the surface, could be happening. The mutual interactions, therefore, could improve the electrostatic repulsion and reduce the adhesion between the adsorbed polar oil components and calcite surface, thereby resulting in desorption from the surface [19]. The reactivity of Mg^{2+} ions could also increase in water, and it can even substitute Ca^{2+} from the calcite surface and thereby displace Ca^{2+} ions that are bridged to carboxylic polar components, leading to further desorption from the carbonate surface. Figure 6.5 illustrates the potential chemical interactions between calcite/crude oil and saline solution. It is worth commenting that the previous adhesion analysis in Chapter 5 revealed a reduction in the adhesion of about 35% when a super saline solution was replaced by seawater. Some imbibition and core flooding experiments also emphasized that seawater could remove some of the light and heavy crude oils from carbonate rocks during secondary flooding [10,12,33,42, 50].

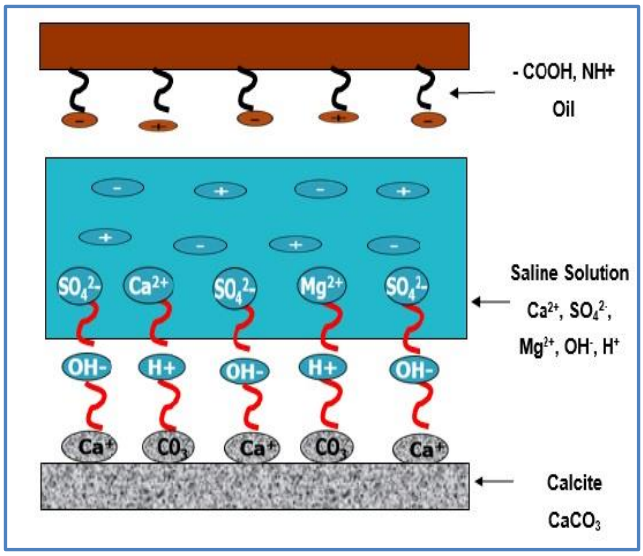

Figure 6.5: Potential interactions between calcite and oil components upon exposure to saline solution.

Furthermore, the significant desorption occurred when the calcite surface with adsorbed oil layer is subjected to solutions of 2dSW and 10dSW, sequentially. Such results differ to some extent from the adhesion force data in the previous chapter, showing a reduction by about 48.6% in the adhesion force as the salinity is diluted twice from seawater concentration, but plateauing after this level. The results nevertheless show a satisfactory agreement with the observations of zeta potential in Chapter 4, confirming that the surface potential of the carbonate surfaces become more negatively charged when the salinity decreased up to 10 times dilution. As the adsorbed oil layer is also negatively charged due to the presence of negative polar active components, it can lead to an increase in the electrostatic repulsion and an improvement in the desorption efficiency. Conversely, very small desorption was noticed with further dilution. This could be explained by 20dSW and 50dSW displayed less negative zeta potential with negligible change in the adhesion force values, as shown previously in Figure 4.1-Chapter 4 and Figure 5.3-Chapter 5, thus limited oil desorption is likely to be expected.

In the case of silica, Table 6.2 illustrates the measured frequency changes and calculated desorption efficiencies, which are summarised in Figure 6.6. It is obvious there is less amount of the adsorbed oil was desorbed than from the calcite surface at the high salinity solution (seawater). Previous studies have suggested that both oil and solid interfaces become charged in the presence of water film [68]. Hence, injecting high salinity solution with the presence of positive divalent ions such as Ca^{2+} and Mg^{2+} can act as a bridge between dissociated negative polar oil components and negative silica surface sites, leading to adverse desorption, as illustrated in Figure 6.7. These results are consistent with the basis of the experimental work of Lager and his co-workers [9] that a conventional high salinity water flood containing the high concentration of Ca^{2+} and Mg^{2+} resulted in low recovery factor compared with the modified brine (depleted in Ca^{2+} and Mg^{2+}).

Table 6.2: Desorption of dead crude oils from silica surface upon exposure to different saline solutions

Dead Oil A-Silica Surface						
Aqueous Solution	**SW**	**2dSW**	**5dSW**	**10dSW**	**20dSW**	**50dSW**
Desorbed Frequency Change Δf (Hz)	-6.94	-17.55	-3.46	-17.93	-9.37	-5.00
Desorbed Mass Δm (mg/m^2)	0.40	1.03	0.20	1.05	0.55	0.26
Desorption Efficiency (%)	9.38	23.71	4.68	24.22	12.66	6.75

Dead Oil B- Silica Surface						
Aqueous Solution	**SW**	**2dSW**	**5dSW**	**10dSW**	**20dSW**	**50dSW**
Desorbed Frequency Change Δf (Hz)	-6.10	-16.00	-3.00	-15.00	-8.00	-4.21
Desorbed Mass Δm (mg/m^2)	0.35	0.94	0.17	0.88	0.47	0.23
Desorption Efficiency (%)	8.12	22.76	4.28	21.42	11.38	5.56

Dead Oil C- Silica Surface						
Aqueous Solution	**SW**	**2dSW**	**5dSW**	**10dSW**	**20dSW**	**50dSW**
Desorbed Frequency Change Δf (Hz)	-2.00	-7.51	-1.80	-8.22	-2.31	-1.41
Desorbed Mass Δm (mg/m^2)	0.12	0.44	0.10	0.47	0.11	0.08
Desorption Efficiency (%)	4.84	17.75	4.00	18.96	4.43	3.22

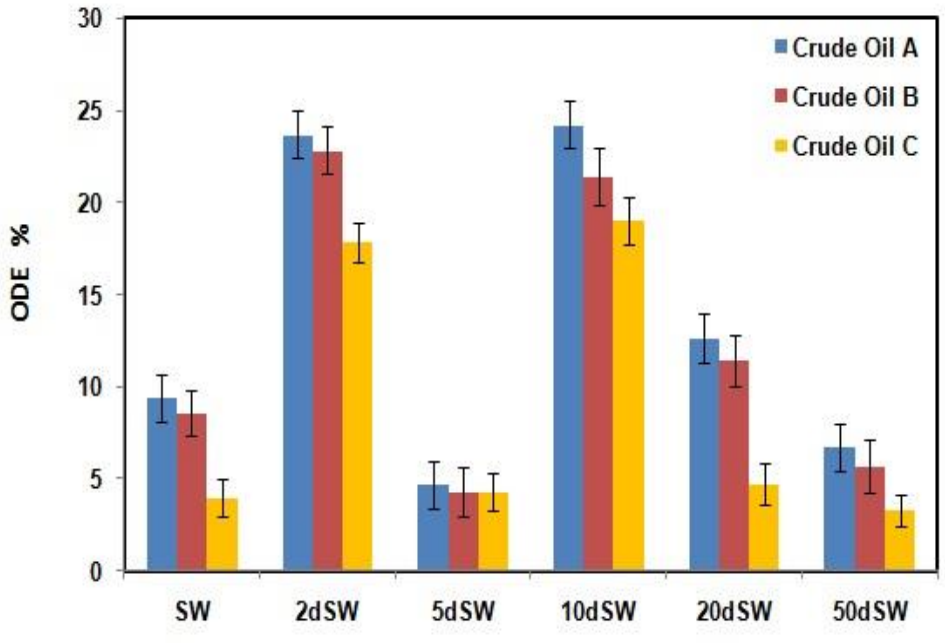

Figure 6.6: Oil desorption efficiency (ODE) from the silica surface upon exposure to seawater and different diluted versions of seawater.

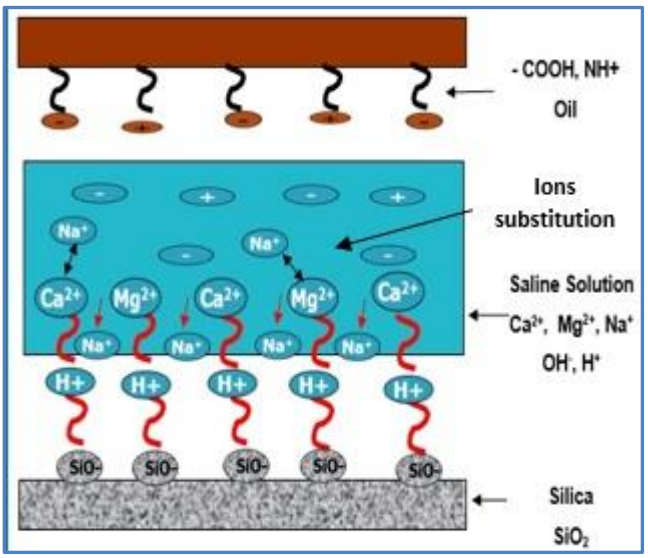

Figure 6.7: Potential interactions between silica and oil components upon exposure to saline solution.

Considering the bridging effect of potential determining ions, it can thus be expected limited desorption (4.8%) of crude oil C, which has the highest polar components, from silica surface upon exposure to seawater [19].

On the other hand, it is obvious from Figure 6.6 that injecting low salinity solution increases the extent of desorption from silica surface in comparison with the high salinity solution. The highest desorption efficiency is observed for 10 times-diluted seawater. It is apparent that a sharp decrease in the attraction force had happened when switching from seawater to 10dSW. This could be explained by promoting the electrostatic repulsion forces. In our system, the interactions occurred between the silica-coated sensor and crude oil in the presence of the aqueous phase. It has previously been suggested that the isoelectric point for silica is about pH 2 and the surface is negatively charged at neutral pH (pH >6) [6,108]. As given before in Table 3.2-Chapter 3, the low salinity solutions have a pH range from 7.01-7.58, which can enhance the negative charges on surface sites. Thus, at low electrolyte concentration and a relatively high surface charges density, the repulsive energy is going to play a vital role in the interactions between silica/brine/oil interfaces, and therefore promoting the desorption efficiency when a solution of 10 times dilution used. In contrast, injected seawater is likely to screen off the surface charges, resulting in a decrease in the repulsion and less desorption efficiency.

Further limited desorption has been observed at 50dSW. In this case, despite the ionic strength of salt solution being reduced at neutral pH value, the repulsive electrostatic force is likely to be insufficient to promote the desorption. Farooq et al. [155] found that a critical expansion of the EDL is required for further desorption from silica by low salinity solution.

Another possible explanation in which the saline solutions impact the desorption of crude oil from silica surface is by considering the effect of mutual ions interaction, as the divalent cations (Ca^{2+} and Mg^{2+}) could be replaced by the monovalent cations, such as Na^{+} (see Figure 6.7). As a result, the divalent ions leave the silica surface along with the crude oil

components [79]. This could provide further proof to explain the limited desorption when utilizing 20 and 50 times-diluted seawater, i.e., when the ionic strength was decreased. The only opposite trend was for 5dSW, and the reason for this behaviour could be related to the reduction in the effect of the ions binding and EDL expansion. As with the 5 times dilution, the concentration of the divalent and monovalent ions is relatively decreased, and correspondingly their binding to the solid/water interface is reduced. Simultaneously, in comparison with the 10dSW, it is expected that the electrical double layer expansion is not large enough to promote the desorption of oil. This means that the two proposed mechanisms are not much dominant for the oil desorption when 5dSW used.

For different diluted versions of seawater, the overall desorption from silica surface was the highest for crude oil A with the low polar contents, acid number= 0.25 mg KOH/g. As illustrated in Figure 6.7, the presence of electrolyte solutions results in the formation of a positively charged water film between silica and oil. Therefore, if the crude oil with a higher acid number (crude oil C) used, then the acidic components are tightly held through the water phase, thereby resulting in less desorption [156]. Generally, the effect of active polar components present in crude oil on the oil desorption efficiency (ODE) is more pronounced for calcite surface than silica surface upon exposure to various salinities. This discrepancy may be because of the difference in electrostatic interactions between charged functional groups in oil and charged mineral surfaces.

6.4 Summary

In this study, Quartz Crystal Microbalance (QCM) has been used to assess the impact of ionic strength and brine salinity on the desorption efficiency of various types of crude oils from calcite and silica surfaces. It is believed that the novel observations of this work are helpful to glean more information on how the variation in the chemical composition of crude oils and the electrostatic properties of surfaces, which significantly affect oil's adhesion, can influence the adsorption/desorption process.

The results clearly show that the potential of low salinity flooding is closely related to the chemical composition of crude oil and the characteristic of surface minerals. The most notable observation to emerge from the data comparison is that the effect of active polar components represented by the acid number on the oil desorption efficiency (ODE) is more pronounced for calcite surface than silica surface upon exposure to different saline solutions. Furthermore, less desorption happened from the silica surface compared to the calcite surface upon exposure to seawater for all three oils examined. The findings also confirm the potential of twice-diluted seawater, showing high desorption efficiency for the calcite surface, which supports the previously discussed results in Chapter 5. However, 10 times diluted seawater gives the highest oil desorption in the case of the silica surface.

The results obtained from this work provide further evidence that either EDL expansion (electrokinetics repulsive) or multiple ions exchange mechanism alone could affect the desorption efficiency, i.e., a combination of these two mechanisms are dominant for the oil desorption.

In summary, the current QCM work helps to give an indication of the oil desorption efficiency during different salinity injection at a micro-scale; however, it was not precisely designed to mimic *in-situ* real reservoir conditions. Thus, for more practical implications, a set of core flooding experiments under high pressure-high temperature conditions have been extensively conducted to get more reliable and conclusive evidence about the correlation between the potential of low salinity flooding and oil

composition. The obtained observations will be discussed in detail in the next Chapter.

CHAPTER 7

Effect of Crude Oil Composition on the Potential of Low Salinity Flooding for Enhanced Oil Recovery in Carbonates

7.1 Introduction

Some of the lab tests on the potential of chemically modified water for EOR have been carried out, yet there are still critical issues. From a comprehensive review of many technical works covering various salinity aspects, it is found that researchers have tended to focus primarily on investigating the impact of salinity and ionic strength on oil recovery without taking into consideration the effect of oil composition and rock mineralogy on the real low salinity impact, especially in carbonate rocks.

In the previous chapter, desorption efficiency of different kinds of crude oils from surfaces has been assessed by Quartz Crystal Microbalance (QCM) approach. It should, however, be noted that despite its efficiency and simplicity, such an approach is limited in its capability to resemble *in-situ* reservoir conditions, which are associated with the use of natural carbonate rocks and providing high pressure-high temperature conditions. In this work, a series of systematic core flooding experiments were carried out under reservoir-like conditions to evaluate the effect of the diversity of crude oil composition on the potential of low salinity flooding for enhanced oil recovery in carbonate rocks.

The same three crude oils that were used in our previous QCM work [19] were used in this study to saturate the core samples prior to brine flooding. Outcrop limestone and subsurface dolomite samples with the properties outlined in Chapter 3 were used to mimic carbonate reservoirs with different mineralogy. Tertiary oil recovery by different diluted versions

of seawater was evaluated relative to the secondary recovery by seawater or formation water.

In this Chapter, the effect of seawater and different diluted versions of seawater on the macroscopic displacement efficiency of the outcrop limestone and subsurface dolomite rocks saturated with different kinds of oil will be first described. Then, the effect of formation water on the performance of low salinity water flooding will be discussed. Finally, the role of potential determining ions such as SO_4^{2-}, Ca^{2+}, and Mg^{2+} on the overall macroscopic displacement efficiency will be qualitatively summarized.

7.2 Effect of Crude Oil Composition and Rock Mineralogy on the Potential of Low Salinity Flooding for EOR

The impact of different salinity solutions on oil recovery of carbonate samples aged with different kinds of dead crude oil is studied. The aim was to verify whether changing the type of crude oil (i.e., the concentration of polar organic components) could affect the potential of low salinity flooding or not. A set of six core flooding experiments were carried out on outcrop limestone and subsurface dolomite cores by injecting seawater in secondary mode. Then, different diluted versions of seawater were flooded sequentially in tertiary mode. An indicative example of the volumes of produced oil and brine collected during one of the flooding experiments is illustrated in Figure 7.1.

Figure 7.2 shows the results of salinity flooding on outcrop core EST-24, saturated with crude oil A with the lowest acidic components (AN=0.25 mg KOH/g). It can be observed that the oil recovery was about 52.6% of the original oil in place (OOIP) at the end of the secondary mode by injecting 3 PVs of seawater. The substantial amount of oil of about 34% of the OOIP was obtained after injecting 0.4 pore volume of seawater, i.e., before breakthrough time, coinciding with a maximum increase in the corresponding pressure drop (4.5 bar). The pressure drop was then

decreased due to oil production to stabilize at the end of the seawater injection at 1.45 ± 0.05 bar. After all moveable oil was displaced by seawater, the core sample was subjected to low salinity solutions, sequentially. Injection twice-diluted seawater in tertiary mode reflected an increase in oil recovery of 4.2% of the OOIP, while flooding 5dSW and 10dSW did not yield significant improvement in oil recovery (1.6% of the OOIP). No enhancement in recovery factor was observed with the further dilutions. Such results are supported by the adhesion work measurements reported in Chapter 4-section 4.7, showing a relatively sharp decrease in the adhesion work values when switching from high saline solution to twice-diluted seawater, and the effect was more pronounced for crude oil A. The differential pressure was decreased steadily as the salinity of water declined to level off at about 0.55 bar.

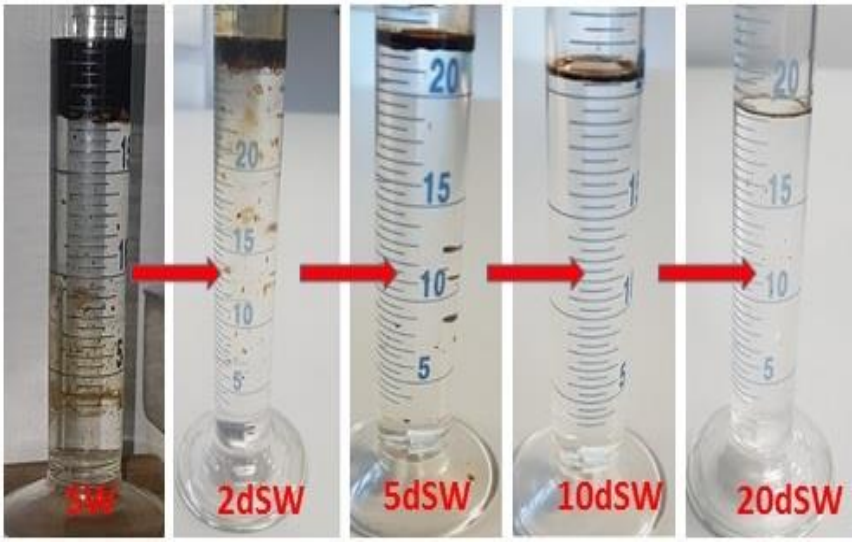

Figure 7.1: Volume of produced oil and brine during one of the sequential flooding experiments on carbonate sample.

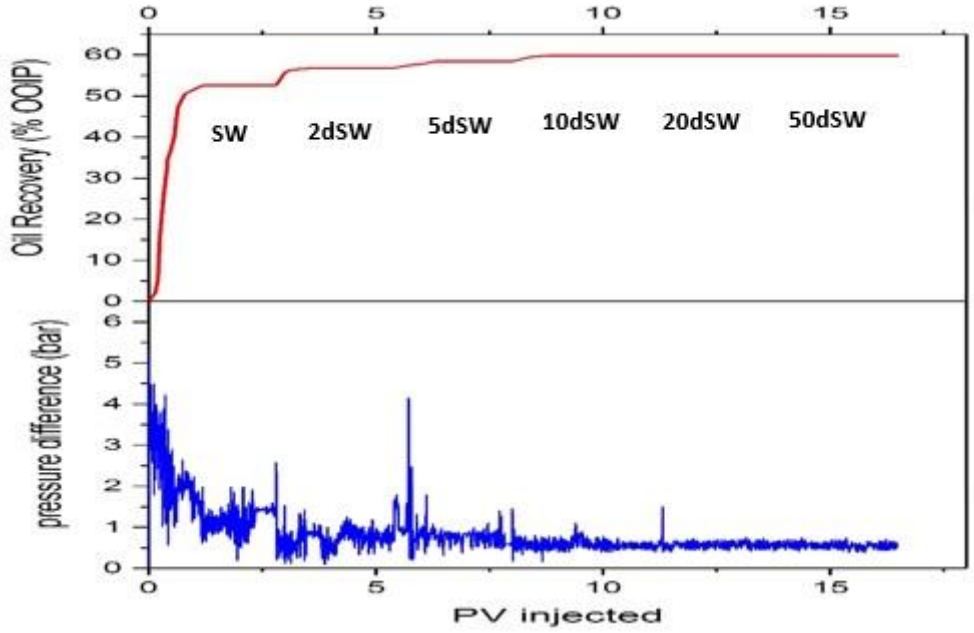

Figure 7.2: Oil recovery and corresponding pressure drop for outcrop core (EST-24) saturated with crude oil A.

In the second flooding test, the macroscopic displacement efficiency of low salinity flooding on reservoir carbonate rock (M-01) was examined. The core was saturated with the same kind of crude oil used in the first experiment. The objective was to test if the potential of low salinity injection is linked to rock mineralogy. The core was subjected to the same flooding sequence as core EST-24. As shown in Figure 7.3, the oil recovery was comparable to the previous experiment (53.2 % of the OOIP) during secondary recovery. Injecting twice-diluted seawater resulted in a significant improvement in oil recovery of 6.8 % of the OOIP. Even though the permeability of M-01 core sample is less than that of EST-24, an overall enhancement of 10 % of the OOIP was obtained due to the tertiary low salinity flooding in M-01 compared to 7.4 % of the OOIP for EST-24 sample. This could be strongly attributed to the difference in the mineralogy of outcrop and reservoir core samples, as will be discussed later in Chapter 9. Like the previous case, a peak pressure drop was observed before breakthrough time, and then it stabilized with the stepwise low salinity injection to end up with the value of about 0.48 ± 0.05 bar, which might refer to the stable resistance to the fluid flow [157].

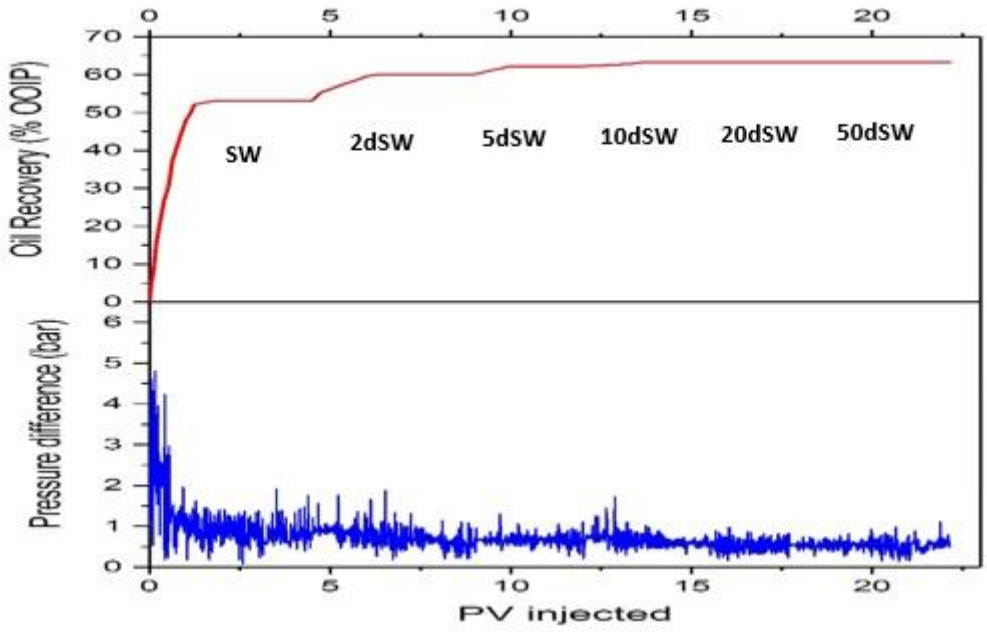

Figure 7.3: Oil recovery and corresponding pressure drop for reservoir dolomite core (M-01) saturated with crude oil A.

Another two core flooding experiments were carried out on the outcrop rock sample (EST-26) and reservoir rock (M-02), saturated with crude oil B, having a higher acid number (AN=0.46 mg KOH/g) compared to crude oil A. Figures 7.4 and 7.5 show the results of oil recoveries and pressure drop profiles for the two samples examined. It is apparent that seawater injection recovered 43% and 47% of the OOIP for both outcrop and reservoir rocks at the end of secondary mode. It can also be seen that injecting twice-diluted seawater in tertiary mode resulted in a relatively less incremental in oil recovery of 2.8% and 5 % of the OOIP for both samples examined in comparison with those yielded from the core samples saturated with crude oil A. This discrepancy could be related to the variation in the chemistry of oil adsorbed onto the rock surfaces, thereby resulting in a more hydrophobic surface and less desorption efficiency. More discussion on the effect of oil composition will be given in Chapter 9. As reviewed previously in Chapter 2, no sufficient data are available in the literature, showing the effect of chemical oil composition on the potential of low salinity flooding to compare with the current results. Nevertheless, the above observations are supported by our previous

QCM analysis at the microscopic scale [19], that the highest desorption efficiency was for crude oil A, having the lowest amount of acidic components (O= 2.2%).

A further slight increase in recovery of about 1-1.4% of the OOIP was obtained with 5dSW and 10dSW for the two samples examined. No more oil was collected after injection of a total of about 6 pore volumes of 20dSW and 50dSW into the carbonate cores, and the oil recovery plateau was reached. Like the previous experiments, the differential pressure was increased sharply at the beginning of injection and was then dropped gradually at each stage of low salinity injection to stabilize at 0.4 ± 0.4 and 0.78 ± 0.5 bar for EST-26 and M-02 core samples, respectively.

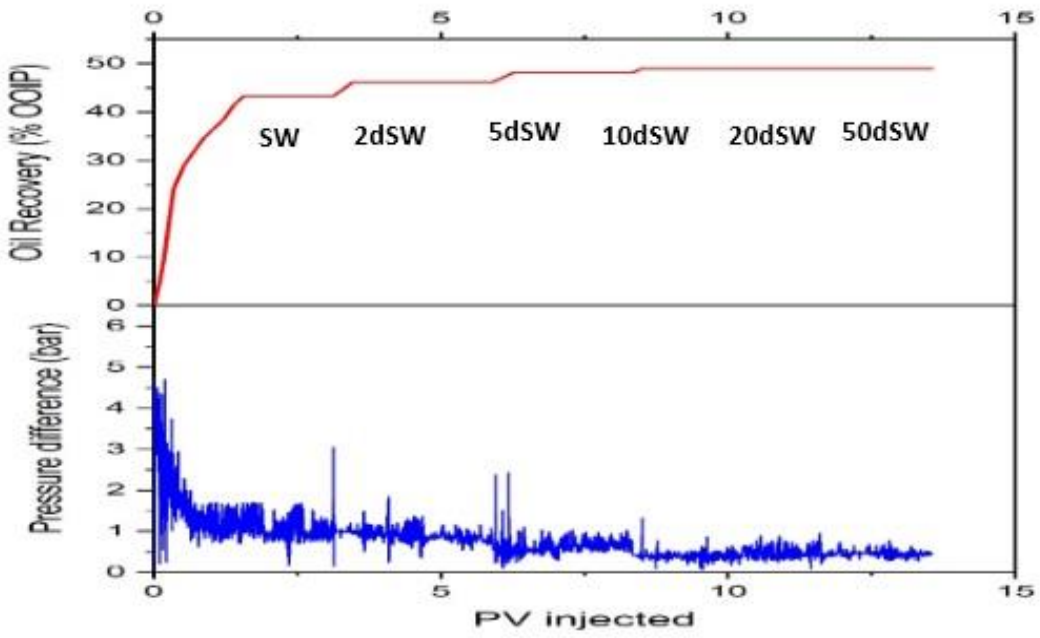

Figure 7.4: Oil recovery and corresponding pressure drop for outcrop core (EST-26) saturated with crude oil B.

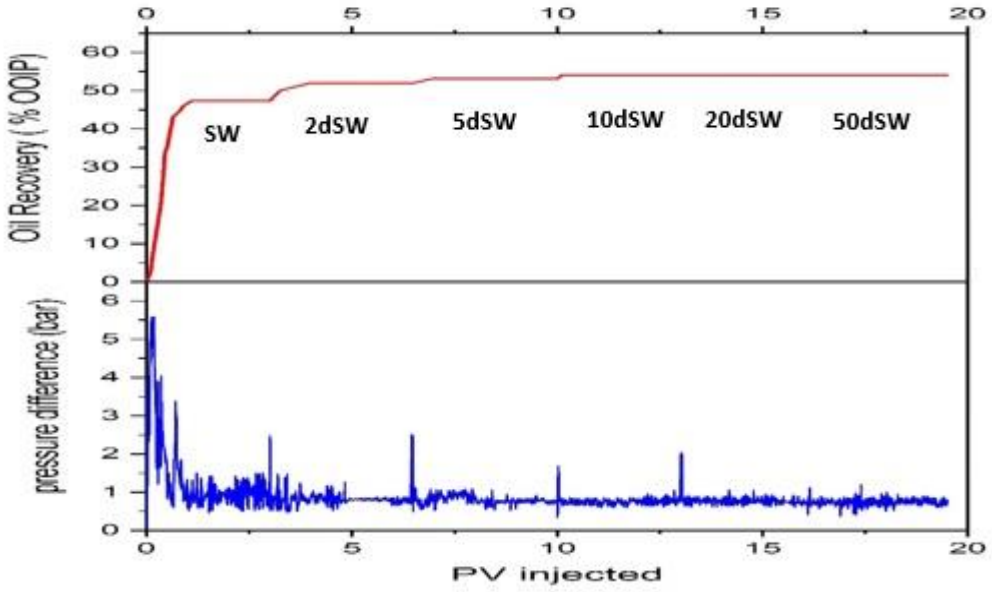

Figure 7.5: Oil recovery and corresponding pressure drop for reservoir dolomite core (M-02) saturated with crude oil B.

To confirm the effect of oil composition on the potential of low salinity flooding for EOR in carbonates, further core flooding tests were performed using outcrop core (EST-31) and reservoir core (M-03). Both samples were saturated with crude oil C, containing the highest amount of polar components (AN=2.54 mg KOH/g). The flooding sequence was similar to the previous tests. From the comparative results, Figures 7.6 and 7.7, it can be seen that 40.5 to 43% of the OOIP was recovered by seawater at the end of secondary flooding. Even though both cores examined in this case have a higher absolute permeability (112 and 290 md for EST-31 and M-03, respectively) in comparison with other core samples examined before, no more oil was collected during the tertiary low salinity flooding into outcrop sample. While a negligible increment in oil recovery was observed upon injecting 2dSW into reservoir dolomite core. To confirm these observations, the injection rate was increased to 1.5 ml/min, but no more oil was recovered. Such results could be strongly traced back to the presence of higher amount of polar organic components in oil C and viscosity effect. These findings are in line with those reported in Chapter 4 that crude oil C showed higher adhesion work compared to other kinds of

crude oil examined, thereby more work is needed to separate the oil phase from the solid, leading to less displacement efficiency. It is evident that the potential of tertiary salinity flooding for improved oil recovery in carbonate formations with high acidity and heavy crude oils is negligible compared to that saturated with the light crude oils.

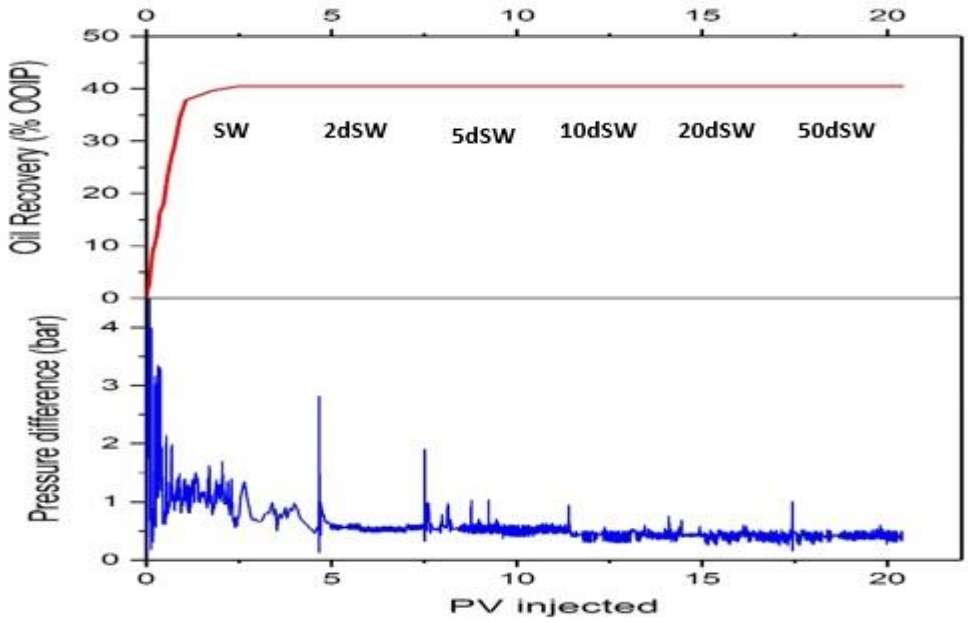

Figure 7.6: Oil recovery and corresponding pressure drop for outcrop core (EST-31) saturated with crude oil C.

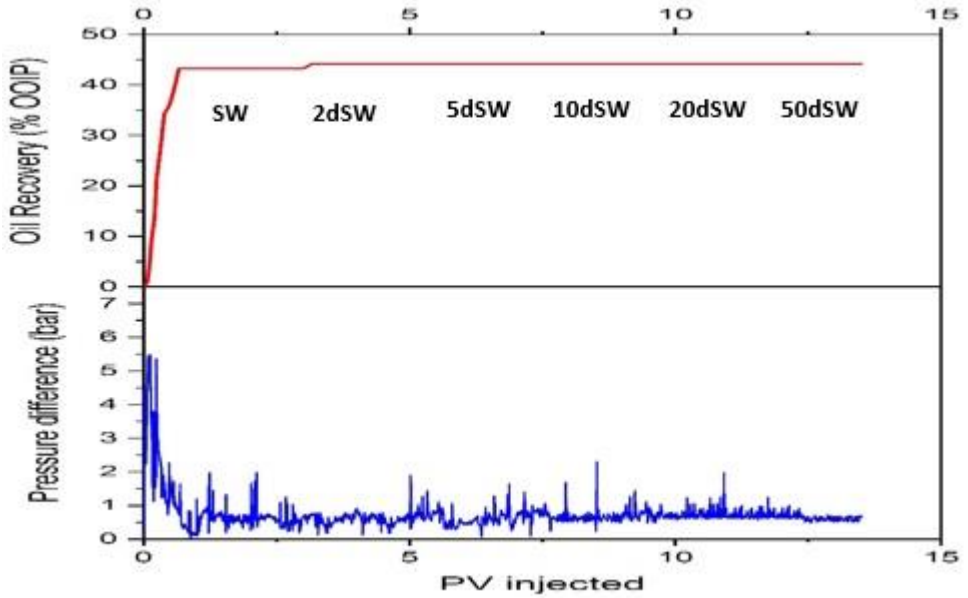

Figure 7.7: Oil recovery and corresponding pressure drop for reservoir dolomite core (M-03) saturated with crude oil C.

7.3 Effect of Formation Water on the Potential of Low Salinity for EOR

Due to the fact that in practical oil field operations formation water may represent a source of injecting water, two flooding tests were performed by injecting formation water with the salinity of 200000 ppm in secondary mode followed by subsequent exposure to different slugs of diluted seawater (2dSW and 5dSW) in tertiary mode.

After a gentle core cleaning, the same outcrop and reservoir core samples (EST-24 and M-01) that used in the first set of experiments were re-utilized in this test. Crude oil A was also used to saturate the rock samples. The aim was to verify that any potential improvement in oil recovery is due to the invading brine, i.e., not because of the petrophysical variation of rock samples or oil composition. Four pore volumes of synthetic formation water were injected in secondary mode until the oil production was stopped and a stable differential pressure profile was attained. This was followed by sequential injection of 2dSW and 5dSW in tertiary mode. The oil recoveries and pressure drop profiles for the two cores tested are illustrated in Figures 7.8 and 7.9, respectively.

A noticeable distinction in the amount of recovered oil than that of seawater injection was observed when formation water used. The cumulative oil recovery was 30 % and 37% of the OOIP for outcrop and reservoir core samples, respectively. Such observation is in line with what was previously obtained by Strand et al. [43] who conducted a study on enhancing oil recovery from naturally fractured chalk reservoir. In addition, the flooding of twice-diluted seawater yielded a minor improvement in oil recovery of about 1.5-2.5% of the OOIP, and no recovery improvement was observed with the 5dSW. In general, it is apparent that the potential of dilution slugs of seawater for enhancing oil recovery was less pronounced when formation water was injected in secondary mode. This might be commonly linked to the scale precipitation formed by formation water, as identified by Nasralla et al. [158].

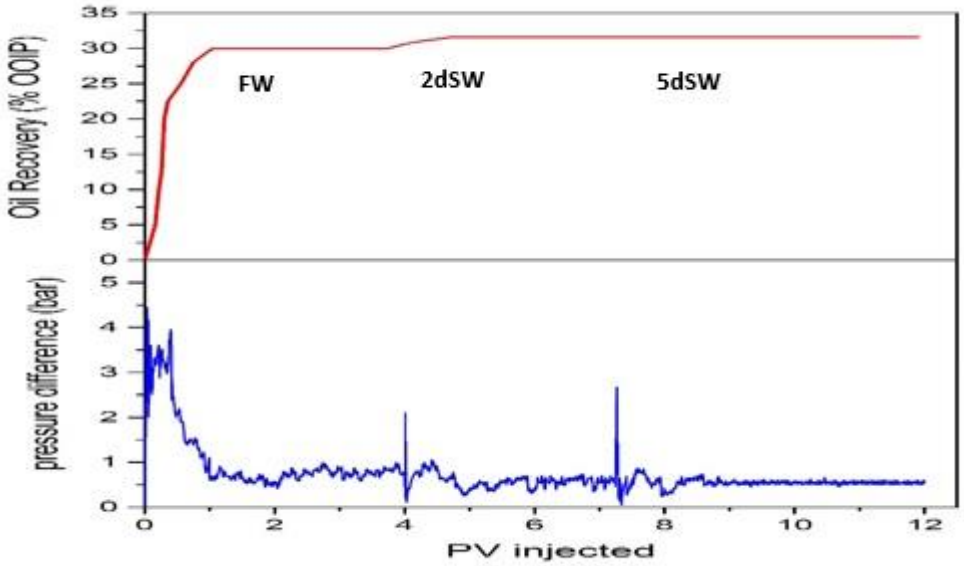

Figure 7.8: Oil recovery and corresponding pressure drop for outcrop core (EST-24) saturated with crude oil A upon injecting formation water in secondary mode and diluted seawater in tertiary mode.

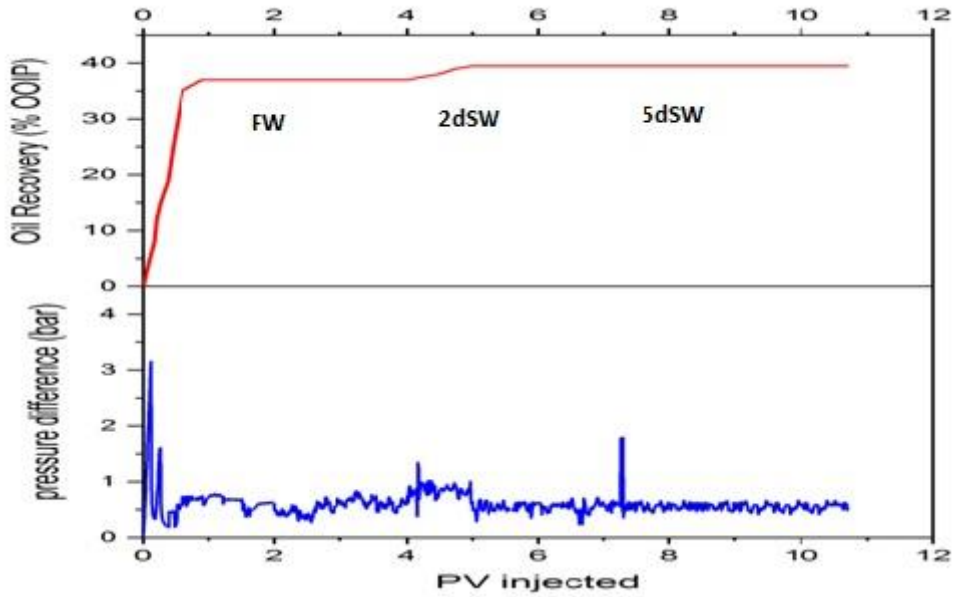

Figure 7.9: Oil recovery and corresponding pressure drop for reservoir dolomite core (M-03) saturated with crude oil A upon injecting formation water in secondary mode and diluted seawater in tertiary mode.

The general differential pressure trends are similar to the previous experiments since the pressure drop over the core sample was increased before breakthrough time and decreased then with the stepwise low salinity injection. It is, however, worth noting that the differential pressure was more stable than the previous cases, which might be attributed to the potential of scale precipitation [158].

7.4 Effect of Potential Determining Ions on Oil Recovery

In this section, the impact of low salinity flooding with respect to the concentration of SO_4^{2-}, Mg^{2+}, and Ca^{2+} ions are qualitatively evaluated. The goal was to find the effective concentration of divalent ions that affect the performance of low salinity solution for enhanced oil recovery. NaCl solution was used as the base brine with a salinity equal to that of twice-diluted seawater (2 wt. %), as a significant low salinity effect was observed upon exposure to this solution, i.e., it represents the optimum saline solution as outlined earlier. The concentration of sulphate, magnesium, and calcium ions was then increased gradually with the proportion of 0.5x, 1x, 2x, 3x, 4x, the concentration of twice-diluted seawater. As mentioned before in Chapter 5, the concentration of sulphate ions in seawater is less than that of Mg^{2+} ions [37]. For this, the concentration of Mg^{2+} ions has been adjusted to be more than the concentration of SO_4^{2-} ions.

A series of core flooding tests were carried out by injection seawater in secondary mode followed by flooding NaCl solution with different concentrations of potential determining ions in tertiary mode. The results of oil recovery and corresponding differential pressure as a function of injected pore volumes are illustrated in Figures 7.10 through 7.12. From Figure 7.10, it is clear that the highest increase in oil recovery (5.5% of the OOIP) was achieved by saline solution 1×SO_4, i.e., when the concentration of sulphate ions equal to that in twice-diluted seawater. Increasing the concentration of SO_4^{2-} ions to 3 times showed a further small increase in oil recovery of about 2.8% of the OOIP, and no

improvement was observed beyond this level. Such observations are supported by the adhesion measurements in Chapter 5, showing a reduction in the adhesion forces when the concentration of sulphate ions was increased 3 times (0.6 wt. %) the concentration of twice-diluted seawater. This finding is also in line with some of the spontaneous imbibition results reported in the literature [37]. Similar to previous core flooding tests, the overall pressure drop across the core was reduced with a sequence injection, which could be linked to the same previously discussed reasons in section 7.2.

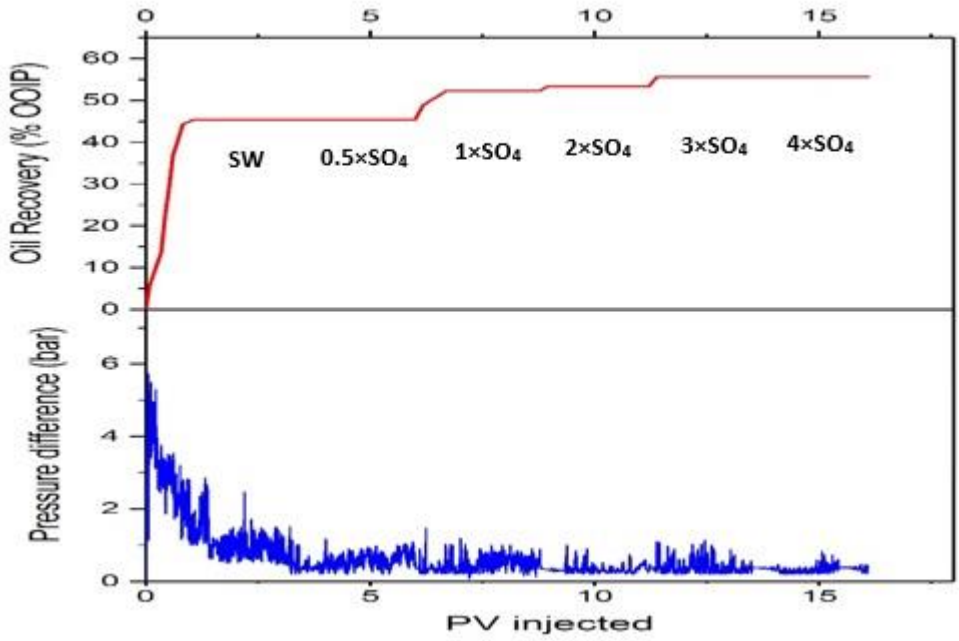

Figure 7.10: Oil recovery and corresponding pressure drop for outcrop core (EST-30) saturated with crude oil A upon exposure to seawater in secondary mode and saline solutions varying in sulphate concentration in tertiary mode.

Likewise, the impact of magnesium concentration on the efficiency of low salinity flooding has been studied, and the results are shown in Figure 7.11. A significant improvement in oil recovery (6.6 % of the OOIP) was obtained when the EST-33 core was subjected to brine solution of 1× Mg^{2+}, after seawater injection in a secondary mode which recovered 42% of the OOIP. A small incremental in oil recovery of about 1.9% of the OOIP was observed when the concentration of magnesium ions

increased to two times that of twice-diluted seawater. No improvement was recorded with the other proportions of magnesium examined. Such results are relatively different from what was previously observed in Chapter 5 by measuring the adhesion forces, indicating that Mg^{2+} ions had a much smaller effect on the adhesion forces compared to SO_4^{2-} ions. This confliction is likely to be attributed to the variation in the test conditions. Since, the core flooding experiments were conducted under high temperature (80 °C) which may, therefore, increase the affinity of magnesium ions toward carbonate surface when the temperature increased, leading to a measurable effect on oil recovery.

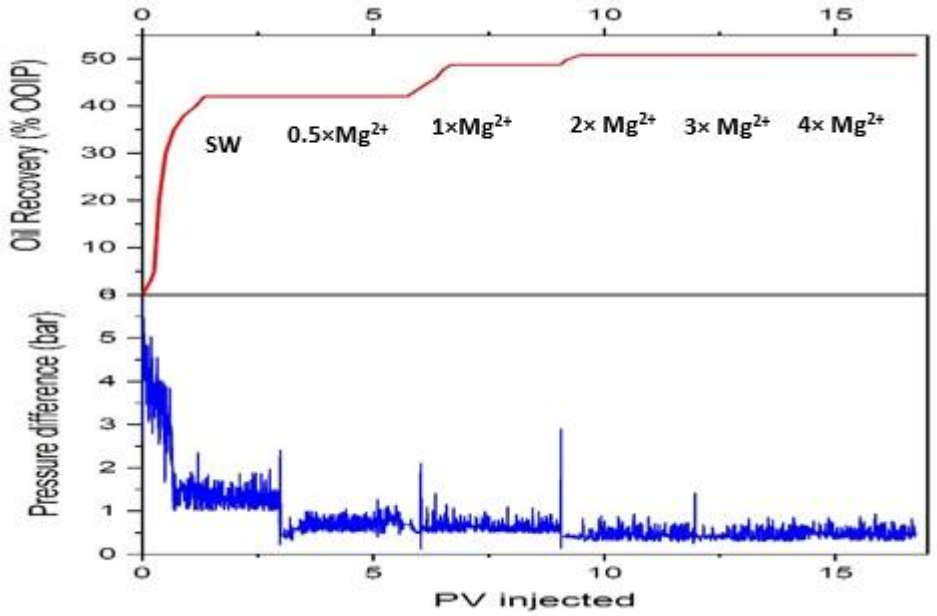

Figure 7.11: Oil recovery and corresponding pressure drop for outcrop core (EST-33) saturated with crude oil A upon exposure to seawater in secondary mode and fluids varying in magnesium concentration in tertiary mode.

The last core flooding test was conducted to evaluate the link between the concentration of Ca^{2+} ions and the performance of low salinity. Seawater was first injected into the core EST-25 in secondary mode, which recovered only 44.44 % of the OOIP, as shown in Figure 7.12. Apparently,

injecting saline solution with the different concentration of Ca^{2+} ions in tertiary mode did not show a substantial effect on oil recovery in comparison with the SO_4^{2-} and Mg^{2+} ions. Hence, only an increment in oil recovery of about 2.5 % of the OOIP was recorded with the brine of $2\times Ca^{2+}$, and no improvement in oil recovery was observed with the other proportions of Ca^{2+} ions. Contrary to expectations and within the accuracy of the test, it is found that the role of Ca^{2+} ions in enhancing oil recovery is almost insignificant compared to other potential determining ions. The present observation differs from the previously reported results [37,41]. This discrepancy could be mostly attributed to the difference in the samples and test conditions.

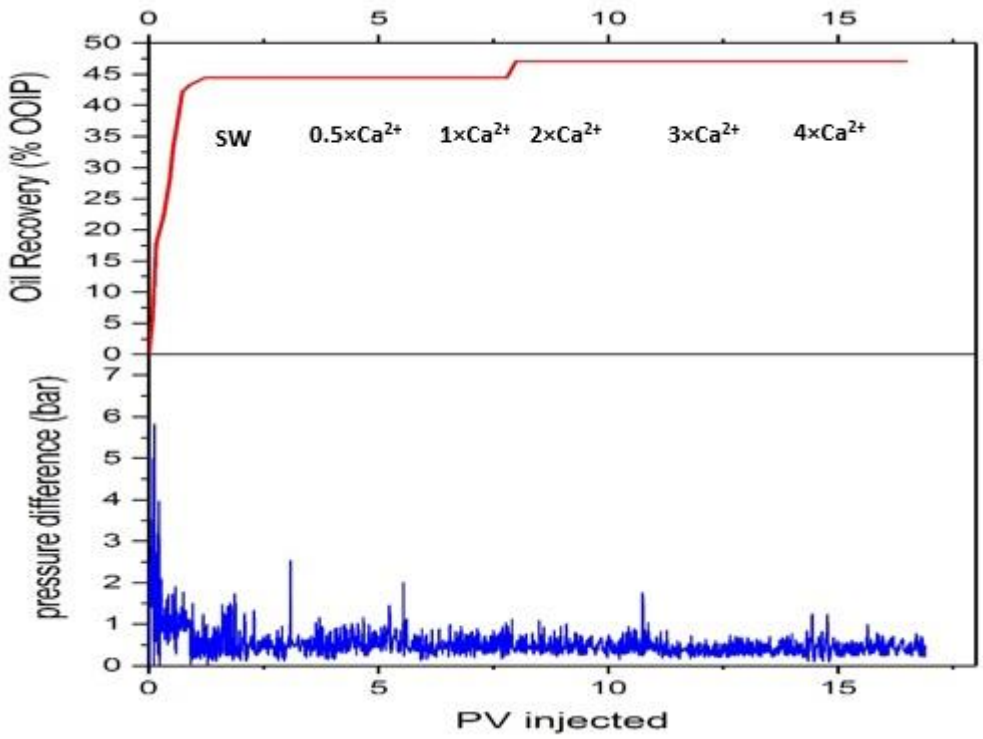

Figure 7.12: Oil recovery and corresponding pressure drop for outcrop core (EST-25) saturated with crude oil A upon exposure to seawater in secondary mode and fluids varying in calcium concentration in tertiary mode.

7.5 Summary

In this Chapter, the macroscopic displacement efficiency by injecting different diluted versions of seawater into outcrop limestone and reservoir dolomite carbonate rocks saturated with different kinds of oils has been evaluated. The effect of divalent ions on the low salinity potential has also been identified.

One of the main conclusions that emerge from this study is that the chemical composition of crude oil existing in the porous media significantly affects the potential of low salinity for EOR. A negligible improvement in the ultimate oil recovery is observed for the two types of carbonate samples examined when crude oil with a high acid number and polar organic content is used, suggesting that low salinity flooding is an unsuitable technique for enhanced oil recovery from such carbonate reservoirs with heavy-polar crude oil.

The overall tertiary low salinity injection demonstrates that twice-diluted seawater provides a substantial increase in oil recovery and its effect is more pronounced for reservoir dolomite rock saturated with crude oil A than outcrop rock; 6.8% of the OOIP for reservoir rock compared to 4.2% of the OOIP for outcrop rock. Such results seem to indicate that the potential of salinity flooding for EOR is not just affected by the composition of oil, but also by the rock mineralogy with respect to the anhydrite concentration. The results also indicate that 5dSW and 10dSW show a minor effect on EOR for both types of carbonate rocks used and no improvement in oil recovery is reported thereafter. It is found that injection formation water in secondary mode affects adversely the performance of salinity flooding for EOR, suggesting that injection seawater in secondary mode could be more favorable than formation water under such conditions.

From the systematic study of the effect of potential determining ions (SO_4^{2-}, Mg^{2+}, and Ca^{2+}), it can be reasoned that the role of SO_4^{2-} and Mg^{2+} ions during salinity flooding are almost stronger than that of Ca^{2+} ions. Also, there is a critical concentration of SO_4^{2-} and Mg^{2+} for a given amount

of NaCl, beyond which no enhancement in the macroscopic displacement efficiency was observed.

In summary, from the combination of the above findings, it is concluded that the main possible reason for the observed EOR effect during low salinity injection is likely to be due to the multiple ions exchange on the rock surface. Nevertheless, electrical double layer expansion (EDL) could also have a role to play.

The results of the current study extend the findings from the previous chapters. However, the core flooding experiments are subject to certain limitations in providing a full visualization of fluid movement and flow patterns inside the core samples. For this, further experimental work using a microfluidic system has been conducted to provide *in-situ* visualization of oil/brine flow. Such work can assist in our understanding of the complexities of the various interfacial phenomena governing surface wetting of crude oil on carbonates in a brine environment. The observed findings of the imbibition displacements at a mesoscale will be presented in the next Chapter.

Chapter 8

Pore-Scale Displacement Efficiency during Different Salinity Water Flooding in Hydrophilic and Hydrophobic Microstructures

8.1 Introduction

From the literature review in Chapter 2, it is found that many studies have been conducted to evaluate the performance of different displacing fluids for improved oil recovery at the pore-scale level. However, it is important to emphasize here that most of these studies up to now have been conducted on strongly water-wet microstructures, but with inconclusive findings in terms of understanding the mechanisms of low salinity flooding. Furthermore, to the best of the author's knowledge, no pore-scale displacement has been carried out in a completely oil-wet porous medium to resemble low salinity flooding in carbonates.

As pointed out in the previous chapter, macroscopic core flooding experiments have shown that injecting twice-diluted seawater can improve oil recovery in carbonate rocks with light crude oil. However, a clarification of low salinity flood performance at the pore-scale level and its related mechanisms need more investigation.

In this study, a microfluidic approach with surrogate rock pore structure is used to provide full *in-situ* visualization of oil/brine flow, which would help in predicting the mechanisms affecting oil sweep efficiency and revealing the potential of enhancing oil recovery by low salinity flooding at the mesoscale. To achieve this work, silicon-glass and polymer-coated physical pore networks were used to mimic the hydrophilic (sandstone) and hydrophobic (carbonate) surfaces, respectively. Two kinds of crude oils were used for the drainage process, while synthetic seawater and

different diluted versions of seawater were used for the imbibition displacements. The dynamics of displacement and the flow pattern of various saline solutions in the water-wet and oil-wet systems are critically compared. The potential of low salinity water flooding to improve the microscopic sweeping efficiency and the associated wettability effects are visually evaluated.

Throughout this Chapter, the observed results of the imbibition displacements are categorized into three main sections. In the first and second sections, the effect of different saline solutions on the pore-scale displacement efficiency and wettability alteration in the hydrophilic and hydrophobic networks will be discussed, respectively. Section three will include a discussion about the effect of low salinity flooding on the secondary recovery for both water-wet and oil-wet surfaces.

8.2 Effect of Salinity on the Pore-Scale Displacement Efficiency in a Hydrophilic Network

As mentioned before in Chapter 2, there is a general agreement that reducing the salinity of water below a certain level (4000-5000 ppm) revealed positive results for sandstone reservoirs by shifting rock wettability from water-wet conditions to mixed-wet [15,16,52,54]. Therefore, it is found that evaluating the effectiveness of low salinity water flooding for enhanced oil recovery in sandstones at the pore-scale level would be of great help to recognize the physicochemical mechanisms for the hydrophilic surfaces. Table 8.1 summarizes the observed results from a series of pore-scale displacement in the hydrophilic and hydrophobic microstructures. The initial oil saturation was almost the same (0.89-0.88) after drainage displacement into the water-wet micromodel saturated with crude oils A and B, respectively.

Table 8.1: Summary of micromodel experiments

Micromodel type	Oil	Wettability	S_{oi}	S_{or} at secondary mode	S_{or} at tertiary mode	Increased recovery %
Silicon-glass	A	Water-wet	0.89	0.23	0.14 - 2dSW	10
Silicon-glass	B	Water-wet	0.88	0.37	0.30 - 2dSW 0.29 - 5dSW	8
Polymer-coated	A	Oil-wet	0.84	0.47	0.46 - 2dSW	1
Polymer-coated	B	Oil-wet	0.87	0.50	0.50	0

The saturation of residual oil at the end of secondary flooding by seawater (imbibition) was determined to be 0.23 and 0.37, i.e. 57.9% of the movable oil was removed from the pore network saturated with crude oil B, but with a significant displacement (74%) for that saturated with crude oil A, having less polar organic components (acid number= 0.25 mg KOH/g). The discrepancy in the sweeping efficiency could be attributed to the difference in the oil composition, represented by the concentration of active polar components [19]. Hence, the presence of concentrated electrolyte solution results in the formation of a positively charged water film between silica and oil [16]. Therefore, if we consider the crude oil with higher polar components (crude oil B), then these components are tightly held through the water phase, thereby resulting in less desorption [19].

The segmented images of the water-wet micromodel, showing oil distribution after high and low salinity water flooding is illustrated in Figure 8.1. Due to the difficulty of measuring *in-situ* single-pore pressure, the overall pressure drop across the micromodel was measured instead, as shown in Figure 8.2.

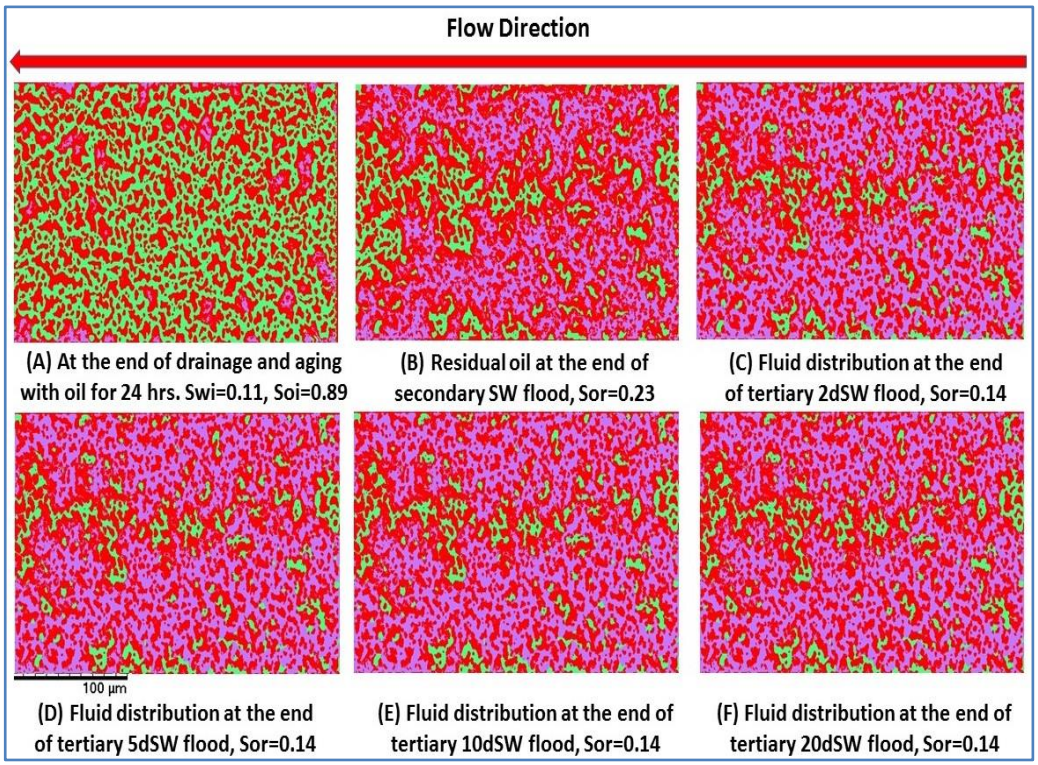

(A)

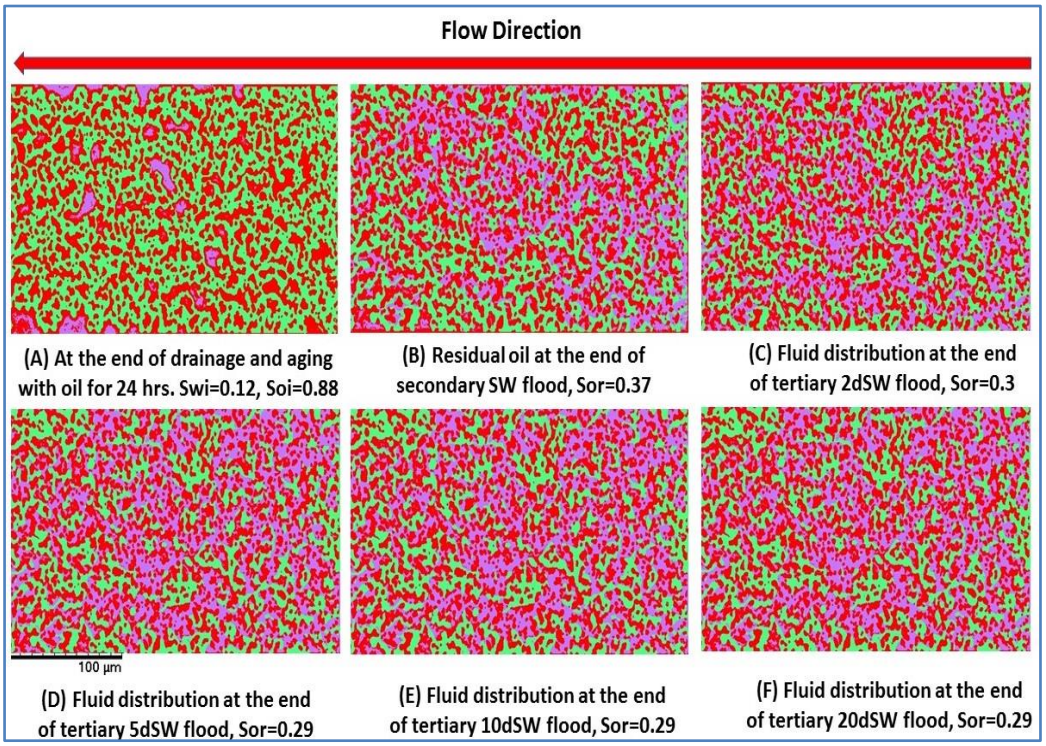

(B)

Figure 8.1: Micromodel images after secondary and tertiary flooding in a hydrophilic surface saturated with (A) crude oil A and (B) crude oil B. Red: grains, green: oil, purple: brine.

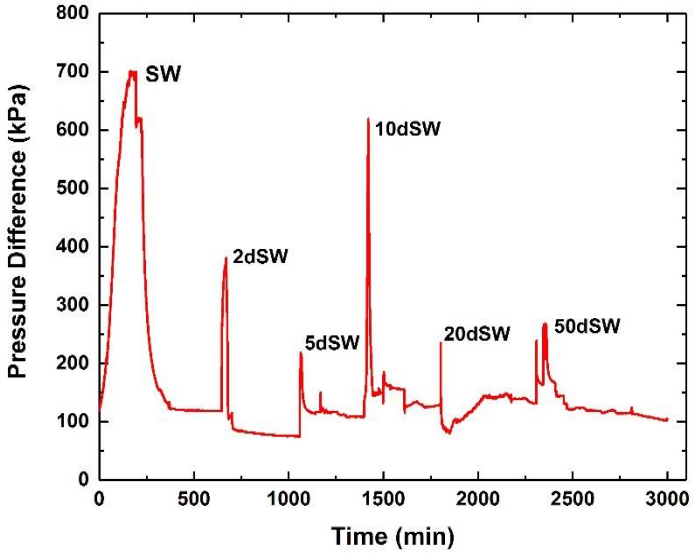

(A)

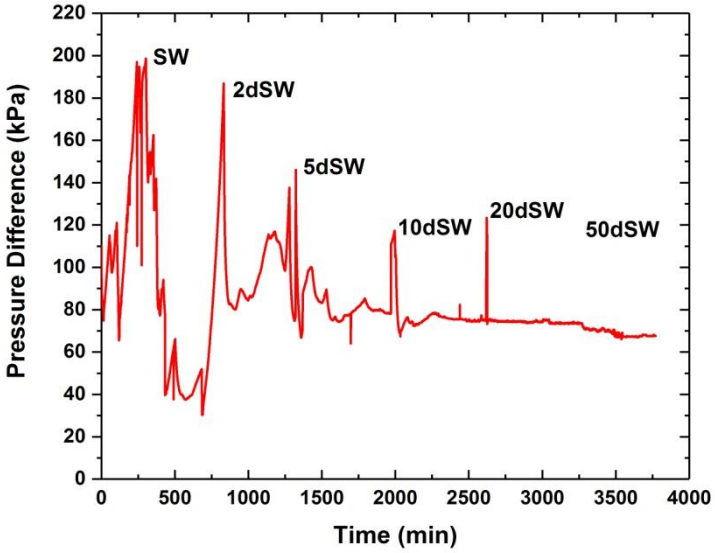

(B)

Figure 8.2: Pressure drop across the hydrophilic micromodel saturated with (A) crude oil A and (B) crude oil B during secondary and tertiary brine flooding.

It is clear that a considerable increase in the pressure difference was observed, particularly at the beginning of seawater flooding, suggesting a high capillary pressure and a strong resistance to the brine flow. Therefore, a higher viscous pressure drop is required to overcome the critical capillary entry pressure and enable brine to invade into the network. Afterward, the pressure drop was decreased and was relatively stable as a result of oil production and an increase in the relative permeability of brine.

It is important to emphasize that during secondary imbibition oil was transported along the pore-throat pairs due to the multiple snap-off and coalescence process, i.e., the flow was under a dynamic ganglion regime. As mentioned before in Chapter 2, the stability of displacement and fluid distributions are controlled by the capillary number ($Nc = \frac{v\mu}{\sigma cos\theta}$), where v is the velocity of the injecting fluid, μ is the viscosity of the injecting fluid, σ is the oil/brine interfacial tension (31.8 dynes/cm for seawater), θ is the contact angle between oil/brine and grain surface, and viscosity ratio (M = μ_w/μ_o, μ_w and μ_o represent the viscosities of the displacing and displaced fluids, respectively). In the case of seawater injection, the capillary number is low (6×10^{-8}) and M <1, indicating that the flow pattern falls within the unstable capillary fingering regime according to Lenormand's stability diagram [30]. The ganglion dynamics happen when oil trapped inside the pore-throat pairs is dominated by capillary forces rather than viscous forces [159].

Figure 8.3 shows two series of magnified images taken at two different locations of the hydrophilic micromodel during secondary seawater imbibition, clarifying snap-off and coalescence events. It is obvious that the snap-off occurred because of water film swelling in a throat between two contiguous pores (marked by a black stippled circle in Fig. 8.3C). This affects the stability of the oil/brine interface at the throat, leading to a discontinuity in the oil phase and forming an isolated cluster (ganglion), which was finally stabilized in a single pore (Fig. 8.3D). These

observations are in agreement with earlier visual studies by Amirian et al. [118] and Rücker et al. [159] for water-wet systems.

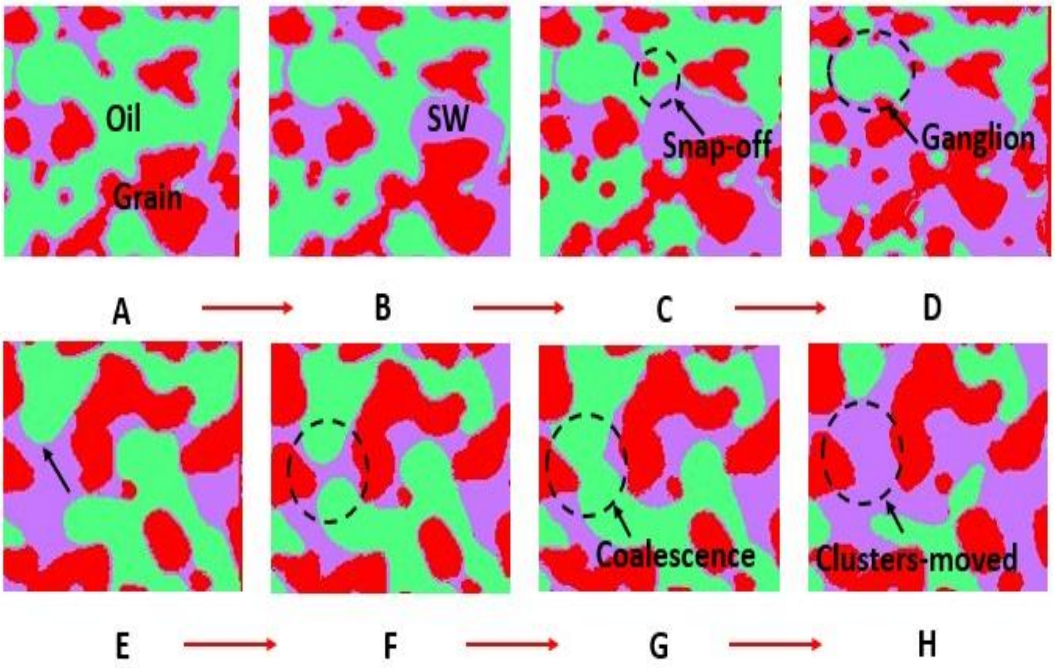

Figure 8.3: Two series of the same magnified sections at two different locations in the hydrophilic pore network during oil-seawater displacement. (A-D) Shows the sequence of snap-off. (E-H) Shows the sequence of coalescence and ganglia movement. Red: grains, green: oil, purple: brine.

At the beginning of brine flooding, the snap-off process frequently occurred due to the capillary disequilibrium and therefore the number of disconnected oil clusters was increased. After snap-off, the local capillary pressure was relatively increased as the individual clusters tend to find a new place with the minimum local energy [160]. For this, it is observed that the disconnected clusters prefer to internally reconnect (coalesce) with other movable clusters in the adjacent pore with lower capillary pressure, moving then along rigorously from pore-to-pore, leading to an improvement in the displacement efficiency and a decrease in the oil saturation. Due to the fact that the viscosity of the injected brine is very low; therefore, it is expected that the viscous forces showed a very small effect on the pore-scale displacement when the high salinity solution was

injected, and the net oil transport was almost due to the ganglion dynamic regime (oil cluster mobilization) even though the associated capillary number is very low (<< 10^{-5}). Figure 8.3E-G illustrates a sequence of coalescence during seawater injection. As the oil saturation was reduced, the coalesced clusters were trapped into pore throats, and the seawater had continuously proceeded in tandem along the walls of the pore without sweeping the receding oil in the pores' center; hence no more oil was produced after 9 hours of continual seawater flooding.

From Figure 8.1, it is obvious that a reduction in the trapped oil clusters was observed in some parts of the network after continuous injection of twice-diluted seawater in tertiary mode (Fig. 8.1C), resulting in an enhancement in oil recovery of about 10% compared to 7% for the case of the micromodel saturated with crude oil B, Table 8.1.

It has been reported that the capillary trapping is mostly dominated by the change in the flooding velocity, pore geometry, and rock-fluid interaction (wettability alteration) [30,117,161,162]. In this case, twice-diluted seawater was injected at the same low rate as seawater (5 µl/hr); therefore, it is expected that the mobilization of oil clusters would not be by viscous forces. Also, a close examination of the pore network images after exposure to twice-diluted seawater showed a minor change in the *in-situ* contact angle over the time scale of injection, and the wetting state remains within the same strongly water-wet condition, Figure 8.4B. Such results are incongruent with what was previously observed from some core floods within a Darcy-scale that a reduction in the residual oil saturation with a decrease in brine salinity was attributed to the wettability alteration from strongly water-wet toward an intermediate-wetness [163]. However, the findings of the present work agree with the results by other researchers [12,164], showing higher oil recovery with water-wet wettability. On the other hand, it was found that the interfacial tension was approximately constant (33.7 and 30.5 dynes/cm for oils A and B, respectively) as the seawater was diluted twice from its original concentration. Consequently, the capillary number remains within the low

range (5.5-6×10^{-8}), which is far smaller than that required for residual oil mobilization (*N*c =10^{-5} for hydrophilic surface) [111,162].

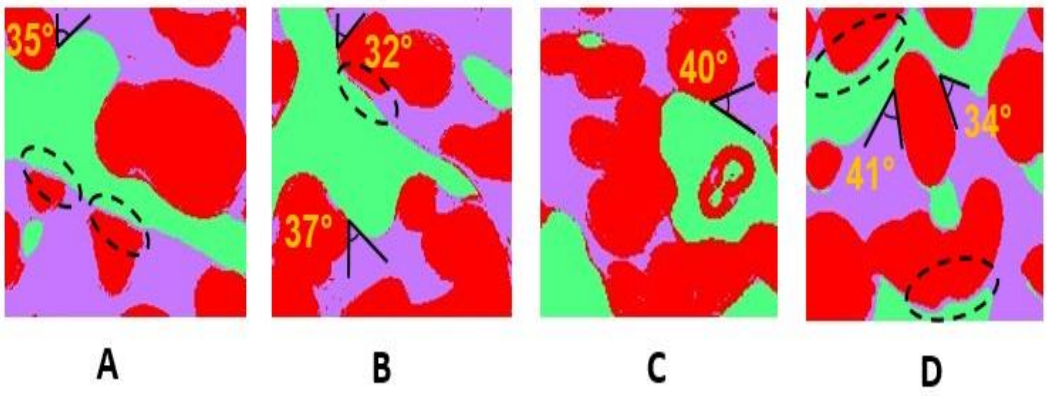

Figure 8.4: Magnified images at different locations in the hydrophilic micromodel show a typical example for *in-situ* contact angle between the oil/brine and brine/solid when the system was flushed with (A) seawater, (B) 2dSW, (C) 5dSW and (D) 10dSW. The stippled circles refer to a thin film of brine coated the walls of the pore, preventing oil from reaching the surfaces. Red: grains, green: oil, purple: brine.

As twice-diluted seawater showed less impact on the interfacial properties and therefore on the capillary forces, it is found that the most likely reason behind oil mobilization is the reduction in the attractive electrostatic forces (adhesive forces) between the trapped oil and silicate surface. It has been reported that in the presence of a water film the oil/solid interface becomes charged [68]. Furthermore, the low salinity solution has a neutral pH (pH =7.58), as illustrated previously in Table 3.2-Chapter 3, meaning that the silica/brine interface is almost negatively charged [6,79,165]. In comparison with other diluted brines, twice-diluted seawater contained a high concentration of monovalent cations such as Na^+, which could substitute the divalent cations (Ca^{2+} and Mg^{2+}) bonded to the negatively charged polar organic components of oil (-COOH) during secondary seawater injection [19,79]. Thereby, the divalent ions leave the silica surface along with the crude oil, helping to improve the pore-scale sweep efficiency. Figure 8.5 shows the potential chemical interactions between

silica/brine/oil at the pore-scale level. The results are qualitatively supported by our previous work to evaluate the desorption efficiency of oil with different compositions from silica surfaces upon exposure to low saline solutions [19].

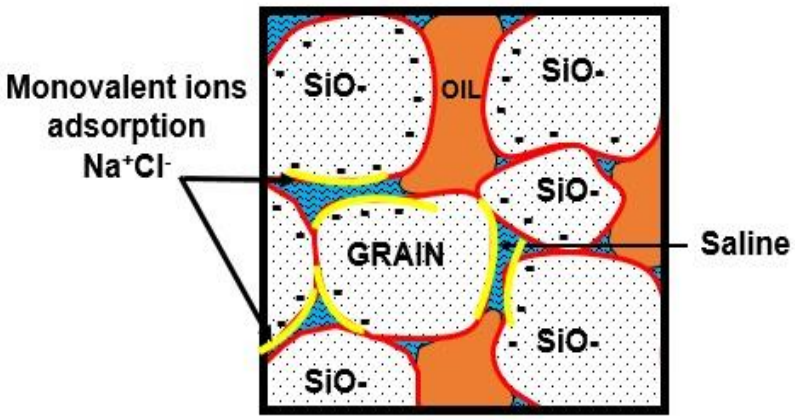

Figure 8.5: Proposed chemical interactions between hydrophilic surface/ brine/ oil at the pore-scale level.

Another probable explanation in which twice-diluted seawater influences the trapped oil mobilization is by considering the effect of the viscoelastic interface. It has been recently suggested that when the low saline solutions come in contact with the polar organic components of oil, a highly viscoelastic film will be formed [166,167]. It is, therefore, speculated that when twice-diluted seawater was flooded continuously for more than 6 hours, an expansion in the electrical double layer (EDL) would happen. This led to screening off all the interactions with the bulk solution, and hence increasing the affinity of polar organic components into the oil/brine interface, which favorably promoted the viscoelasticity at the interface. As a result, the trapped oil clusters were dispersed in the saline solution, i.e., the sweeping process can be much easier.

Injecting 5dSW into the hydrophilic porous media displayed a minor increase (1% of the OOIP) in oil recovery for the micromodel saturated with oil B (see Figure 8.1) but with no improvement in recovery factor for the case of oil A. Any further decrease in the salinity also did not show an

increase in the displacement efficiency for the two kinds of crude oils examined. Such results could be traced back to the reduction in the concentration of monovalent ions (Na^+) and therefore, their binding at the solid-water interface could be reduced. The EDL expansion could also be not large enough to stimulate the attraction of negative polar components toward the interface to form the viscoelastic interface. The previous study suggested that a critical expansion of the EDL is required for oil displacement [106]. These results also substantiate previous macroscopic core flooding experiments discussed in the literature that the low salinity effect on EOR from sandstone (silica) is mostly dominated by the presence of significant clay minerals [12]. The pressure drop was relatively constant with the stepwise low salinity injection, consistent with a constant resistance to the brine flow.

8.3 Effect of Salinity on the Pore-Scale Displacement Efficiency in a Hydrophobic Network

From the second set of microfluidic experiments, examining the impact of different saline solutions on the pore-scale sweeping efficiency in a hydrophobic microstructure, it is found that the initial oil saturation at the end of drainage displacement were 0.84 and 0.87 for oils A and B, respectively. More than half of the oil was trapped in the hydrophobic pore network at the end of secondary flooding by seawater, as the sweeping efficiency were calculated to be 44% and 42.5% for oils A and B, respectively. Figure 8.6 shows the binary analysis of the micromodel images for the hydrophobic pore networks saturated with crude oil A and B, respectively, while Figure 8.7 displays the corresponding pressure drops.

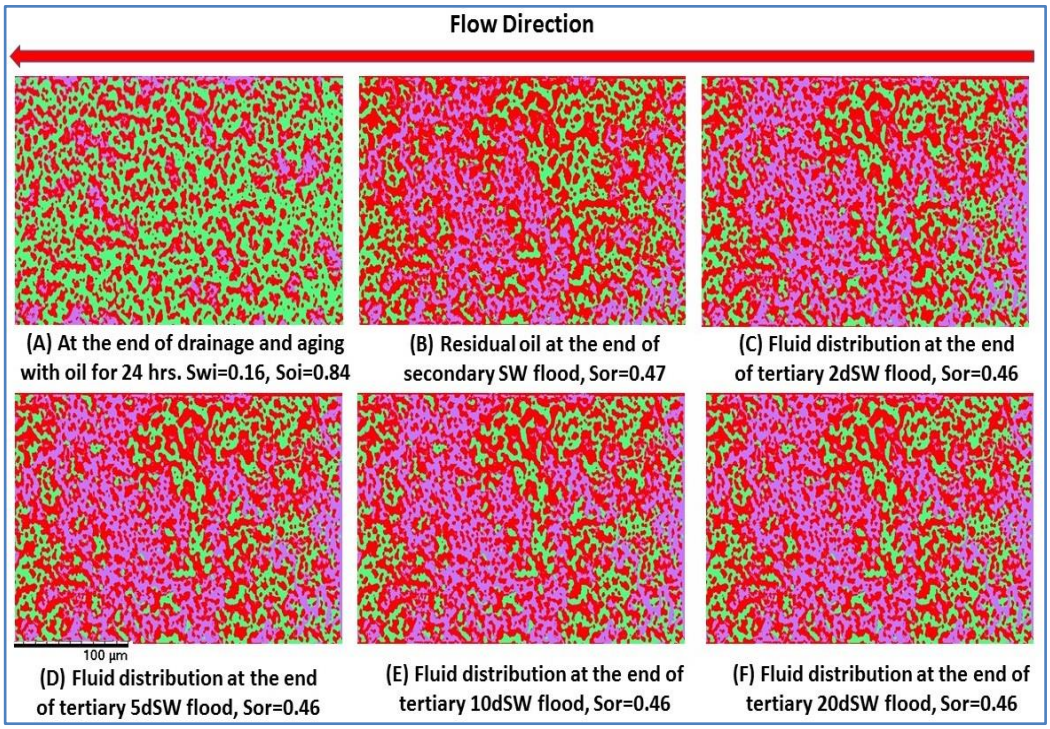

(A)

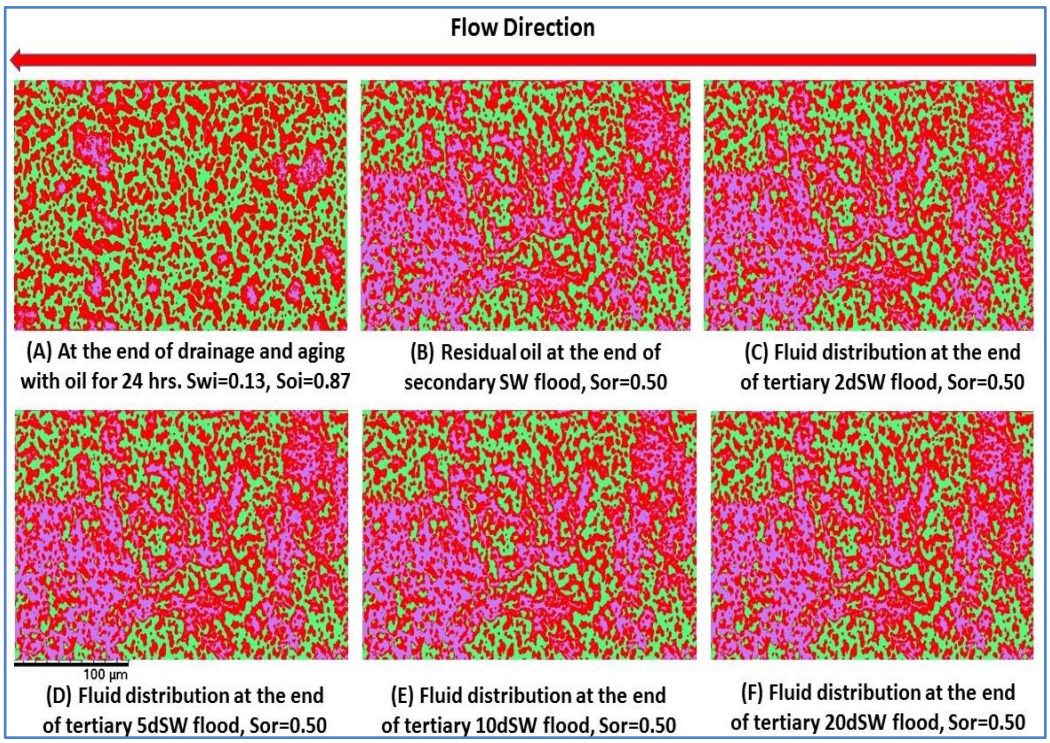

(B)

Figure 8.6: Segmented micromodel images after secondary and tertiary flooding in a hydrophobic surface saturated with (A) crude oil A and (B) crude oil B. Red: grains, green: oil, purple: brine.

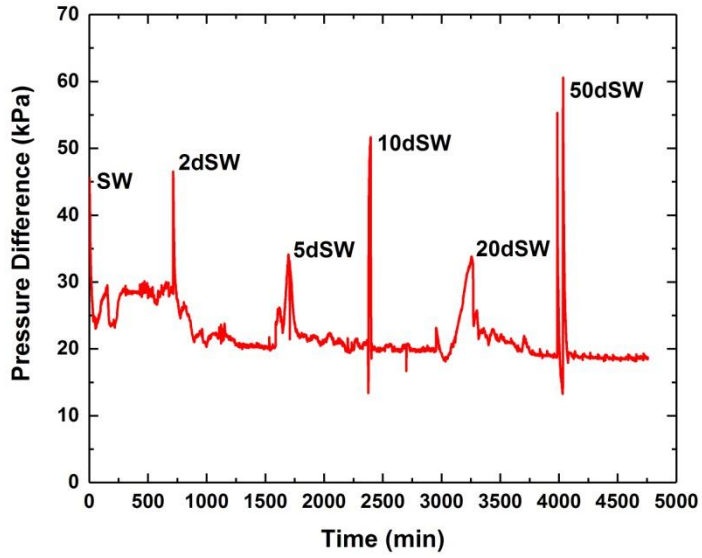

(A)

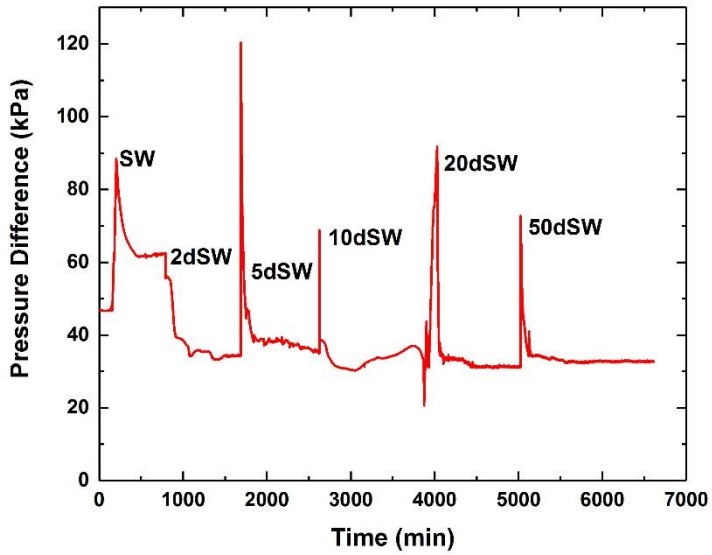

(B)

Figure 8.7: Pressure drop across the hydrophobic micromodel during secondary and tertiary flooding saturated with (A) crude oil A and (B) crude oil B during secondary and tertiary brine flooding.

Like the hydrophilic microstructure, the corresponding pressure drop at the beginning of seawater flooding was increased, and then it decreased once the brine displacement front began to cross-flow through the micromodel. This was followed by pressure stabilization at a certain level with the successive low salinity injection. Such observations could be explained by the fact that the viscosity of the injected brines showed relatively the same values as given in Table 3.2-Chapter 3, and all these brines were injected at the same low injection rate. Thus, it is expected that the viscous forces would be nearly the same during the sequential brine flooding, resulting in constant pressure drops.

It is worth noting that the snap-off-coalescence phenomenon was not observed when brine was flooded through the hydrophobic pore network and brine smoothly displaced oil in a piston-like way with a stable or sometimes irregular displacement front, as the oil was moved ahead of the brine, and only the irreducible oil was left behind the displacement front. Figure 8.8 illustrates a typical example of the brine front, advancing with time from the right-hand side of the micromodel.

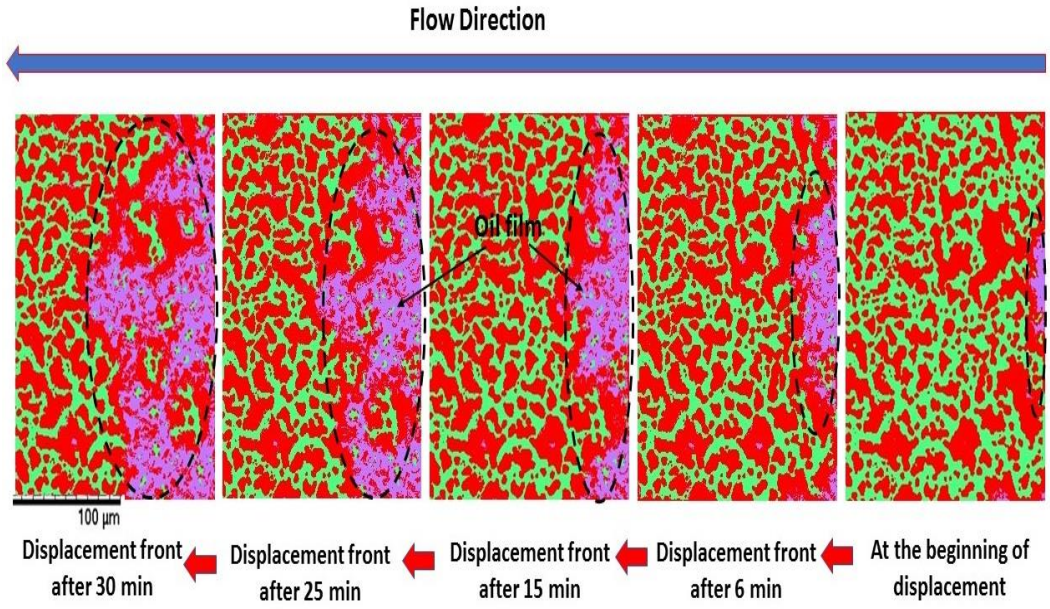

Figure 8.8: Segmented images, showing brine front advancing during secondary injection in the hydrophobic micromodel. Red: grains, green: oil, purple: brine.

Contrary to expectations, the analysis of recorded images did not show any substantial change in the residual oil saturation during the sequential flooding of different diluted versions of seawater, Figure 8.6C-F, and thereby no positive effect on the pore-scale sweeping efficiency. The results also revealed that injecting twice-diluted seawater in the hydrophobic micromodel saturated with crude oil A showed a minor improvement (1%) in oil recovery, as shown in Table 8.1. Although the results contradict previous macroscopic core flooding experiments in Chapter 7, which show a positive effect of twice-diluted seawater on EOR in carbonate surfaces, the findings are in agreement with those of Lager et al. [16] and Fathi et al. [39].

The foremost reason for results inconsistency is due to the fact that in this mesoscale study there is definitive evidence that the wetting state at the pore level did not change during low salinity displacements and all the pore walls remain within an oil-wet condition. This could be related to the coated-polymer pore surface. Consequently, the affinity of active ions toward the coated surface, ion exchange, and desorption should be weak. It has been reported that the constituents and conditions for solid influence the wetting preference [68]. Therefore, no change in the wettability of coated-pore surface was observed under such test conditions. Figure 8.9 presents the contact angle and oil/brine interfaces at typical locations at the end of the imbibition displacements.

Another possible explanation for the lack of oil recovery enhancement during low salinity injection into the hydrophobic micromodel might be that the pore diameter and geometry of micromodel are different to some extent from those of real natural carbonate rocks, which were used in the macroscopic flooding displacements. The previous study showed that besides the effect of interfacial tension and contact angle, the pore diameter and geometry could also have a role to play in the magnitude of capillary forces during imbibition displacement [30,161].

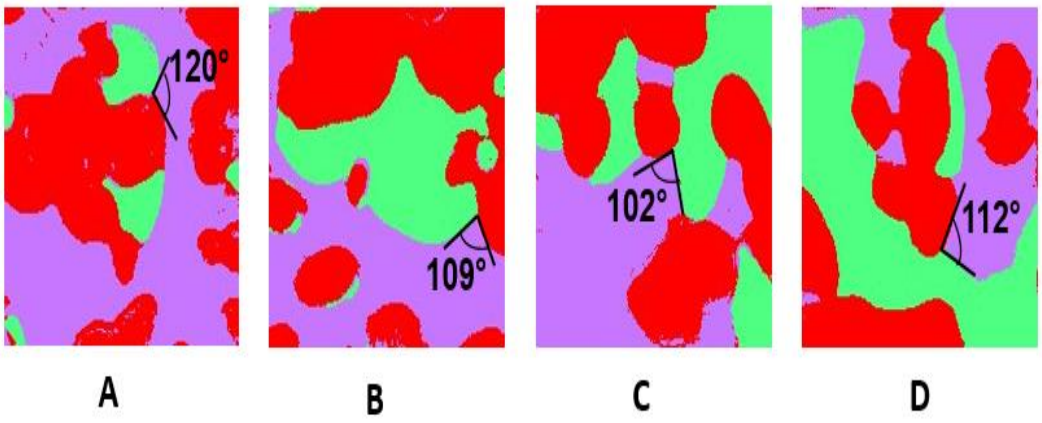

Figure 8.9: Segmented images of *in-situ* contact angle measured at different locations in the hydrophobic micromodel when the system was flushed with (A) seawater, (B) 2dSW, (C) 5dSW and (D) 10dSW. Red: grains, green: oil, purple: brine.

It has also been reported that it is difficult to detach carbon chains that adsorbed to the hydrophobic surface by low salinity solution and the only way to remove them is by increasing the salinity of the injected water, which can promote the reactivity of the surface and modify the wettability to water-wetness [16]. Such a hypothesis is consistent with what is observed in this mesoscale study. A close inspection of the recorded images in Figure 8.10 illustrates that a thin oil film coated the walls of the pore that were already invaded by brines, meaning that the surface had a higher affinity to oil than water and therefore promoting the interaction between oil components and grain surfaces. For this, streaming brine toward the grains was not able to replace the attached oil film, and the grain surfaces remain within oil-wet conditions. This could provide compelling evidence that the multiphase flow of the oil/brine system and *in-situ* contact angle over a pore-scale with a length of micrometres are different from those reported in the literature within the macroscopic scale level [5,50].

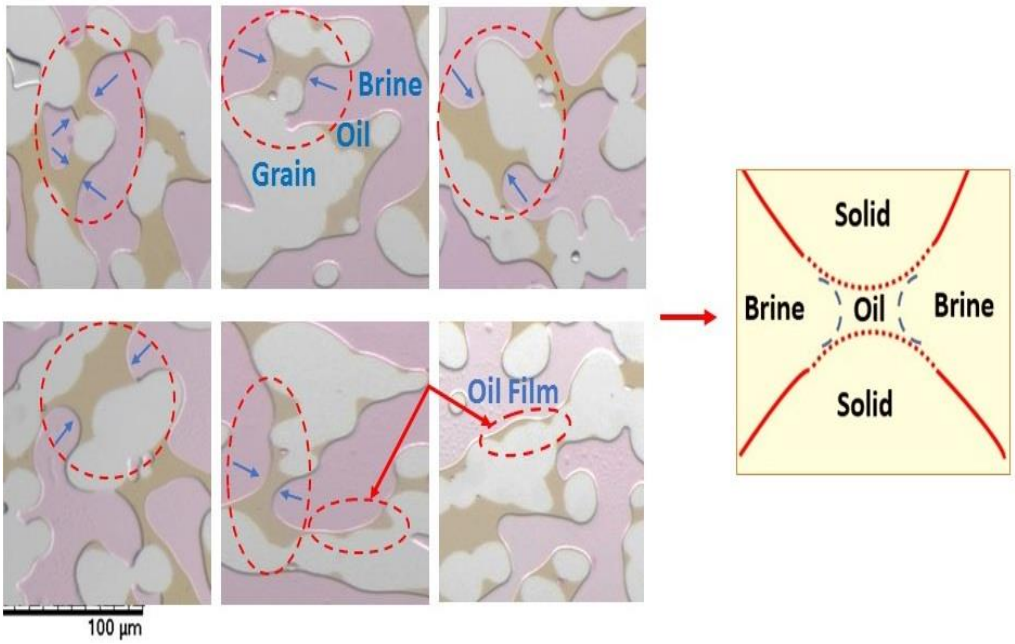

Figure 8.10: Magnified images at different locations in the hydrophobic micromodel during low salinity flooding, illustrating strongly oil-wet surfaces as the oil occupies the smallest pores and brine advances over it. Thin oil films are left on the walls of some invaded pores, showing strong adhesive forces between oil and grain surfaces.

8.4 Effect of Low Salinity Flooding on the Secondary Recovery of the Hydrophilic and Hydrophobic Networks

The other two series of pore-scale displacement were conducted on hydrophilic and hydrophobic microstructures saturated with crude oil A to examine the efficiency of secondary low salinity injection on oil production compared to high salinity solution (seawater). For this, 5 times dilution of seawater was flooded in secondary mode, while 10 times dilution of seawater (4366 ppm) was selected to inject in tertiary mode since previous core flood studies indicated that reducing the salinity of water below 5000 ppm revealed positive results for sandstone and carbonate reservoirs [10,15,16,52,54]. Figure 8.11 shows oil distribution after

secondary and tertiary low salinity flooding through the hydrophilic and hydrophobic pore networks.

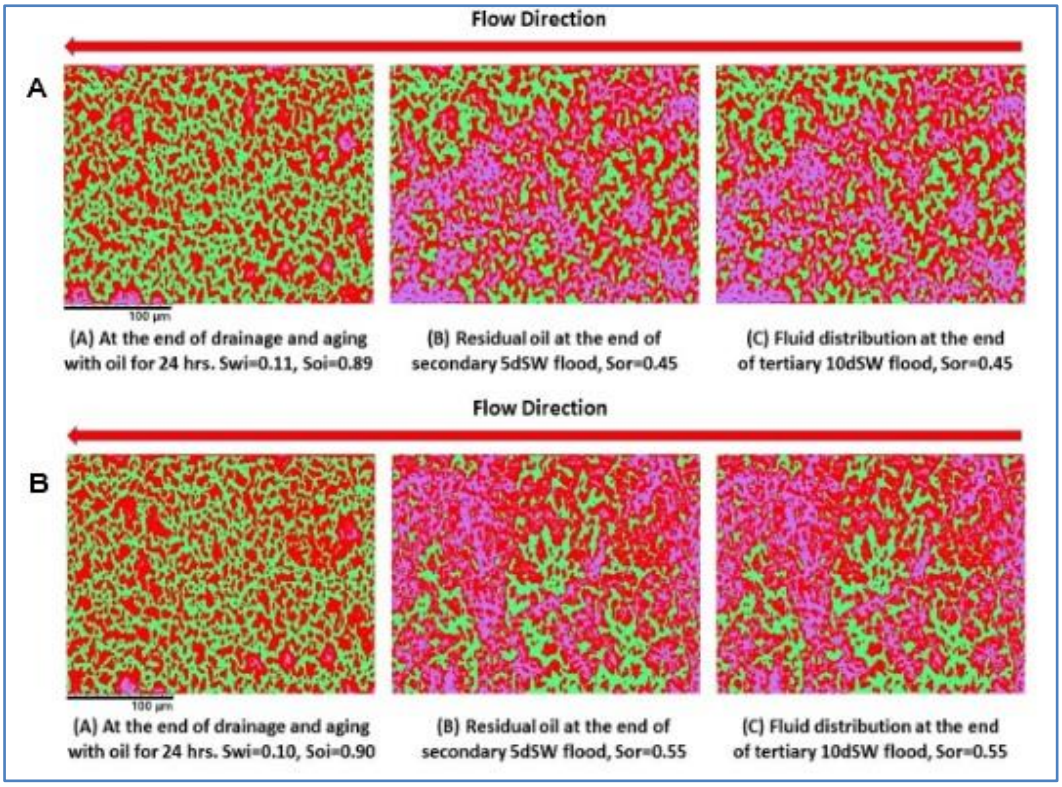

Figure 8.11: Segmented micromodel images after secondary and tertiary low salinity flooding for (A) hydrophilic micromodel and (B) hydrophobic micromodel. Red: grains, green: oil, purple: brine.

Obviously, a clear distinction in the magnitude of oil recovery from that of secondary seawater injection was observed (Figure 8.11A), 49% compared to 74% recovered from the seawater secondary flooding under the same test conditions. This might be commonly traced back to the reduction in the ionic strength of the solution, particularly in terms of monovalent ion concentration, which is supposed to play the greatest role in the oil desorption efficiency from the water-wet surfaces [9]. However, the discrepancy between high and low salinity secondary flooding was less pronounced for a hydrophobic surface. Hence, 38.8% of the oil was produced by injecting 5 times dilution of seawater in secondary mode compared to 44% when seawater was flooded through the hydrophobic

surface. Injecting 10 times dilution of seawater in tertiary mode did not reveal any positive effect on the incremental oil recovery for both surfaces examined. This could provide compelling evidence that the sequence of displacement did not heavily affect the potential of low salinity water to enhance oil recovery, as the same impact of 10 times dilution was observed when high salinity seawater was injected in secondary mode.

The overall corresponding pressure drop across the hydrophilic and hydrophobic microstructures recorded during the secondary and tertiary low salinity water flooding is shown in Figure 8.12. Peak pressure drops of 93 kPa and 48 kPa were observed before the breakthrough time for the hydrophilic and hydrophobic surfaces, respectively. The pressure was then stabilized at 80 ±3 kPa and 37±2 kPa with the continuous 5 diluted seawater flooding. Injecting 10 times dilution revealed a little further increase in the pressure drop for both surfaces examined with a small fluctuation in the pressure values for the oil-wet microstructure. This could be attributed to the disequilibrium in the local capillary pore pressure and occasional resistance to flow through the hydrophobic pore network. Such results are in line with what was previously observed by Cissokho et al. [168], who stated that there was an increase in pressure drop when the low saline solution was injected into the sandstone cores even if no extra oil was recovered.

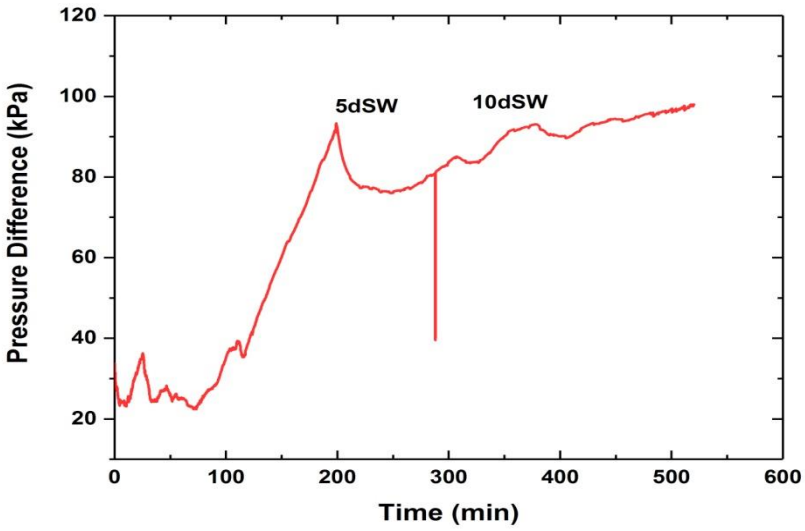

(A)

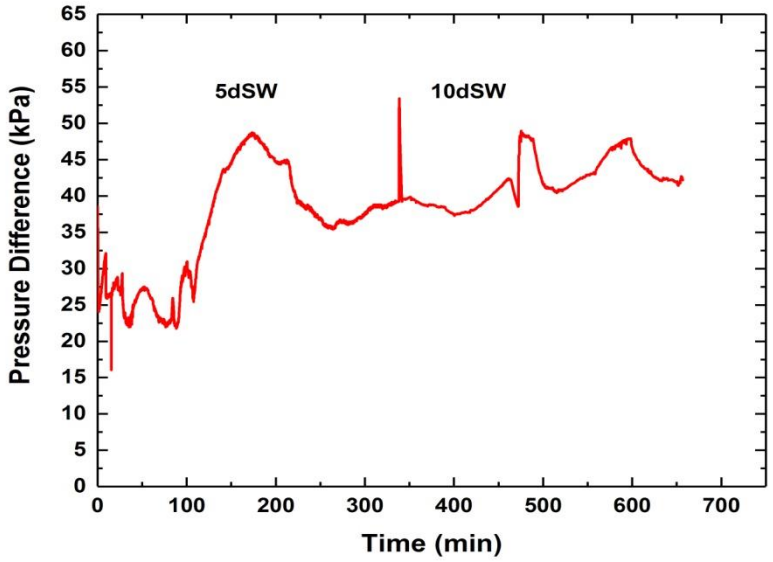

(B)

Figure 8.12: Pressure drop for (A) hydrophilic micromodel and (B) hydrophobic micromodel during secondary and tertiary low salinity flooding.

8.5 Summary

In this Chapter, the impact of ionic strength and brine salinity on the pore-scale displacement efficiency is experimentally investigated using two types of micromodel with the same pore geometries but different wetting properties. The dynamic flow behaviour and flow pattern of oil/brine during imbibition displacements are also explored.

The results reveal that the dynamics of displacement during secondary flooding by seawater (high salinity) is different in the hydrophilic and hydrophobic surfaces. For the hydrophilic system, oil moves through the multiple snap-off and coalescence process, while a piston-like displacement of oil by brine was dominant the flow in the oil-wet microstructure.

For the hydrophobic microstructure, it is found that no change in the initial wettability is observed during a sequential low salinity injection as the pore

surfaces remain within a strongly oil-wet condition due to the highly bonding effect between carbon chains and pore surfaces. Such observation is consistent to some extent with our previous macroscopic contact angle measurements for limestone rock, showing an oil-wet condition for different crude oils examined [19]. Thereby, tertiary low salinity flooding does not show any positive effect on the pore-scale displacement efficiency for the oil-wet system. However, an improvement in oil recovery of 7-10% is observed by injecting twice-diluted seawater through a hydrophilic micromodel due to a reduction in the attractive electrostatic forces (i.e., adhesive forces) and electrical double layer expansion, which could promote the viscoelasticity at the interface. The results also confirm that the potential of low salinity for enhanced oil recovery is not affected by the sequence of flooding.

The present findings provide direct evidence that the multiphase flow of an oil/brine system and *in-situ* contact angle trend at the pore-scale are different to some extent from some of those reported previously at the macroscopic-scale level for both oil-wet and water-wet porous media, suggesting extra cautions are needed to predict and/or interpret the effect of low salinity injection on reservoir performance.

Chapter 9

Discussion and Conclusions

As mentioned in Chapter 1, this project aims to provide a multi-scale understanding of the complex interactions of solid/brine/oil system. This contributes to developing new knowledge about the feasibility of low salinity injection specifically in carbonate reservoirs and offers a unified interpretation of its associated mechanisms. Integrated macroscopic and microscopic experimental works have been conducted to meet the objectives of this research, and coherent interpretation of these works is given in the respective chapters. In this Chapter, a summary of the main findings obtained from each test method with the subsequent analytical discussion and general conclusions will be described. This will be followed by the recommendations and suggestions for future work.

9.1 Discussion

In this thesis, the key parameters that dominate the composite interactions of rock/brine/oil in carbonate reservoirs at the macroscopic scale are first investigated through systematic contact angle, IFT, IFR, and SEM-EDX measurements, as discussed in Chapter 4. It is found that the salinity effect is more salient at the liquid/rock interface than the liquid/liquid interface, and the response to the brine composition is highly governed by the oil composition with respect to its content of polar organic components. The results also reveal that there is a reduction of contact angle as the seawater is diluted twice while its influence on the IFT is small, and the effect is more pronounced for dolomite rock, showing different results for different crude oils used. This suggests that wettability alteration of carbonate rock is an intricate phenomenon that is influenced not only by the salinity but also by the chemical composition of crude oil existing in the porous media and rock mineralogy.

The observed change in the contact angle when switching from super saline solution (200000 ppm) to seawater and then to twice-diluted seawater could be explained by a relatively sharp decline in the work of adhesion (W_A), and the effect is more pronounced for dolomite/crude oil A system. This means a decrease in the electrostatic adhesive force, i.e., an increase in the repulsion energy has happened due to the synergic effects of sulphate ions binding, salting-out, and EDL expansion. Thus, less work is needed to separate the aqueous phase from the solid surface, resulting in a change in the wetting-state of the rock. The current macroscopic contact angle study adds more knowledge about the effect of crude oil composition on the wettability trend, evidenced by the higher adhesive forces and preferentially oil-wet condition for surfaces saturated with crude oil having the high polar atoms, as a result of strong interaction between these polar components and the positively charged carbonate surfaces.

Taken these together, the above macroscopic contact angle observations suggest a reduction in the work of adhesion at a certain level of salinity, which is significantly affected by the chemical composition of crude oil in the porous media. Such conclusions are supported by the molecular AFM study presented in Chapter 5. In the AFM study, the molecular interaction of polar organic components with the carbonates has been highlighted by measuring the adhesion forces between the functionalized tips and carbonate minerals at different levels of salinity. The results reveal a reduction by about 49% in the interaction force as the salinity is diluted twice from seawater concentration, but with minimal gains (3-5%) thereafter, meaning no measurable difference in the W_A/σ_{ow} ratio when the concentration of ions is decreased, i.e., a minor effect on the carbonates wettability.

The results also show that a model system of $NaCl/Na_2SO_4$ has a larger effect on adhesion. While the greater reduction in adhesion in this more basic model system proves that it is the ionic strength of the solution that plays a significant role, it also indicates that there are other components in the seawater sample that are modifying and reducing this response.

Binding of divalent ions at the solid/water interface could also affect the adhesion. It could be supposed that seawater and twice-diluted seawater have almost a high concentration of SO_4^{2-} compared to the super saline solution (formation water). A possibility arises that this ion could penetrate the solid/water interface and increase the negative charges (Figure 5.8), causing a reverse interaction between the negatively charged tip (-COOH carboxyl group) and calcite surface, and thus a noticeable decrease in the adhesion with the seawater and twice-diluted seawater. This hypothesis fits with the basis of the experimental work of Zhang and his co-workers [41,42]. It should be noted that the observed adhesion trend further supports the idea of *in-situ* chemical interactions between SO_4^{2-} and carbonate surfaces during low salinity injection, which has been discussed in Chapter 4. Either way, with the further dilution of seawater, the concentration of the SO_4^{2-} is relatively decreased or correspondingly, its binding to the solid/water interface is reduced, leading to almost a small variation in the adhesion values.

From the micro-scale AFM study, it is proposed that while the expansion of the electric double layer (EDL) at lower salt concentration is responsible for changing oil adhesion on carbonates, it is modulated by surface ions binding. Overall, based on the results of macroscopic contact angle and microscopic adhesion forces, which are used to consider the solid/brine/oil interactions, it is suggested that either ions binding or EDL expansion (electrokinetics repulsive) alone could affect the adhesion of oil onto the surfaces. A combination of these two mechanisms, as well as, salting-out phenomenon shall be responsible for the adhesion changes, hence the wettability alteration of carbonate surfaces.

The effect of oil composition on the low salinity effect has been corroborated by QCM work, as mentioned in Chapter 6. The adsorption/desorption efficiency of various types of crude oils onto/from calcite and silica surfaces at different salinity is evaluated. The results indicate that the amount of adsorption is strongly correlated to the concentration of polar organic components present in the oil and the type of surface minerals. Subsequent desorption shows that low amounts of

desorption are reported upon exposure to seawater for both surfaces examined. It is also found that two and ten times dilution of seawater achieve high desorption efficiency due to an improvement in the electrostatic repulsion forces, which lead to reduce the adhesion between the adsorbed oil components and crystal surfaces.

On one side, the desorption observations are qualitatively in line with the measured adhesion force values, showing a considerable decrease in adhesions as the salinity is diluted twice from seawater; on the other side, the QCM findings seem not to support the molecular AFM results that insignificant change in adhesions was observed as the salinity decreased to 10 times dilution. Such discrepancy in the results could be due to the difference in the experimental test protocol. The results also indicate that limited desorption is observed when utilizing 20 and 50 times-diluted seawater, i.e., when the ionic strength is decreased, and thereby negligible change in the adhesion is obtained, resulting in less desorption efficiency. Generally, it is inferred that increasing the content of polar components in crude oil leads to reduced desorption from calcite surfaces compared to the silica surfaces. This could be explained by the difference in the electrostatic properties between calcite and silica surfaces which, therefore, leads to high bonding strength between the negatively charged polar components of oil and the positively charged calcite surface.

The observed results in Chapters 4 through 6 indicate that the potential of low salinity flooding is closely correlated to the chemical composition of crude oil and the characteristics of surface minerals. For more practical implications, a series of core flooding experiments were precisely designed under reservoir-like conditions to get more reliable and conclusive evidence about the synergetic effect of rock mineralogy and oil composition on the potential of low salinity flooding for EOR.

From Chapter 7, the results of relative EOR contributions by different diluted versions of seawater show that a substantial increase in oil recovery (6.8% of the OOIP) is observed for reservoir dolomite rock saturated with crude oil A, containing the lowest amount of polar organic

components compared to 4% for outcrop limestone sample saturated with the same type of oil when the salinity of seawater is decreased to 21828 ppm. No tertiary low salinity effect has been observed for the rock samples saturated with the heavy crude oil, having a high acid number and polar content. Insignificant improvement in oil recovery has also been seen with the 5 and 10 times dilution of seawater for the two types of carbonate rocks examined.

As mentioned before, several researchers argued that wettability alteration from oil-wet to intermediate-wet is the plausible mechanism which affects the EOR significantly during low salinity water flooding in carbonates [10,20,80]. From the above macroscopic contact angle analysis, it is found that a change in the contact angle with the significant alteration in adhesion work was when twice-diluted seawater used, which has almost a high concentration of potential determining ions compared to the other dilution versions. This can, therefore, lead to a measurable increase in oil recovery and almost higher salinity effect. As mentioned before, further dilutions of seawater cause a reduction in the concentration of the SO_4^{2-}, Ca^{2+}, and Mg^{2+} ions, and correspondingly their binding to the solid/water interfaces is reduced, suggesting a minor effect on the oil adhesion and insignificant salinity effect. This could provide a further explanation of why no extra oil was recovered with the 20 and 50 times dilution. The macroscopic core flooding results confirm that the EOR by low salinity injection is likely to be due to the ions binding at the rock/water interface. However, EDL could also have a role in oil recovery enhancement.

On the other hand, the core flooding results show that the potential of twice-diluted seawater and other dilutions of seawater for EOR are strongly affected by the chemical composition of crude oils used. Hence, low salinity flooding reveals a negligible impact on EOR for core samples saturated with crude oil C. In comparison with other investigated oils (crude oil A and B), crude oil C has the highest mass ratio of polar organic components, therefore it is supposed that the oil/water interface has a high magnitude of negative charges. Consequently, the ionized acidic

components could adsorb at the carbonate surface and the strongest interactions between these polar atoms and the polar surface site may occur, i.e., the electrostatic force is attractive, leading to preferentially oil-wet surface and no incremental oil recovery. Previous studies argue that the polar organic components in the crude oil play a major role in the wettability alteration of mineral surfaces, hence oil recovery enhancement [68]. Such data match in some ways those reported in Chapter 4, confirming that no significant wettability alteration is seen for crude oil C, and the contact angle of carbonate rocks remains within the oil-wet conditions. Jackson et al. [169] also argues that the incremental oil recovery is only observed if the controlled low salinity water flooding (CSW) can induce a repulsive electrostatic force at interfaces with respect to the type of oils used.

Another possible explanation is by considering the effect of viscous fingering, as the viscosity of the saline solution is much smaller than that of displaced fluid, i.e., crude oil C. Consequently, the saline solution would preferentially flow through the flow channel, i.e., viscous fingering, and therefore most crude oil situated out of this channel would not be recovered [161,170].

In addition, the observed tertiary low salinity effect is rather high when reservoir dolomite rock is used. This is most likely attributed to the presence of dissolvable anhydrite ($CaSO_4$) as a part of the core material, which could enrich the injected brine with sulphate, coinciding with the adsorption of sulphate ions onto the rock surface, helping to promote the electrostatic repulsion forces and detach hydrophobic layer from the carbonate surfaces. It is found in the previous studies by Austad et al. [55,59] that sulphate is a catalyst for the wettability alteration process and oil recovery enhancement, and this effect is similar to sandstones with clay minerals.

On the other hand, a closer inspection of differential pressure profiles for all core flooding tests exhibits a considerable increase in the maximum pressure drop when seawater or formation water was flooded in

secondary mode, coincided with pressure drop fluctuations, which are manifested as either increase or decrease in differential pressure values. It is expected that the magnitude of capillary forces is likely to be large at the beginning of injection. Consequently, to overcome the strong capillarity and enable brine to invade into the porous media, a higher viscous pressure drop is required [14,30,161]. Such competition between two forces at the flood front might lead to a noticeable fluctuation in the differential pressure profiles, particularly at the earlier time of brine injection. Afterward, the pressure drop was relatively stable as a result of oil production and an increase in the relative permeability of brine. It decreased then steadily during tertiary low salinity injection, and it is less than the stabilized pressure by seawater, suggesting that the interaction between the charged surface and fluid reaches equilibrium, hence stable resistance to the flow of injected fluid [157].

Furthermore, comparing the quantity of oil recovered from fluids with different concentrations of SO_4^{2-}, Mg^{2+}, and Ca^{2+} exhibits that the oil recovery increases as the concentration of SO_4^{2-} and Mg^{2+} ions in the solution is increased to a certain level, beyond which the concentration of these ions has a negligible impact on oil recovery. This implies that SO_4^{2-} and Mg^{2+} ions have strong potential to interact with the carbonate surfaces than the Ca^{2+} ions, and multiple ions exchange seems likely to be happening at a high temperature. As mentioned before, such interaction could improve the electrostatic repulsion between oil components and carbonate surfaces, leading to an improvement in the oil desorption efficiency. The macroscopic displacements also show that the performance of low salinity water for EOR was affected adversely when formation water was injected in secondary mode due to the probability of scale deposition, indicating that pumping seawater in secondary mode would be more favourable compared to the formation water.

Generally, the core flooding data confirm that the potential of low salinity for EOR in carbonate reservoirs is enormously influenced by the rock mineralogy with respect to the anhydrite concentration, as well as the

amount of polar organic components in crude oil, supporting the previous conclusions of macroscopic contact angle measurements.

Further full visualization of oil/brine flow inside the porous media has been investigated by using microfluidic chips with different wettabilities, to represent different reservoir characteristics. In contrast to the macroscopic core flooding, the overall findings summarised in Chapter 8 show that tertiary low salinity flooding does not produce any improvement in the oil recovery for the hydrophobic microstructure. The wettability of the surfaces also remains within a strongly oil-wet condition, evidenced by the thin oil films left on the walls of some invaded pores, showing strong adhesive forces between oil and grain surfaces upon exposure to different levels of salinity. It is found that while the pore-scale flow does not substantiate the macroscopic core flooding experiments, which is likely due to the lack of temperature effect and variation in the pore geometry, it provides additional evidence about the highly bonding effect between oil components and pore surfaces. On the other hand, such observations corroborate the previous macroscopic contact angle measurements for outcrop limestone rock in Chapter 4, showing strong hydrophobic conditions upon exposure to low saline solutions for different crude oils examined.

The mesoscale study also reveals that imbibing low salinity fluids into the hydrophilic (strongly water-wet) microstructure caused a reduction by 8-10% in the residual oil. This improvement could be explained by the electrical double layer expansion, which could promote the viscoelasticity at the oil/brine interface. As mentioned before, previous macroscopic studies for sandstones confirm that injecting brines with salinities below 5000 ppm could improve oil recovery from water-wet reservoirs. However, the evidence from the current mesoscale study for the hydrophilic microstructure does not support the occurrence of such observations. A possible explanation for this contradiction is that the displacements were conducted into non-coated (clay free) chips which could, therefore, affect adversely the pore-scale sweeping efficiency of low salinity solutions. The presence of clay minerals in the sandstone formations has been

considered by some researchers as a pre-condition for the observed low salinity effect in the water-wet surfaces [117].

The mesoscale study extends the existing knowledge of the pore-flow in the water-wet and oil-wet systems. It is observed that the flow dynamics of the hydrophilic and hydrophobic microstructures are different, as the snap-off-coalesce phenomenon governs the flow in the water-wet system, while oil moved by a piston-like displacement with a stable or irregular front in the hydrophobic system. Furthermore, the potential of low salinity for enhanced oil recovery is not affected by the sequence of flooding.

In general, the present multi-scale study suggests that the solid/brine/oil interactions, flow pattern, and corresponding low salinity effect in the oil-wet pore surfaces are different from those in the water-wet system.

9.2 Summary of Conclusions

The main conclusions drawn on the basis of a series of experiments conducted in this study are summarised as follows:

1. A combination of three mechanisms including ions binding, EDL expansion (electrokinetics repulsive), and salting-out are responsible for the oil adhesion changes, and hence the potential of low salinity injection.
2. Low salinity flooding shows more effect on the fluid/solid interaction than the fluid/fluid interaction for the different crude oils examined.
3. Twice-diluted seawater provides a high potential to enhance oil recovery from carbonate rocks at the macroscopic-scale as a result of the decrease in the adhesions between polar oil and carbonate surfaces.
4. The observed potential of low salinity flooding is strongly affected by the chemical composition (polar components) of crude oil existing in the porous media, as well as the type of carbonate formations.

5. Low salinity water flooding seems to be an unsuitable technique to improve oil recovery from carbonate reservoirs with heavy and polar crude oils.
6. The pore-flow of oil/brine inside the hydrophilic and hydrophobic porous media is entirely different, thereby the feasibility and associated mechanisms of low salinity injection are rather different.
7. Low salinity flooding reveals a measurable effect on the macroscopic oil displacement efficiency for the oil-wet system, but with no influence on the microscopic sweeping efficiency.

9.3 Recommendations

Throughout this research, the potential of low salinity flooding to enhance oil recovery in carbonate reservoirs and its associated mechanisms have been extensively investigated at the macroscopic, meso, and microscopic scales. However, like many other studies, additional avenues of investigation can be considered to fully acknowledge the feasibility of low salinity flooding in carbonates. For future experimental work, the following recommendations are proposed:

- Atomic force microscopy, quartz crystal microbalance, and microfluidic apparatus have been accurately used to assess the polar oil adhesion and desorption into/from the carbonate surfaces. The aim was to understand the solid/brine/oil interactions and evaluate low salinity potential at the pore-scale level. It would be more beneficial if these methodological approaches can be improved by conducting the same multi-scale experiments at *in-situ* (HPHT) reservoir conditions.

- The current study reveals that low salinity flooding has an insignificant effect on the fluid/fluid interface. It would be interesting to develop a hybrid of low salinity-surfactant or low salinity-nanoparticles to assess its impact on the interfacial tension (IFT)

and thereby, on the capillary forces and pore-scale sweeping efficiency.

- Taking into consideration the diversity of carbonate formations and pore fluids, more focus on carbonate reservoirs with a wide range of heterogeneities could lead to supportive findings for further confirmation on the feasibility of low salinity flooding at the field scale.

- It would be useful to explore the rheological behaviour and viscoelastic properties of the oil/brine interface.

- The observed findings from this multi-scale study could be extended to use in a field wide scale. One such example is the carbonate formations with light crude oils in the Middle East.

References

1. Ayirala, S.C., & Yosef, A.A. A State-of-the-Art Review to Develop Injection-Water-Chemistry Requirement Guidelines for IOR/EOR Projects*. SPE Production and Operations.* 2015*,* 30 (1), pp. 26-42*.*

2. Thomas, S. Enhanced Oil Recovery-An Overview. *Oil & Gas Science and Technology-Revue de IFP.* 2008*,* 63 (1), pp. 9-19.

3. Alvarado, V., & Manrique, E. Enhanced Oil Recovery: An Update Review. *Energies*. 2010, 3, pp.1529-1575.

4. Sohal, M. Wettability Modification in Chalk. Thesis. Aalborg University, 2016.

5. Alshakhs, M.J., & Kovscek, A.R. Understanding the Role of Brine Ionic Composition on Oil Recovery by Assessment of Wettability from Colloidal Forces. *Advances in Colloid and Interface Science*. 2016, 233, pp.126-138.

6. Anderson, A., & William, G. Wettability Literature Survey-Part 1: Rock/Oil/Brine Interactions and the Effects of Core Handling on Wettability. *Society of Petroleum Engineer.* 2016, 38 (11), pp.1125-1127.

7. Kokal, S., & AL-Kaabi, A. Enhanced Oil Recovery: Challenges and Opportunities. *World Petroleum Council*. 2010, pp. 65-69.

8. Ligthelm, D.J., Gronsveld, J., Hofman, J., Brussee, N., & Marcelis, F. Novel Waterflooding Strategy by Manipulation of Injection Brine Composition. In: *EUROPEC/EAGE Conference and Exhibition*, January 2009, Amsterdam, Netherlands.

9. Lager, A., Webb, K.J., & Collins, I.R. LoSal Enhanced Oil Recovery: Evidence of Enhanced Oil Recovery at the Reservoir Scale. In: *SPE Symposium on Improved Oil Recovery*, April 2008a, Tulsa, Oklahoma, USA.

10. Yousef, A.A., Al-Saleh, S., Al-Kaabi, A., & Al-Jawfi, M. Laboratory Investigation of Injection-Water Salinity and Ionic Content on Oil Recovery from Carbonate Reservoirs. *SPE Reservoir Evaluation & Engineering*. 2011, 14 (5), pp. 578-593.

11. Gupta, R., Smith, G.G., Hu, L., Willingham, T., Cascio, M.L., Shyeh, J.J., & Harris, C.R. Enhanced Waterflood for Carbonate Reservoirs - Impact of Injection Water Composition. In: *SPE Middle East Oil and Gas Show and Conference*, January 2011, Manama, Bahrain.

12. Tang, G.O., & Morrow, N.R. Influence of Brine Composition and Fines Migration on Crude Oil / Rock Interactions and Oil Recovery. *Journal of Petroleum Science and Engineering*. 1999, 24 (2-4), pp. 99-111.

13. Webb, K.J., Black, C.J.J., & Al-Ajeel, H. Low Salinity Oil Recovery Log-Inject-Log. In: *SPE/DOE Symposium on Improved Oil Recovery*, April 2004, Tulsa, Oklahoma, USA.

14. McGuire, P.L., Chatham, J.R., & Paskvan, F.K. Low Salinity Oil Recovery: An Exciting New EOR Opportunity for Alaska's North Slope. In: *SPE Western Regional Meeting*, January 2005, Irvine, California, USA.

15. Vledder, P., Fonseca, J.C., Wells, T., Gonzalez, I., & Ligthelm, D.J. Low Salinity Water Flooding: Proof of Wettability Alteration on a Field Wide Scale. In: *SPE Improved Oil Recovery Symposium*, April 2010, Tulsa, Oklahoma, USA.

16. Lager, A., Webb, K.J., Black, C.J.J., Singleton, M., & Sorbie, K.S. Low Salinity Oil Recovery-An Experimental Investigation1. *Petrophysicists and Well Log Analysts*. 2008b, 49 (1).

17. Doust, A.R., Puntervold, T., Strand, S., & Austad, T. Smart Water as Wettability Modifier in Carbonate and Sandstone: A Discussion of Similarities/Differences in the Chemical Mechanisms. *Energy & Fuels.* 2009*,* 23, pp. 4479-4485.

18. Fathi, S.J., Austad, T., & Strand, S. Water-Based Enhanced Oil Recovery (EOR) by 'Smart Water': Optimal Ionic Composition for EOR in Carbonates. *Energy & Fuels*. 2011, 25, pp. 5173-5179.

19. Al-Khafaji, A., Neville, A., Wilson, M., & Wen, D. Effect of Low Salinity on the Oil Desorption Efficiency from Calcite and Silica Surfaces. *Energy & Fuels*. 2017, 31(11), pp.11892-11901.

20. Romanuka, J., Hofman, J., Ligthelm, D.J., Suijkerbuijk, B., Marcelis, F., Oedai, S., & Austad, T. Low Salinity EOR in Carbonates. In: *SPE Improved Oil Recovery Symposium*, April 2012, Tulsa, Oklahoma, USA.

21. Mohanty, K.K., & Chandrasekhar, S. Wettability Alteration with Brine Composition in High Temperature Carbonate Reservoirs. In:

SPE Annual Technical Conference and Exhibition, September 2013, New Orleans, Louisiana, USA.

22. Al-Hashim, H., Kasha, A., Abdallah, W., & Sauerer, B. Impact of Modified Seawater on Zeta Potential and Morphology of Calcite and Dolomite Aged with Steric Acid. *Energy & Fuels*. 2018, 32, pp.1644-1656.

23. Austad, T., Strand, S., Høgnesen, E.J., & Zhang, P. Seawater as IOR Fluid in Fractured Chalk. In: *SPE International Symposium on Oil Field Chemistry*, January 2005, Woodlands, Texas.

24. Olajire, A.A. Review of ASP EOR (Alkaline Surfactant Polymer Enhanced Oil Recovery) Technology in the Petroleum Industry: Prospects and Challenges. *Energy*. 2014, 77, pp. 963-982.

25. Wei, B., Romero-Zerón, L., & Rodrigue, D. Oil Displacement Mechanisms of Viscoelastic Polymers in Enhanced Oil Recovery (EOR): A Review. *Journal of Petroleum Exploration and Production Technology*. 2014, 4 (2), pp.113-121.

26. Lyons, W.C., & Plisga, G.J. Standard handbook of petroleum & natural gas engineering 2nd ed. Burlington, MA: Elsevier, 2005.

27. Rao, D.N., & Sharma, A.P. Scaled Physical Model Experiments to Characterize the Gas-Assisted Gravity Drainage EOR Process. In: *SPE Symposium on improved oil recovery*, April 2008, Oklahoma, USA.

28. Al-Menhali, A., Niu, B., & Krevor, S. The Effect of Reservoir Conditions on Wetting and Multiphase Flow Properties in CO2-*Brine-Rock System. In: International Petroleum Technology Conference,* December 2015, Doha, Qatar.

29. Kazemifar, F., Blois, G., Kyritsis, D.C., & Christensen, K.T. Quantifying the Flow Dynamics of Supercritical CO2–Water Displacement in a 2D Porous Micromodel Using Fluorescent Microscopy and Microscopic PIV. *Advances in Water Resources*. 2016, 95, pp. 352-368.

30. Lenormand, R., Touboul, E., & Zarcone, C. Numerical Models and Experiments on Immiscible Displacements in Porous Media. *Journal of Fluid Mechanics*. 1988,189, pp.165-187.

31. Zhang, C., Oostrom, M., Wietsma, T.W., Grate, J.W., & Warner, M.G. Influence of Viscous and Capillary Forces on Immiscible Fluid Displacement: Pore-Scale Experimental Study in a Water-Wet Micromodel Demonstrating Viscous and Capillary Fingering. *Energy & Fuels*. 2011, 25 (8), pp. 3493-505.

32. London, F. The General Theory of Molecular Forces. *Transactions of the Faraday Society*. 1937, 33, 8b-26.

33. Hognesen, E.J., Strand, S., & Austad, T. Water Flooding of Preferential Oil-Wet Carbonates: Oil Recovery Related to Reservoir Temperature and Brine Composition. In: *SPE Europec/EAGE Annual Conference*, June 2005, Madrid, Spain.

34. Cuiec, L., Bourbiaux, B., & Kalaydijian, F. Oil Recovery by Imbibition in Low-Permeability Chalk. *SPE formation Evaluation.* 1994, 9 (3), pp. 200-208.

35. Puntervold, T., Strand, S., & Austad, T. New Method to Prepare Outcrop Chalk Cores for Wettability and Oil Recovery Studies at Low Initial Water Saturation. *Energy & Fuels*. 2007, 21(6), pp. 3425-3430.

36. Agbalaka, C., Dandekar, A.Y., Patil, S.L., & Khataniar, S. The Effect of Wettability on Oil Recovery: A Review. In: *SPE Asia Pacific Oil and Gas Conference*, October 2008, Perth, Australian.

37. Strand, S., Hognesen, E.J., & Austad, T. Wettability Alteration of Carbonates--Effects of Potential Determining Ions (Ca^{2+} and SO_4^{2-}) and Temperature. *Colloids and Surfaces A: Physicochemical and Engineering Aspects*. 2006, 275 (1-3), pp.1-10.

38. Zhang, P., & Austad, T. Wettability and Oil Recovery from Carbonates: Effects of Temperature and Potential Determining Ions. *Colloids and Surfaces A: Physicochemical and Engineering Aspects*. 2006a, 279 (1-3), pp. 179-187.

39. Fathi, S.J., Austad, T., & Strand, S. "Smart Water" as a Wettability Modifier in Chalk: The Effect of Salinity and Ionic Composition. *Energy & Fuels.* 2010, 24(4), pp. 2514-2519.

40. Al-Attar, H.H., Mahmoud, M.Y., Zekri, A.Y., Al-Mehaideb, R., & Ghannam, M. Low–Salinity Flooding in a Selected Carbonate Reservoir: Experimental Approach. *Journal of Petroleum Exploration and Production Technology*. 2013, 3 (2), pp.139-149.

41. Zhang, P., Tweheyo, M.T., & Austad, T. Wettability Alteration and Improved Oil Recovery by Spontaneous Imbibition of Seawater into Chalk: Impact of the Potential Determining Ions Ca^{2+}, Mg^{2+}, and

SO_4^{2-}. *Colloids and Surfaces A: Physicochemical and Engineering Aspects*. 2007a, 301(1-3), pp.199-208.

42. Zhang, Y., Sie, X., & Morrow, N.R. Water Flooding Performance by Injection of Brine with Different Salinity for Reservoir Cores. In: *SPE Annual Conference and Exhibition*, November 2007b, California, CA.

43. Strand, S., Puntervold, T., & Austad, T. Effect of Temperature on Enhanced Oil Recovery from Mixed-Wet Chalk Cores by Spontaneous Imbibition and Forced Displacement Using Seawater. *Energy & Fuels*. 2008, 22 (5), pp. 3222-3225.

44. Puntervold, T., Strand, S., & Austad, T. Co-Injection of Seawater and Produced Water to Improve Oil Recovery from Fractured North Sea Chalk Oil Reservoirs. *Energy & Fuels.* 2009, 23 (5), pp. 2527-2536.

45. Strand, S., Standnes, D.C., & Austad, T. Spontaneous Imbibition of Aqueous Surfactant Solutions into Neutral to Oil-Wet Carbonate Cores: Effects of Brine Salinity and Composition. *Energy & Fuels*. 2003,17 (5), pp. 133-1144.

46. Webb, K.J., Black, C.J.J., & Tjetland, G.A. Laboratory Study Investigating Methods for Improving Oil Recovery in Carbonates. In: *International Petroleum Technology Conference*, November 2005, Doha, Qatar.

47. Karimi, M., Al-Maamari, R.S., Ayatollahi, S., & Mehranbod, N. Impact of Sulphate Ions on Wettability Alteration of Oil-Wet Calcite in the Absence and Presence of Cationic Surfactant. *Energy & Fuels*. 2016, 30 (2), pp. 819-829.

48. Karoussi, O., & Hamouda, A.A. Imbibition of Sulfate and Magnesium Ions into Carbonate Rocks at Elevated Temperatures and their Influence on Wettability Alteration and Oil Recovery. *Energy & Fuels*. 2007, 21 (4), pp. 2138-2146.

49. Puntervold, T., & Austad, T. Injection of Seawater and Mixtures with Produced Water into North Sea Chalk Formation: Impact on Wettability, Scale Formation and Rock Mechanics Caused by Fluid-*Rock Interaction.* In: *PE/EAGE Reservoir Characterization and Simulation Conference,* October 2007, Abu Dhabi, UAE.

50. Zhang, P., Tweheyo, M.T., & Austad, T. Wettability Alteration and Improved Oil Recovery in Chalk: The Effect of Calcium in the *Presence of Sulfate*. *Energy & Fuels*. 2006b, 20 (5), pp. 2056-2062.

51. Seccombe, J., Lager, A., Jerauld, G., Jhaveri, B., Buikema, T., Bassler, S., Denis, J., Webb, K.J., Cockin, A., Fueg, E., & Paskvan, F. Demonstration of Low-salinity EOR at Inter Well-Scale, Endicott Field, Alaska. In: *SPE Improved Oil Recovery Symposium,* April 2010, Tulsa, Oklahoma, USA.

52. Morrow, N., & Buckley, J. Improved Oil Recovery by Low-Salinity Water Flooding. *Journal of Petroleum Technology*. 2011, 63 (5), pp.106-112.

53. Nasralla, R.A., Bataweel, M.A., & Nasr-El-Din, H.A. Investigation of Wettability Alteration and Oil-Recovery Improvement by Low-Salinity Water in Sandstone Rock. *Journal of Canadian Petroleum Technology*. 2013, 52 (2), pp.144-154.

54. Xie, Q., Liu, Y., Wu, J., & Liu, Q. Ions Tuning Water Flooding Experiments and Interpretation by Thermodynamics of Wettability. *Journal of Petroleum Science and Engineering*. 2014,124, pp. 350-358.

55. Austad, T., Shariatpanahi, S.F., Strand, S., Black, C.J.J., & Webb, K.J. Conditions for a Low-Salinity Enhanced Oil Recovery (EOR) Effect in Carbonate Oil Reservoirs. *Energy & Fuels*. 2012, 26 (1), pp. 569-575.

56. Al-Harrasi, A.S., Al-Maamari, R.S., & Masalmeh, S. Laboratory Investigation of Low Salinity Water Flooding for Carbonate Reservoirs. *In: Abu-Dhabi International Petroleum Exhibition and Conference*, November 2012, Abu-Dhabi, UAE.

57. Al-Adasani, A., Bai, B., & Wu, Y.S. Investigating Low Salinity Water Flooding Recovery Mechanisms in Carbonate Reservoirs. *In: SPE Oil and Gas West Asia Conference*, January 2012, Muscat, Oman.

58. Hamouda, A.A., & Maevskiy, E. Oil Recovery Mechanisms by Low Salinity Brines and Their Interaction with Chalk. *Energy & Fuels.* 2014, 28 (11), pp. 6860-6868.

59. Austad, T., Shariatpanahi, S.F., Strand, S., Aksulu, H., & Puntervold, T. Low Salinity EOR Effects in Limestone Reservoir Cores Containing Anhydrite: A Discussion of the Chemical Mechanism. *Energy & Fuels.* 2015, 29 (11), pp. 6903-6911.

60. Gupta, R., & Mohanty, K. Wettability Alteration of Fractured Carbonate Reservoirs. In: *SPE Symposium on Improved Oil Recovery*, April 2008, Tulsa, Oklahoma, USA.

61. Alotaibi, M.B., Nasralla, R.A., & Nasr-El-Din, H.A. Wettability Challenges in Carbonate Reservoirs. In: *SPE Improved Oil Recovery Symposium,* April 2010, Tulsa, Oklahoma, USA.

62. Lashkarbolooki, M., Ayatollhi, S., & Riazi, M. The Impact of Aqueous Ions on Interfacial Tension and Wettability of Asphaltenic-Acidic Crude Oil Reservoirs during Smart Water Injection. *Journal of Chemical and Engineering Data.* 2014*,* 59 (11), pp. 3624-3634.

63. Vijapurapu, C.S., & Rao, D.N. Compositional Effects of Fluids on Spreading, Adhesion and Wettability in Porous Media. *Colloids and Surfaces A: Physicochemical and Engineering*. 2004, 241(1-3), pp. 335-342.

64. Xu, W. Experimental Investigation of Dynamic Interfacial Interactions at Reservoir Conditions. MSc. Thesis. Louisiana State University, Louisiana, 2005.

65. Moeini, F., Sarapardeh, A.H., Ghazanfari, M.H., Masihi, M., & Ayatollahi, S. toward Mechanistic Understanding of Heavy Crude Oil/Brine Interfacial Tension: The roles of salinity. *Fluid Phase Equilibria*. 2014, 375, pp.191-200.

66. Speight, J.G. Chemistry and Technology of Petroleum. 4th Ed. Hoboken: Taylor and Francis, 2006.

67. Sayyouh, M.H., Hemeida, A.M., Al-Blehed, M.S., & Desouky, S.M. Role of Polar Compounds in Crude Oils on Rock Wettability. *Journal of Petroleum Science and Engineering.* 1991, 6 (3), pp. 225-233.

68. Buckley, J.S., & Liu, Y. Mechanisms of Wetting Alteration by Crude Oils. *Journal of Petroleum Science and Engineering.* 1998, 3 (1), pp. 54-61.

69. Buckley, J.S., & Fan, T. Crude Oil/Brine Interfacial Tensions. *Petrophysics*. 2007, 48 (3), pp.157-187.

70. Meredith, W., Kelland, S.J., & Jones, D.M. Influence of Biodegradation on Crude Oil Acidity and Carboxylic Acid Composition. *Organic Geochemistry*. 2000, 31(11), pp.1059-1073.

71. Barth, T., Høiland, S., Fotland, P., Askvik, K.M., Pedersen, B.S. & Borgund, A. Acidic compounds in biodegraded petroleum. *Organic geochemistry*. 2004, 35 (11-12), pp.1513-1525.

72. Abdel-Wali, A.A. Effect of Single Polar Compounds and Salinity on Interfacial Tension and Wettability of Rock/Oil/Brine System. *Journal of King Saud University*, *Engineering Sciences*. 1996, 8 (2), pp.153-163.

73. Brandal, Ø., Hanneseth, A.D., & Sjöblom, J. Interactions between Synthetic and Indigenous Naphthenic Acids and Divalent Cations

across Oil–Water Interfaces: Effects of Addition of Oil-Soluble Non-Ionic Surfactants. *Colloid and Polymer Science*. 2005, 284 (2), pp.124-133.

74. Lashkarbolooki, M., Riazi, M., Ayatollahi, S., & Hezave, A.Z. Synergy Effects of Ions, Resin, and Asphaltene on Interfacial Tension of Acidic Crude Oil and Low-High Salinity Brines. *Fuel*. 2016a, 165, pp. 75-85.

75. Lashkarbolooki, M., & Ayatollahi, S. Effects of Asphaltene, Resin and Crude Oil Type on the Interfacial Tension of Crude Oil/Brine Solution. *Fuel*. 2018a, 223, pp. 261-267.

76. Nasralla, R.A., Bataweel, M.A., & Nasr-El-Din, H.A. Investigation of Wettability Alteration by Low Salinity Water. In: *Offshore Europe*, January 2011, Aberdeen, United Kingdom.

77. Robert, H.J. Foundations of colloid science. Oxford university press, 2001.

78. Winsauer, W.O., & McCardell, W.M. Ionic Double-Layer Conductivity in Reservoir. Petroleum Transactions, *Journal of Petroleum Technology*. 1953, 5 (5), pp.129-134.

79. Buckley, J.S., & Liu, Y. Some Mechanisms of Crude/Brine/Solid Interactions. *Journal of Petroleum Science and Engineering*. 1998, 20 (3-4), pp.155-160.

80. Alotaibi, M.B., & Nasr-El-Din, H.A. Electrokinetics of Limestone and Dolomite Rock Particles. *SPE Reservoir Evaluation and Engineering*. 2011, 14 (5), pp. 594-603.

81. Mahani, H. , Keya, A.L., Berg, S., & Nasralla, R. The Effect of Salinity, Rock Type and pH on the Electrokinetics of Carbonate-Brine Interface and Surface Complexation Modeling. In: *SPE Reservoir Characterization and Simulation Conference and Exhibition*, September 2015a, Abu Dhabi, UAE.

82. Kasha, A., Al-Hashim, H., Abdallah, W., Taherian, R., & Sauerer, B. Effect of Ca^{2+}, Mg^{2+} and SO_4^{2-} Ions on the Zeta Potential of Calcite and Dolomite Particles Aged with Stearic Acid. *Colloids and Surfaces A: Physicochemical and Engineering*. 2015, 482, pp. 290-299.

83. Hiorth, A., Cathles, L.M., Kolnes, J., Vikane, O., Lohne, A., & Madland, M.V. A Chemical Model for the Seawater-CO2-Carbonate System-Aqueous and Surface Chemistry. In: *International Symposium of the Society of Core Analysts*, October 2008a, Abu Dhabi, UAE.

84. Hiorth, A., Cathles, L.M., Kolnes, J., Vikane, O., Lohne, A., & Madland, M.V. Chemical Modeling of Wettability Change in Carbonate Rocks. In: *International Symposium of the Society of Core Analysts,* October 2008b, Abu Dhabi, UAE.

85. Austad, T., Strand, S., & Puntervold, T., 2009. Is Wettability Alteration of Carbonates by Seawater caused by Rock Dissolution? In: *International Symposium of the Society of Core Analysts*, September 2009, Netherland, 3 (1), pp. 27-30.

86. Mahani, H., Keya, A.L., Berg, S., Bartels, W.B., Nasralla, R., & Rossen, W.R. Insights into the Mechanism of Wettability alteration by Low-Salinity Flooding (LSF) in Carbonates. *Energy & Fuels*. 2015b, 29 (3), pp.1352-1367.

87. Buckley, J.S., & Lord, D.L. Wettability and Morphology of Mica Surfaces after Exposure to Crude Oil. *Journal of Petroleum Science and Engineering*. 2003, 39 (3-4), pp. 261-273.

88. Toulhoat, H., Prayer, C., & Rouguet, G. Characterization by Atomic Force Microscopy of Adsorbed Asphaltenes. *Colloids and Surfaces A: Physicochemical and Engineering Aspects*. 1994, 91(3), pp. 267-283.

89. Hassenkam, H., Pedersen, C.S., Dalby, K., Austad, A., & Stipp, S.L.S. Pore Scale Observation of Low Salinity Effects on Outcrop and Oil Reservoir Sandstone. *Colloids and Surfaces A: Physicochemical and Engineering Aspects.* 2011*,* 390 (1-3), pp.179-188.

90. Brady, P.V., & Thyne, G. Functional Wettability in Carbonate Reservoirs. *Energy & Fuels*. 2016, 30 (11), pp. 9217-9225.

91. Kumar, K., Dao, E.K., & Mohantly, K.K. Atomic Force Microscopy Study of Wettability Alteration by Surfactants. *Society of Petroleum Engineers*. 2008, 13 (2), pp.137-145.

92. Seiedi, O., Rahbar, M., Nabipour, M., Emadi, M.A., Ghatte, M.H., & Ayattollahi, S. Atomic Force Microscopy (AFM) Investigation on the Surfactant Wettability Alteration Mechanism of Aged Mica Mineral Surfaces. *Energy & Fuels*. 2011, 25 (1), pp.183-188.

93. Hilner, E., Andersson, M.P., Hassenkam, T., Matthiesen, J., Salino, P.A., & Stipp, L.S. The Effect of Ionic Strength on Oil Adhesion in Sandstone-the Search for the Low Salinity Mechanism. *Scientific Report*. 2015, 5, p. 9933.

94. Mathiesene, J., Bovet, N., Hilner, E., Andersson, M.P., Schmidt, D.A., Webb, K.J., Dallby, K.N., Hassenkam, T., Crouch, J., Collins, I.R., & Stipp, L.S. How Naturally Adsorbed Material on Minerals

Affects Low Salinity Enhanced Oil Recovery. *Energy & Fuels*. 2014, 28 (8), pp. 4849-4858.

95. Pedersen, N.R., Hassenkam, H., Ceccato, M., Dalby, K.N., Mogensen, K., & Stipp, S.L.S. Low Salinity Effect at Pore Scale: Probing Wettability Changes in Middle East limestone. *Energy & Fuels*. 2016, 30 (5), pp. 3768-3775.

96. Generosi, J., Ceccato, M., Andersson, M.P., Hassenkam, T., Dobberschutz, N.B., & Stipp, S.L. Calcite Wettability in the Presence of Dissolved Mg^{2+} and SO_4^{2-}. *Energy & Fuels.* 2016*,* 31(1), pp. 1005-1014*.*

97. Guo, Y., Wang, D., Yang, L., & Liu, S. Nanoscale Monolayer Adsorption of Polyelectrolytes at the Solid/Liquid Interface Observed by Quartz Crystal Microbalance. *Polymer Journal*. 2017, 49 (7), pp. 543-548.

98. Li, J., Zhang, Z., Zhou, X., Chen, T., Nie, J., & Du, B. PNIPAmx–PPO36–PNIPAmx Thermo-Sensitive Triblock Copolymers: Chain Conformation and Adsorption Behaviour on a Hydrophobic Gold Surface. *Physical Chemistry Chemical Physics.* 2016*,* 18 (1), pp. 519-528.

99. Dubey, S.T., & Doe, P.H. Base Number and Wetting Properties of Crude Oils. *SPE Reservoirs Engineering.* 1993*,* 8 (3), pp.195-200.

100. Pernyeszi, T., Patzko, A., Berkesi, O., & Dekany, I. Asphaltene Adsorption on Clays and Crude Oils Reservoir Rocks. *Colloids and Surfaces A: Physicochemical and Engineering Aspects.* 1998*,* 137 (1-3), pp. 373-384.

101. Ekholm , P., Blomberg, E., Claesson, P., Auflem, I.H., Sjöblom, J., & Kornfeldt, A. A Quartz Crystal Microbalance Study of the Adsorption of Asphaltenes and Resins onto a Hydrophilic Surface. *Journal of Colloidal and Interface Science.* 2002, 247(2), pp. 342-350.

102. Tapio, L., Subramanian, S., Simon, S., & Sjöblom, J. Solvent Desorption of Asphaltenes from Solid Surfaces. *Journal of Dispersion Science and Technology*. 2016, 28 (3), pp. 355-360.

103. Buckley, J.S. Mechanisms and Consequences of Wettability Alteration by Crude Oils. Doctoral Thesis. Herriot Watt University 1996.

104. Donaldson, E.C. Oil-Water-Rock Wettability Measurement. *American Chemical Society, Division of Petroleum Chemistry*. 1981, 1, pp.110-122.

105. Farooq, U., Sjøblom, J., & Øye, G. Deorption of Asphaltenes from Silica-Coated Quartz Crystal Surfaces in Low Saline Aqueous Solutions. *Journal of Dispersion Science and Technology.* 2011a, 32 (10), pp. 1388-1395.

106. Farooq, U., Asif, N., Tweheyo, M.T., Sjoblom, J., & Qye, G. Effect of Low-Saline Aqueous Solutions and pH on the Desorption of Crude Oil Fractions from Silica Surfaces. *Energy & Fuels.* 2011b, 25 (5), pp. 2058-2064.

107. Nourani, M., Tichelkamp, T., Gawel, B., & Oye, G. Desorption of Crude Oil Components from Silica and Aluminosilicate Surfaces upon Exposure to Aqueous Low Salinity and Surfactant Solutions. *Fuel.* 2016,180, pp.1-6.

108. Liu, X., Yan, W., Stenby, E.H., & Thormann, E. Release of Crude Oil from Silica and Calcium Carbonate Surfaces: On the Alternation of Surface and Molecular Forces by High-and Low-Salinity Aqueous Salt Solutions. *Energy & Fuels.* 2016, 30 (5), pp. 3986-3993.

109. Nilghaz, A., Wicaksono, D.H.B., Gustiono, D., Abdul Majid, F.A., Supriyanto, E., & Rafiq Abdul Kadir, M. Flexible Microfluidic Cloth-Based Analytical Devices Using a Low-Cost Wax Patterning Technique. *Lab on a Chip.* 2012, 12 (1), pp. 209-218.

110. Martinez, A.W., Phillips, S.T., Whitesides, G.M., & Carrilho, E. Diagnostics for the Developing World: Microfluidic Paper-Based Analytical Devices. *Analytical Chemistry.* 2009, 82, pp. 3-10.

111. Xu, W., Ok, J.T., Xiao, F., Neeves, K.B., & Yin, X. Effect of Pore Geometry and Interfacial Tension on Water-Oil Displacement Efficiency in Oil-Wet Microfluidic Porous Media Analogs. *Physics of Fluids*. 2014, 26 (9), pp.1-16.

112. Joseph, J., Gunda, N.S.K., & Mitra, S.K. On-Chip Porous Media: Porosity and Permeability Measurements. *Chemical Engineering Science.* 2013, 99, pp. 274-283.

113. Nilsson, M.A., Kulkarni, R., Gerberas, L., Hammond, R., Singh, R., Baumhoff, E., & Rothstein, J.P. Effect of Fluid Rheology on Enhanced Oil Recovery in a Microfluidic Sandstone Device. *Journal of Non-Newtonian Fluid Mechanics.* 2013, 202, pp.112-119.

114. Conn, C.A., Ma, K., Hirasaki, G.J., & Biswal, S.L. Visualizing Oil Displacement with Foam in a Microfluidic Device with Permeability Contrast. *Lab on a Chip*. 2014, 14 (20), pp. 3968-3977.

115. He, K., Xu, L., Gao, Y., Yin, X., & Neeves, K.B. Evaluation of Surfactant Performance in Fracturing Fluids for Enhanced Well Productivity in Unconventional Reservoirs Using Rock-on-a-Chip *Approach*. *Journal of Petroleum Science and Engineering*. 2015, 135, pp. 531-541.

116. Xu, K., Zhu, P., Tatiana, C., Huh, C., & Balhoff, M. A Microfluidic Investigation of the Synergistic Effect of Nanoparticles and Surfactants in Macro-Emulsion Based EOR. In*: SPE Improved Oil Recovery Conference*, April 2016, Tulsa, Oklahoma, USA.

117. Barnaji, M.J., Pourafshary, P., & Rasaie, M.R. Visual Investigation of the Effects of Clay Minerals on Enhancement of Oil recovery by Low Salinity Water Flooding. *Fuel*. 2016, 184, pp. 826-835.

118. Amirian, T., Haghighi, M., & Mostaghimi, P. Pore Scale Visualization of Low Salinity Water Flooding as an Enhanced Oil Recovery Method. *Energy & Fuels.* 2017, 31(12), pp. 13133-13143.

119. Emadi, A., & Sohrabi, M. Visual Investigation of Oil Recovery by Low Salinity Water Injection: Formation of Water Micro-Dispersions and Wettability Alteration. In: *SPE Annual Technical Conference and Exhibition*, *Society of Petroleum Engineers*, October 2013, Louisiana, USA.

120. Fredriksen, S.B., Rognmo, A.U., & Fernø, M.A. Pore-Scale Mechanisms during Low Salinity Water flooding: Oil Mobilization by Diffusion and Osmosis. *Journal of Petroleum Science and Engineering*. 2018,163, pp. 650-660.

121. Adamson, A.W., & Alice, P.G. Physical Chemistry of Surfaces. New York: John Wiley and Sons, Inc., 1997.

122. Kranias, S. Effect of Drop Volume on Static Contact Angles. Technical Note 310e, 2012.

123. Al-Khafaji, A., & Wen, D. Quantification of Wettability Characteristics for Carbonates Using Different Salinities. *Journal of Petroleum Science and Engineering.* 2018, 173, pp. 501-511*.*

124. Dixon, M.C. Quartz Crystal Microbalance with Dissipation Monitoring: Enabling Real-time Characterization of Biological Materials and Their Interactions. *Journal of Bimolecular Techniques*. 2008, 19 (3), pp. 151-158.

125. Sauerbrey, G.Z. Use of Quartz Crystal Vibrator for Weighting Thin Films on a Microbalance. *Physics*.1959,155, pp. 206–222; Bottom VE, Introduction to Quartz Crystal Unit Design.

126. Kanazawa, K.K., & Gordon, G. Frequency of a Quartz Microbalance in Contact with Liquid. *Analytical Chimica Acta*. 1985, 175, pp. 99-105.

127. Hutter, J.L., & Bechhoefer, J. Calibration of Atomic-Force Microscope Tips. *Review of Scientific Instruments*. 1993, 64 (7), pp.1868-1873.

128. Gavara, N. A Beginner's Guide to Atomic Force Microscopy Probing for Cell Mechanics. *Microscopy Research and Technique.* 2017*,* 80 (1), pp. 75-84.

129. Fulcher Jr, R.A., Ertekin, T., & Stahl, C.D. Effect of Capillary Number and Its Constituents on Two-Phase Relative Permeability Curves. *Journal of Petroleum Technology.* 1985, 37(2), pp. 249-260.

130. Gomari, R. Different Approaches to Understand Mechanism of Wettability Alteration of Carbonate Reservoirs. In: *SPE Europec /Eage Annual Conference and Exhibition*, January 2009, Amsterdam, Netherlands.

131. Marouf, R., Marouf-Khelifa, K., Shott, J., & Khelifa, A. Zeta Potential Study of Thermally Treated Dolomite Samples in Electrolyte Solutions*. Microporous and Mesoporous Materials.* 2009*,* 122 (1-3), pp. 99–104.

132. Pokrovsky, O.S., Schott, J., & Thomas, F. Dolomite Surface Speciation and Reactivity in Aquatic Systems*. Geochimica Cosmochimica Acta.* 1999, 63 (19-20), pp. 3133-3143.

133. Chen, G., & Tao, D. Effect of Solution Chemistry on Floatability of Magnesite and Dolomite. *International Journal of Mineral Processing.* 2004, 74 (1-4), pp. 343-357.

134. Vdović, N. Electrokinetic Behaviour of Calcite-the Relationship with Other Calcite Properties. *Chemical Geology.* 2001, 177(3), pp. 241-248.

135. Austad, T., Strand, S., Madland, M.V., Puntervold, T., & Korsnes, R. I. Seawater in Chalk: An EOR and Compaction Fluid. In: *SPE International Petroleum Technology Conference*, January 2007, Dubai, UAE.

136. Derrick, M.R., Stulik, D., & Landry, J.M. Infrared Spectroscopy in Conservation Science. Los Angeles, CA: The Getty Conservation Institute, 1999.

137. Stuart, B.H. Infrared Spectroscopy: Fundamentals and Applications. New York: John Wiley and Sons Ltd., 2004.

138. Varadaraj, R., & Brons, C. Molecular Origins of Heavy Oil Interfacial Activity Part 1: Fundamental Interfacial Properties of Asphaltenes Derived from Heavy Crude Oils and their Correlation to Chemical Composition. *Energy & Fuels.* 2007, 21(1), pp. 195-198.

139. Kummar, B. Effect of Salinity on the Interfacial Tension of Model and Crude Oil Systems. Master Thesis, University of Galgary, 2012.

140. Skauge, A., Standal, S., Boe, S.O., Skauge, T., & Blokhus, A.M. Effects of Organic Acids and Bases, and Oil Composition on Wettability. In: *Society of Petroleum Engineers, Annual Technical Conference and Exhibition*, October 1999, Houston, Texas.

141. Bai, J.M., Fan, W.Y., Nan, G.Z., Li, S.P., & Yu, B.S. Influence of Interaction between Heavy Oil Components and Petroleum Sulfonate on the Oil–Water Interfacial Tension. *Journal of Dispersion Science and Technology*. 2010, 31(4), pp. 551-556.

142. Brandal, Ø., Hanneseth, A.M.D., & Sjöblom, J. Interactions between Synthetic and Indigenous Naphthenic Acids and Divalent Cations across Oil–Water Interfaces: Effects of Addition of Oil-Soluble Non-Ionic Surfactants. *Colloid and Polymer Science*. 2005, 284 (2), pp.124-133.

143. Hu, X., Li, Y., Sun, H., Song, X., Li, Q., Cao, X., & Li, Z. Effect of Divalent Cationic Ions on the adsorption behaviour of zwitterionic surfactant at silica/solution interface*. Journal of Physical Chemistry*. 2010, 114 (27), pp. 8910-8916.

144. Lashkarbolooki, M., & Ayatollahi, S. Investigating Injection of Low Salinity Brine in Carbonate Rock with the Assist of Works of Cohesion and Adhesion and Spreading Coefficient Calculations. *Journal of Petroleum Science and Engineering.* 2018b, 161, pp. 381-389.

145. Lashkarbolooki, M., & Ayatollahi, S. Performance of Sea Water Dilution on the Surface Free Energies of the Crude Oils in Water-Flooded Carbonate Rock. *Journal of Adhesion Science and Technology*. 2018c, 32 (12), pp.1359-1368.

146. Israelachvili, J.N. Intermolecular and Surface Forces. Third edition, Amsterdam: Academic Press, 2011.

147. Yi, Z., & Sarma, H.K. Improving Waterflood Recovery Efficiency in Carbonate Reservoirs through Salinity Variations and Ionic Exchanges: A Promising Low-Cost "Smart-Waterflood" Approach. In: *SPE International Petroleum Conference and Exhibition*, November 2012, Abu Dhabi, UAE.

148. Zhang, Y., & Sarma, H.K. Improving Waterflood Recovery Efficiency in Carbonate Reservoirs through Salinity Variations and Ionic Exchanges: A Promising Low-Cost “Smart-Waterflood” Approach. In: *Abu Dhabi International Petroleum Exhibition and Conference*, November 2012, Abu Dhabi, UAE.

149. AlShaikh, M., & Mahadevan, J. Impact of Brine Composition on Carbonate Wettability: A Sensitivity Study. In: *SPE Saudi Arabia Section Technical Symposium and Exhibition*, April 2014, Al-Khobar, Saudi Arabia.

150. Awolayo, A., Sarma, H., & AlSumaiti, A.M. A Laboratory Study of Ionic Effect of Smart Water for Enhancing Oil Recovery in Carbonate Reservoirs. In: *SPE EOR Conference at Oil and Gas West Asia*, April 2014, Muscat, Oman.

151. Lashkarbolooki, M., Riazi, M., Hajibagheri, F., & Ayatollahi, S. Low salinity Injection into Asphaltenic-Carbonate Oil Reservoir, Mechanistical Study. *Journal of Molecular Liquids*. 2016b, 216, pp. 377-386.

152. Donaldson, E., & Alam, W. Wettability. Houston: Gulf Publishing Company, 2008.

153. Butt, H.J., Cappella, B., & Kappl, M. Force Measurements with the Atomic Force Microscope: Technique, Interpretation and Applications. *Surface Science Reports*. 2005, 59 (1), pp.1-152.

154. Samanta, A., Ojha, K., & Mandal, A. Interactions between Acidic Crude Oil and Alkali and Their Effects on Enhanced Oil Recovery. *Energy & Fuels*. 2011, 25 (4), pp.1642−1649.

155. Farooq, U., Tweheyo, M.T., Sjøblom, J., & Øye, G. Surface Characterization of Model, Outcrop, and Reservoir Samples in Low

Salinity Aqueous Solutions. *Journal of Dispersion Science and Technology.* 2011c, 32 (4), pp. 519-531.

156. Abdolmohsen, S.A., Abdalla, A.M., Mohd, S.I., & Jose, V.P. P. Experimental Investigation into Effects of Crude Oil Acid and Base Number on Wettability Alteration by Using Different Low Salinity Water in Sandstone rock. *Journal of the Japan Petroleum Institute*. 2015, 58 (4), pp. 228-236.

157. Hamouda, A.A., & Gupta, S. Enhancing Oil Recovery from Chalk Reservoirs by a Low-Salinity Water Flooding Mechanism and Fluid/Rock Interactions. *Energies*. 2017, 10 (4), p. 576.

158. Nasralla, R.A., Sergienko, E., Van der Linde, H.A., Brussee, N.J., Mahani, H., Suijkerbuijk, B.M.J., Al-Qarshubi, I.S.M., & Masalmeh, S.K. Demonstrating the Potential of Low-Salinity Waterflood to Improve Oil Recovery in Carbonate Reservoirs by Qualitative Coreflood. In: *Abu Dhabi International Petroleum Exhibition and Conference*, November 2014, Abu Dhabi, UAE.

159. Rücker, M., Berg, S., Armstrong, R.T., Georgiadis, A., Ott, H., Schwing, A., & Wolf, M. From Connected Pathway Flow to Ganglion Dynamics. *Geophysical Research Letters.* 2015, 42 (10), pp. 3888-3894.

160. Singh, K., Menke, H., Andrew, M., Lin, Q., Rau, C., Blunt, M.J., & Bijeljic, B. Dynamics of Snap-off and Pore-Filling Events during Two-Phase Fluid Flow in Permeable Media. *Scientific Reports.* 2017, 7(1), p. 5192.

161. Zheng, X., Mahabadi, N., Yun, T.S., & Jang, J. Effect of Capillary and Viscous Force on CO_2 Saturation and Invasion Pattern in the Microfluidic Chip. *Journal of Geophysical Research: Solid Earth.* 2017, 122 (3), pp.1634-1647.

162. Moore, T.F., & Slobod, R.L. Displacement of Oil by Water-Effect of Wettability, Rate, and Viscosity on Recovery. In: *Meeting of the Petroleum Branch of AIME*, October 1955, New Orleans, Louisiana.

163. Agbalaka, C.C., Dandekar, A.Y., Patil, S.L., Khataniar, S., & Hemsath, J.R. Core flooding Studies to Evaluate the Impact of Salinity and Wettability on Oil Recovery Efficiency. *Transport Porous Media.* 2009, 76 (1), pp. 77-94.

164. Zhang, Y., & Morrow N.R. Comparison of Secondary and Tertiary Recovery with Change in Injection Brine Composition for Crude Oil/Sandstone Combinations. In: *SPE/DOE Symposium on Improved Oil Recovery,* April 2006c, Tulsa, USA.

165. Lake, L.W. Enhanced Oil Recovery. Upper Saddle River, New Jersey: Prentice Hall, 1989.

166. Chávez-Miyauchi, T.E., Firoozabadi, A., & Fuller, G.G. Nonmonotonic Elasticity of the Crude Oil–Brine Interface in Relation to Improved Oil Recovery. *Langmuir.* 2016, 32 (9), pp. 2192-2198.

167. Morin, B., Liu, Y., Alvarado, V., & Oakey, J. A Microfluidic Flow Focusing Platform to Screen the Evolution of Crude Oil–Brine Interfacial Elasticity. *Lab on a Chip.* 2016, 16 (16), pp. 3074-3081.

168. Cissokho, M., Baussour, S., Cordier, P., Bertin, H., & Hamon, G. Low Salinity Oil Recovery on Clayey Sandstone: Experimental Study. *Petrophysics*. 2010, 51(5), pp. 305-313.

169. Jackson, M.D., Al-Mahrouqi, D., & Vinogradov, J. Zeta Potential in Oil-Water-Carbonate Systems and its Impact on Oil Recovery during Controlled Salinity Water-Flooding. *Scientific Report*s. 2016, 6, p. 37363.

170. Zhang, C.Y., Oostrom, M., Wietsma, T.W., Grate, J.W., & Warner, M.G. Influence of Viscous and Capillary Forces on Immiscible Fluid Displacement: Pore-Scale Experimental Study in a Water-Wet Micromodel Demonstrating Viscous and Capillary Fingering. *Energy & Fuels*. 2011, 25 (8), pp. 3493–3505.

Appendix A

Measured Zeta Potential

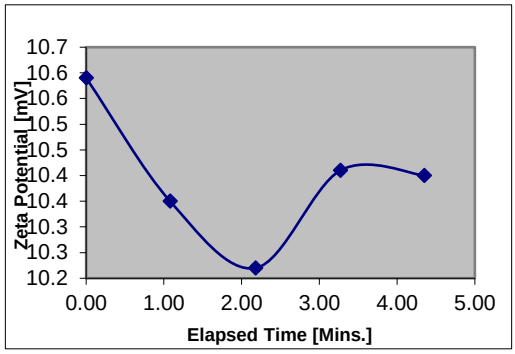

FW

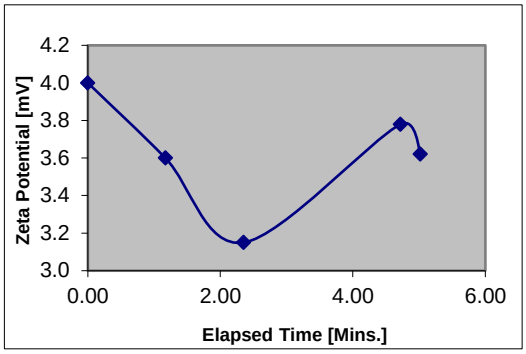

SW

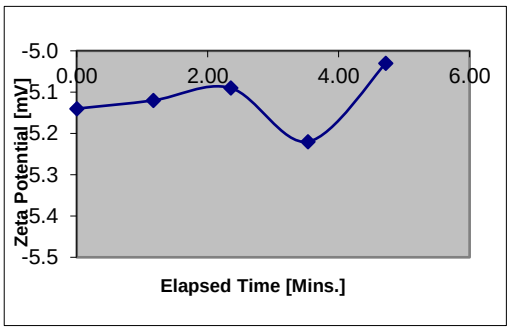

2dSW

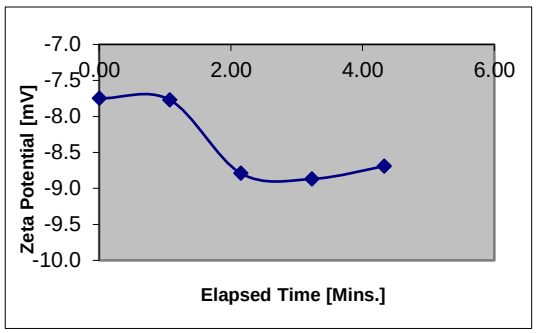

5dSW

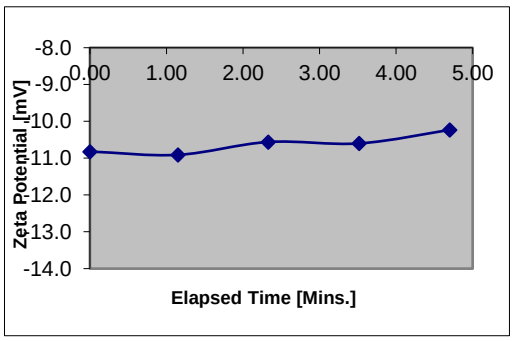

10dSW

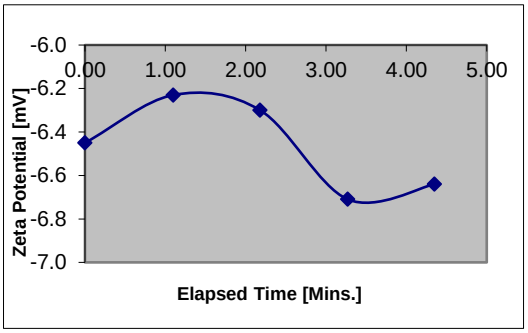

20dSW

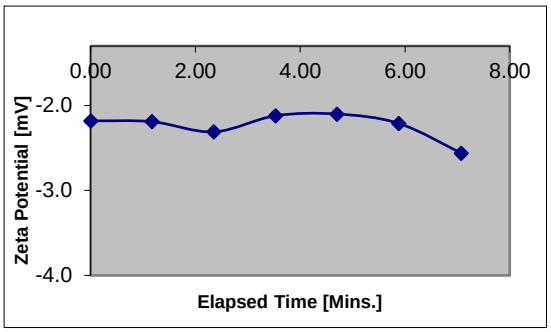

50dSW

Figure 1: Measured zeta potential vs. elapsed time for outcrop limestone suspensions.

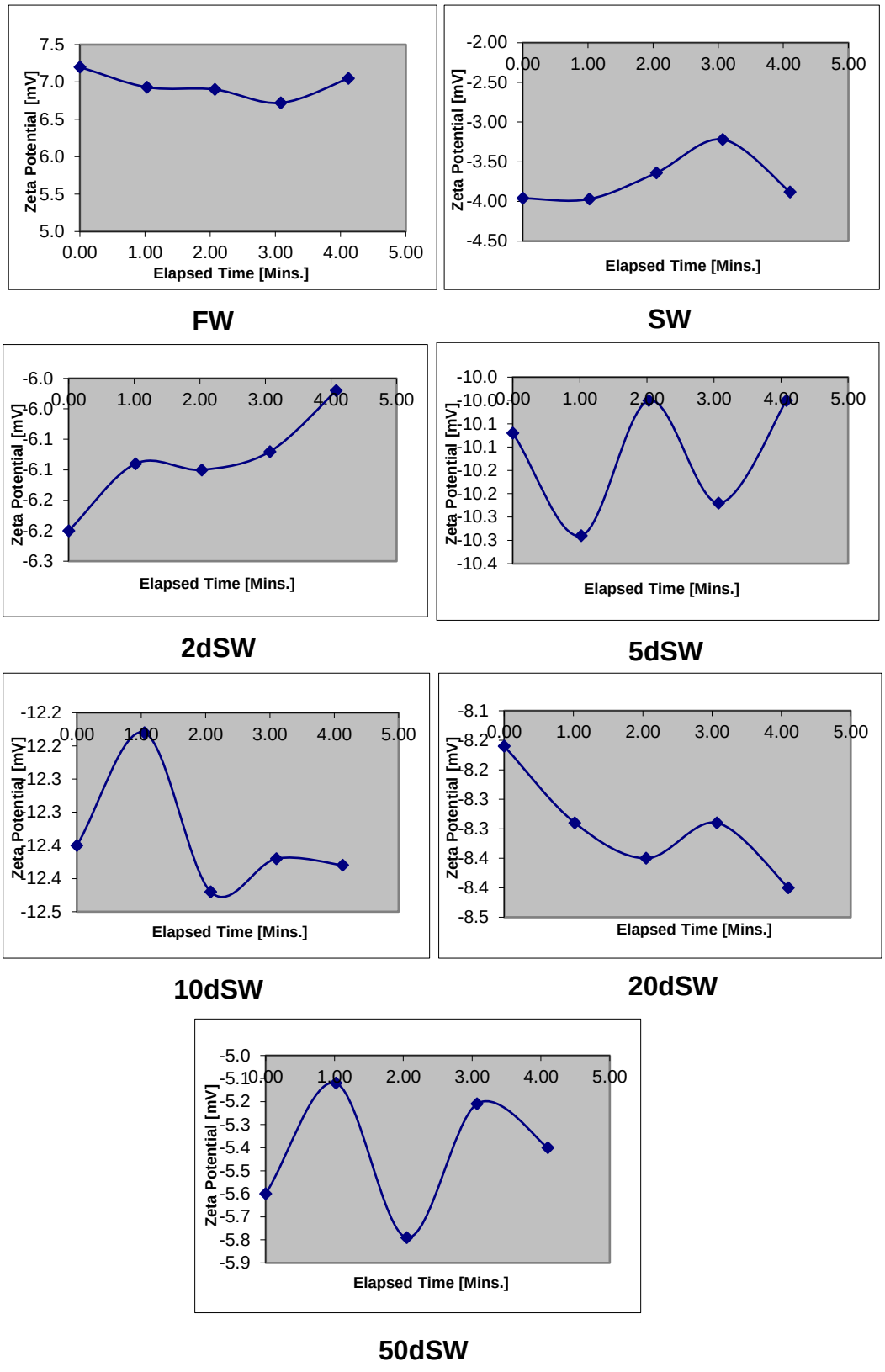

Figure 2: Measured zeta potential vs. elapsed time for reservoir dolomite-brine suspensions.